1-1-2011

Method Development And Applications To Screening And Characterization Of Rrna-Targeting Small Molecules

Papa Nii Asare-Okai
Wayne State University

METHOD DEVELOPMENT AND APPLICATIONS TO SCREENING AND CHARACTERIZATION OF rRNA-TARGETING SMALL MOLECULES

by

PAPA NII ASARE-OKAI

DISSERTATION

Submitted to the Graduate School

of Wayne State University,

Detroit, Michigan

in partial fulfillment of the requirements

for the degree of

DOCTOR OF PHILOSOPHY

2011

MAJOR: CHEMISTRY

Approved by:

_____

Advisor   Date

_____

_____

_____

DEDICATION

To my father Dr. S. Asare-Okai, my sister Pamela Zormelo and in memory of my mother Theresa

Asare-Okai. Thank you for investing in my education.

ACKNOWLEDGEMENTS

my undergraduate advisor Prof. Roger DeKock, and also, Dr. Kumar Sinniah and Dr. Douglas Vander Griend for encouraging me to apply to graduate school.

Most importantly, I would like to thank my wife Kwartekai for keeping me grounded, and well-fed. Thank you for your support and providing me with a safe haven at home. Thank you for your prayers, encouragement and love.

TABLE OF CONTENTS

LIST OF TABLES

LIST OF FIGURES

xvi

LIST OF ABBREVIATIONS

A site   aminoacyl-transfer site

ACC   acetyl-CoA- dependent acetyltransferase

AM   antibiotic modification

ANT   ATP-dependent nucleotidyl-transferase

antiSD   anti Shine Dalgarno

APCI   atmospheric pressure chemical ionization

APH   ATP-dependent phosphotransferase

Arm   aminoglycoside resistance methyltransferase

ddNTP   dideoxynucleotidetriphosphate

DEPC   diethylpyrocarbonate

DMS   dimethylsulfate

E site   exit site

EF   efflux

EF-G   elongation factor G

EF-TU   elongation factor Tu

ESI-MS   electrospray ionization mass spectrometry

FID   fluorescent intercalator displacement

fMet-tRNA^{fmet} formyl-methionine tRNA

FTICR   Fourier transform ion cyclotron resonance

GDP	guanosine diphosphate
GrmA	gentamicin-resistance methyltransferase
GTP	guanosine triphosphate
HIV	human immunodeficiency virus
IF	initiation factor 2
IF1	initiation factor 1
IF3	initiation factor 3
IPA	isopropyl alcohol
ITC	isothermal titration calorimetry
Kd	dissociation constant
KgmB	kanamycin-gentamicin-resistance methyltransferase
Krm	kanamycin-resistance methyltransferase
m/z	mass-to-charge ratio
MALDI	matrix assisted laser desorption ionization
mRNA	messenger RNA
NMR	nuclear magnetic resonance
NTP	nucleotide triphosphate
P site	peptidyl transfer site
PNK	polynucleotide kinase
RF1	release factor 1
RF2	release factor 2

RF3	recycling factor 3
RMP	reduced membrane permeability
RmtA	ribosomal methyltransferase A
RmtB	ribosomal methyltransferase B
RmtC	ribosomal methyltransferase C
RmtD	ribosomal methyltransferase D
rRNA	ribosomal RNA
SD	Shine Dalgarno
Sgm	sisomicin-gentamicin methylase
SPR	surface plasmon resonance
TAR	trans-activation responsive region
TAT	trans-activator of transcription
TM	target modification
TOF	time of flight
TO-PRO	3-methyl-2-((1-(3-(trimethylammonio)propyl)-4-quinolinylidene)methyl)benzothiazolium
tRNA	transfer RNA
UTR	untranslated region

CHAPTER 1

INTRODUCTION

From time in memorial, humans have tried to make sense of their environment and develop new tools to conquer the ever-increasing challenges they face in life every day. Human disease is no exception; the advances in science have propelled the development of tools and medicines to fight many deadly diseases. However, seemingly harmless but dangerous micro-organisms continue to plague and torment the human race in a non-relenting fashion. The antibiotic revolution began after the accidental discovery of penicillin by Alexander Fleming in 1928.[1] Since then, new and better antibiotics have been developed, but the increasing use and misuse of existing antibiotics in humans and agriculture has resulted in bacteria that are highly resistant to current antibiotics (superbugs). Nowadays, over 70% of bacterial infections in the hospitals are resistant to at least one of the drugs most commonly used to treat them.[2] This has resulted in increased mortality rate and longer hospital stays, placing a huge economic burden on patients and the government.[2] The total cost of antimicrobial resistance in the U.S.A. is approximately $30 billion annually.[2] Development of new and effective antibiotics is therefore a high priority for the healthcare industry. The long-term goal of this project is to develop new and effective antibiotics. Before going into the details of the project, it is worthwhile discussing current antibiotics, their mechanism of action against bacteria, and how bacteria develop resistance.

1.1   Mechanism of Action of Current Antibiotics

A variety of antibiotics target different parts of the bacterium cell. They can be grouped into three major classes, depending on their site of action. There are antibiotics that kill bacteria by inhibiting cell wall synthesis, nucleic acid metabolism, or protein synthesis.

First of all, antibiotics such as penicillins, cephalosporins, carbapenems, and monobactams target the cell wall of bacteria. This group of antibiotics is collectively known as the β-lactams.[3] In actively dividing bacteria, β-lactams inhibit the enzymes needed for the proper synthesis of the bacterial cell wall. Inhibition of these enzymes subsequently activates the autolytic system of the cell, leading to lysis and cell death.[4]

Furthermore, fluoroquinolones (examples: norfloxacin and ciprofloxacin) inhibit bacterium cell growth by interacting with DNA gyrase and DNA topoisomerase IV.[5] DNA gyrase is responsible for relieving torsional stress that accumulates ahead of the replication fork by introducing negative supercoils. DNA topoisomerase IV aids this process by introducing nicks at the appropriate DNA sites. Interaction of fluoroquinolones with these two enzymes inhibits DNA replication, and accumulation of nicked DNA triggers pathways that eventually lead to cell death.[5]

The last class of antibiotics inhibits protein synthesis in bacteria. Protein synthesis is an essential process for all living organisms; hence, a wide variety of antibiotics target the protein synthesis machinery of bacteria. Among these antibiotics are tetracyclines, chloramphenicol, and aminoglycosides, just to mention a few.[6-8] The mechanism by which these antibiotics inhibit

protein synthesis will be discussed in detail in the next section. The different antibiotics, their

target sites, and mechanism of resistance are summarized in Table 1.1.

Table 1.1: Bacterial antibiotic targets and resistance mechanisms associated with different antimicrobial agents.

Target	Antimicrobial Agent	Resistance Mechanism	Reference
Cell wall synthesis	β-Lactams	AM, TM, EF, RMP	9
	Glycopeptides	TM	10
	Aminoglycosides	AM, TM, EF, RMP	11-14
	Macrolides	TM, AM, EF	15-16
	Linsosamides	TM, AM, EF	15-16
	Ketolides	TM, AM, EF	15-16
	Sterptogramins	TM, AM, EF	15-16
	Tetracyclines	TM, EF	17
	Chloramphenicol	AM, TM, EF, RMP	18
	Oxazolidinones	TM	19
RNA synthesis	Rifamycin	TM	20
DNA synthesis	Coumarins	TM, EF, RMP	21-22
	Naphthyridines	TM, EF, RMP	22
	Quinolones	TM, EF, RMP	22
	2-Pyridones	TM, EF, RMP	22
Intermediary metabolism	Sulfonamides	TM	23
	Trimethoprim		

TM: target modification, AM: antibiotic modification, EF: efflux, RMP: reduced membrane permeability.

1.2   Antibiotic Resistance

In spite of the availability of diverse antibiotics, antibiotic resistance against all the

different classes of antibiotic has compromised their effectiveness. Antibiotic resistance

mechanisms include target modification; the antibiotic target is modified by mutation or

methylation so that the antibiotic is no longer able to effectively bind to it.[9-10] This kind of

resistance mechanism is seen in all the major classes of antibiotics. Resistance can also occur when membrane proteins are modified, resulting in reduced uptake of the antibiotic.[11-12] Conversely, over-expression of efflux pumps in the membrane could result in reduced accumulation of the antibiotic in the cell, thereby reducing its effectiveness.[14] Antibiotics can also be rendered ineffective by enzymatic modifications or hydrolysis. There are enzymes that catalyze the addition of certain functional groups to the antibiotic, thereby rendering it inefficient in binding to its target.[15-16] Refer to Table 1.1 for a summary of the different resistance mechanisms and the antibiotics that they affect.

All of the antibiotic resistance mechanisms described above are different strategies that antibiotic-producing bacteria use to protect themselves from the antibiotics that they produce. It is probable that current antibiotic resistant pathogens derived these antibiotic-resistance determinants through gene transfer.[24-25] Gene exchange occurs in the soil or the gastrointestinal tract of humans and animals where selection pressure of antibiotics is heaviest. Bacteria can exchange genetic information through transformation, phage-mediated transduction, conjugation, or transposition. These processes can spread antibiotic resistance determinants among bacteria.[24-26]

The antibiotic resistance problem is now at the highest peak and there is a dire need to develop new and effective antibiotics. Many researchers have taken up this challenging task. My thesis work focused on developing new aminoglycoside antibiotics that inhibit protein synthesis. Therefore, the next section will focus on structure and function of the protein synthesis machinery of the cell, the ribosome.

1.3 The Ribosome

1.3.1 Ribosome Structure

The bacterial ribosome is the protein synthesis machinery of the cell. It is composed of two subunits, the 50 S subunit, which is made up of 23 S rRNA, 5 S rRNA, and 34 proteins (L1-L31 there are 4 copies of L12) and the 30 S subunit, which is composed of 16 S rRNA and 21 proteins (S1-S21)[27]. "L" and "S" in the nomenclature of the ribosomal proteins refer to the large and small subunit, respectively. The "S" in the nomenclature of the ribosomal subunit (for example, 50 S) is a measuring unit known as the Svedberg unit, which is a measure of the rate of sedimentation of a component upon centrifugation. A summary of the components of the *E. coli* ribosome is shown in Table 1.2.

Table 1.2: RNA components of the bacterial ribosome (*E. coli*) [27-32]

Type of RNA	Approximate number of nucleotides	subunit Location	Proteins present in subunit
16 S	1,541	30 S	S1-S21
5 S	120	50 S	L1-L34
23 S	2,904	50 S	L1-L34

The secondary structure of the ribosome is formed as a result of the specific base pairing of the different parts of the RNA molecule.[33] The secondary structure of the 16 S rRNA (**Figure 1.1**)[34] is divided into three major domains; the 5' domain, the central domain, and the 3' major domain, and a fourth domain called the 3' minor domain. There are 45 helices in the 16 S r RNA, which are named with a lower case "h" followed by the helix number (for example, h31).

The 23 S rRNA on the other hand is made up of 6 domains (I to IV) (**Figure 1.2**).[35] The domains consist of over a hundred helices, which are named with an upper case "H" followed by the helix number (for example H69). Unlike DNA that exists as a double strand, single strands of RNA can fold into more complex patterns resulting from unpaired nucleotides and mismatches that form bulges, loops and junctions.[36] These structural elements allow the RNA to adopt complex three-dimensional structures. Even more complexity is achieved upon binding of ribosomal proteins.[37] Typically ribosomal proteins have one or more globular domains with long N- or C- terminal domain extensions that penetrate to fill the gaps in the rRNA (**Figure 1.3**).[38] The ribosomal proteins are post-translationally modified by methylation (S11, L3, L7/L12, L11, L16, and L33), acetylation (S5, S18, and L12), glutamic acid residues (S6), and an isoaspartate residue (S11).[39-42] Furthermore, all the ribosomal proteins lack sequence homology with the exception of L12 and L7, which have identical amino acid sequences with the exception of an acetyl group. L12 is converted to L7 when acetylated.[39] The abundance of these post-translational modifications in the ribosomal proteins suggests that they may play a significant role in fine tuning the ribosome structure and or function.[38]

1.3.2 Ribosome Assembly/Biogenesis

The 16 S, 23 S, and the 5 S rRNAs are transcribed as a single primary transcript from one of the rrn operons.[43-44] The new transcript starts to fold during transcription into local secondary structures. Simultaneously, ribosomal modifications and binding of some ribosomal proteins occur.
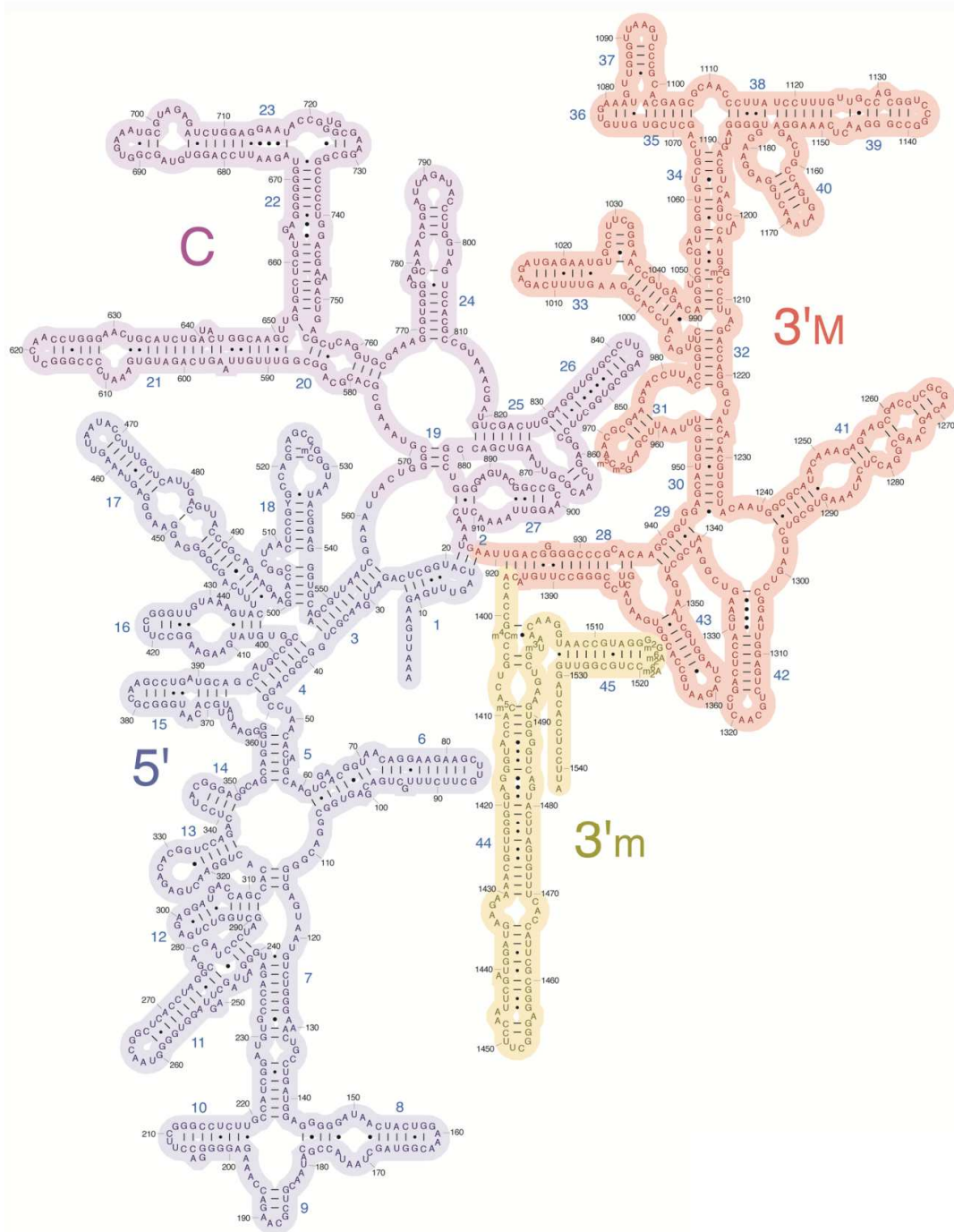
Figure 1.1: The secondary structure of *E. coli* 16 S rRNA shows the different helix numbers in blue color and the different domains; 5' domain (5'), 3' major domain (3'M), 3' minor domain (3'm) and the central domain (C).[34, 45]
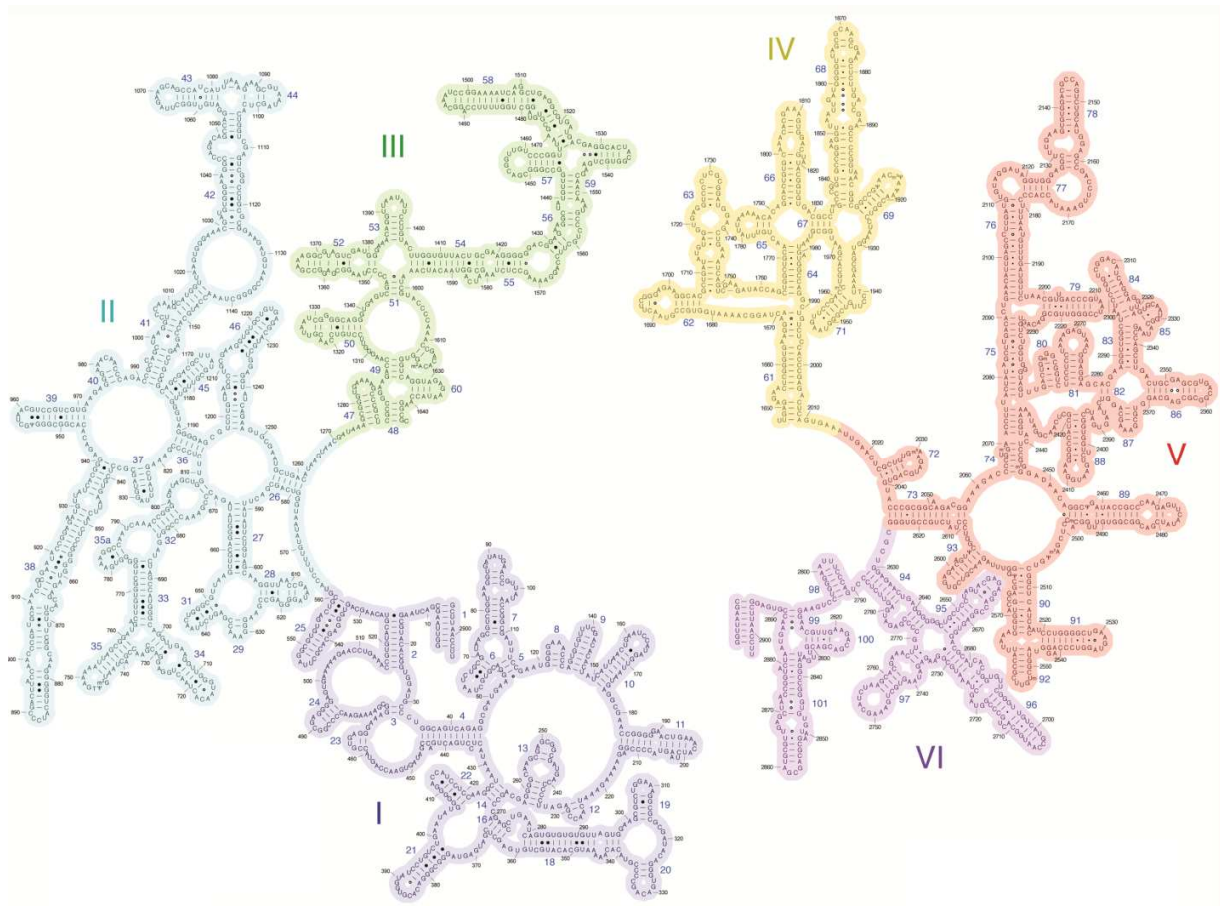
Figure 1.2: The secondary structure of *E. coli* 23 S and rRNA is shown. The different domains are numbered I-VI.[35, 45]

The 16 S RNA is modified at 11 positions, ten of which are methylations and one is pseudouridine.[46-47] The 23 S on the other hand is modified at 25 positions with 14 methylations, nine pseudouridines and one unknown modification.[46-47] Binding of ribosomal proteins to the rRNA happens in a hierarchical and cooperative manner in which early binding proteins arrange the binding sites for late-binding proteins.[48] In general, ribosomal proteins S4-S9, S11-S13, and

S15-S20 assemble first, and after undergoing conformational changes, proteins S2,S3, S10-S14, and S21 bind to form the 30 S particle.[48]
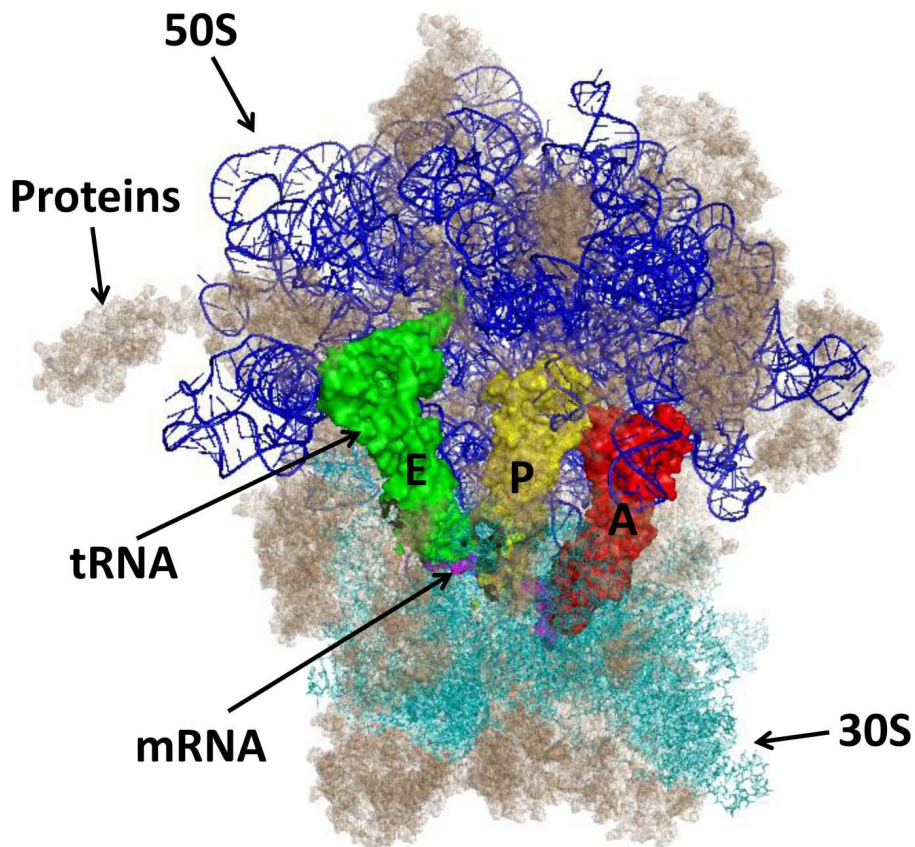
Figure 1.3: Structure of the bacterial ribosome is shown. This figure was generated with PyMol software[49] using coordinates from PDB file 2WDG.[50]

Assembly of the 50 S particle is much more complex and requires metal ions such as Mg^{2+} to help stabilize the RNA structure.[32] Herold and Nierhaus presented a detailed assembly map of the 50 S subunit in 1987,[32] which has since been updated by Williamson.[51] The primary transcript is further processed by RNases to generate mature 30 S and 50 S rRNAs. The whole

process of maturation and assembly of ribosomal subunits takes approximately 2 minutes at 37 °C.[52]

There is an abundance of complementary sequences present in the rRNA;[28, 31] therefore, there is a high probability for mis-folding of the rRNA. RNA chaperones, helicases, and GTPases help manage RNA folding.[53] These proteins in addition to maturation factors help lower the activation energy required for maturation and also rescue kinetically trapped intermediates or mis-folded RNAs to their native state.[32, 53-54] Mature ribosomes are now ready and available for protein synthesis.

1.4 Ribosome Function

1.4.1 Protein Synthesis

Protein synthesis or translation is a process by which a sequence of codons on an mRNA is used as a template for polypeptide synthesis by the ribosome.[55] The 70 S ribosome has three tRNA binding sites on each of its subunits (30 S and 50 S) known as the aminoacyl (A), peptidyl (P) and the exit (E) sites (**Figure 1.3**).[56] The initiation of protein synthesis is promoted by initiation factors IF1, IF2, and IF3. At the onset of translation, IF3 binds to the 30 S subunit and promotes dissociation of the 70 S into the 50 S and 30 S subunits. Binding of IF3 to the 30 S prevents re-association of 30 S with the 50 S subunit. It also helps in the selection of the initiator tRNA (fMet-tRNA^{fMet}) by destabilizing the binding of other tRNAs to the P site.[57] IF1 also binds to the base of the A site and directs the initiator tRNA to the P site by blocking the A

site.[58] Next, IF2, mRNA, and fMet-tRNA^{fMet} are recruited to the 30 S subunit in an unknown order. The anti-Shine-Delgarno (antiSD) sequence at the 3' end of the 16 S rRNA interacts with its complementary sequence (typically GGAGG) on the 5' untranslated region (5' UTR) of the mRNA.[59] This positions the initiation codon in the P site of the ribosome. Current data suggests that the Shine-Delgarno is not the sole determinant for identification of the start codon. However, more importantly, the mRNA folds in a specific manner making the start codon uniquely available for interaction with the 30 S subunit.[60-62] This idea is supported by evidence from other groups who demonstrated that initiation of protein synthesis is possible without an SD-antiSD interaction.[62-63] Furthermore, there have been reports of translation of leaderless mRNAs[64] and translation of prokaryotic mRNAs with translation initiation regions similar to eukaryotic ribosome entry sites[65], which do not involve SD-antiSD interactions for translation initiation to occur.

After the mRNA docks at the P site of the 30 S ribosome, the anti-codon of the initiator tRNA interacts with the start codon (usually AUG, GUG or UUG). This complex constitutes the 30 S initiation complex.[66] Next, IF1 and IF3 are ejected and the 50 S subunit associates with the 30 S subunit with subsequent hydrolysis of GTP to GDP, which leads to the release of IF2. The fMet-tRNA^{fMet}-bound 70 S initiation complex is now ready for elongation. One critical step in the initiation process is the accuracy of selection of the initiator tRNA. This process is promoted by IF2, which interacts directly with the initiator tRNA on the ribosome and IF3, which acts has a proof-reading capability by destabilizing non-cognate tRNAs (**Figure 1.4**).[67]
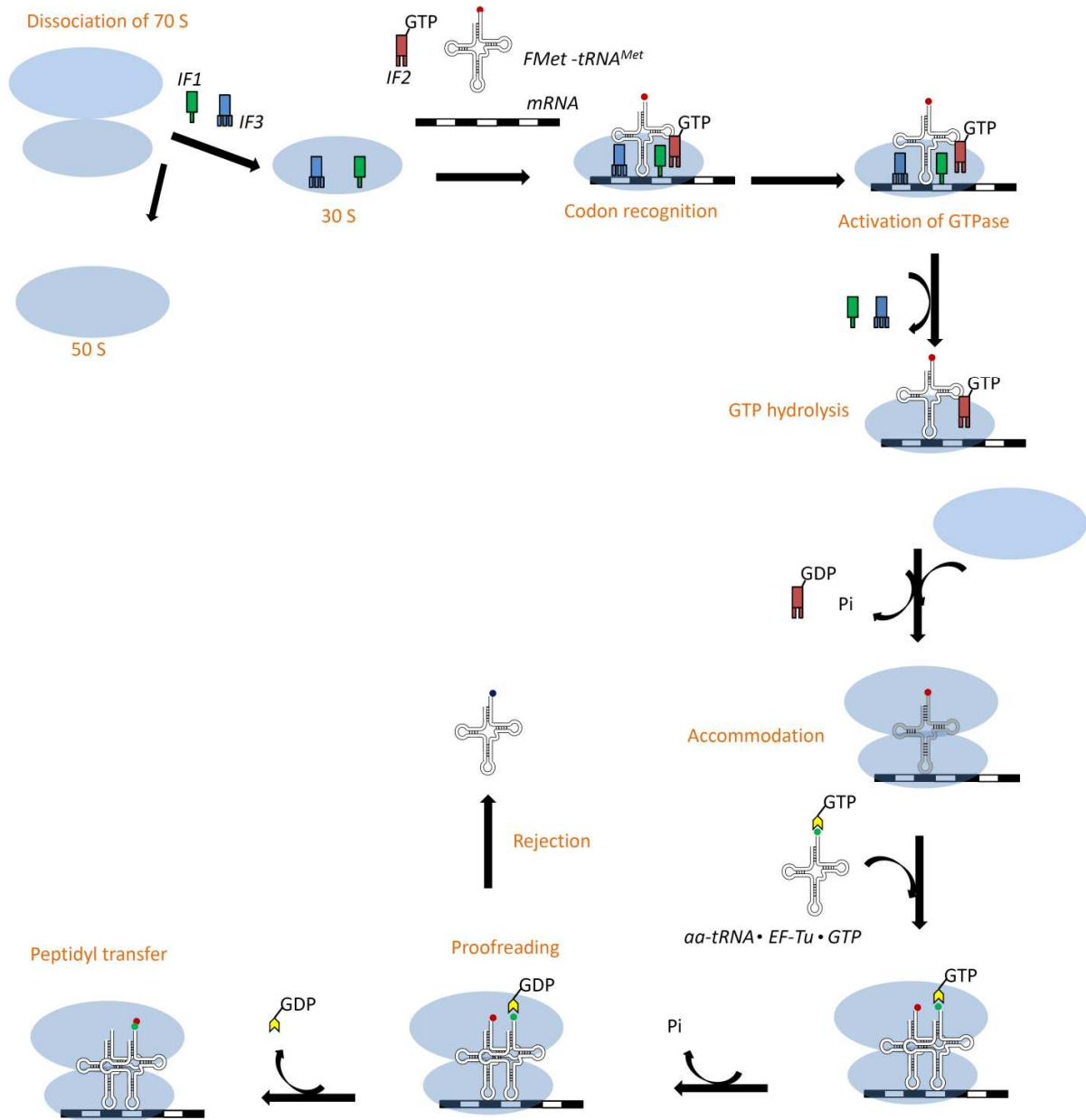
Figure 1.4: A schematic diagram depicts the process of translation initiation through to peptide-bond formation in a bacterial system. Refer to the text for a detailed description of the process.

The elongation process involves repetitive cycles of aminoacyl-tRNA (aa-tRNA) selection, peptide-bond formation, and mRNA-tRNA translocation. This process takes place at an estimated rate of about 15-20 amino acids per second, with an error rate less than 10^{-4}.[68] This amazing fidelity is achieved by concerted efforts of elongation factor Tu (EF-Tu), elongation factor G (EF-G), and a series of ribosomal conformational changes discussed below. The elongation process begins with the delivery of the aa-tRNA to the fMet-tRNA[fMet]-bound 70 S initiation complex in the form of a ternary complex consisting of aa-tRNA bound to EF-Tu and GTP.[69-70] Correct anti-codon–codon interaction triggers the hydrolysis of GTP, which causes the dissociation of EF-Tu.[71-72] The 3' acceptor arm of the tRNA is accommodated into the P site of the 50 S and peptide-bond formation occurs.[73] Selectivity of this process is achieved by a double-checking mechanism, consisting of the initial selection and a proof-reading step. During the initial selection process, aa-tRNA reversibly interacts with the 30 S decoding region for initial codon recognition.[74] Conformational changes occur in the aa-tRNA (described as a molecular spring model) such that only the correct aa-tRNA can sufficiently be stabilized in the decoding center.[72, 75] The interaction between the cognate tRNA and the ribosome induces conformational changes in the 30 S subunit; specifically, nucleotides A1492 and A1493 flip out of the internal loop of helix 44 and nucleotide G530 changes conformation from *syn* to *anti* to interact with the sugar edge of the cognate tRNA.[75-76] This favorable interaction triggers the GTPase activity of EF-Tu. During the proof-reading step, GTP is hydrolyzed, and the release of inorganic phosphate induces conformational changes in EF-Tu leading to its dissociation from the ribosome.[77] At this point, any near-cognate tRNA that may have survived the initial

selection process is likely to dissociate from the ribosome due to unfavorable interactions between partial mismatch interaction between the tRNA and the decoding center.[75] Next, the 3' CCA of the tRNA is positioned at the P site of the 50 S subunit, which catalyzes peptide-bond formation between the α–amino group of the incoming amino acid and the carboxyl group of the amino acid attached the P-site tRNA (**Figure 1.4**).[73]

After peptide-bond formation, translocation occurs. This process involves the movement of the mRNA-tRNA complex from the A and P sites to the P and E sites, respectively. This process requires GTP hydrolysis from elongation factor G (EF-G). The binding of EF-G to the ribosome triggers a ratchet motion in which there is a counterclockwise movement of the small subunit with respect to the large subunit, [78-79] this movement shifts the mRNA bound tRNA to the P/E hybrid state. Next there is hydrolysis of GTP, and a reversal motion occurs where the small subunit moves back to its original position.[80] This movement shifts the mRNA up by one codon, which leaves the A site vacant and ready for another aa-tRNA to bind and repeat the cycle of protein synthesis. The description of the translocation process given above was refined by major contributions made in the past decade by Joachim Frank and co-workers among others (**Figure 1.5**).[78-80]

The process of decoding and translocation continues until a stop codon (UAA, UAG or UGA) docks in the A site of the ribosome. This step leads to recruitment of release factors RF1, RF2 and RF3 to the ribosome, and triggers the release of the polypeptide chain from the P site.[81] After the release of the polypeptide, GTP binds to RF3, resulting in a conformational change in RF3, which leads to the dissociation of RF1 and RF2.[82]
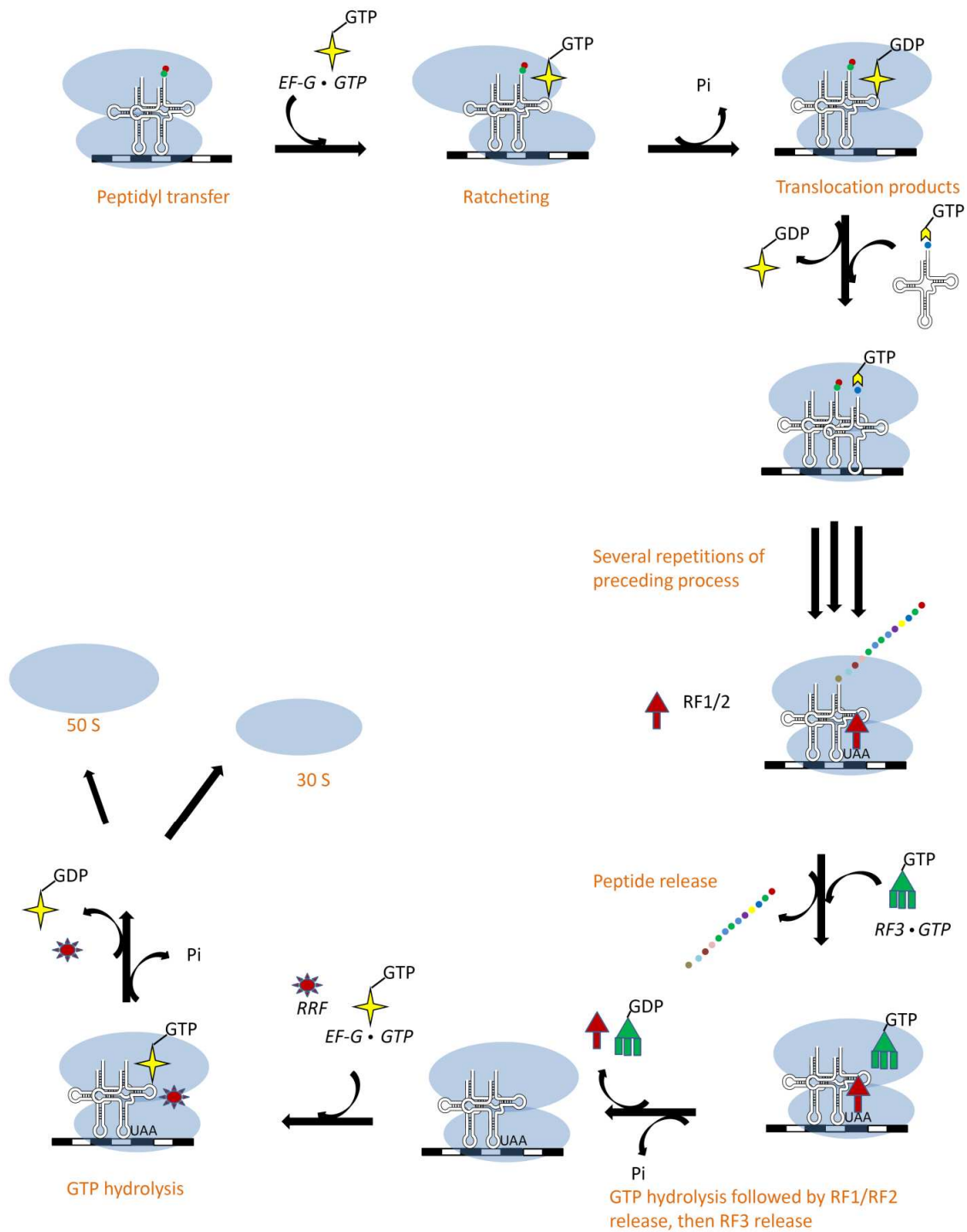
Figure 1.5: A schematic diagram depicts the process of translocation through to ribosome recycling in a bacterial system. Refer to the text for a detailed description of the process.

Upon GTP hydrolysis, RF3 also dissociates from the ribosome leaving the mRNA and deacylated tRNA in the P site of the ribosome. The ribosome is recycled with the help of the ribosome recycling factor (RRF) and EF-G. The binding of these two factors to the ribosome and subsequent hydrolysis of GTP leads to the dissociation of the 70 S ribosome from the mRNA and tRNA (**Figure 1.5**).[83]

1.4.2 A Closer Look at the Decoding Region of the Ribosome

The decoding region is one of the most important parts of the ribosome that ensures the correct synthesis of proteins by accurately decoding the message embedded in the mRNA. Different conformational changes occur in the decoding region (especially helix 44 (**Figure 1.6A**)) to aid this process.[84] One such conformational change is the flipping out of A1492 and A1493, which has been well characterized by different biochemical and biophysical approaches.[85-87] The highly dynamic nature of the decoding region has made it a target of many antibiotics. Many antibiotics such as aminoglycosides bind to the decoding region and induce structural changes that compromise the fidelity or abort the synthesis of the polypeptide.[88-89] To simplify the study of the decoding region, Purohit and Stern were able to show that a 50-nucleotide model of the decoding region (**Figure 1.6B**) is able to fold into the right conformation and bind to antibiotics with affinities similar to that observed in the context of the whole ribosome.[90] This work opened the door to new experiments geared toward understanding the function of the decoding region. Since then, it has also been shown that even shorter RNA constructs representing the A site are able to bind to antibiotics effectively

(**Figure 1.6C**).[89, 91] This work has facilitated the understanding and design of antibiotics to target the A site of the ribosome. Various A-site RNA analogues from different species and analogues representing different mutants can be easily studied by using shorter A-site RNA model representations. [92]
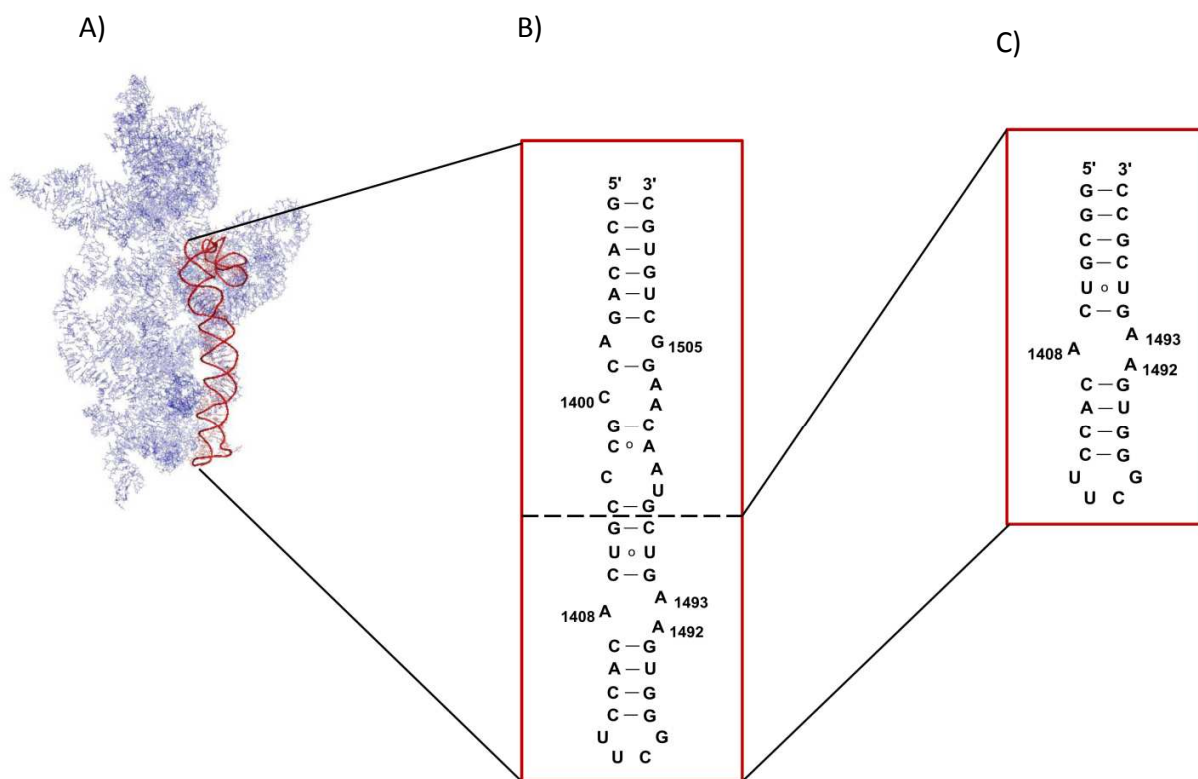
Figure 1.6: Reduction of the decoding region into shorter RNA models is depicted: a) the structure of the ribosomal 30 S subunit with the decoding region (helix 44) highlighted in red the figure was generated with PyMol using coordinates from PDB file 3I8G; b) the 50-nucleotide model of the decoding region introduced by Purohit and Stern;[90] c) the 27-nucleotide model of the A site introduced by Puglisi and Yokoyama.[89, 91]

1.5   The Ribosome as a Drug Target

The ribosome serves as an attractive drug target for a variety of reasons. First of all, it is composed of diverse structural motifs that serve as good binding sites for small molecules.[36] Unlike DNA, rRNA has no known repair mechanisms and is located outside the nucleus; rRNA is more accessible compared to DNA. The structure of the ribosome is conserved across phylogeny; however, there still remain subtle sequence differences and conformational variations that can be utilized for species-specific targeting of antibiotics.[93] Even though there are a wide variety of structural motifs present in the ribosome, most of the current antibiotics target a narrow section of the ribosome with some overlapping sites, utilizing distinct modes for protein-synthesis inhibition (**Figure 1.7**).[94-96] Some of the modes of inhibition include inducing miscoding,[88, 95] interfering with ribosome dynamics,[94, 97] competing with substrate binding,[97] blocking the peptide-exit tunnel,[8] and inhibiting movement of the mRNA chain.[97]

The success of crystallographic studies has expanded our understanding of antibiotic rRNA interactions such that it is not uncommon to find that one antibiotic may exerts its inhibitory action by one major mode in addition to several minor modes due to minor or secondary interactions with other sites on the ribosome.[7, 87, 95] This is not surprising, because some ribosomal antibiotics share common chemical elements and similar structures. Some antibiotics that exert these different modes of inhibition are discussed below.

Aminoglycoside antibiotics, such as paromomycin, bind the ribosomal A site and induce miscoding by increasing the initial binding affinity of non-cognate tRNA by stabilizing helix 44 in a specific conformation.[88, 95]

A)

B)
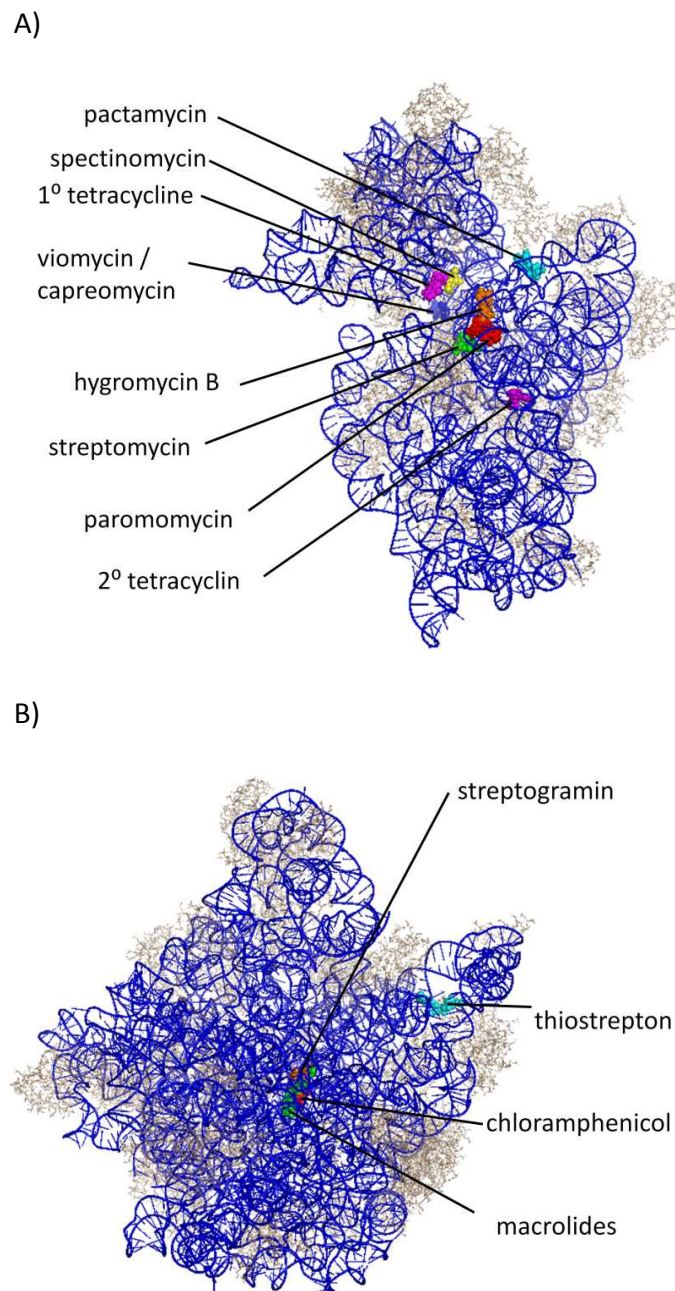
Figure 1.7: A) Structure of the 30 S ribosomal subunit shows the binding sites of current antibiotics. This figure was generated using coordinates from PDB files 1FJG, 1HNZ, 1HNW, 1HNX, and 3KNN.[94-96] B) Structure of the 50 S ribosomal subunit shows the binding sites of current antibiotics. This figure was generated using coordinates from PDB files 1N8R, 1NJI, and 3CF5.[7, 98]

Other aminoglycosides, such as kanamycin and tetracycline interact with the decoding region and block interactions of tRNA.[6, 94] Also, the aminoglycoside hygromycin B binds to helix 44 of the 30 S subunit and has been shown to inhibit the movement of tRNA to the P site by restricting a conformational change in helix 44 that is crucial for the translocation of tRNA.[94] It is worth noting that aminoglycosides are a class of antibiotics that have very similar structures; however, they are able to inhibit protein synthesis by a variety of modes described above. A more detailed description of the structure of aminoglycosides will be discussed in the next section. Antibiotics such as clindamycin, chloramphenicol, sparsomycin, and streptogramin A interfere with tRNA binding to the P site.[99-100] Also, ketolides, macrolides, and streptogramin B have been shown to bind to the peptide-exit tunnel and block the progression of the extending poplypeptide.[100-101] Inhibition of the ribosome has been a good avenue for developing antibiotics. As our understanding of the structure and function of the ribosome increases, it is expected that more potent antibiotics will be developed to counteract the resistance problem. Recent efforts to identify new potential drug target sites in the ribosome will be discussed in the next section.

1.5.1 New Potential Drug Target Sites

Clinically useful antibiotics target functionally important sites of the ribosome. In the small subunit (30 S), they interfere with tRNA binding or translocation, or displace/hinder mRNA progression during protein synthesis.[6, 94, 97] In the large subunit (50 S), most antibiotics target the peptidyl-transferase center, peptide-exit tunnel, GTPase-association center, or the

translation-factor-binding region.[99-102] The above-mentioned regions represent a very narrow section of the ribosome considering its enormous size. This fact has prompted researchers to explore and discover other sites on the ribosome that can serve as good drug targets. Advances in ribosome crystallography and NMR have aided in the identification of several potential antibiotic target sites such as helix 69 (H69) and helix 31 (h31). H69, from the large subunit of the ribosome, is located in the inter-subunit bridge B2a region and makes important contacts with the small ribosomal subunit, A- and P-site bound tRNAs, as well as translation factors. [103-104] The small subunit hairpin h31 serves as a promising drug target because it is located near the P site and is proposed to be involved in the decoding process. [105-107]

Furthermore, advances in sequencing technology allow for identification of conserved sequences that can be utilized as potential drug target sites. Despite the success of this process, conservation of a nucleotide does not always correlate with its functional importance.[108] This is one drawback of the nucleotide conservation approach to identifying new drug target sites.

Using mutational studies, Mankin and co-workers have explored the prospect of finding new potential drug target sites in the ribosome in a more random manner. Their results identified several deleterious mutations that coincide with current antibiotic target sites, as well as interesting new sites. In the 30 S subunit, Makin and co-workers identified a cluster of mutation in helices 5 and 15 that moderately inhibited translation with the exception of A55G and A373G that completely abolished translation due to interference with subunit association.[109] This section of the 30 S subunit is not part of the already identified functionally important sites; nonetheless, it is an important player in ribosome biogenesis and this makes it

a potential antibiotic target.[109] Also a cluster of moderately deleterious mutations in the middle portion of helix 24 were identified. This portion of helix 24 is important because it makes contact with protein L2 and is proposed to be part of a signal pathway linking the large and small ribosomal subunits. Similar to helices 5 and 15, deleterious mutations were identified in helices 21 and 12. Compromising of these helices may result in hindrance of 30 S assembly, because these helices make important contacts with the primary assembly proteins of the 30 S subunit. Lastly, strong deleterious mutations identified in helices 35-37, which are located on the solvent side far from all known functional sites, induced unidentified severe functional defects not related to subunit association or the translation process itself.[109] A summary of these new potential drug target sites in the 30 S subunit is shown in **Figure 1.8A**.

Similarly, other potential drug targets have been identified in the large subunit (60 S) using the same methodology.[110] These sites include H38, H32, H55, H61, H19, and H20, which were identified to contain deleterious mutations. The mutations have been proposed to result in functional defects ranging from inhibition of 50 S biogenesis, subunit association, and perturbation of ribosome structure, to inhibition of binding of elongation factors.[110] Refer to **Figure 1.8B** for the spatial location of these new potential drug target sites on the 50 S subunit.

1.6   Aminoglycoside Antibiotics

Aminoglycosides are antibiotics used to treat infections from both gram-positive and gram-negative bacteria.[111-112] The chemical structure consists of amino sugars linked to a 2-

deoxystreptamine ring. Aminoglycosides are classified into two groups, based on how the different sugar rings are linked to the central 2-deoxystreptamine ring.

A)

h44   aminoglycosides
h18   streptomycin
h34   tetracyclin
h35   spectinomycin
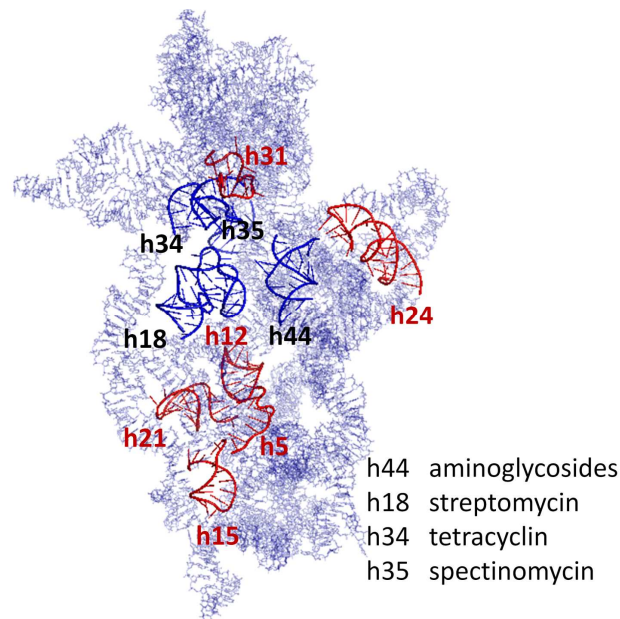
B)
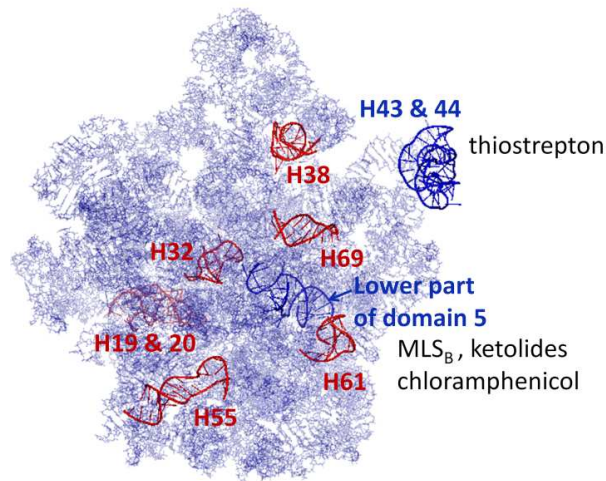
Figure 1.8: A) Structure of the 30 S subunit shows current drug target sites (blue helices) and new potential drug target sites (red helices). B) Structure of the 50 S subunit shows current drug target sites (blue helices) and new potential drug target sites (red helices). The figures were generated with PyMol software[49] using coordinates from PDB file 3I8F and 3I8G.[109-110,113]

The two classes are the 4,5-linked also known as the neomycin class, and the 4,6-linked, also

known as the kanamycin class. The conserved structural motif between these two classes is the

neamine core (**Figure 1.9**).[114]

A)

	R_1
Paromomycin	OH
Neomycin B	NH_2
Neamine	NH_2

B)

	R_1	R_2	R_3	R_4
Amikacin	OH	OH	OH	AHB
Kanamycin A	OH	OH	OH	H
Tobramycin	NH_2	H	OH	H
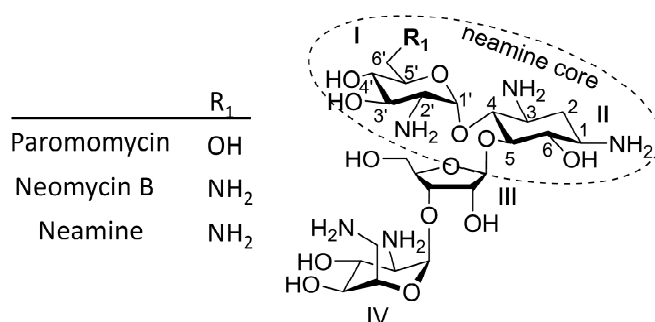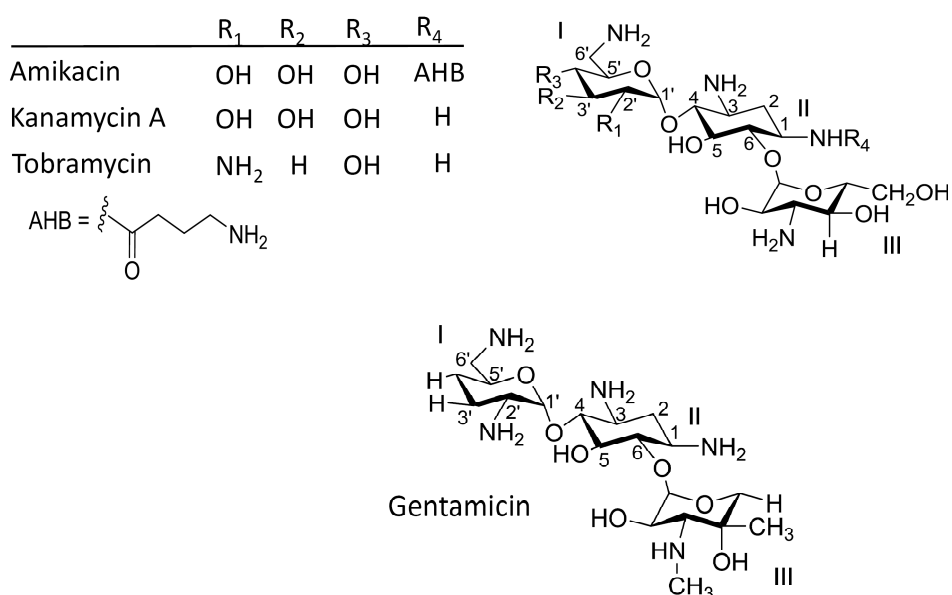
Figure 1.9: Chemical structures of A) 4, 5-linked and B) 4, 6-linked aminoglycosides are shown.

Aminoglycosides have been shown to exhibit their antibiotic activity by binding to the 16 S rRNA and inhibiting protein synthesis by a variety of modes such as inducing miscoding,[88, 95] blocking interactions with tRNA,[6, 94] and inhibiting the movement of tRNA to the P-site.[94]

Traditionally, aminoglycosides have been used to target the ribosome; however, more recent efforts have seen the use of aminoglycosides and its derivatives to target the human immunodeficiency virus (HIV).[115-117] Aminoglycosides have been shown to bind to the trans-activation responsive region (TAR) and inhibit the binding of a viral regulatory protein, known as the trans-activator of transcription (Tat).[115-117] This Tat-TAR interaction is crucial for the successful replication of HIV-1; therefore, the binding of aminoglycosides to TAR inhibits the propagation of HIV-1.[118-120]

Furthermore, premature termination codons (PTCs) have been linked to many genetic disorders. Suppression of PTCs has emerged as an attractive treatment option for a variety of genetic diseases.[121] Aminoglycosides, such as gentamicin, tobramycin, and amikacin, have been explored for the treatment of cystic fibrosis by inducing read-through of PTCs associated with this disease.[122-124] Although aminoglycosides have been used successfully to treat many diseases, there are a lot of problems associated with their usage. The major problems include toxicity, synthetic access, and bacterial resistance.

1.6.1 Problems Associated with Aminoglycoside Therapy

1.6.1.1   Toxicity

The long-term use of aminoglycosides is discouraged because of toxicity issues associated with this class of antibiotic. The primary toxicity effects that arise from aminoglycoside usage are nephrotoxicity and ototoxicity.[125-127] Nephrotoxicity arises from kidney malfunction caused by accumulation of aminoglycoside compounds in the kidney.[127] Aminoglycoside metabolites are eliminated by the kidney through a series of processes that involve the transfer of aminoglycoside metabolites through the lysosome.[127] The polycationic nature of the aminoglycosides facilitates its binding to negatively charged phospholipids in the lysosome, resulting in decreased activity of lysosomal phospholipase and eventually causes the arrest of the aminoglycoside secretion pathway.[127] This kind of aminoglycoside induced nephrotoxicity is fully reversible upon hydration treatment; however, prolonged usage of aminoglycosides may result in permanent damage to the kidney.

Unlike nephrotoxicity, ototoxicity is irreversible and it is characterized by vestibular hypofunction (disorientation or dizziness due to issues of the ear) or high-frequency hearing loss.[126] These symptoms arise from degeneration of hair cells and neurons in the cochlea, which do not regenerate once damaged. This condition is brought about by accumulation of free radicals in the ear induced by the use of aminoglycosides. The free radicals initiate the apoptotic pathway leading to degeneration of cochlear and vestibular cells.[126, 128]

Current efforts have been geared toward the development of new aminoglycosides that are less toxic. For example, Tulkens and co-workers have shown that placing a non-ionizable acyl group at the N1 position reduces the binding of aminoglycosides to phospholipids, thereby reducing the nephrotoxicity effect of these aminoglycosides.[129] Also, Mazurek and co-workers have shown that induction of heat shock protein 70 can lead to reduced ototoxicity arising from the use of gentamycin.[130] These examples show the steady progress toward developing new aminoglycosides with reduced side effects.

1.6.1.2   Synthetic Access

Total chemical synthesis of aminoglycosides is very challenging. Current synthetic methodologies require numerous steps resulting in very poor overall yields.[131-132] Another drawback is the lack of appropriate protection group chemistry that will allow for fewer steps in the synthetic pathway.[132] Researchers are now working on developing new methodologies that will allow for better yields and large quantity production. One promising method is using chemoenzymatic methods to generate large libraries of compounds.[133-134]

1.6.1.3   Bacterial Resistance to Aminoglycosides

There are three main mechanisms by which bacteria develop resistance against aminoglycosides, namely: a) aminoglycoside-binding-site modification by mutation or methylation;[135] b) reduction of intracellular concentrations of aminoglycosides by modification

of the bacterial outer membrane or by efflux;[136-137] c) modification of the amino and hydroxyl groups of the aminoglycoside by acetylation, adenylation or phophorylation.[138]

Many aminoglycoside-producing bacteria protect themselves by expressing rRNA methylases that methylate the target site of the aminoglycoside in their ribosomes. This reduces the affinity of the aminoglycoside for the ribosome target, thereby protecting the host bacterium.[139] These methylases can be transferred to other pathogenic bacteria, thereby granting them resistance to aminoglycosides.[135, 140] For example, methylation of G1405 of the 16 S rRNA confers resistance to 4,6-linked aminoglycosides.[141] A summary of resistance methlyases and the nucleotides they methylate is given in Table 1.3.

Reduction of intracellular concentrations of aminoglycosides by modification of the bacterial outer membrane or by efflux is a major contributor to some types of antibiotic resistance.[14, 142] Changes in the bacterial membrane components can occur, resulting in poor uptake or low interaction with aminoglycoside antibiotics, thereby leading to resistance.[11, 142] Also, over-expression of ATP-dependent pumps resulting from mutations in their regulatory genes can give rise to reduced accumulation of the aminoglycoside in the bacterial cell, thereby reducing the effectiveness of the drug.[11, 142]

Aminoglycoside modification is the most common type of resistance mechanism seen in aminoglycosides. Resistance occurs when the amino groups at positions 1, 3, 2' and 6' and hydroxyl groups at positions 3', 4' and 2'' are modified by aceylation, adenylation or phosphorylation thereby rendering them inert (**Figure 1.10**).[12]

There are three types of aminoglycoside modifying enzymes, nucleotidyl-transferases that are ATP dependent (ANT), phosphotransferases that are ATP or GTP dependent (APH), and acetyltransferases that are acetyl-CoA dependent (AAC).[12] The aminoglycoside-modifying enzymes are regiospecific; however, there are also bi-functional enzymes that can catalyze both 6'-acetylation and 2'-phosphorylation of its substrate.[114, 143]

Table 1.3: Summary of 16 S rRNA resistance methylases is given.

Resistance methylase	Family	Position methylated	Drug resistance conferred	Reference
RmtA	Arm	ND		
RmtB	Arm	G1405	Kan, Apr, 4,6-DOS	144
RmtD	Arm	ND		
ArmA	Arm	G1405	Kan, Apr, 4,6-DOS	13
RmtC	Arm	ND		
FmrO	Kgm	ND		
Krm	Kgm	G1405	4,6-DOS	145
KgmB	Kgm	G1405	4,6-DOS	139
NbrB	Kgm	ND		
Kmr	Kgm	ND		
GrmA	Kgm	G1405		145
Sgm	Kgm	G1405		145
Srm1	Kgm	ND		
GrmB	Kgm	ND	Kan, Gen, 4,5-DOS	
NpmA	Pam	G1408	4,5-DOS	146
KamB	Kam	G1408	4,5-DOS	147
KamA	Kam	G1408	4,5-DOS	148

ND; not determined, Kan; kanamycin, Apr; apramycin, 4,6-DOS; 4,6-disubstituted deoxystreptamine, 4,5-DOS; 4,5-disubstituded deoxystreptamine.
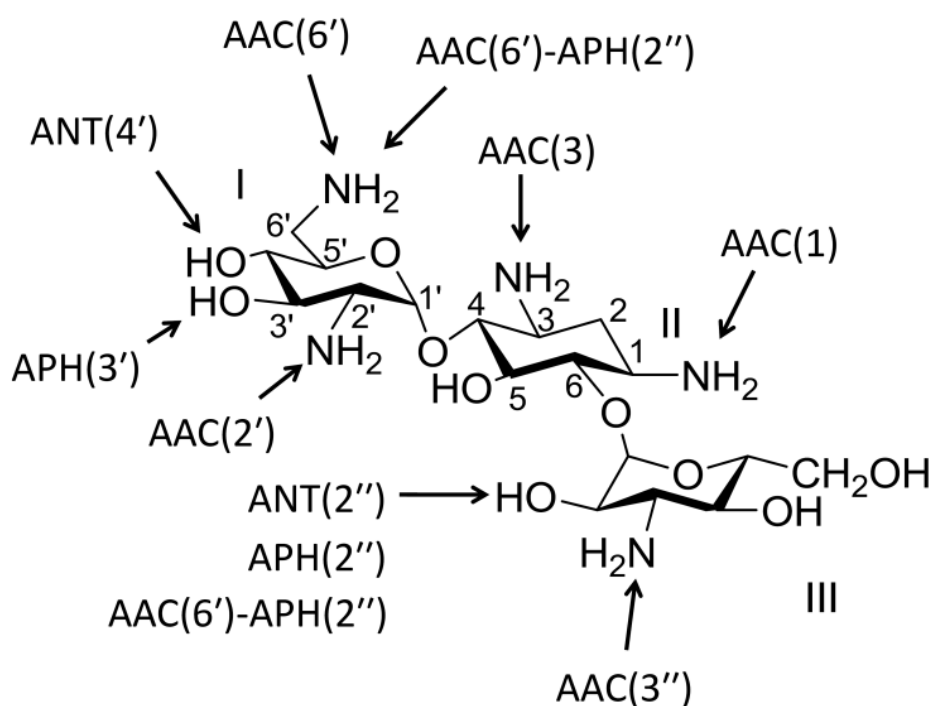
Figure 1.10: Aminoglycoside resistance enzyme modification sites on kanamycin are shown.[12]

Also, researchers have recently isolated genes from *S. marcescens and P. aeruginosa* that encode for bi-functional enzymes designated as AAC(3)-lb/AAC(6')-lb', AAC(6')-30/AAC(6')-lb', and ANT(3'')-li/ACC(6')-lld.[149-152] The success of aminoglycosides has been compromised because of the spread of the resistance enzymes. Hence, current research efforts have been geared toward designing new aminoglycoside analogues that can evade these resistance mechanisms.

1.7   Tools for Exploring RNA-Ligand Interactions

A variety of techniques are used as tools for screening RNA-binding ligands. Among them are biophysical methods such as NMR, SPR, ITC, ESI-MS, fluorescence assays, and biochemical methods such as RNase and chemical footprinting. A general overview of these techniques is provided below.

Nuclear magnetic resonance (NMR) is a desirable technique because it can be used to determine the binding site and capture conformational changes that occur upon ligand binding to the RNA target.[153-154] By monitoring imino proton shifts, standard 1D NMR experiments can be used to detect binding of ligands to RNA.[155] The drawback of using NMR is that a large amount of RNA is required to conduct experiments, and isotope labeling of the RNA or ligand may be necessary in some experiments.

Surface plasmon resonance (SPR) employs the use of immobilized RNA on a metal surface (chip), over which the dissolved ligand is continuously flowed. Binding is detected by changes in the angle of refraction of incident light focused on the chip.[156] Binding parameters such as dissociation constants and on and off rates can be determined with this technique.[156-157] Even though low concentrations of RNA and ligand are required, SPR is not widely used because of its high cost and low throughput nature.[158]

Isothermal titration calorimetry (ITC) is the gold standard for obtaining dissociation constants and thermodynamic parameters for RNA-ligand binding.[158] It operates by measuring the heat change upon ligand binding in a closed system.[159] Although it is a desirable method, its

use is limited because it requires a large amount of RNA to conduct a single experiment, it is low throughput, and it cannot be applied to ligands with poor solubility in aqueous solutions.[158]

Many techniques available today employ the use of fluorescence to monitor RNA-ligand binding. For example there are methods that employ fluorescently end-labeled RNA or ligands. Binding of the ligand to the RNA results in conformational changes that affect the fluorescence of the fluorophore, thereby providing a readout for the binding event.[160] This technique has been used extensively in characterizing the binding of aminoglycosides to RNA.[160-161] The drawback with this technique is that the fluorescence change depends on how far the fluorophore is from the binding site, and therefore cannot be applied to larger RNA constructs.[158] Assays that require fluorescently labeled ligands cannot be used for ligand discovery because it requires a known ligand that can be fluorescently labeled. Other methods employ the use of 2-aminopurine as a site-specific probe to monitor ligand binding events.[162-163] Usually an adenine which is at, or close to, the ligand binding site is replaced with 2-aminopurine, which acts as a fluorescent reporter.[162-164] The disadvantage with this technique is that the incorporated 2-aminopurine has to be close to the binding site and the presence of the 2-aminopurine may cause structural changes that may affect ligand binding.[165] Fluorescent indicator displacement is another technique which can be used to assess RNA-ligand interactions.[166-167] This technique, as well as ESI-MS, were utilized as screening tools in this thesis work, and will be discussed in more detail in the next chapter.

Biochemical methods such as RNase and chemical footprinting are very popular techniques used to validate ligand binding sites and obtain dissociation constants.[168] These

assays utilize end-labeled RNA (usually radio-labeled). The labeled RNA is incubated with varying concentrations of ligand. After binding equilibrium is reached, the RNA is degraded with RNases or chemical reagents.[168] The binding site of the ligand can be identified by protection from degradation, and binding constants can be determined by quantifying the protected bands as a function of ligand concentration.[169] These biochemical methods will also be discussed in the next chapter.

1.7 Thesis Overview

The clinical usefulness of aminoglycosides has been compromised due to widespread resistance to this class of antibiotics. The long-term goal of this project is to develop new aminoglycoside antibiotics that target the A site (or other regions) of the bacterial ribosome. The strategy is to simplify the aminoglycosides by generating derivatives of the neamine core in order to maintain the minimal motif for binding, but avoid enzymatic modification.To achieve this goal, a series of compounds were synthesized by our collaborators and screened for their affinity to a model A-site RNA in our laboratory. The binding site and mode of action of the top candidates were characterized by using biochemical methods and enzymatic footprinting (Chapter 3). The binding sites of the ligands were compared to that of the parent compounds in order to gain insights to why the ligands had good or poor antibacterial activity. This information will also be helpful in designing the next generation of ligands.

In the second part of the thesis work, a new high-throughput fluorescent intercalator displacement assay was developed to aid in rapid screening of ligand libraries for RNA binding.

The assay employed dye molecules as the fluorescent indicators. Furthermore, electrospray ionization mass spectrometry (ESI-MS) was used to investigate the mechanism of the assay. The assay was optimized for screening a variety of RNA-binding ligands with a set of small hairpin RNAs (A site, TAR, h31, and H69) (Chapter 4).

The specificity of the top candidates and the parent compounds were tested against a variety of RNA models using ESI-MS (Chapter 5). The aim was to identify ligands that prefer certain RNA structural motifs (duplex, hairpin loop, or internal bulge), and also identify the ligands that had significant preference for the human A-site RNA. This information will help us to design the next generation of ligands to be more specific and less toxic.

Modified nucleotides have been well characterized for the roles that they play in antibiotic sensitivity and resistance; however, the role that modified nucleotides play in antibiotic binding is not well understood. In Chapter 6, the role that modified nucleotides play in the binding of a variety of antibiotics was investigated.

An overview of the various biophysical and biochemical techniques that were used to achieve our goals is given in the next chapter.

CHAPTER 2

BIOPHYSICAL AND BIOCHEMICAL METHODS

A variety of techniques were utilized in this thesis work to investigate RNA-ligand interactions. This section will focus on providing a general background and introduction to these techniques. Detailed experimental will be provided in the chapters that utilize these techniques.

2.1   Mass Spectrometry Applied to Macromolecular Analysis

2.1.1 General Set-up of a Mass Spectrometer

The process of mass spectrometry analysis involves the formation of analyte ions in the gaseous phase, followed by sorting and selection of wanted masses and finally detection of ions by their mass-to-charge ratios (m/z). To achieve this, the mass spectrometer uses several functional units, which consist of three main parts: the ion source, mass analyzer, and detector (**Figure 2.1**).[170]

Depending on the ionization process, the analyte may already exist as ions in solution or may be ionized during the volitisation process in the ion source. The ions are deflected by an electric or magnetic field in the mass analyzer (maintained at vacuum pressure), thereby sorting the ions according to their m/z values.[170] The detector then converts the detected ions into a proportional electric current, followed by generation of a spectrum, in which the electric current is recorded as a function of m/z.[170]
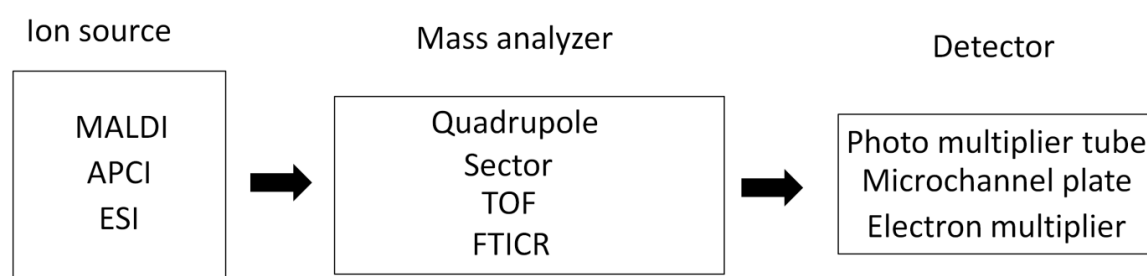
Figure 2.1: The general set-up of a mass spectrometer for molecular analysis is outlined.

2.1.1.1 Ion Source

There are different techniques used to transfer the analyte into the gas phase (**Figure 2.1**). For elemental analysis, very harsh techniques such as inductively coupled plasma (ICP) are used to fragment and ionize the sample.[171] On the other hand, softer ionization techniques are used for macromolecular analysis. Matrix assisted laser desorption ionization (MALDI) is considered to be a soft ionization process, in which the analyte is co-crystallized with a solid matrix (for example 3-hydroxypicolinic acid) that can absorb light energy emitted from a laser.[172] Upon irradiation, the analyte is ionized by the energy transferred from the matrix.[172-173] The precise mechanism by which ionization occurs in MALDI is still unknown.[172] One advantage of MALDI is that usually only singly charged ions are produced, and therefore MALDI can be used to provide molecular weight information for more than one analyte without complicated analyses.[174]

Atmospheric pressure chemical ionization (APCI) is another soft ionization process that can be used to ionize weakly polar analytes and samples that do not exist as pre-formed ions in solutions.[170] Reagent and solvent molecules are ionized at atmospheric pressure by electrons

from a fine needle maintained at a high voltage (~ 1-5 kV). Chemical reactions occur between the thermally vaporized analyte and the ionized solvent or reagents, which lead to the ionization of the sample.[170] APCI has the advantage of having a reduced salt susceptibility as compared to ESI, and therefore APCI is usually used to complement ESI.[175] The mechanism of ESI will be discussed in detail in the next section.

2.1.1.2   Mass Analyzer

After ionization, the analyte is transferred to the mass analyzer where a specific mass range can be focused onto the detector. The quadrupole mass analyzer consists of four cylindrical rods with radio frequency and DC current flowing through them. By tuning the radio frequency and DC current, only ions of a certain mass range maintain a stable trajectory through the quadrupole, whereas other mass ranges are deflected and prevented from reaching the detector.[176] Compared to all of the available contemporary mass analyzers, the resolution of the quadrupole is very low and also has a limited mass range (usually < 4000 m/z). In spite of its limitations, the quadrupole mass analyzer is widely used because of its relatively low cost, low voltage requirement and small physical size.[176]

Sector mass analyzers utilize magnetic sectors that bend the trajectories of ions into circular paths.[177] The radii of the paths depend on the mass-to-charge ratio of the ions. This allows only ions with certain m/z values to pass through a slit and reach the detector.[175, 178] These analyzers have very high mass accuracy and resolution; however, magnetic sectors are not widely used because of their high cost and enormous size.[175]

A time-of-flight (TOF) mass analyzer sorts ions by applying a fixed potential to a pulse of ions generated from the ion source.[170] The potential imparts kinetic energy to the ions and accelerates them through a drift region with a set distance. Since the potential energy delivered is constant, ions with a smaller size obtain greater kinetic energy and therefore travel through the drift tube faster.[170] The m/z of the ions is determined by measuring the time it takes for the ions to reach the detector. Usually TOF analyzers are operated with reflectrons. These are electrostatic mirrors that send the ions along a second flight distance toward the detector. The use of the reflectron helps to compensate for any discrepancies in velocities of ions with the same m/z arising from the ionization process.[175] TOF mass analyzers can achieve higher resolutions as compared to the quadrupole, and can also achieve mass accuracy up to 50 ppm.[179]

Fourier transform ion cyclotron resonance (FTICR) mass analyzers employ the use of a magnetic field.[175] Analyte ions are transferred into the magnetic field with a low velocity, and hence they become trapped in the magnetic field instead of deflected as in the case of sector analyzers. The trapped ions are excited by an electric field held perpendicular to the magnetic field causing the ions to oscillate with covalent orbital (cyclotron) frequencies inversely proportional to their m/z values. The oscillating frequencies of the ions are converted to m/z readings using a Fourier transform.[175] FTICR is the most powerful instrument available for accurate mass determination; its resolution power is in the high parts per billion.[175]

2.1.2 Application of ESI-MS to Nucleic Acids

Electrospray ionization (ESI) is the method of choice commonly used for the ionization of biological molecules such as nucleic acids, peptides, and proteins. This is because it is a soft ionization process that allows for analyte detection with minimal fragmentation.[180] ESI-MS was first applied to the detection of non-covalent interactions in 1991.[180] Since then, ESI-MS has been extended to the study of non-covalent interactions between nucleic acids and ligands as a screening tool for drug discovery.[181-182] ESI-MS allows for examination of multiple-stoichiometry complexes, even at very low abundance. [183]

2.1.2.1   Mechanism of Electrospray Ionization

In ESI, ions are generated by passing the analyte through a small heated capillary maintained at high voltage (~4.5 kV). A continuous flow of an inert gas such as nitrogen is used to facilitate nebulization of the sample, allowing it to emerge from the tip of the capillary in an aerosol of charged droplets (**Figure 2.2**).[182] The polarity of the droplets depends on the sign of the applied voltage. For nucleic acids, the negative ion mode is used, such that positive charges are removed from the capillary wall and negative charges are drawn toward the liquid front as the analyte emerges from the capillary.[182] Following nebulization, the solvent around the charged droplets evaporates as they travel to the mass analyzer, which reduces the size of the droplets to a point where Coulomb repulsion forces between the charged droplets are very high, causing them to break into even smaller droplets. This process continues to a point where

single ions are isolated, surrounded by residual counter ions such as Na$^+$. The analyte ions are then passed through a skimmer and toward the mass analyzer (**Figure 2.2**).
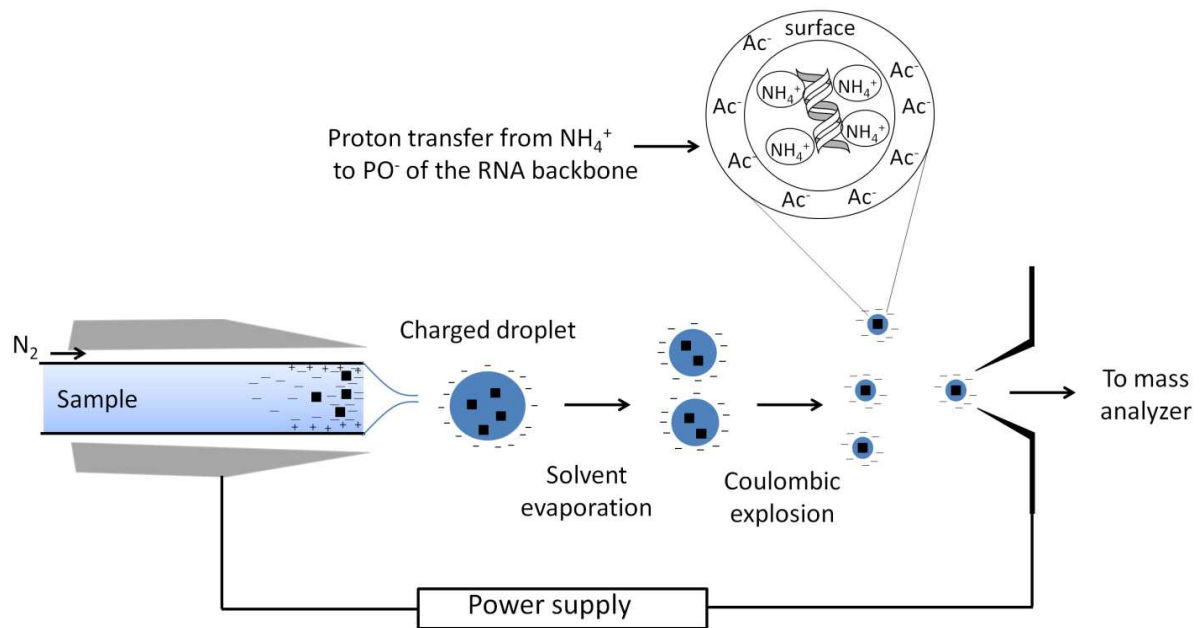
Figure 2.2 A schematic diagram of the electrospray ionization process is shown.

ESI-MS has a low salt tolerance; therefore, even minute amounts of sodium or potassium ions will condense on nucleic acids during droplet formation, resulting in detection of a wide distribution of salt adducts, which drastically reduces the resolution and complicates data analysis.[182] To solve this problem, ammonium acetate is usually used as the buffer. In the negative ion mode, droplets of negatively charged RNA polyanions can be neutralized by proton transfer from NH$_4^+$ to PO$^-$ of the RNA backbone. Using a solution with 150 mM ammonium acetate usually results in a small fraction of phosphates that remain negatively charged (on

average, 5 out of 22 in a 12-mer duplex DNA).[182] When analyzing nucleic acids with ESI-MS, a volatile solvent such as isopropyl alcohol (IPA) or methanol is usually added to the sample prior to injection. Presence of the alcohol decreases the surface tension of the droplets and favors droplet formation. It also gives a significant signal enhancement (**Figure 2.3**) and helps minimize the risk of analyte conformational changes in solution.[182]
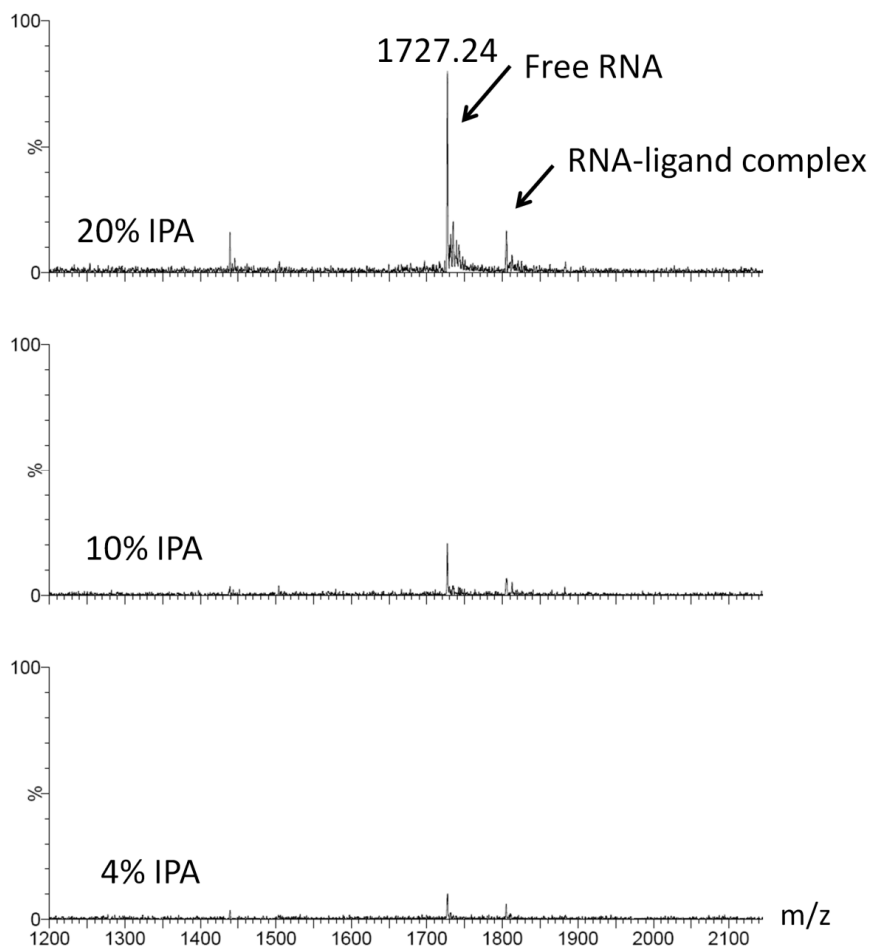
Figure 2.3: ESI-MS spectra show signal enhancement upon increasing concentrations of isopropyl alcohol (IPA) with a representative RNA molecule and RNA-binding ligand.

2.1.2.2   Determination of Equilibrium Binding Constants

ESI-MS can be used for quantitative measurements. The position of the peaks in a mass spectrum allows for the determination of stoichiometries of complexes that are present in the sample. By monitoring the relative intensities of sample peaks, ESI-MS can be used to perform binding assays to determine equilibrium dissociation constants, and can also be used to perform competition assays provided that the ligands being used do not have overlapping m/z signals.

2.1.2.3   Binding Assays

One method for determining equilibrium binding constants is to perform a binding assay to obtain seven or more data points to generate a binding curve. Generally, different concentrations of ligand ranging from low to high depending on the estimated K_d of the ligand are allowed to equilibrate with a constant concentration of RNA (~ 1 µM) in 150 mM ammonium acetate. Right before injection, 50% IPA is added to the sample and the sample is infused into the instrument. Sixty scans per sample are taken and averaged.

2.1.2.4   Obtaining Binding a Curve

Each spectrum is smoothed, integrated, and the area under each peak is calculated using Masslynx (Micromass Ltd. Manchester, UK). A plot of ligand concentration vs fraction of ligand bound is generated. The faction of ligand bound (Fr) is calculated using the equation; Fr =

RL / R + RL, in which RL is the peak area of RNA-ligand complex, and R is the peak area of free RNA.

The peak areas of the different species are proportion to their concentrations in solution.[184]

2.1.2.5   Curve Fitting

One advantage of ESI-MS is that the stoichiometry of the non-covalent complex of interest can be determined directly by the location of the peaks on the mass spectrum. With the stoichiometry already known, the curve can be fitted to the appropriate binding model. For a 1-to-1 binding assay expressed in the form RL $\rightleftharpoons$ R + L, a quadratic equation is derived as follows to fit the data:

The dissociation constant, K_d, can be expressed as:

$$K_d = \frac{R*L}{RL}$$

in which R is the concentration of free RNA, L is the concentration of ligand, and RL is the concentration of RNA-ligand complex.

But,

$$R_f = R_t - RL$$
$$L_f = L_t - RL$$

In which R_f is the concentration of free RNA, Lf is the concentration of free ligand, R_t is the concentration of total RNA, and L_t is the concentration of total ligand.

Therefore,

$$K_d \;=\; \frac{(R_t - RL)\,(L_t - RL)}{RL}$$

Both sides are multiplied by RL to give:

$$K_d * RL \;=\; (R_t - RL)\,(L_t - RL)$$

The equation is expanded to give:

$$K_d * RL \;=\; (R_t * L_t) - (R_t * RL) - (RL * L_t) + RL^2$$

$$0 = (R_t * L_t) - (R_t * RL) - (RL * L_t) - K_d * RL + RL^2$$

After rearrangement,

$$0 = 1\,RL^2 - (R_t - L_t - K_d)\,RL + (R_t * L_t)$$

$$0 = ax^2 + bx + c$$

and solving for x,

$$x = \frac{- b - \mathrm{sqrt}\,(b^2 + 4ac)}{2}$$

Hence,

$$RL = \frac{-\,(R_t - L_t - K_d) - \mathrm{sqrt}\,[(R_t - L_t - K_d)^2 + 4(R_t * L_t)]}{2} \qquad \text{Equation 1}$$

Equation 1 is used to fit binding curves describing a 1:1 binding model.[184]

2.2 Fluorescence Spectroscopy

Fluorescence is a phenomenon that describes the light energy emitted by a molecule that falls from an excited singlet state to various vibrational levels of the electronic ground state.[185] The fluorescence intensity of a molecule at a given wavelength carries information about the physical and chemical nature of the molecule's microsurroundings. Fluorescence emission is one of several processes by which an excited molecule can release energy. Others include non-radiative processes such as internal conversion, vibrational relaxation, intersystem crossing and longer-lifetime relaxation from the triplet state to the ground state known as phosphorescence (**Figure 2.4**).[186] Other relaxation processes include collisional quenching, solvent relaxation, energy transfer, and photochemical reactions.[186] The fluorescence intensity and quantum yield (the fraction of excited molecules that undergo fluorescence) can be influenced by any interactions of the fluorescing molecule which can favor the other competing relaxation processes or can introduce a new relaxation pathway. Therefore, careful characterization of the experimental system is necessary in order to ensure accurate interpretations of the data acquired. The basic set-up of instrumentation for fluorescence detection is shown in **Figure 2.5**. Fluorescence spectroscopy can be applied to a wide range of problems in biology and biochemistry. Fluorescence measurements can provide information about molecular processes including binding interactions,[187] conformational changes,[188] and distances between two sites on a biomolecule.[189] More advanced fluorescence techniques can achieve very high resolutions, even up to single molecule detection.[190-191]
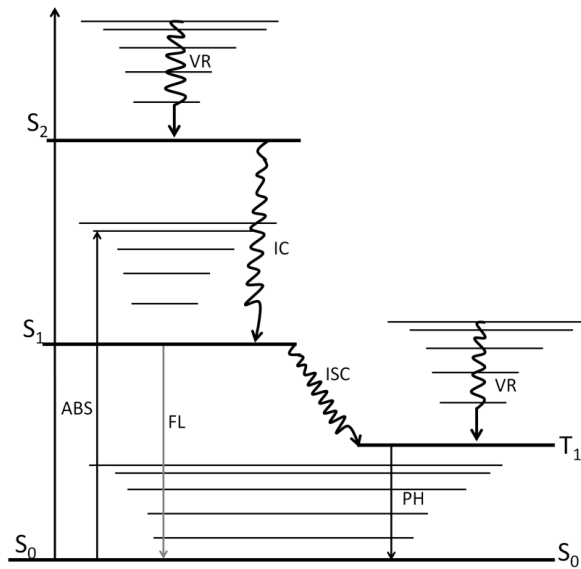
Figure 2.4: A Jablonski diagram shows the different relaxation processes that an excited molecule can undertake after absorption (ABS) of energy. The relaxation processes include fluorescence (FL), phosphorescence (PH), vibrational relaxation (VR), internal conversion (IC), and intersystem crossing (ISC). The single and triplet states are designate as S_0-S_2 and T_1 respectively.
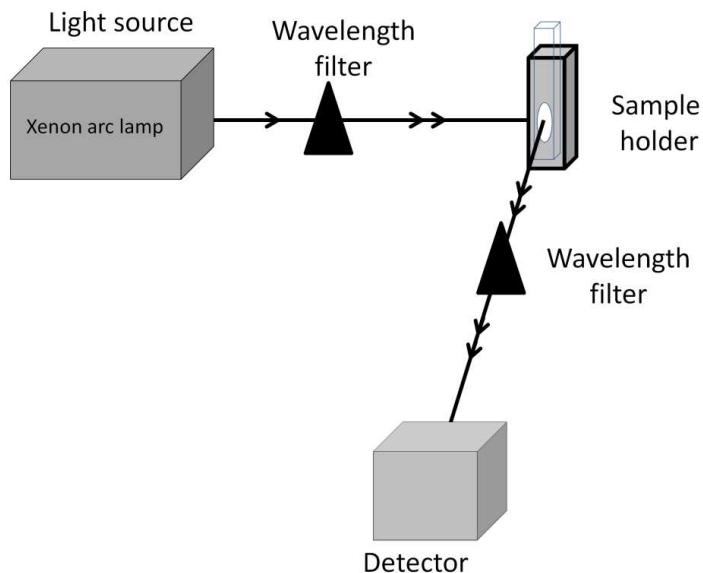
Figure 2.5: Basic instrumentation for fluorescence detection is represented.

2.2.1 Fluorophores

Fluorophores or fluorescent dyes are molecules that can absorb light at a specific wavelength and emit light at a longer wavelength upon relaxation.[185] The chemical structure of fluorescent dyes usually consists of conjugated functional groups or aromatic rings (**Figure 2.6**). The delocalized electrons in such structures absorb energy and stabilize the molecule in the excited state.[185] Fluorophores can absorb and emit light over and over again; however, in some instances the structure of the fluorophore can be damaged and it will not be able to fluoresce any longer.[185] This process is known as photobleaching, and it is important to check for photobleaching when performing fluorescence experiments. The planar structure of most fluorophores makes them very good intercalating agents, and they are therefore widely used as nucleic-acid- staining agents.
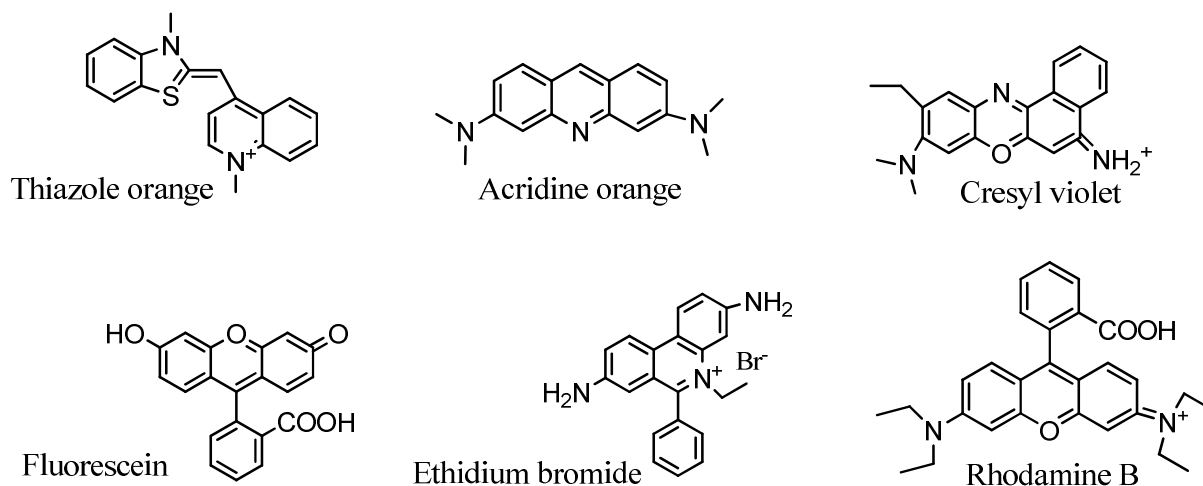
Figure 2.6: The chemical structures of some common fluorophores are shown.

2.2.1 Fluorescence Intercalator Displacement

Fluorescent intercalator displacement assay is based on the theory that a fluorescent probe bound to RNA is displaced by a ligand, leading to reduction in fluoresce intensity. The extent of decrease in fluoresce is proportional to the affinity of the ligand for the RNA (**Figure 2.7**). The structure of B DNA provides a wide and deep major groove that allows for intercalation of dyes.[158] Unlike DNA, RNA has a narrow and deep "major groove" that is not conducive for intercalation. Therefore, a number of dyes that readily intercalate into DNA do not bind to RNA.[158] In spite of this drawback, unpaired or mismatched bases in RNA provide binding pockets for small molecules and fluorephores.[158] In this thesis work, an assay based on DNA fluorescent intercalator displacement was developed to assess and rank the binding affinity of ligands to RNA.
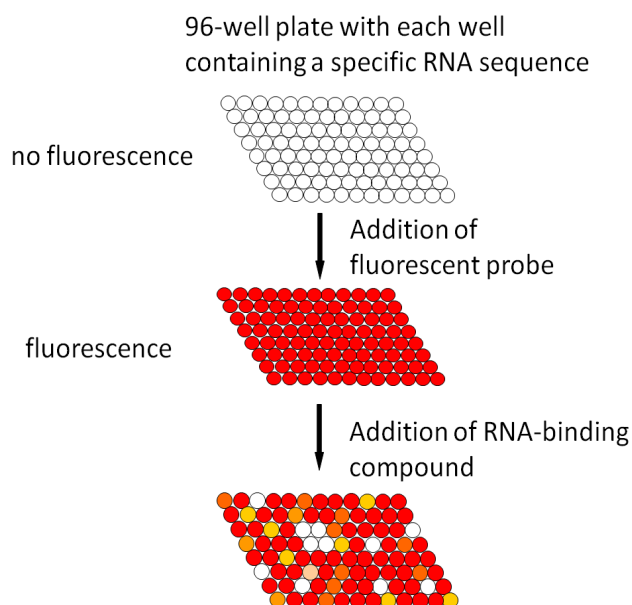
Figure 2.7: The FID assay is summarized. The degree of reduction in fluorescence intensity correlates to the affinity of the compound for the RNA.

2.2.1.1 General Procedure for RNA FID Using TO-PRO

The generalized instrumentation set-up for the experiment is shown in **Figure 2.5**. A range of dyes may be appropriate, but the discussion will be limited to a single dye. 3-Methyl-2-((1-(3-(trimethylammonio)propyl)-4-quinolinylidene)methyl)benzothiazolium (TO-PRO) has essentially no fluorescence when free in solution, but exhibits a 400-fold increase in fluorescence when bound to RNA such as the A site (**Figure 2.8**). Initially, the optimal excitation and emission wavelengths of the dye are determined by generating an absorption and emission profile. For example, the excitation and emission wavelengths of TO-PRO were determined to be 512 nm and 533 nm, respectively, at room temperature in 100 mM KCl and 20 mM Tris-Cl pH 7 (**Figure 2.9**). Next, the dye is titrated into a constant concentration of RNA to determine the appropriate concentration of dye needed to provide the highest fluorescence signal. At this concentration of dye, it is assumed that all of the binding sites of the RNA are occupied by dye molecules. This dye:RNA ratio is then used for the screening experiments. For this study, all fluorescence readings were taken on a Cary Eclipse Spectrophotometer (Varian Inc., Walnut Creek, CA). Typically, 2 μM of RNA is incubated with 2 μM of TO-PRO in 100 mM KCl and 20 mM Tris-Cl, pH 7, for 5 minutes. The initial fluorescence reading is taken and the appropriate concentration of drug is then added, mixed thoroughly, and allowed to equilibrate for another 5 minutes. Five scans per sample are taken with an excitation wavelength of 512 nm (5 nm slit width). The level of fluorescence change (either enhancement or quenching) is determined and converted to a percent change in fluorescence using the formula $(F_1/F_0)*100$, in which F_0 is the

initial fluorescence of dye bound to RNA before the addition of drug and F_1 is the fluorescence

after addition of drug.
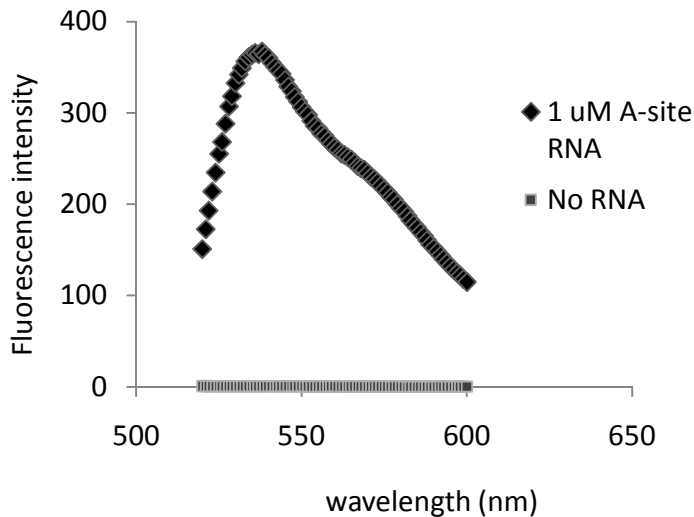
Figure 2.8: Fluorescence enhancement of the TO-PRO dye after association with 1 µM A-site RNA is shown. In this case, excitation occurred at 510 nm and emission was monitored between 520 and 600 nm.
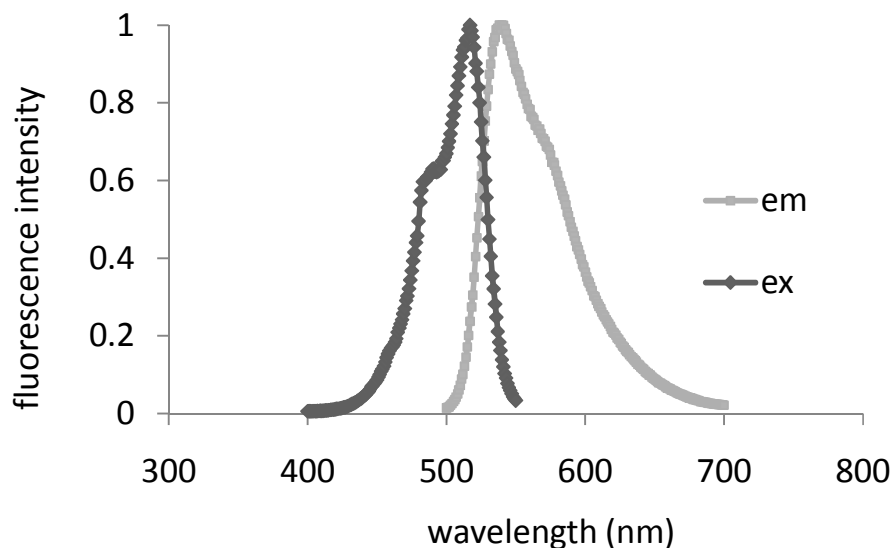
Figure 2.9: An overlay of the excitation and emission profiles of TO-PRO is shown.

2.3   RNA Probing

A wide variety of chemical probes are available for obtaining distinct information about RNA structure. Among them are base-specific reagents that carry out methylations or alkylations with one or more of the four RNA bases. They provide structural information about hydrogen bonding, base stacking, and electrostatic environments close to the position of modification on the base.[192] Examples of these chemical probes include dimethyl sulfate (DMS), which modifies N7 of guanine, N1 of adenine and N3 of cytosine,[193] diethylpyrocarbonate (DEPC), which modifies N7 of adenine,[193] and hydrazine, which modifies uracils and preferentially modifies cytosine at high salt concentrations.[192-195] Furthermore, sequence and base-specific restriction enzymes such as RNase A, RNase T1, and RNase V1, just to mention a few, can be used as footprinting probes to determine the binding sites of small molecules on RNA. Brunel and Romby provide a good review of chemical and enzymatic probes that are employed in RNA sequencing and footprinting applications.[192]

RNA probing with chemical reagents and enzymes is performed in such a way that only a limited amount of the RNA is modified. The modifications can result in either RNA cleavage that can be detected by polyacrylamide gel analysis of end-labeled RNA or covalent modification of the RNA that can be detected as primer extension stops by reverse transcriptase.[196] By utilizing these techniques, one can gain more understanding about the binding sites and modes of action of different compounds such as antibiotics.[197] The next section provides a discussion of the mechanisms of the chemical probes used in this thesis work.

2.3.3 DMS Reaction

The N7 cyclic amine of guanosine in a single- or double stranded A-form RNA is usually accessible for methylation by DMS unless it is involved in tertiary interactions or non Watson-Crick base pairing.[198] Addition of a methyl group on the N7 position by DMS generates a positive charge that weakens the 7,8-double bond, which can easily be reduced by sodium borohydride (**Figure 2.10**).[198] The resulting methylated dihydroguanosine hydrolyzes, and provides a site for aniline to react.[198]
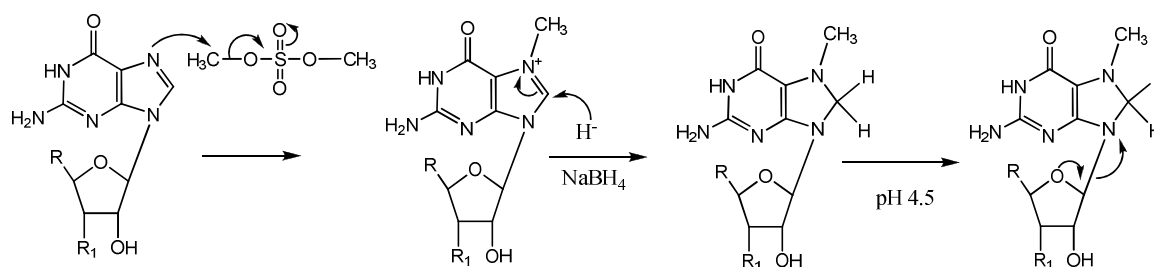
Figure 2.10: The mechanism of DMS reaction is shown. Refer to the text for the description of the reaction process.

2.3.2 Aniline Reaction

Reaction with DMS leads to hydrolysis of the glycosidic bond between the base and ribose, which leads to formation of a ribose tautomer.[198] Formation of the open ring tautomer can be encouraged by maintaining the reaction at 60 °C.[192] The aldehyde group of the tautomer reacts with aniline and the 3'-phosphodiester bond is cleaved by β-elimination (**Figure 2.11**).[193]
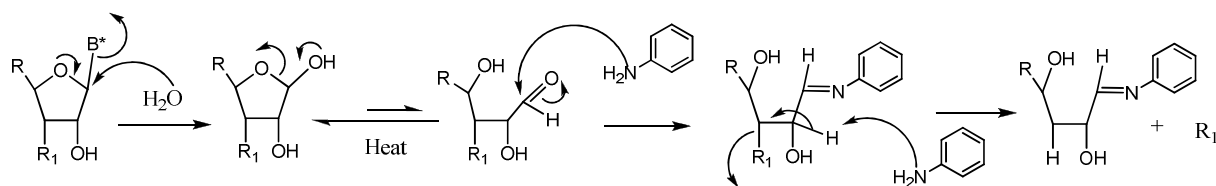
Figure 2.11: The mechanism of aniline reaction is shown. Refer to the text for the description of the reaction process.

2.3.3 DEPC Reaction

Diethylpyrocarbonate modifies the N7 position of adenosine. Carbethoxylation of N7 of adeninosine destroys the resonance of the heterocyclic ring, leading to ring opening between N7 and N8, thereby creating a site for strand scission by aniline (**Figure 2.12**).[198-199] The reaction with aniline proceeds as described in Section 2.3.2.
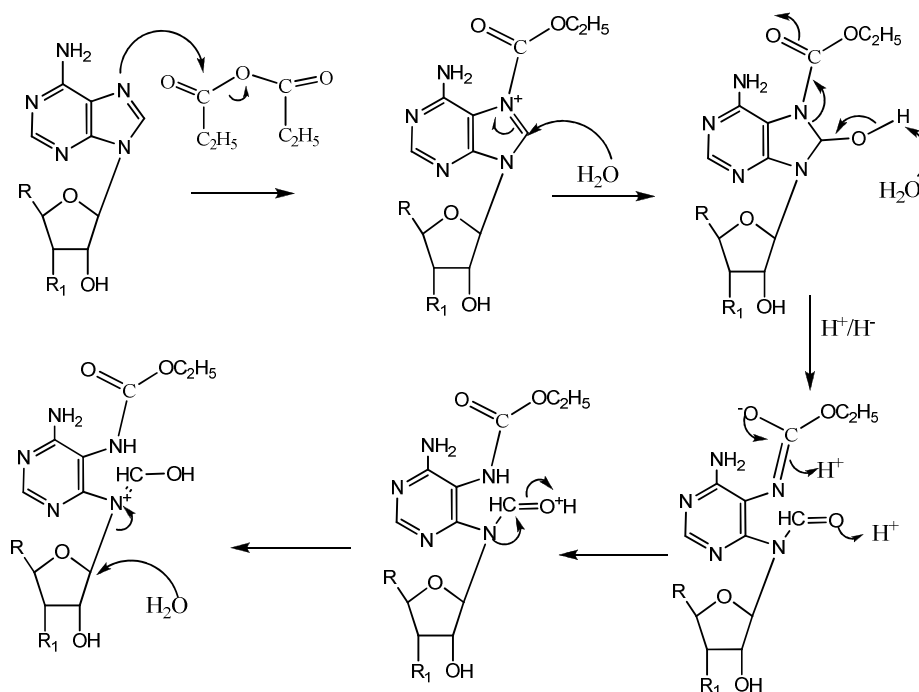
Figure 2.12: The mechanism of DEPC reaction is shown. Refer to the text for the description of the reaction process.

2.3.4 Hydrazine Reaction

Hydrazine attacks uridine at C-4 and C-6, opens the pyrimidine ring and forms a new 5-membered ring. Further reaction leads to release of the pyrazolone ring, leaving a hydrazone product exposed for aniline attack (**Figure 2.13**).[194, 200] The reaction with aniline proceeds as described in section 2.3.2.
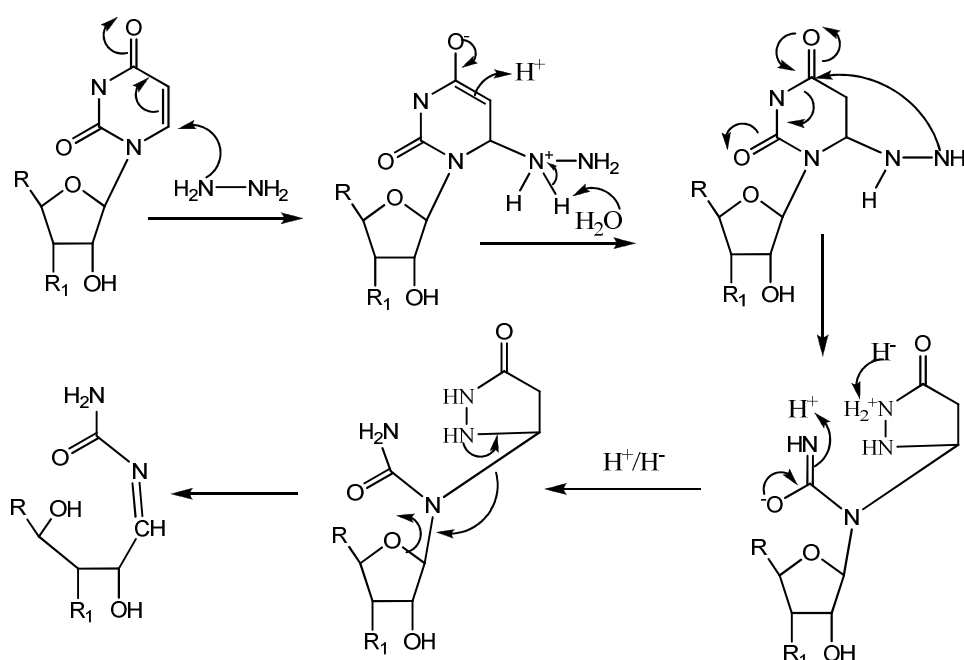
Figure 2.13: The mechanism of hydrazine reaction is shown. Refer to the text for the description of the reaction process.

The chemical probes discussed above were used to gain some insights to the binding sites and mode action of the single-ring neamine analogues designed in this thesis work. A detail experimental will be provided in the chapters in which these chemical probes are utilized. The next chapter addresses the first objective of the project, characterizing the binding of single-ring aminoglycoside analogues to the A site.

CHAPTER 3

SMALL MOLECULES TARGETING THE RIBOSOMAL AMINOACYLTRANSFER SITE*

3.1 Abstract

The structure of the aminoglycoside neamine was used as the basis for design of new small molecules targeting the amino-acyltransfer site (A site) of the bacterial 16 S ribosomal RNA. A series of molecules of such design was tested for binding to a model RNA representing the A site. Several of the synthetic analogues with low molecular weights were found to bind to the RNA with affinities comparable to the parental aminoglycoside neamine, with apparent dissociation constants in the low micromolar range. Footprinting experiments revealed that one of the compounds (DHR23) has a similar binding site as the antibiotic paromomycin. DMS chemical probing also revealed that the binding of DHR23 to the A site leads to the stabilization of the stacked in conformation of A1492 and A1493. The use of these minimal single-ring motifs for further design and modulation of RNA-binding activity could prove fruitful for generation of new antibiotics that would survive the action of the existing antibiotic-resistance mechanisms.

3.2 Introduction

Aminoglycosides are antibiotics that bind to the A site of the ribosome and inhibit proteins synthesis.[202-204] The chemical structures of aminoglycosides consist of amino sugars linked to a 2-deoxystreptamine ring (ring II). There are two classes of aminoglycosides, the 4,5-linked (such as neomycin) and the 4,6-linked (such as kanamycin), in which the conserved structural component between them is the neamine core, containing rings I and II (**Figure 3.1**).[114] Although aminoglycosides are effective antibiotics, their use has been compromised because of wide-spread resistance to this class of antibiotics.[114] Resistance to aminoglycosides can occur in a variety of ways; however, the most common type is enzymatic modification of their hydroxyl and amino groups, which affects the ability of the compounds to bind to the target RNA.[114, 205] The mechanism of action and resistance to aminoglycosides antibiotics were discussed in Chapter 1.

Data from X-ray crystal and NMR structures have revealed specific interactions between aminoglycosides and the A site of the decoding region of 16 S rRNA (**Figure 3.2**).[6, 95, 206-209] Due to extensive contacts with the A site, rings I and II appeared to contain the minimal structural components for specific binding of both classes of aminoglycosides. Recent strategies to overcome resistance include simplifying the structures of aminoglycosides by generating derivatives of the neamine core[210-216] in order to maintain the minimal motif for ribosome binding, but avoid enzymatic modification. For example, semi-synthetic aminoglycoside derivatives such as amikacin contain a γ-amino-α-hydroxybutyryl group at N1 position (**Figure**

3.1).[217-218] This modification makes amikacin less susceptible to certain resistance enzymes, compared to other aminoglycosides.[219-220] Other studies identified a series of neamine core analogues that had comparable or better antimicrobial activities and binding affinities than the clinically used aminoglycosides (**Figure 3.1**).[212-213] Also, the potential efficacy of some neamine derivatives are increased by attachment of different lengths of polyamine groups at the O6 position of ring II. This is because the presence of the polyamine group enhances interactions with the phosphate backbone of RNA.[212-213]
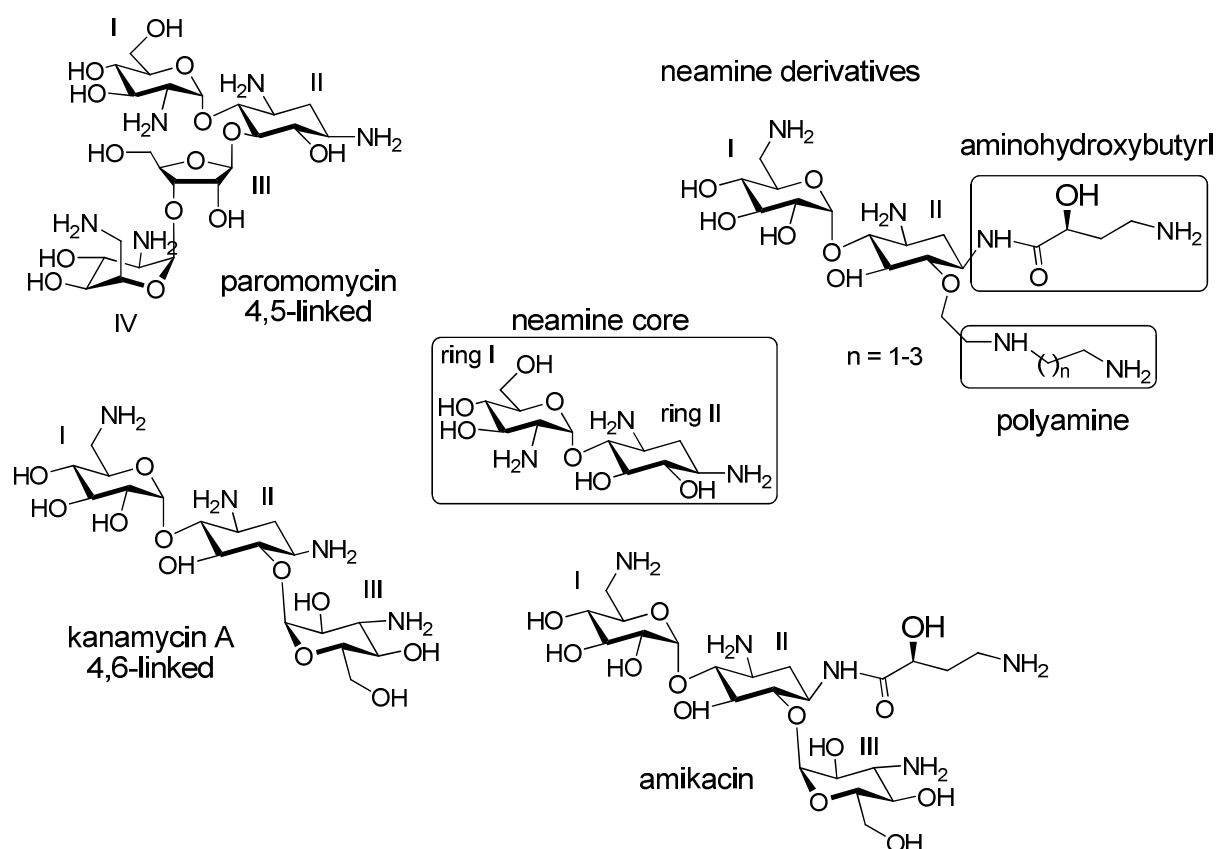
Figure 3.1: The chemical structures of paromomycin (4,5-linked), kanamycin (4,6-linked), amikacin, neamine derivatives, and neamine core are shown.
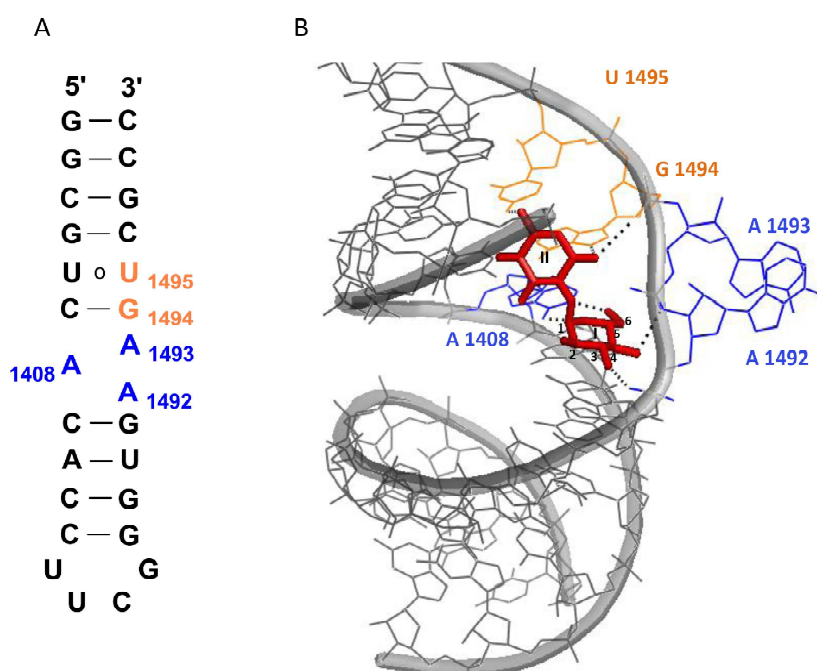
Figure 3.2: A model representing the decoding region A-site RNA is shown. The RNA is numbered based on *E. coli* 16S rRNA. B) Structure shows rings I and II from kanamycin complexed with a model A-site RNA.[221] Nucleotides that make contact with ring I are shown in blue and those that contact ring II are shown in orange. Hydrogen bonds are indicated by dashed lines. The Figure was generated with PyMol software[222] using coordinates from PDB file 2ESI.[221]

A series of compounds was synthesized (by Dr. Mobashery's lab) based on the chemical structure of neamine. The compounds were investigated in order to understand the roles of the individual rings in binding to the decoding region A-site model and also gain insights to the effect of various functional groups such as polyamine and γ-amino-α-hydroxybutyryl groups at different positions of the ring I moiety. It was anticipated that these derivatives would maintain the minimal structural motif for RNA binding, but at the same time, prevent modification by the resistance enzymes. The neamine analogues were screened by Pei-Wen Chao using

electrospray ionization mass spectrometry (ESI-MS).[201] The results she obtained indicated that charge formation at the N1 and N6 positions is important for binding to the A-site RNA. Also placing an amino group at the N2 position did not seem to contribute significantly to binding. Aminohydroxybutyryl and polyamine groups at position one enhanced binding (**Figure 3.3**). Furthermore, placing a second hydroxybutyryl group at position six reduced binding to the A-site RNA. The single-ring neamine analogue with the best affinity to the A-site RNA was DHR23 ($Kd \sim 10$ μM) (**Figure 3.3**).
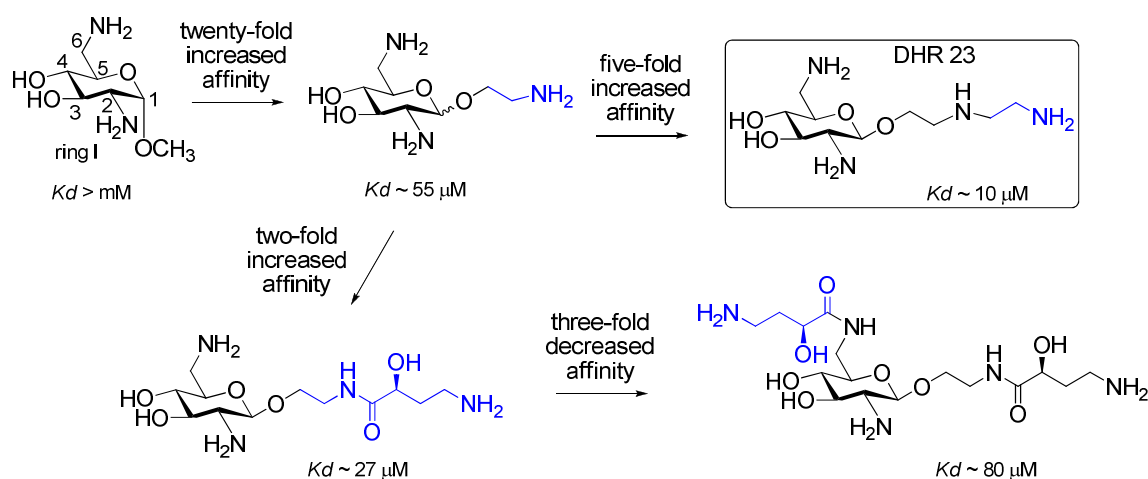
Figure 3.3: The effects of coupling various functional groups to ring I are shown. The apparent K_d values were determined by using ESI-MS in 150 mM ammonium acetate buffer, pH 7.6, with 50% isopropyl alcohol.[201]

In this study, the binding of DHR23 to the A-site RNA was further characterized using ESI-MS and footprinting assays. Salt and pH-dependence studies were performed to investigate the interactions that favor the binding of DHR23 to the A-site RNA. Also, the binding site and mode of action of DHR23 were investigated using footprinting and primer extension assays.

3.3 Experimental

3.3.1 RNA Synthesis and Purification

The A-site RNA hairpin with the sequence 5'-GGCGUCACACCUUCGGGUGAAGUCGCC-3', was purchased from Dharmacon Research Inc. (Lafayette, CO). The 2'-*O*-ACE-protected RNA was deprotected by incubating in tetramethylethylenediamine acetate buffer (TEMED-acetate) (pH 3.8) for 30 min at 60 °C.[223] The RNA was purified by electrophoresis on 20% denaturing polyacrylamide gels, followed by electroelution with 1/2× TBE (45 mM Tris-HCl, 45 mM boric acid, 1.25 mM Na$_2$EDTA, pH 8.3) in an Amicon centrilutor. The RNA was desalted by ethanol precipitation using a final concentration of 2 M ammonium acetate buffer, pH 7.8 (RNA for ESI-MS experiments) or 0.3 M sodium acetate pH 4.5 (RNA for enzymatic reactions). The concentration of the RNA was determined using Beer's law with the single-stranded extinction coefficients ($\varepsilon_{260\ nm}$) of 253,390 M^{-1}cm^{-1}.[224] For ESI-MS experiments, the A-site RNA (100 μM) was re-natured in 100 mM ammonium acetate, pH 7.6, by heating to 95 °C for 5 min in a heat block and slowly cooling to room temperature.

3.3.2 Neamine Analogue

DHR23 was obtained from Shahriar Mobashery and Dusan Hesek (University of Notre Dame). It was dissolved in double-distilled water to generate 2.5 mM stock solutions for all of the analyses.

3.3.3 Electrospray Ionization Mass Spectrometry

Electrospray ionization mass spectrometry (ESI-MS) experiments were performed on a Quattro LC tandem quadrupole mass spectrometer equipped with electrospray ionization in the negative ion mode (Micromass, Manchester, UK). The samples were injected via a Harvard 11 syringe pump at a flow rate of 6 μL/min. The following tuning parameters were used: capillary voltage 2.5 kV, cone voltage 50 V, extractor voltage 2 V, RF lens voltage 0.6 V, source block temperature 100 °C, and disolvation temperature 120 °C. The RNA-ligand samples were prepared in 150 mM ammonium acetate, pH 7.0. To aid sample disolvation, isopropyl alcohol was added to the samples to achieve a 1:1 (isopropyl alcohol: sample) solution prior to injection. In varying ionic strength experiments, 1 μM RNA was incubated with 10 μM of DHR23 in different ammonium acetate concentrations (80–225 mM) for 10 min before each measurement. The pH-dependece experiments were carried out in 150 mM ammonium acetate buffers at pH 5.5 to 8.6. Sixty scans per sample were taken and averaged. The spectra obtained were smoothed and the area under each peak was calculated using Masslynx (Micromass Ltd. Manchester, UK). The percentage of the different complex peaks were calculated using the formula (CP/ ($\sum$Cp + RNA)) * 100, in which Cp is the peak area of the complex (including all salt adducts), RNA is the peak area corresponding to the free RNA and its salt adducts, and $\sum$Cp is the summation of the peak areas corresponding to all complex peaks (including all salt adducts).

3.3.4 Transcription of 16 S rRNA

The 16 S rRNA was transcribed from vector pWK1 (Figure 3.4),[225] which was graciously

provided by Dr. Phil Cunningham of Wayne State University. The pWk1 was first linearized by

using restriction enzyme BSU 36I (New England Biolabs, Ipswich, MA). Approximately 10 μg of

plasmid DNA was incubated with 1x NEB buffer 3, 1x BSA (provided with the enzyme), and 10

units of BSU 36I in a reaction volume of 100 μL. The sample was incubated at 37 °C for 4 hours.
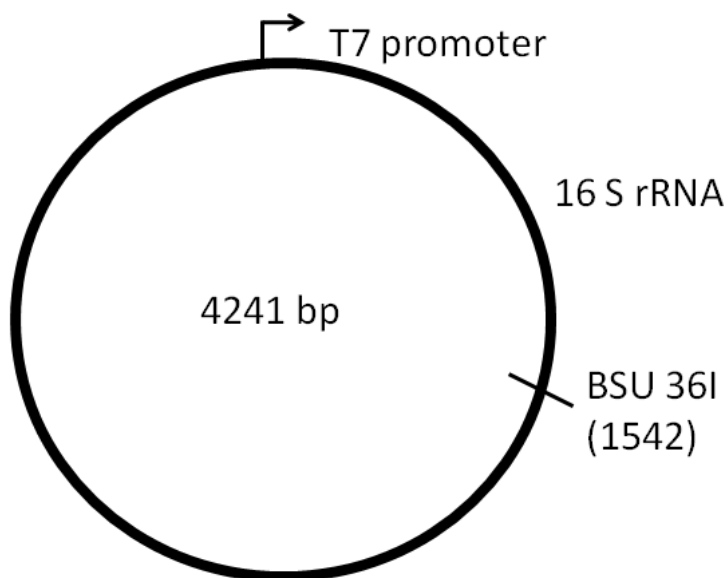
Figure 3.4: The map of the pWK1 plasmid is shown.

The digested product was verified by running a 1% agarose gel. Next, 1.5 μg of the linearized

plasmid was used for a 100 μL transcription reaction which contained 1x reaction buffer (80

mM Hepes-KOH pH 7.5, 12 mM $MgCl_2$, 2 mM spermidine), 40 mM dithiothreitol, 2.5 mM NTPs,

and 40 u of T7 polymerase. Inorganic pyrophosphatase (5 u/mL) was added to improve the

yield.[226] The reaction was incubated at 37 °C for 5 hours and the transcription product was

verified by running a 1% agarose gel. Finally, the transcription product was purified using size-exclusion chromatography. Before purification, the plasmid DNA in the transcription reaction was digested using DNase 1 (New England Biolabs, Ipswich, MA) in a 100 µL reaction that contained six units of DNase 1, 1x reaction buffer (10 mM Tris-HCl pH 7.6, 2.5 mM $MgCl_2$, 0.5 mM $CaCl_2$) and 87 µL of transcription product, which contained about 1.5 µg of plasmid DNA. The transcription product was then purified using pre swollen-Sephacryl 200 HR (Sigma Aldrich, St. Louis, MO). The resin was loaded in a Pasteur pipette to obtain a bed height of about 6 cm. Next, the resin was equilibrated with about 6 mL of running buffer (20 mM Hepes pH 7.5 or 20 mM Tris-HCl pH 7.5) and a 100 µL sample volume was loaded onto the column. The column was run at an approximate rate of 10 drops per minute and 0.3 mL fractions were collected. The fractions were checked for the presence of RNA using UV absorbance and the concentration of 16 S was determined using Beer's law and an extinction coefficient of 15,291,800 $M^{-1}cm^{-1}$.

3.3.5 3′-^{32}P Radiolabeling

Radiolabeling of the 3′ end of the A-site RNA was achieved by using 5′-^{32}P [$_pC_p$] (Perkin-Elmer, Waltham, MA).[227] In general, 25 pmoles of purified RNA was incubated in 1x T4 RNA ligase buffer (50 mM Tris-HCl, 10 mM MgCl2, 1 mM ATP, 10 mM dithiothreitol, pH 7.8), 10% dimethyl sulfoxide, 20 µCi of 5′-^{32}P [$_pC_p$] and 20 units of T4 RNA ligase (New England Biolabs, Ipswich, MA) in a reaction volume of 30 µL at 4 °C for 4 hours. The reaction was quenched by addition of 3 M ammonium acetate, followed by ethanol precipitation using 5 µg of tRNA[Phe] as co-precipitant.

3.3.6 5′-^{32}P Radiolabeling

Radiolabeling of the 5′ end of the DNA primers were achieved by using ^{32}P-γ ATP (Perkin-Elmer, Waltham, MA). In general, 25 pmoles of the DNA was incubated in 30 μL reaction containing 1x PNK buffer (70 mM Tris-HCl, 10 mM MgCl$_2$, 5 mM dithiothreitol, pH 7.6 at 25 °C), 10 μCi of ^{32}P-γ ATP and 20 units of T4 PNK (New England Biolabs, Ipswich, MA). The reaction was incubated at 37 °C for 30 minutes and quenched with 10 μL of 7.5 M ammonium acetate. The labeled sample was purified using a G-25 microspin column (GE healthcare, Piscataway, NJ).

3.3.7 RNA Chemical Probing

3.3.7.1 G Reaction

Dimethylsulfate (DMS) methylates N7 position of guanine, N1 position of adenine and N3 position of cytosine. Modification of adenines can be detected by primer extension (blocks the progression of reverse transcriptase); however, modification of guanines can only be detected after further reduction reaction with NaBH$_4$ followed by aniline treatment, which leads to strand scission.[193, 198] Truncated products can be detected by reverse transcription.[193] For the G reaction, 1 μg of 16 S rRNA or 1,000,000 cpm of labeled RNA was incubated with 1 mM DMS (Sigma Aldrich, St. Louis, MO) in a 300 μL reaction volume containing 10 mM MES buffer pH 7 and 100 mM KCl. For the end-labeled A-site RNA, 5 μg of tRNA^{phe} was added to the

reaction. The reaction was then incubated at 90 °C for 60 seconds and quenched by addition of 1.5 M sodium acetate followed by ethanol precipitation.

The dry RNA pellet obtained after ethanol precipitation was re-suspended in 10 mL of 1 M Tris-HCl (pH 8.2) and kept on ice. Next, 10 μL of freshly prepared 0.2 M NaBH$_4$ was added to the RNA sample and incubated on ice for 30 minutes. The reaction was quenched by ethanol precipitation with 0.3 M sodium acetate (pH 4.5) and dried down. Next, 40 μL of 1 M aniline acetate buffer (pH 4.5) was added to the dry RNA sample and incubated at 60 °C for 30 minutes protected from light. The sample was placed in dry ice to quench the reaction and the aniline was removed from the sample by two rounds of dissolving in water, freezing and lyophilizing.

3.3.7.2 A Reaction

Adenine specific reaction was achieved by using diethylpyrocarbonate (DEPC) (Sigma Aldrich, St. Louis, MO).[228-229] One microgram of 16 S rRNA or 500,000 cpm of radio labeled A-site RNA was incubated with 1 μL of DEPC in 200 μL of buffer containing 50 mM of sodium acetate (pH 4.5) and 1 mM EDTA for 5 minutes at 90 °C. For the end-labeled A-site RNA, 5 μg of tRNA^{Phe} was added to the reaction mixture. The reaction was quenched with 5 M ammonium acetate followed by ethanol precipitation. A second ethanol precipitation was performed using sodium acetate, followed by aniline treatment as described for the G reaction. The mechanism of this reaction was discussed in Chapter 2.

3.3.7.3   U Reaction

The U reaction was performed using 97% hydrazine (Sigma Aldrich, St. Louis, MO).[228-229] Ten microliters of hydrazine was added to the dry RNA sample (1 µg of 16 S rRNA or 500,000 cpm of end-labeled RNA) and incubated on ice for 10 minutes. The reaction was terminated with 200 µL of 0.3 M sodium acetate, followed by ethanol precipitation. A second round of ethanol precipitation was performed and the sample was dried in the speed vac. Next, the sample was subjected to aniline treatment as described previously. The mechanism of this reaction was discussed in Chapter 2. The chemical modifications in the 16 S rRNA were detected using a primer extension assay.

3.3.8 Primer Extension

The dry 16 S rRNA sample modified by DMS, DEPC or hydrazine was dissolved in water and quantified using UV absorption spectroscopy. Approximately 0.5 µg of the RNA was incubated with 20 pmol or 200,000 cpm of 5'-labeled DNA primer in a total volume of 5 µL. The sample was heated to 90 °C for two minutes and slowly cooled down to room temperature to allow the primer to anneal.[228-229] Next, the annealed sample was incubated with 1x reaction buffer (50 mM Tris-HCl, pH 8.3, 60 mM NaCl, 10 mM dithiothreitol,) 3 mM $MgCl_2$, 1 mM DNTPs, and 10 units of AMV reverse transcriptase (Promega, Madison, WI), in a 20 µL reaction volume. The reaction was incubated at 42 °C for one hour. For sequencing reactions, four samples were prepared containing the appropriate ddNTP at a ratio of 1 ddNTP to 10 dNTP (2.5 mM dNTP :

0.25 mM ddNTP). The reactions were terminated by addition of 2 mL of loading dye, boiled for two minutes and quickly cooled on ice. The reactions were resolved on an 8 % denaturing PAGE gel.

3.3.9 Enzymatic Footprinting

Enzymatic footprinting was carried out by incubating 3'-^{32}P-labeled A-site RNA (~250,000 cpm) with various concentrations (0–100 μM) of the drug being investigated in buffer containing 10 mM Tris-HCl, pH 7.2, 15 mM NaCl, and 1 mM Na$_2$EDTA at 37 °C for 1.5 h. Next, 0.002 U of RNase A was added to the RNA and the mixture was incubated at 37 °C for 30 minutes. The reactions were stopped by placing the samples on dry ice, followed by denaturing in a boiling water bath for 2 min in the presence of 1× formamide loading buffer (6× stock solution of loading buffer contains 0.1% bromophenol blue, 0.1% xylene cyanol, 80% formamide, and 20% glycerol). The A, U, and G sequencing ladders of the RNA were generated as described previously (3.3.7.1-3.3.7.3). The reaction samples (50,000 cpm/each) were loaded onto a pre-run 20% denaturing polyacrylamide gel and run at 1800 V for 3 h. The gel was exposed overnight at -20 °C to a storage phosphorscreen, which was then scanned on a Typhoon (GE, Piscataway NJ) phosphorimager.

3.4   Results and Discussion

3.4.1 Effects of Ionic Strength and pH on Binding of DHR23 to A-Site RNA

DHR23 had the highest affinity to the A-site RNA relative to the other single-ring aminoglycoside derivatives. It is expected to have a charge of +3 or +4 at neutral pH. We hypothesized that the binding of DHR23 to the A-site RNA is mainly driven by electrostatics. To verify this, the effects of ionic strength and pH on the relative affinity of DHR23 to A-site RNA were examined. In this experiment, A-site RNA and 10 uM DHR23 were incubated at different ammonium acetate concentrations (80 mM to 225 mM, pH 7.6) and varying pH values (150 mM ammonium acetate, pH 5.5 to 8.6) and analyzed by ESI-MS. The competing ammonium ions were expected to reduce binding of DHR23 to the A-site RNA, if the interactions were mainly driven by electrostatics. Increasing ionic strength reduced the amount of both 1:1 and 2:1 (DHR23: A site) complex (**Figure 3.5**). The amount of 3:1 complex was minimal or negligible in all cases. The ratio of 1:1 to 2:1 complexes increased with increasing ammonium ion concentration, suggesting a greater role for electrostatics in higher order complex formation (**Figure 3.5**).
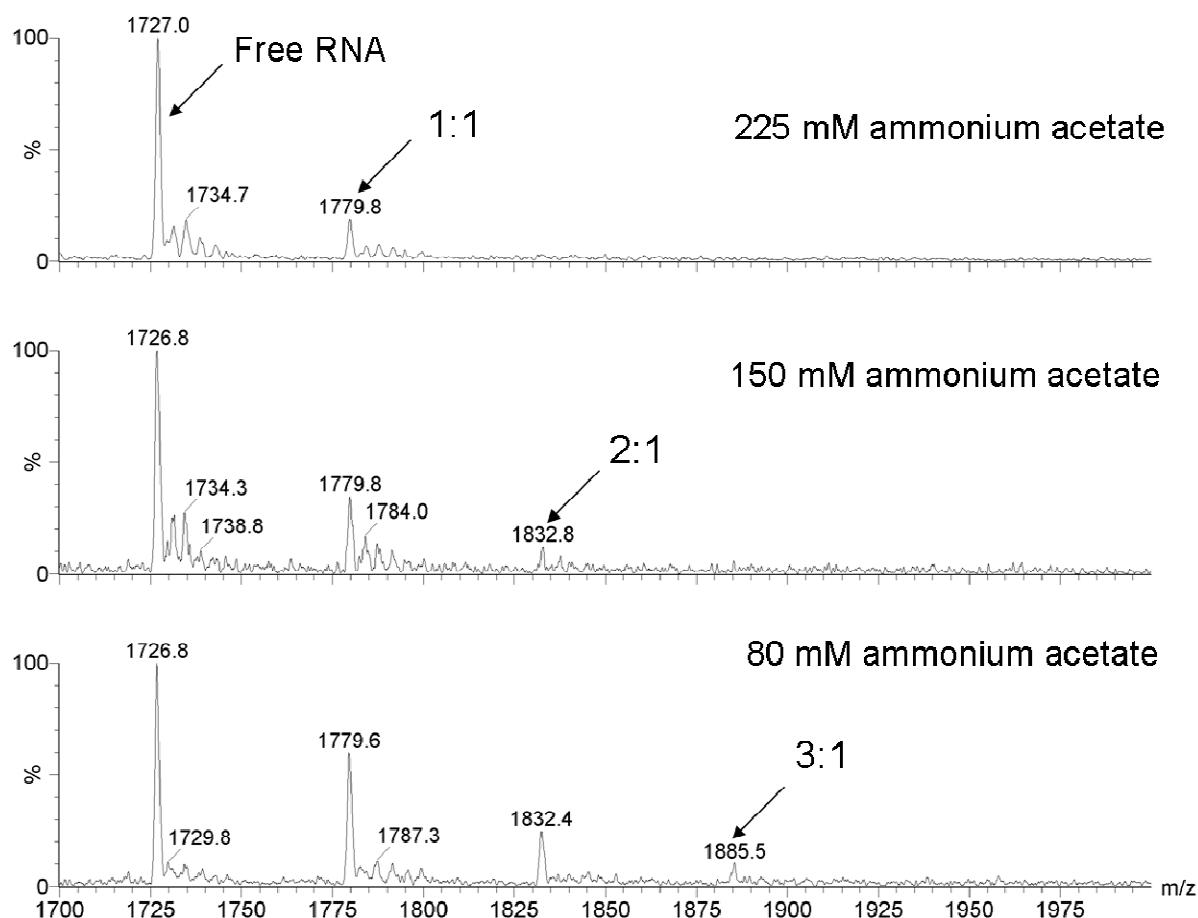
Figure 3.5: ESI-MS spectra in the m/z range of 1700-2000 of A-site RNA complexed with DHR23 at various concentrations of ammonium acetate (80 to 225 mM) at pH 7.6 are shown. The free RNA and 1:1, 2:1, and 3:1 complexes (DHR23:A-site RNA) are in the -5 charge state.

A similar trend was observed in experiments to determine the pH-dependence of complex formation. Raising the pH from 7.6 to 8.6 led to a reduction of both 1:1 and 2:1 complexes, and the 3:1 complex was not observed (**Figure 3.6**). A lowering of pH to 5.5 led to increased binding. These results suggest that there is a significant electrostatic component to the binding of DHR23 to the A-site RNA. These results are summarized in Table 3.1
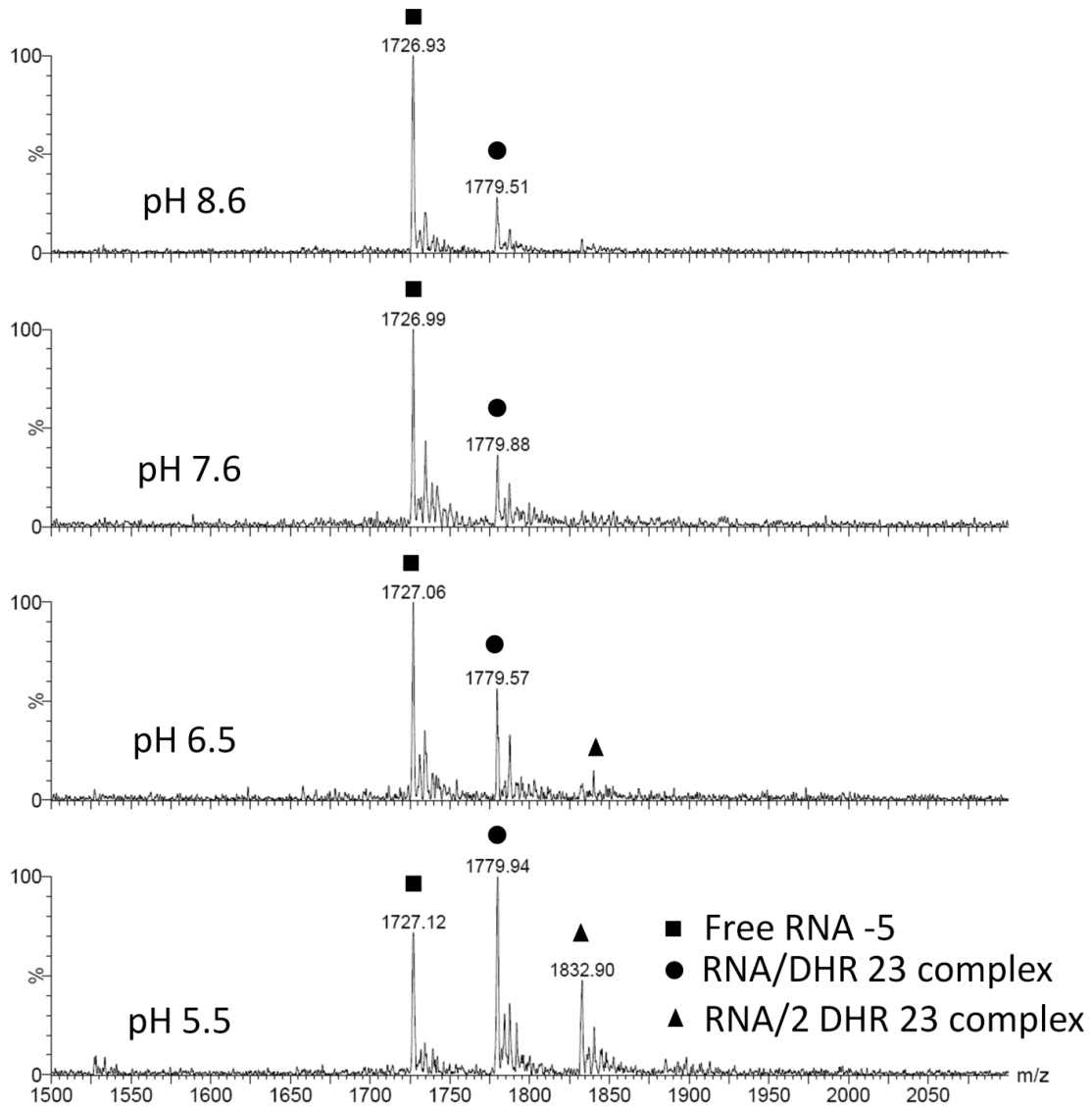
Figure 3.6: ESI-MS spectra of A-site RNA complexed with DHR23 at various pH values (5.5 to 8.6) are shown. The free RNA and 1:1, 2:1, and 3:1 complexes (DHR:A-site RNA) are in the -5 charge state.

Table 3.1: Effects of pH and ionic strength on A-site RNA binding by DHR23.

[ammonium acetate]	pH	free RNA (%)	1:1 complex (%)	2:1 complex (%)	3:1 complex (%)
80 mM	7.6	41	39	16	4
150 mM	7.6	60	31	9	0
225 mM	7.6	78	20	2	0
150 mM	5.5	27	42	26	5
150 mM	6.6	57	33	8	1
150 mM	7.6	60	31	9	0
150 mM	8.6	69	23	7	0

3.4.2 Binding Site of DHR23 on the A-site RNA

Previous ESI-MS competition studies performed by addition of paromomycin to pre-formed DHR23-A-site RNA complex revealed that DHR23 has a similar binding site on A-site RNA as paromomycin.[201] To locate the binding site of DHR23 on the A-site RNA, enzymatic footprinting analysis with RNase A was performed. RNase A catalyzes the cleavage of the phosphodiester bond in single-stranded RNA via a 5' RNA-2'-3' cyclic phosphate intermediate, eventually resulting in 3' RNA-OH and 5' RNA-PO_4 products.[230] In general, 3'-radiolabeled A-site RNA was incubated with varying concentrations of ligand and allowed to equilibrate. The samples were treated with RNase A for 30 minutes. The idea here is that the bound ligand would protect the RNA from cleavage by RNase A, resulting in increased protection upon an increase in ligand concentration.

As seen in **Figure 3.7**, increasing the concentration of DHR23 from 5 to 100 µM resulted in protection of nucleotides A1492, A1493, and G1494. This result indicates that the binding site of DHR23 is in the internal bulge region of the A-site RNA.
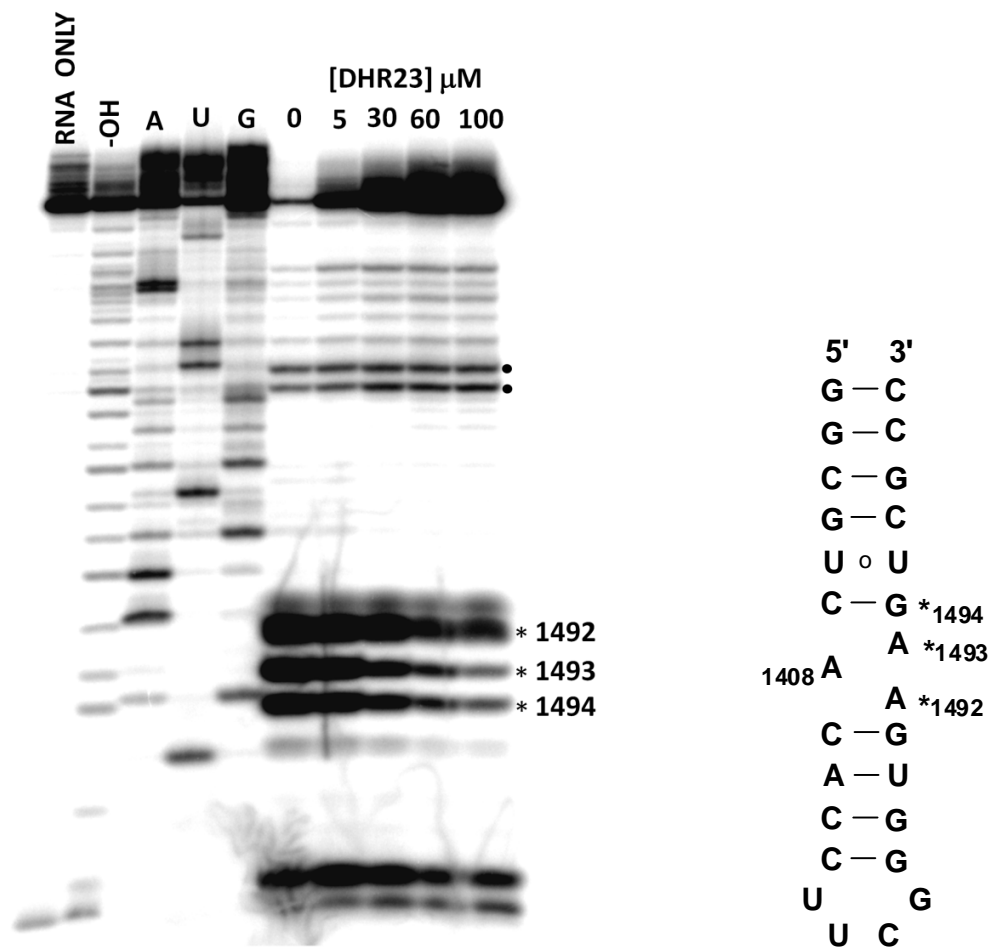
Figure 3.7: Enzymatic footprinting analysis of DHR23/A-site RNA complex is shown. On the left, an autoradiogram of the 20% denaturing polyacrylamide gel reveals RNase A cleavage sites on 3'-^{32}P-labeled A-site RNA. Lane 1: RNA control; lane 2: alkaline hydrolysis ladder; lanes 3–5 A, U, G chemical sequencing reactions, respectively; lane 6: RNase A cleavage in the absence of DHR23; lanes 7–10 RNase A cleavage in the presence of 5 to 100 µM of DHR23. The A-site RNA model is shown on the right, with stars (*) indicating the residues protected by DHR23. The filled circles (●) represents cleavage sites corresponding to the uridines in the hairpin loop.

The bands that were protected from RNase A cleavage, A1492, A1493, and G1494, were quantified and binding curves of fraction bound vs. ligand concentration were generated and fitted to Equation 1 to obtain dissociation constants. The fraction bound was calculated by dividing the intensity of the bands corresponding to A1492, A1493, or G1494 by the total intensities of all bands in the lane. The bands in the lane in which no DHR23 was added (lane 6, **Figure 3.7**) represent 0% protection; hence, the bands in the other lanes were normalized accordingly. The dissociation constants obtained were: 21 ± 10 µM, 11 ± 3 µM, and 27 ± 8 µM for A1492, A1493, and G1494, respectively. The average K_d was 19.6 ± 8 µM, which is consistent with ESI-MS data for DHR23, will be discussed in the next chapter. The error of the individual K_d values is the error of the fit and the error of the average K_d value is the standard deviation of the three different K_d values.
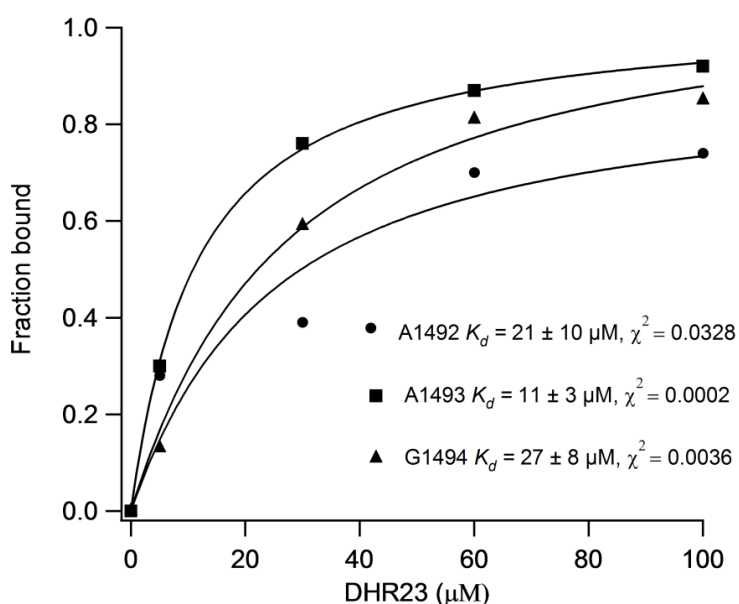
Figure 3.8: Binding curves and dissociation constants generated from the RNase A footprinting data are shown. The data was fit to a 1:1 binding model using Equation 1.

RNase A is reported to specifically catalyze cleavage of the 3' end of single-stranded pyrimidines;[231] however, it can be seen in **Figure 3.7** that RNase A catalyzed the cleavage of A1492, A1493, and G1494 in addition to the uridines present in the loop of the A-site RNA, highlighted with black dots in **Figure 3.7**. This seemed surprising at first; however, Libonati and other groups have shown that RNase A is able to catalyze the cleavage of poly-adenine ribonucleotide, though the rate is 10^3-10^4 less than that of poly-uridine.[232-233] The preference of RNase A for pyrimidine bases is reported to be due to specific hydrogen bonding that occurs between the pyrimidine bases and the amino acid threonine 45, present in the active site of RNase A. This hydrogen bond interaction is sterically excluded for purine bases;[232] however, the fact that RNase A is able to catalyze the cleavage of poly-adenine nucleotides at a slower rate indicates that its specificity is not very stringent. The internal bulge of the A-site RNA is a dynamic region, and therefore it could be adopting a conformation that allows A1492, A1493 and G1494 to be accommodated in the active site of RNase A. This could explain the unusual cleavage pattern of RNase A observed in this assay.

To verify if the protection observed with DHR23 was not due to inhibition of the enzyme by DHR23, control experiments were performed with paromomycin, chloramphenicol, and varying salt concentrations. The results are shown in **Figure 3.9**. Chloramphenicol was chosen as a negative control because it is a potent RNA binder, but it is not known to bind to the A site.[100, 234] Consequently, no protection was observed with increasing concentrations of chloramphenicol (**Figure 3.9**, lanes 5-8). RNase A cleavage in the presence of increasing concentrations of paromomycin on the other hand resulted in protection of nucleotides A1493

and G1494 (**Figure 3.9**, lanes 10-12). This result is similar to what was observed with DHR23, and consistent with previous competition experiments in which DHR23 was found to bind to a similar region as paromomycin.[201]
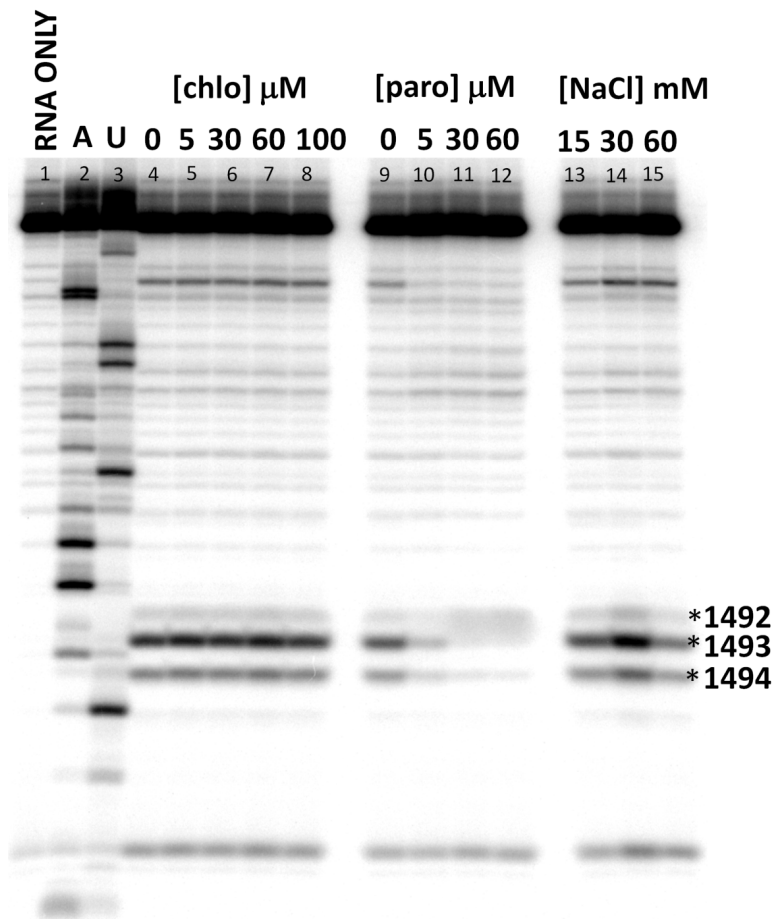
Figure 3.9: Enzymatic footprinting analyses of chloramphenicol/A-site RNA complex, paromomycin/A-site RNA, and A-site RNA under varying NaCl concentrations are shown. The autoradiogram of the 20% denaturing polyacrylamide gel reveals RNase A cleavage sites on 3'-^{32}P-labeled A-site RNA: lane 1: RNA control; lane 2 and 3: A, U, chemical sequencing reactions, respectively; lane 4: RNase A cleavage in the absence of chloramphenicol; lanes 5–8: RNase A cleavage in the presence of 5 to 100 μM of chloramphenicol; lane 9: RNase A cleavage in the absence of paromomycin; lanes 10–12: RNase A cleavage in the presence of 5 to 60 μM of paromomycin; lanes 13-15: RNase A cleavage in the presence of additional 15-60 mM NaCl.

RNase A is cationic at physiological pH.[235] Coulombic interactions between the cationic side chains of RNase A and its substrate are crucial for substrate binding. As result, the activity of RNase A is inhibited at high salt concentrations.[236] To verify if the protection seen with cationic DHR23 was not due to inhibition of the enzyme, a control experiment was run in the presence of 5 – 60 mM NaCl. Lane 13 in **Figure 3.9** shows RNase A cleavage of A-site RNA in identical buffer used for the DHR23 footprinting experiments, but with additional 15 mM NaCl. When the salt concentration was increased to 30 mM, an increase in enzymatic activity was observed (**Figure 3.9**, lane 14). When the salt concentration was increased to 60 mM a reduction of RNase A activity was observed (**Figure 3.9** lane 15), but not to the level of protection seen with DHR23. Moreover, the salt concentration in lane 15 was 600-fold greater than the amount of DHR23 added. These results confirm that in spite of the unusual cleavage pattern of RNase A observed in the footprinting assay, the protection bands observed were caused by the protection of the RNA by DHR23. After determining that DHR23 binds to a similar site on the A-site RNA as paromomycin, the next objective was to investigate if DHR23 is able to cause conformational changes in A1492 and A1493, as observed with paromomycin.[6, 85, 163]

3.4.3 Mode of Binding of DHR23

Studies have shown that aminoglycosides such as paromomycin exhibit antibacterial activity by binding to the internal bulge region of the aminoacyltransfer center of the 16 S rRNA and stabilizing a flipped-out conformation of A1492 and A1493.[95, 207, 237] This conformational change leads to the stabilization of non-cognate aminoacyl-tRNA, thereby compromising the

fidelity of protein synthesis. The objective was to use dimethylsulfate (DMS) to probe the conformation of A1492 and A1493 after incubation with DHR23. The extent of DMS modification of A1492 and A1493 would depend on their accessibility (flipped out or stacked in the helix). A primer-extension assay was used to detect DMS modified adenines. The reaction mechanism of DMS was discussed in Chapter 2. Initially the assay was validated by using paromomycin as a positive control. The results are shown in **Figure 3.10**.
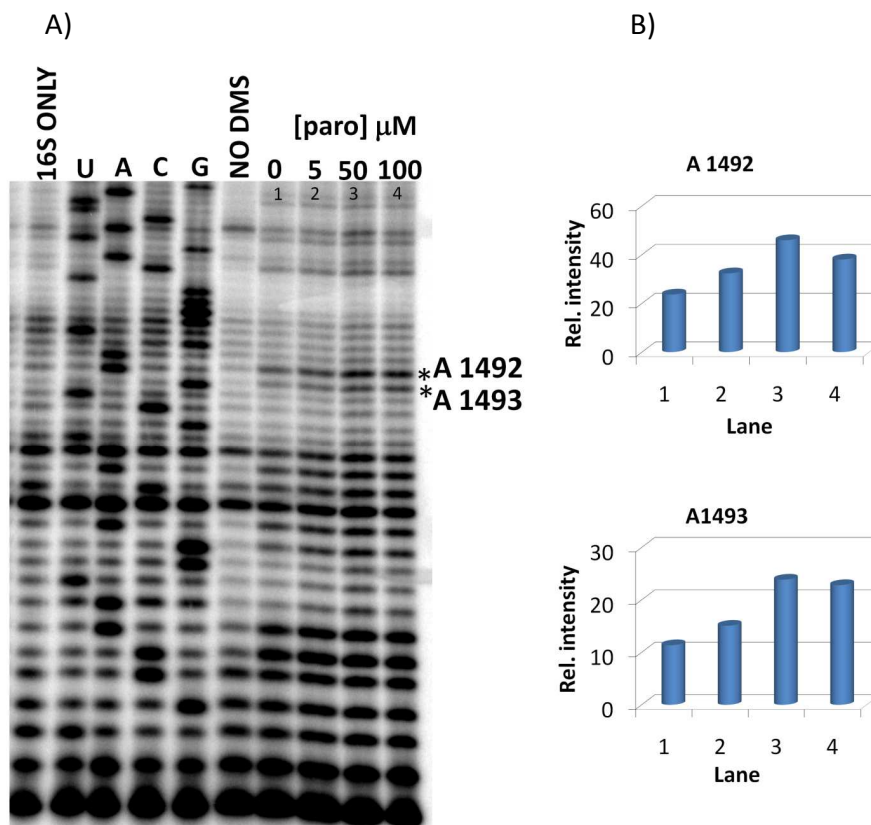
Figure 3.10: A) Autoradiogram of a 10% denaturing polyacrylamide gel. The lanes on the left show primer extension products of the 16 S RNA and U, A, C, G dideoxy sequencing. The lanes 1-4 on the right show primer extension products in the absence of DMS, and DMS reactions in the presence of 0, 5, 50, and 100 µM, respectively, of paromomycin. B) Band quantification results for A1492 and A1493 are shown. The band intensities of A1492 and A1493 were normalized to the total intensities of all bands in each lane.

In the presence of increasing concentrations of paromomycin, approximately two-fold enhancement of DMS reactivity is observed at A1492 and A1493 (**Figure 3.10**). This result is consistent with literature reports in which binding of paromomycin to the A site leads to stabilization of the flipped out conformation of A1492 an A1493 resulting in increased reactivity with DMS.[87, 95]

In the next experiment, the DMS assay was repeated with DHR23. Binding of DHR23 to the 16 S rRNA did not lead to increased reactivity of A1492 and A1493 with DMS as observed with its parent compound paromomycin (**Figure 3.11**). In contrast, DHR23 seemed to cause protection. In the presence of increasing concentrations of DHR23, there was an approximate two-fold decrease in DMS reactivity at A1492 and A1493, suggesting that DHR23 stabilized the stacked-in conformation of these nucleotides. Previous reports indicate that in the absence of aminoglycosides, A1492 and A1493 sample both the stacked in and flipped out conformations.[238] In contrast, the presence of aminoglycosides such as paromomycin, causes nucleotides A1492 and A1493 to flip out of the helix.[6, 238] Also molecular dynamics data provided evidence that the two nucleotides are flipped out simultaneously,[238] but interestingly a crystal structure of the ribosome termination complex showed that upon binding of release factor 1, A1493 remained stacked in the helix; however, A1494 was flipped out in order to accommodate the release factor.[239] The above examples go to show that the A site is very dynamic and can adopt different conformations in the presence of different molecules; therefore, the stabilization of the stacked-in conformation of the two bases by DHR23 is not surprising. However, this result implies that even though the RNase A footprinting data

localized the binding site of both DHR23 and paromomycin to the internal bulge region of the A-site RNA, the specific contacts made between the RNA and the two ligands are different. This difference may influence the A-site RNA to adopt different conformations in the presence of DHR23 or paromomycin.
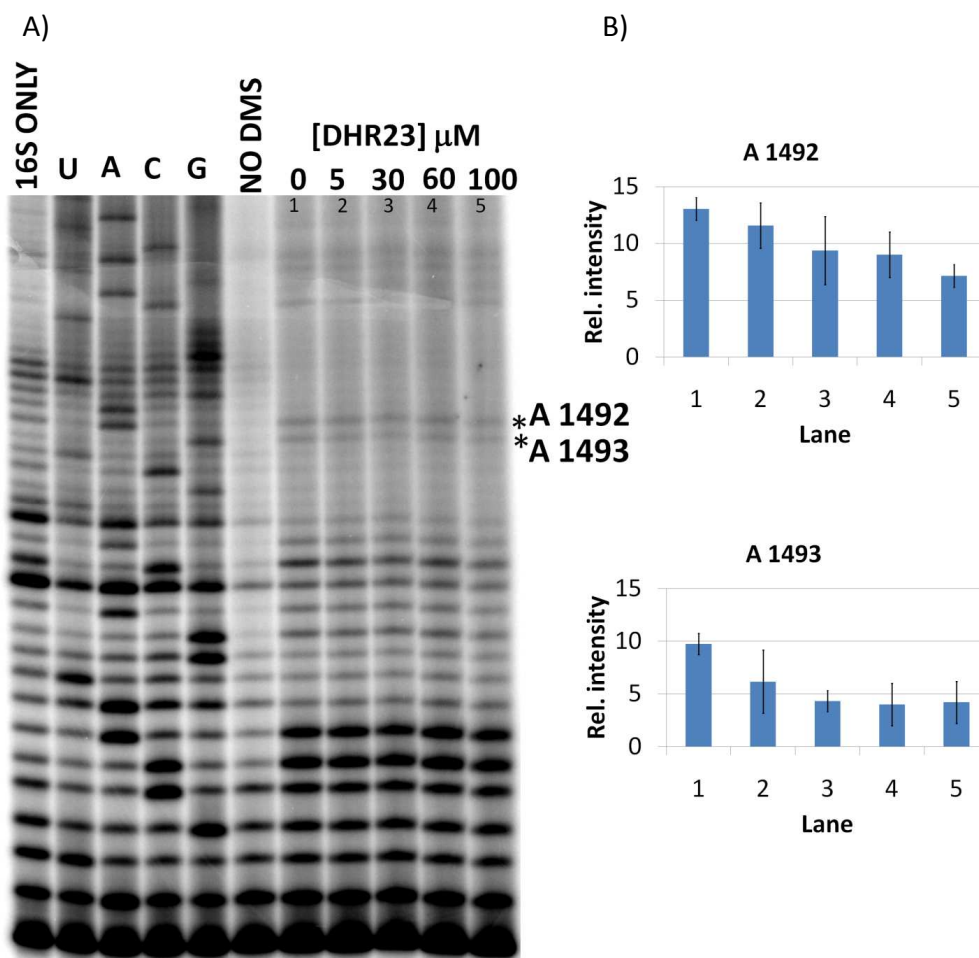
Figure 3.11: Autoradiogram of a 10% denaturing polyacrylamide gel. The lanes on the left show primer extension products of the 16 S RNA and U, A, C, G dideoxy sequencing. The lanes on the right show primer extension products in the absence of DMS, and DMS reactions in the presence of 0, 5, 30, 60, and 100 µM, respectively of DHR23. B) Band quantification results for A1492 and A1493 are shown. The band intensities of A1492 and A1493 were normalized to the total intensities of all bands in each lane.

In the future design of aminoglycoside analogues, it would be prudent to utilize molecular modeling to select side chains or functionalities that mimic the contacts made between paromomycin and the RNA. Future efforts to improve the efficacy of DHR23 include coupling DHR23 with a peptide (HPVHHYQ) known to cause base flipping of A1492 and A1493.[169] Our hope is that the hybrid molecule will adopt the specificity of DHR23 and the efficacy of HPVHHYQ.

CHAPTER 4

A MODIFIED FLUORESCENT INTERCALATOR DISPLACEMENT ASSAY FOR RNA LIGAND DISCOVERY*

4.1   Abstract

Fluorescent intercalator displacement (FID) is a convenient and practical tool for identifying new nucleic-acid-binding ligands. The success of FID is based on the fact that it can be fashioned into a versatile screening assay for assessing the relative binding affinities of compounds to nucleic acids. FID is a tagless approach; the target RNAs and the ligands or small molecules under investigation do not have to be modified in order to be examined. In this study, a modified FID assay for screening RNA-binding ligands was established using 3-methyl-2-((1-(3-(trimethylammonio)propyl)-4-quinolinylidene)methyl)benzothiazolium (TO-PRO) as the fluorescent indicator. Electrospray ionization mass spectrometry (ESI-MS) results provide direct evidence that correlates the reduction in fluorescence intensity observed in the FID assay with displacement of the dye molecule from RNA. The assay was successfully applied to screen a variety of RNA-binding ligands with a set of small hairpin RNAs. Ligands that bind with moderate affinity to the chosen RNA constructs (A-site, TAR, h31, and H69) were identified.

* The results presented in this chapter have been published.[166]

4.2 Introduction

Developing new antibiotics requires a detailed understanding and characterization of drug-RNA interactions. A significant challenge, however, is the development of systems for efficient screening and discovery of ligands of interest for new RNA targets. Thus, a relatively simple and high-throughput method such as fluorescent intercalator displacement (FID)[1][240-241] for RNA applications would be very useful in the drug-discovery process. FID has become an increasingly important tool for identifying new nucleic-acid-binding ligands. Its success is based on the fact that it can be fashioned into a versatile high-throughput assay that can be used to assess the relative binding affinities of compounds to nucleic acids in a relatively simple manner, requiring only a moderate level of specialized expertise. FID has been used successfully to identify and establish relative binding selectivities and affinities, as well as distinguish binding modes for a variety of DNA-binding ligands.[240-244] More recently, work in the laboratories of Beal, Hergenrother, and Nakatani has shown that FID is useful for ranking and determining selectivity of RNA-binding ligands.[245-247] FID is becoming an increasingly attractive method because it is a tagless approach; neither the RNA nor the small molecule under investigation are modified. A dye molecule is employed, which has a greater fluorescence intensity when intercalated (or bound) to the nucleic acid than when free in solution.[240-241, 244-245] The FID assay is based on the model in which a fluorescent probe is bound to RNA and displaced by a ligand, leading to a reduction in fluorescence intensity (**Figure 4.1**). Although the traditional assay involved intercalation of the dye molecule into DNA, the mode of binding to RNA may actually

differ. Nonetheless, the extent of decrease in fluorescence is still proportional to the affinity of

the ligand for the RNA.
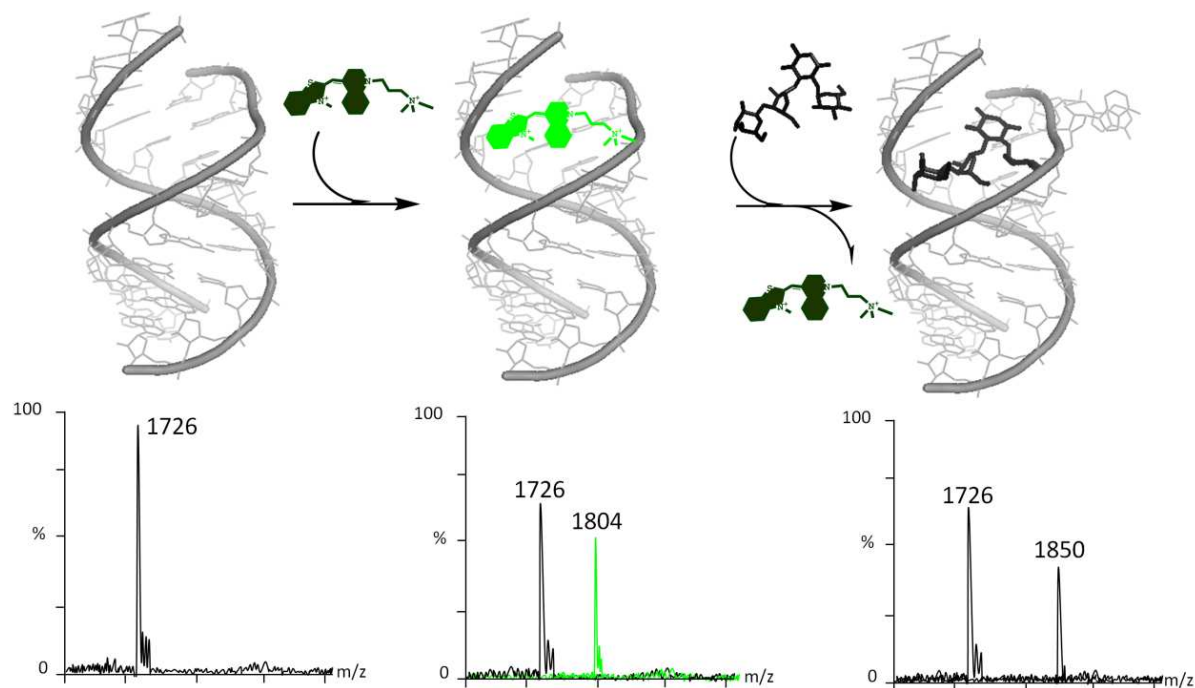
Figure 4.1: A dipiction of the displacement of a fluorescent indicator from A-site RNA by promomycin examined by ESI-MS. The Figure was generated using coordinates from the PDB file 1J7T.[207]

In this study, a modified FID method for screening RNA-binding ligands was established,

and electrospray ionization mass spectrometry (ESI-MS) was used to investigate its mechanism

(**Figure 4.1**). ESI-MS is a soft ionization process that was first used to detect non-covalent

interactions in 1991.[180] Since then, ESI-MS has been extended to the study of non-covalent

interactions between nucleic acids and ligands as a screening tool for drug discovery.[181-182] ESI-

MS has been successful due to the fact that it is a powerful and reliable method that can be

used to determine stoichiometry, relative binding affinities with multiple ligands or targets, and equilibrium binding constants in one set of experiments.[182-183, 248-249] In traditional spectroscopic methods, the bound concentration of ligand has to be relatively high in order for its contribution to be detected, and multiple stoichiometries complicate the analysis. ESI-MS on the other hand allows for examination of multiple stoichiometry complexes even at very low abundance.[183] Unfortunately, ESI-MS is limited to non-physiological buffers due to cationic complexation with nucleic acids.[250-251] ESI-MS is nevertheless a powerful tool that can be used to elucidate the mechanism of FID and verify relative binding affinities obtained from this method.

The traditional FID assays employed ethidium bromide or thiazole orange as dyes;[240-242, 245] however, these dyes were either not suitable for RNA FID and/or ESI-MS assays, or not compatible with certain types of ligands. In this study, the binding of a range of ligands from aminoglycosides to peptides was examined by FID using an alternative dye, namely 3-methyl-2-((1-(3-(trimethylammonio)propyl)-4-quinolinylidene)methyl)benzothiazolium (TO-PRO), and a variety of bacterial and viral RNA targets (A-site RNA and helix 31 (h31) of 16 S rRNA, helix 69 (H69) of 23 S rRNA, and TAR of HIV-1 RNA).

4.3   Materials and Methods

4.3.1 RNA Preparation

The RNA hairpins with the following sequences were purchased from Dharmacon Research Inc. (Lafayette, CO):

5'-GGCGUCACACCUUCGGGUGAAGUCGCC-3' (A-site RNA),

5'-GGCAGAUCUGAGCCUGGGGAGCUCUCUGCC-3' (TAR RNA),

5'-GUUCGAUGCAACGCGAAC-3' (h31), and

5'- GGCCGAψACm^{3}ψAψAACGGUC-3' (H69), in which ψ is pseudouridine and m^{3}ψ is 3-methylpseudouridine.

The RNAs were deprotected and purified as previously described in Chapter 3. The concentration of RNAs were determined using Beer's law with the following single-stranded extinction coefficients: $\varepsilon_{260\ nm}$ of 253,390 M^{-1}cm^{-1} for A-site RNA hairpin, 268,900 M^{-1}cm^{-1} for TAR RNA, 176,900 M^{-1}cm^{-1} for h31, and 189,400 M^{-1}cm^{-1} for H69.[224]

4.3.2 Ligands

TO-PRO was purchased from Invitrogen (Carlsbad, CA). Paromomycin, neomycin and chloramphenicol were purchased from Sigma Aldrich (St. Louis MO). Tat peptide and KkN were purchased from Bachem (Torrance CA). CR1119 was obtained from the lab of Dr. Mark Spaller (Dartmouth Medical School). Single-ring aminoglycoside analogues were obtained from Shahriar Mobashery and Dusan Hesek (University of Notre Dame).

4.3.3 FID Assay

All fluorescence readings were taken on a Cary Eclipse Spectrophotometer (Varian Inc., Walnut Creek, CA). Typically, 2 μM of RNA was incubated with 2 μM of TO-PRO in 150 mM ammonium acetate buffer, pH 7, or 100 mM KCl and 20 mM Tris-Cl, pH 7, for 5 minutes. The initial fluorescence reading was taken and the appropriate concentration of drug was then added and mixed thoroughly and allowed to equilibrate for another 5 minutes. Five scans per sample were taken with an excitation wavelength of 512 nm and emission wavelength of 533 nm. The level of fluorescence change (either enhancement or quenching) was determined and converted to a percent change in fluorescence using the formula $(F_1/F_0)*100$, where F_0 is the initial fluorescence of dye bound to RNA before the addition of drug and F_1 is the fluorescence after addition of drug.

4.3.4 Electrospray Ionization Mass Spectrometry (ESI-MS)

Electrospray ionization mass spectrometry (ESI-MS) experiments were performed on a Quattro LC tandem quadrupole mass spectrometer equipped with electrospray ionization in the negative ion mode (Micromass, Manchester, UK). The tuning parameters, sample preparation, data processing and fraction bound determination were discussed previously in Chapters 2 and 3. In these studies, the mass of the compounds were small compared to that of the RNA target (i.e., <10%). Based on literature reports, an assumption was made in these studies that the binding of ligand to the RNA does not alter the ionization efficiency of the complex.[252-254]

Therefore, a correction factor for different ionization efficiencies of the free RNA and RNA complexes was not used.[184]

For competition experiments, the RNA and dye solution were incubated for 5 minutes after which the appropriate drug was added and incubated for another 5 minutes before injection. The final concentrations of RNA and dye were 1 μM.

4.4   Results and Discussion

4.4.1 TO-PRO Association with the A-site RNA

A series of commercial dye molecules was screened for one that had ideal fluorescent changes in the presence of RNA and no detectable fluorescence in the absence of RNA. A common staining dye referred to as TO-PRO (3-methyl-2-((1-(3-(trimethylammonio)propyl)-4quinolinylidene)methyl)benzothiazolium) (**Figure 4.2**) has essentially no fluorescence in the unbound form in buffer; however, it has fluorescence enhancement of approximately 400-fold when bound to A-site RNA. The A-site RNA is the aminoacyl-tRNA site of the decoding region of bacterial 16 S rRNA, and a known antibiotic target site for aminoglycosides.[6, 89, 206] A series of titrations were performed with TO-PRO and the A-site RNA construct (**Figure 4.2**). The intersection of the pre- and post-saturation data points for fluorescence titrations indicate that TO-PRO associates with the A-site RNA with a stoichiometry of one (**Figure 4.3A**). Similarly, by measuring the fluorescence as a function of the molar fraction of TO-PRO, a Job plot of TO-PRO

binding to the A-site RNA was generated.[255-256] The two straight lines intersected at a mole

fraction of 0.52, which indicates the presence of a 1:1 complex (**Figure 4.3B**).
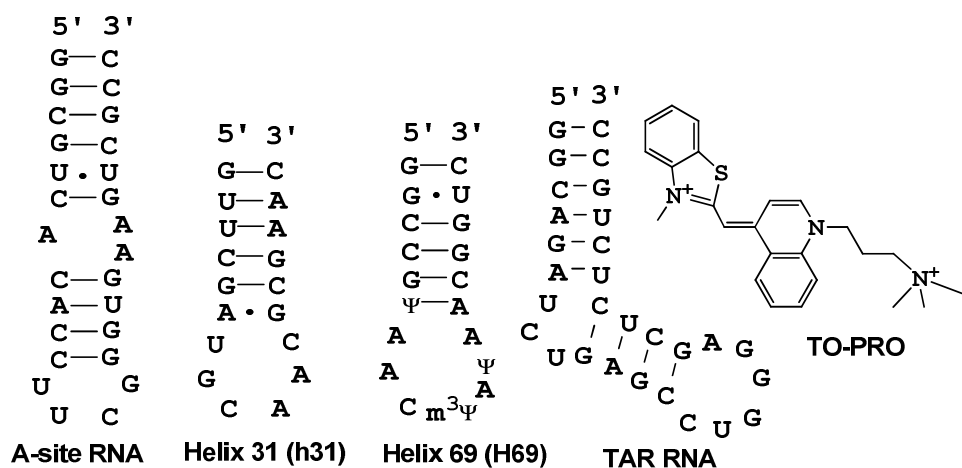
Figure 4.2: The RNA constructs and dye indicator (TO-PRO) used in this study are shown.
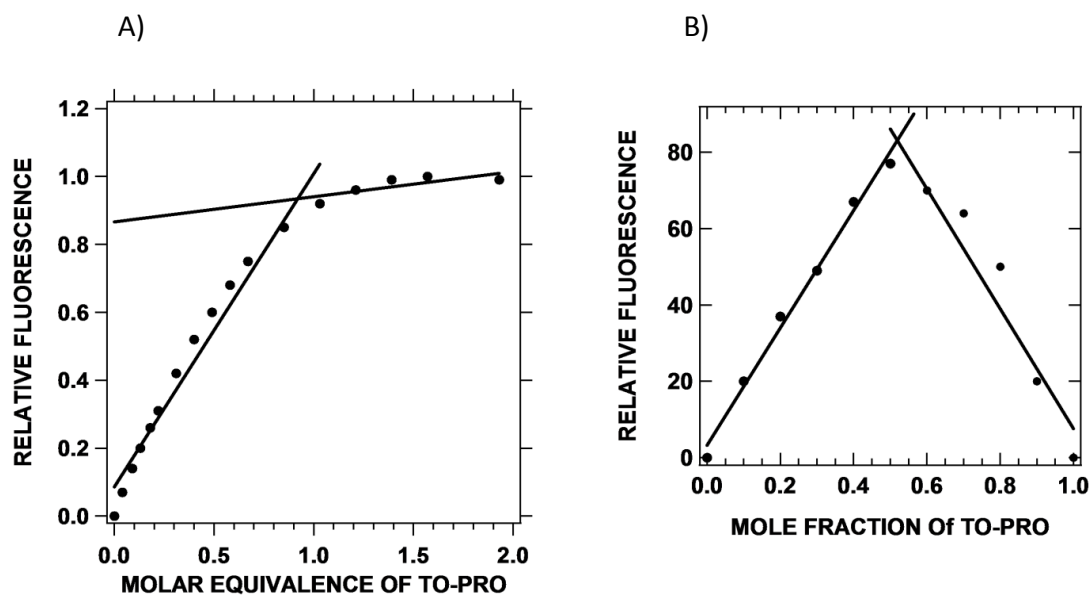
Figure 4.3: A) Fluorescence titration data of the A-site RNA (3 µM) with TO-PRO is shown. B) A Job plot of TO-PRO binding to the A-site RNA (3 µM) is given (buffer conditions were 100 mM KCl, 20 mM Tris, pH 7).

4.4.2 FID Experiments with Paromomycin and A-site RNA

Paromomycin, an aminoglycoside that is known to bind to the A-site RNA,[6, 87, 203, 257] was titrated against 2 µM of the A-site construct bound to 2 µM TO-PRO. The level of fluorescence change (either enhancement or quenching) was determined and converted to a percent change in fluorescence (see Materials and Methods). The results are shown in **Figure 4.4**. Paromomycin was able to displace pre-bound TO-PRO from the A-site RNA. Upon addition of 31 µM of paromomycin, the fluorescence intensity of TO-PRO was reduced to less than 30%. The buffer conditions used were 150 mM ammonium acetate, pH 7. These conditions were chosen to match the ESI-MS conditions for data comparison purposes. Binding experiments using A-site RNA and paromomycin were performed in 20 mM Tris, 100 mM KCl, pH 7, and similar results were obtained. All results shown are the average of three experiments.
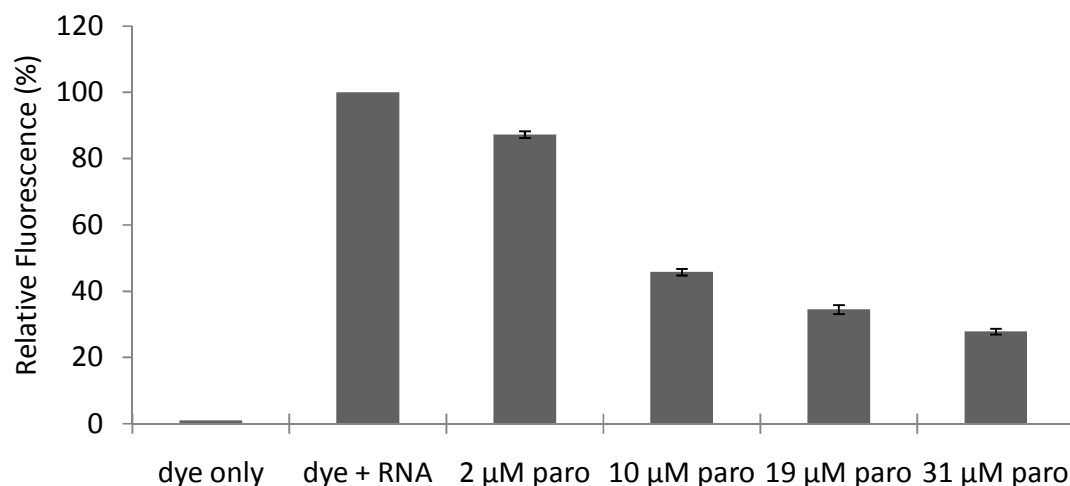
Figure 4.4: FID assay results with paromomycin are shown. Equimolar concentrations of A-site RNA and TO-PRO dye (1 µM) were pre-bound in buffer (150 mM ammonium acetate, pH 7) prior to paromomycin addition. An average of three separate experiments is shown.

4.4.3 FID Mechanism Examined by ESI-MS

To determine if the change in fluorescence observed was due to displacement of TO-PRO by paromomycin, ESI-MS was utilized. There could be several outcomes when dye (TO-PRO) bound to RNA is treated with various RNA-binding ligands (summarized in **Figure 4.5**). One possibility is that the ligand may compete for the same binding site as the dye, thereby displacing the dye from the RNA, leading to a decrease in fluorescence intensity (**1**). Alternatively, the ligand may bind to a different part of the RNA, in which case fluorescence intensity is unchanged (**2**), or the ligand may interact with the dye leading to quenching of fluorescence (**3**). Some ligands may not have affinity for the RNA; in this case, the fluorescence value will be unchanged (**4**).
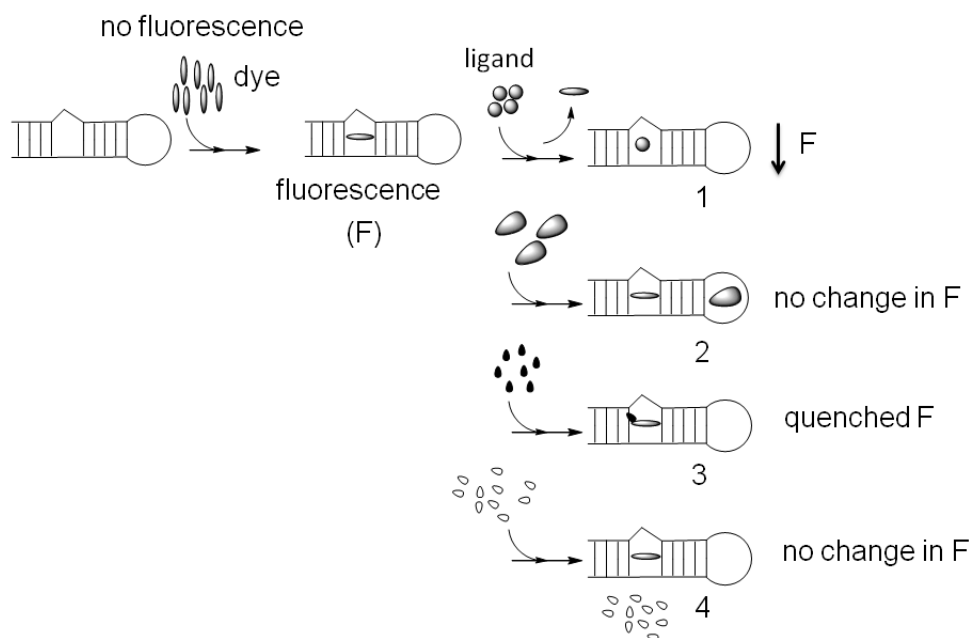
Figure 4.5: Four possible outcomes of the FID process are depicted. Refer to text for a description of the process.

FID is based on a model in which displacement of a fluorescent dye molecule from the host or target results in a decrease of fluorescence intensity.[240-243] In the ESI-MS experiment, we sought evidence to support this model. Competition assays with ESI-MS allows for analysis of the FID mechanism. ESI-MS is useful in this case because the stoichiometry of ligands to RNA can be determined. By monitoring a titration of paromomycin into 1 µM of 1:1 A-site hairpin:TO-PRO complex with ESI-MS, it can be observed that with increasing concentrations of paromomycin, the amount of RNA/TO-PRO complex diminishes and the RNA/paromomycin complex increases (**Figure 4.6**). This result indicates competition between the TO-PRO dye and paromomycin for binding to the RNA hairpin. The appearance of a peak representing a complex of RNA/paromomycin/TO-PRO indicates that paromomycin and TO-PRO have additional non-competing binding sites on the RNA hairpin. This result is not surprising since paromomycin is known to be a promiscuous RNA binder.[258-259]

The extent of TO-PRO displacement by binding of paromomycin in ESI-MS was quantified and the results are shown in **Figure 4.6**. At 15 µM paromomycin, only a negligible amount of TO-PRO remains bound to the RNA. These data are consistent with a displacement model and corresponding decrease in fluorescence intensity of TO-PRO as it is dissociated from the RNA target (as shown in **Figure 4.5**, example **1**).

[paro] μM	fraction bound (TO-PRO)
0	0.29
1	0.25
3	0.20
6	0.19
10	0.13
15	0.04
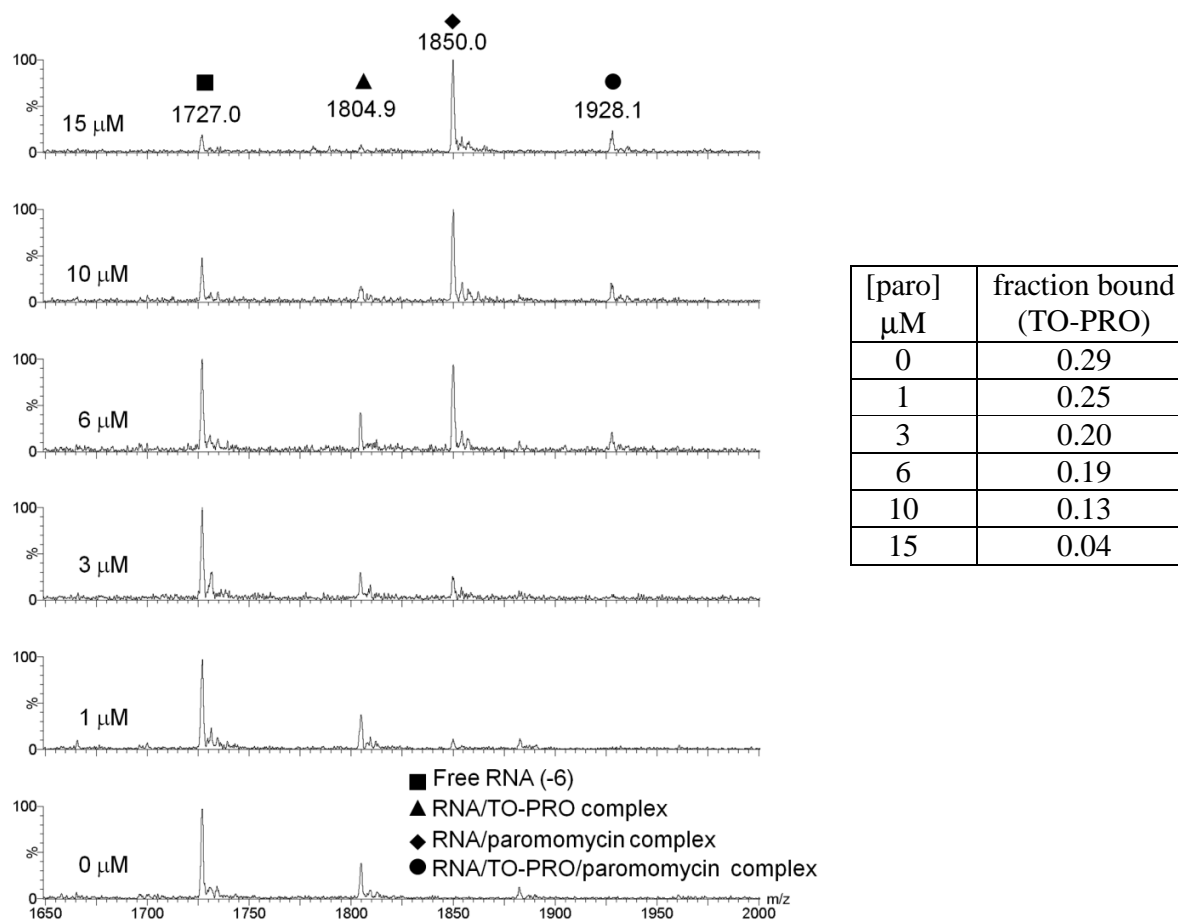
Figure 4.6: ESI-MS spectra showing a titration of paromomycin (0–15 μM) into equimolar concentrations of A-site RNA and TO-PRO complex (1 μM). Buffer conditions are 150 mM ammonium acetate, pH 7. The insert table shows quantification of the ESI-MS peak areas of the TO-PRO:A-site RNA complex after titration with 0–15 μM of paromomycin.

4.4.4 A-Site RNA and Chloramphenicol

Chloramphenicol is a potent antibiotic that binds to 23 S rRNA in the petidyl-transferase center of the ribosome and inhibits protein synthesis.[260-262] Chloramphenicol was chosen to serve as negative control because it is a strong RNA binder, but is not known to bind to the A-

site RNA. A titration of chloramphenicol into the A-site/TO-PRO complex showed no significant

change in fluorescence, even after addition of 31 µM of Chloramphenicol (**Figure 4.7**) In

contrast, more than 70% reduction in fluorescence was observed in the case of paromomycin

(**Figure 4.4**).
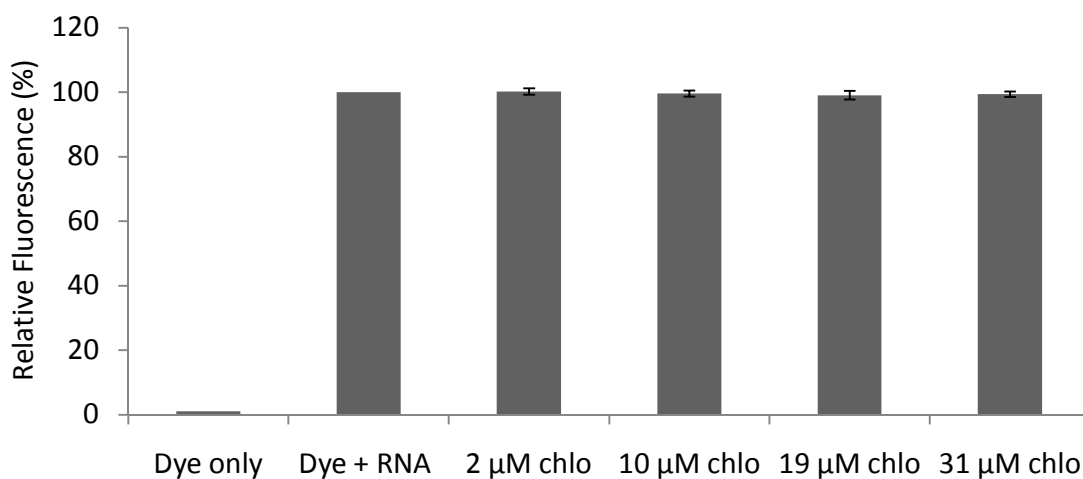
Figure 4.7: FID assay results with chloramphenicol are given. Equimolar concentrations of A-site RNA and TO-PRO (1 µM) were pre-bound in buffer (150 mM ammonium acetate, pH 7) prior to chloramphenicol addition. An average of three separate experiments is shown.

The ESI-MS data also confirm the FID result with chloramphenicol. There was no

significant change in peak areas of the RNA:TO-PRO complex upon addition of 100 µM of

chloramphenicol (**Figure 4.8**). There was no observable peak representing the binding of

chloramphenicol to the A-site RNA, which was expected at an m/z value of 1790. A control scan

confirmed that at 40 µM of chloramphenicol, there is a high concentration of chloramphenicol

in the injected solution as compared to RNA (inset of **Figure 4.8**). This result would be consistent with example **4** in **Figure 4.5**.

[chlo] μM	fraction bound (TO-PRO)[a]
0	0.23
5	0.26
40	0.29
100	0.26
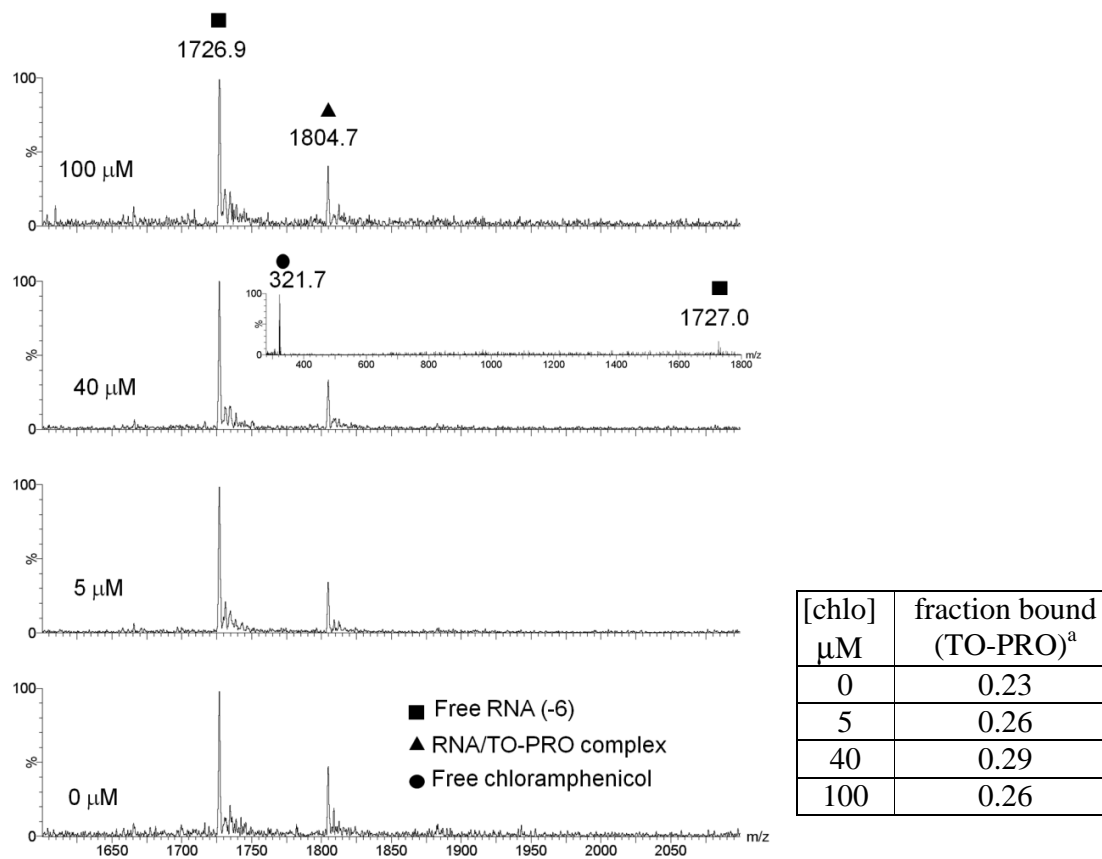
Figure 4.8: ESI-MS spectra show a titration of chloramphenicol into equimolar concentrations of A-site RNA and TO-PRO complex (1 μM). Buffer conditions are 150 mM ammonium acetate, pH 7. Insert shows the relative concentrations free RNA and free chloramphenicol after 40 μM of chloramphenicol was titrated into the pre-bound A-site RNA and TO-PRO complex. The insert table shows quantification of the ESI-MS peak areas of TO-PRO:A-site RNA complex after titration with 0–100 μM of chloramphenicol.

4.4.5 TAR RNA and Tat

Human immunodeficiency virus type 1 (HIV-1) gene expression is controlled by binding of a viral regulatory protein, known as the trans-activator of transcription (Tat), to its RNA target, the trans-activation responsive region (TAR).[118-120] This Tat-TAR interaction is crucial for the successful replication of HIV-1.[118-120] Consequently, disruption of this Tat-TAR interaction has been a good prospect for developing new HIV therapies.[263-265] Studies have identified the minimal motifs for the specific interaction of Tat-TAR to be the 9mer basic amino-acid region of Tat (residues 49-57) and the UCU bulge of the TAR RNA (**Figure 4.2** and **Figure 4.11**).[263-265] This well-characterized Tat-TAR system was used in the modified FID assay.

FID and ESI-MS experiments were both carried out using the Tat-TAR system. The FID results from the Tat-TAR system show a similar trend as observed with the A-site/aminoglycoside system. Upon addition of 31 μM Tat peptide, a 70% decrease in fluorescence is observed (**Figure 4.9**). The reduction in fluorescence was confirmed by using ESI-MS to be due to the displacement of pre-bound TO-PRO from the TAR RNA (**Figure 4.10**).
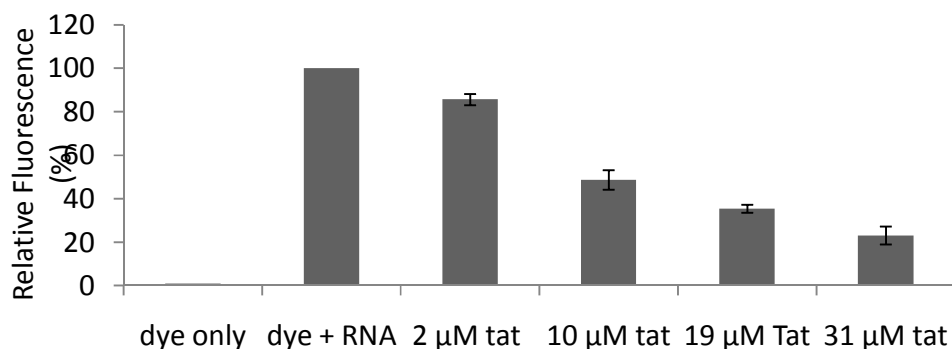
Figure 4.9: FID assay of Tat peptide utilizing pre-bound equimolar concentrations of TAR RNA and TO-PRO (1 µM each). Buffer conditions were 150 mM ammonium acetate, pH 7. The data shown is an average of three separate experiments.
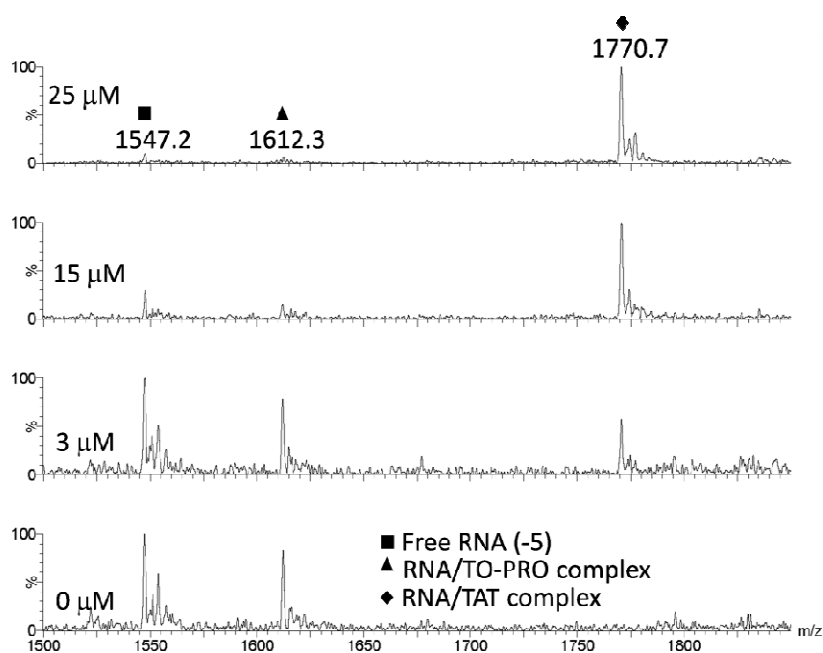
[Tat] µM	fraction bound (TO-PRO)
0	0.42
3	0.35
15	0.13
25	0.05

Figure 4.10: ESI-MS spectra showing a titration of Tat peptide into equimolar concentrations of TAR RNA and TO-PRO complex (1 µM). Buffer conditions are 150 mM ammonium acetate, pH 7. The insert table shows quantification of the ESI-MS peak areas of TO-PRO:A-site RNA complex after titration with 0–25 µM Tat peptide.

4.4.6 FID Screening Results with RNA Constructs and Ligands

As shown in the previous sections, two well-studied RNAs and known ligands were used to validate the modified FID assay with TO-PRO, namely the Tat-TAR system [119, 266-267] and the A-site RNA-aminoglycoside (paromomycin) system.[92, 268-270] Since the binding sites of paromomycin and Tat are well characterized, these results suggest that the TO-PRO dye molecule associates with the RNAs in the secondary structure elements, namely the nucleotide bulge regions. Our next goal was to test new ligands against the A-site RNA and TAR RNA, and carry out FID with previously untested RNA model systems, namely helix 69 (H69) and helix 31 (h31). These RNAs represent functionally important sites of the bacterial ribosome. H69, from the large subunit of the ribosome, is located in the intersubunit bridge B2a region and makes important contacts with the small ribosomal subunit, A- and P-site bound tRNAs, as well as translation factors.[103-104] This RNA contains two modified nucleotides, pseuduridine (Ψ) and 3-methylpseudouridine ($m^3\Psi$), which can be inserted into the RNA model systems by using synthetic approaches.[271] The small subunit hairpin h31 is located in the 970-loop region of 16S rRNA. Helix 31 serves as a promising drug target because it is located near the P-site (peptidyl-tRNA site) and is proposed to be involved in the decoding process.[105-107] This region is also modified, but we chose the unmodified variant for this study. The h31 and H69 RNAs contain secondary structure elements that differ from the A-site RNA and TAR RNA, such as larger loop regions and nucleotide mismatches.

The FID assay was used to identify ligands for the four RNA constructs shown in **Figure 4.2**. The structures of the ligands employed are shown in **Figure 4.11**. Among the compounds screened, the cationic aminoglycosides, paromomycin and neomycin, are known to target the A-site RNA.[92] Simplified aminoglycoside, or single-ring derivatives of paromomycin, referred to as DHR23, DHR36, DHR37, DHR42, and DHR51, were also screened. These compounds were designed with the goal of retaining their RNA-binding ability, but reducing their affinity for resistance enzymes, which are known to modify aminoglycosides and reduce their association with RNA.[205, 272] KkN is a tri-peptide containing D-lysine (k) that was selected by Hwang and coworkers to target TAR RNA.[273] CR1119 is a peptide-based compound that contains potential intercalating groups for nucleic-acid binding.
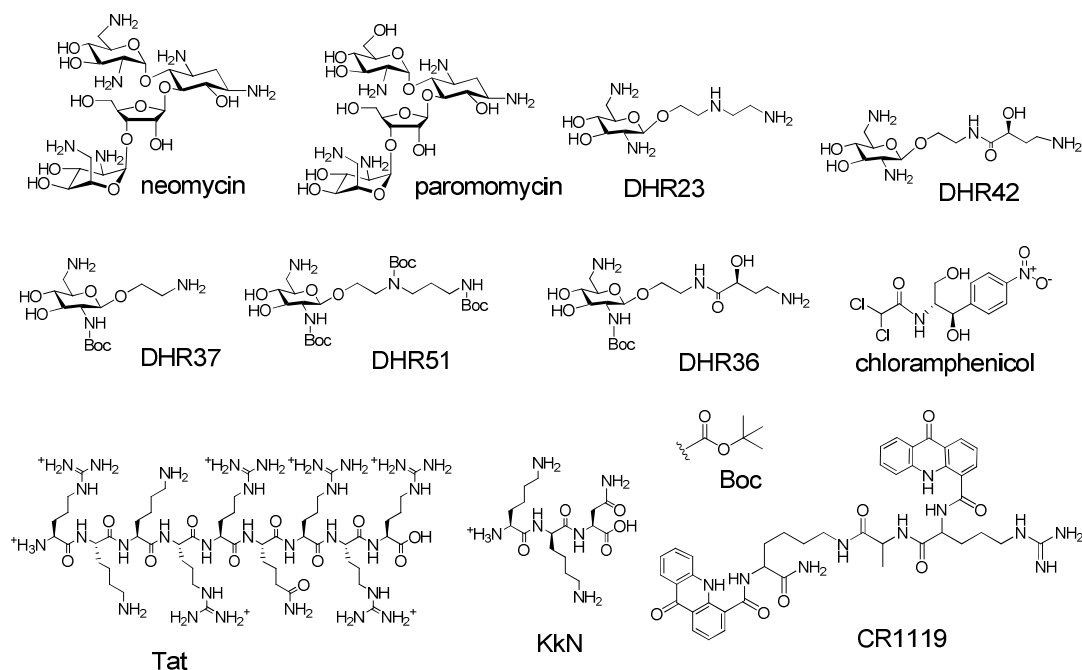
Figure 4.11: The RNA binding ligands used in this study are shown.

The results of the screen reveal that FID is a promising method for rRNA or TAR RNA ligand discovery. The assay was suitable for RNAs with different sequences and secondary structures, as well as modified nucleotides. Perhaps not surprising, the cationic RNA ligands, paromomycin, neomycin, and Tat, show binding to all four constructs, the A-site, h31, H69, and TAR RNAs (**Figure 4.12**).
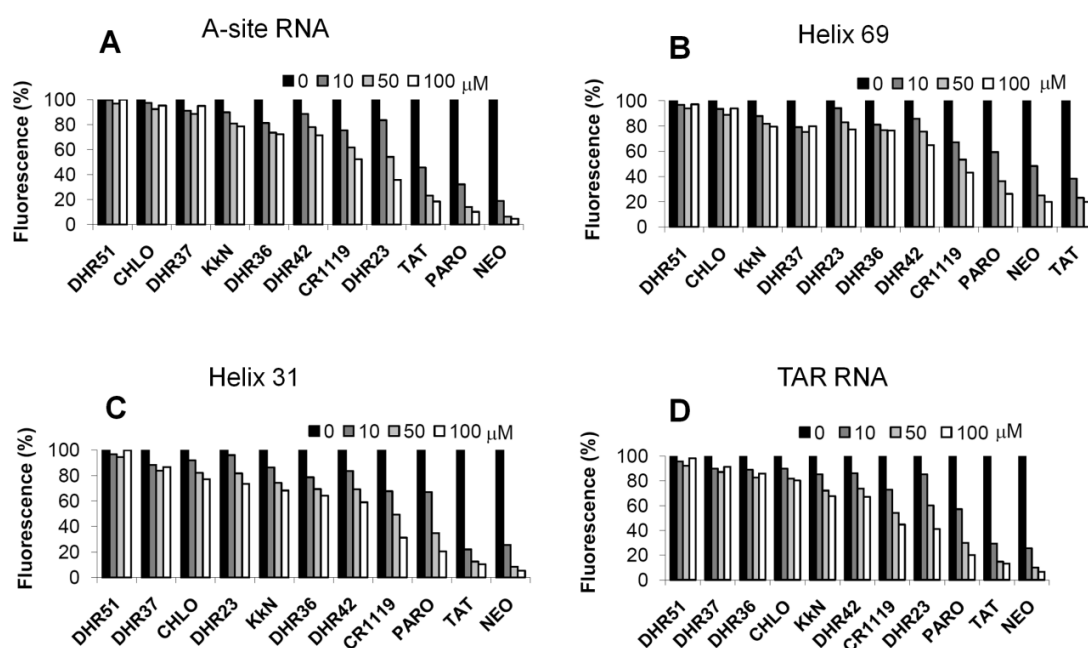
Figure 4.12: FID screening results obtained for the different RNA constructs upon addition of ligand concentrations ranging from 0–100 µM: A) A-site RNA, B) H69 RNA, C) h31 RNA, and D) TAR RNA (buffer conditions are 20 mM Tris, 100 mM KCl, pH 7).

As expected chloramphenicol, which is known to be specific for the peptide exit tunnel in the 50S rRNA,[261-262] had only slight affinity for the RNA constructs. DHR23, a single-ring analogue of paromomycin, had a slight preference for the A-site RNA and TAR RNA, and CR1119 had a preference for h31 (**Figure 4.12**). In contrast, DHR51, which is similar in structure to

DHR23 but contains *tert*-butyloxycarbonyl (BOC) groups at the amine positions (**Figure 4.11**), had reduced affinity to all of the RNA constructs.

The FID results for paromomycin and DHR23 with H69 and A-site RNA were further evaluated by ESI-MS. Dissociation constants obtained from ESI-MS experiments show that DHR23 has a higher affinity for A-site RNA as compared to H69 (K_d = 19 and 42 µM, respectively). Paromomycin also demonstrated a higher affinity for the A-site RNA as compared to H69 (K_d = 1.3 and 21 µM, respectively). These dissociation constants are therefore consistent with the FID data (Table 4.1).

Table 4.1: Comparison of the FID results and dissociation constants for DHR23 and paromomycin binding to H69 and A-site RNA.

	DHR23		paromomycin	
	fluorescence (%)	K_d (µM)[a]	fluorescence (%)	K_d (µM)[a]
A-site RNA	54	19	14	1.3
H69	83	42	36	21

In summary, a modified FID assay for RNA applications has been developed and the ESI-MS data provide molecular evidence that correlates the reduction in fluorescence observed in the FID assay with the displacement of the TO-PRO dye molecule from RNA. FID with TO-PRO is an appropriate method for obtaining relative binding affinities of a variety of ligands to RNA, including amino sugars, peptides, and planar aromatic compounds. The FID assay will be amenable to high-throughput screening because it is a sensitive, fluorescence-based method

that can be done on a 96- or 384-well plate format. The system is compatible with cationic buffer components, including Mg^{2+}, Na^+, and K^+, which are not suitable for ESI-MS screening. The moderate selectivity of DHR23 for the A-site and TAR RNAs relative to the ribosomal targets H69 and h31 is encouraging. In contrast, the aromatic compound CR1119 has a slight preference for h31, which contains a six-nucleotide loop and mismatch at the loop-closing base pair. These results suggest that generation of compounds based on these simplified structures in combination with FID screening may lead to selective reagents for RNA internal bulges, loops, mismatches, or other unique secondary structure elements.

CHAPTER 5

SPECIFICITY OF DHR23

5.1 Abstract

Aminoglycosides are known to be promiscuous ligands. Their ability to bind to a wide variety of RNAs has been exploited for new applications in HIV and genetic disease therapy. Investigating the specificity of aminoglycosides is worthwhile in order to understand their mode of action, and also to identify new drug targets.

In this study, the specificity of DHR23 (a single-ring analogue) and its parent compound paromomycin were tested for binding to a variety of RNA models using electrospray ionization mass spectrometry (ESI-MS). The results show that DHR23 has preferred binding to structured RNA as compared to ssRNA, as well as a modest preference for the A-site RNA. The absence of the other three rings of paromomycin reduced the affinity of DHR23 for the A site RNA by about 10-fold. Even with the reduction in affinity, DHR23 was still able to retain a slight level of selectivity for the A-site RNA.

5.2 Introduction

Aminoglycosides are a group of antibiotics that have been used successfully against many disease-causing bacteria.[111-112] They work by binding to the highly conserved region of the ribosome (A site) and inhibit protein synthesis.[274-275] In spite of its success, aminoglycoside therapy is associated with severe side effects, which may be due to the binding of

aminoglycosides to other targets besides the A site.[276] The promiscuity of aminoglycosides is not a new phenomenon; they have been reported bind to a variety of RNA structures, including TAR RNA,[277] mRNA,[278] and the hammerhead ribozyme.[279] Their lack of selectivity has been attributed to their electrostatically driven binding mode and conformational flexibility.[280-281] However, some studies have shown that aminoglycosides do have a strong preference for structured RNA and A-form RNA.[282] Also, the flexibility around their glycosidic bonds provides an advantage to target conformationally flexible RNAs such as the A site.[237, 283-285] Therefore, in spite of the fact that aminoglycosides are recognized for their promiscuity, studies suggest that there may be certain sequence-structure and conformation-dependent elements in their recognition of their target RNAs.[87, 282-283]

In this study, the specificity of DHR23; a single-ring aminoglycoside analogue discussed in Chapter 3 and its parent compound paromomycin were tested against a variety of RNA models using electrospray ionization mass spectrometry (ESI-MS). Among the RNA models used are an A-site RNA duplex and the A-site RNA hairpin model, which has an artificial GNRA tetraloop added to increase stability (**Figure 5.1**).[207] GNRA teteraloops are very common structural motifs found in rRNA.[286-287] They serve as protein binding sites and participate in tertiary structure interactions that contribute to the formation of proper three-dimensional structures.[286] There have been several reports of aminoglycosides binding to hairpin loops.[288] The reason for choosing this pair (duplex and hairpin A-site models) is to determine whether the affinity of the ligands for the A-site RNA is affected by the artificial tetraloop in the A-site RNA hairpin model. Furthermore, helix 69 (H69) of the large ribosomal subunit and helix 31

(h31) of the small ribosomal subunit represent functionally important sites of the bacterial ribosome. H69 is located in the inter-subunit bridge, B2a, and makes important contacts with the small ribosomal subunit, A- and P-site bound tRNAs, as well as translation factors.[103-104] Helix 31 is the 970-loop region located in the 16 S rRNA. It serves as a promising drug target because it is located near the P site and it is proposed to be involved in the decoding process.[105-107] Other RNA models used the bacterial A-site mutant RNA, human A-site RNA, and a 16-nucleotide single-stranded RNA.

5.4 Experimental

5.4.1 RNA Preparation

The RNA hairpins with the following sequences were purchased from Dharmacon Research Inc. (Lafayette, CO):

5'-GGCGUCGUACUUCGGUAAAAGUCGCC -3' (human A-site)

 5'-CAGCGUCACACCACCC -3' (A-strand),

5'- CAGCGUCAUCACCACCC-3'

5'-GGUGGUGAAGUCGUGG -3' (A-site duplex), and

5'-CAGCGUCAUCACCACCC -3'

5'-GGUGGUGAAGUCGCUGG -3' (A-site mutant),

Information for the other RNAs used in this study was provided in Chapter 4. The RNAs were deprotected and purified as previously described in Chapter 3. The concentrations of RNAs

were determined using Beer's law with the following single-stranded extinction coefficients: $\varepsilon_{260\ nm}$ of 252,900 $M^{-1}cm^{-1}$ for human A-site, 143,300 $M^{-1}cm^{-1}$ for A-strand RNA, 316,800 $M^{-1}cm^{-1}$ for A-site duplex, and 322,000 $M^{-1}cm^{-1}$ for A-site mutant.[224]

5.4.2 Electrospray Ionization Mass Spectrometry (ESI-MS)

Electrospray ionization mass spectrometry (ESI-MS) experiments were performed on a Quattro LC tandem quadrupole mass spectrometer equipped with electrospray ionization in the negative ion mode (Micromass, Manchester, UK). The tuning parameters, sample preparation, data processing and dissociation constant determination were discussed previously in Chapters 2 and 3.

5.3　Results and Discussion

As determined by ESI-MS, paromomycin had the same affinity for both the A-site hairpin and the A-site duplex RNA (1.3 μM). Buffer conditions used were 150 mM ammonium acetate pH 7 (**Figure 5.1**). Similarly, there was no significant difference observed between the affinity of DHR23 for the A-site hairpin and A-site duplex RNAs (K_ds were 19 μM and 20 μM, respectively; Figure 5.1). This result suggests that the teteraloop had no significant effect on the affinity of the two ligands for the A-site RNA.

Figure 5.1: A) The chemical structures of the ligands tested for specificity are shown. B) A summary of affinities of DHR23 and paromomycin for the different RNA constructs is given. The conserved A-site sequence from the bacterial 16 S rRNA is highlighted in black on the A-site hairpin, A-site duplex, and A-site mutant, and for comparison, indicated on the 18 S rRNA construct. The nucleotides that differ from the bacterial 16 S rRNA A site are highlighted in blue on the A-site mutant and the human A site.

DHR23 and paromomycin were both able to discriminate between the A-site duplex RNA and an A-site mutant RNA. As compared to the A-site RNA, the A-site mutant has a uridine in the internal bulge region, affording base pairing between uridine and adenosine just below the A·A mismatch (**Figure 5.1**). The ESI-MS spectra and binding curves as well as the RNA structures are shown in **Figures 5.2** to **5.30.** This base pairing disrupts the formation of the internal bulge, leading to reduced binding affinity of DHR23 and paromomycin to the A-site mutant. This result suggests that the internal bulge structure is important for binding of both paromomycin and DHR23 to the A site.

Nucleotides 1404-1407 and 1492-1497 are universally conserved in all 16 S rRNA of bacteria (**Figure 5.1A**).[289] The highly conserved nature of this region of the ribosome suggests that its function is dependent on the sequence.[289] Aminoglycosides preferentially target bacterial over eukaryotic ribosomes.[290] The only difference between the nucleotide sequence of the bacterial and the eukaryotic A site internal bulge is the presence of an adenosine at position 1408 in bacteria and a guanosine in eukaryotes (highlighted in blue on the human A-site RNA structure in **Figure 5.1**).[289] Consequently, an A1408G mutation in *E. coli* confers a high level of resistance to aminoglycosides with a 6′ NH_2 (*e.g.*, neomycin) and low level resistance to aminoglycosides with a 6′ OH (*e.g.*, paromomycin).[197] Our data is consistent with previous results; DHR23 and paromomycin both had a higher preference for the bacterial A-site RNA as compared to the human A-site RNA. This result further corroborates structure,[291] studies suggesting that the binding pocket created A1408 and A1492 base pair present in the bacterial

A site cannot be mimicked by replacement with a G1408 and A1492 base pair, such as the one present in the human ribosomal A site.[291]

Aminoglycoside antibiotics have been recently reported to bind to H69;[292-293] therefore, it was not surprising that in our hands, paromomycin had moderate affinity to H69 (K_d of 21 µM). Helix 31 displayed two-fold weaker binding to paromomycin compared to helix 69. DHR23 on the other hand had weaker affinity for both H69 and h31 (47 µM and 95 µM, respectively; (**Figure 5.1**). Compared to H69, h31 has a bigger hairpin loop. These two RNAs also contain different mismatch base pairs and different modified nucleotides. Crystal structure data indicate that neomycin binds to the stem region of H69, in the vicinity of the G1907·U1923 mismatch.[293] Ring I of neomycin makes contacts with G1906, and ring II interacts with G1921 and U1923.[293] This region of H69 adopts a conformation similar to that of the A-site internal bulge. The tertiary structure of h31 on the other hand adopts a conformation completely different from H69 and the A-site RNA (**Figure 5.2**). This structure may be unsuitable to provide appropriate contacts for either paromomycin or DHR23 to bind. H69 was able to accommodate the parent aminoglycoside more readily than the smaller derivative. Clearly rings II-IV of paromomycin play a role in governing selectivity, and future designs of selective compounds will have to take that into consideration. Since aminoglycosides prefer to bind to structured RNA,[282] it was not surprising that both ligands had poor affinity for the A-strand RNA (**Figure 5.1**).

In general, DHR23 has preferred binding to structured RNA as compared to ssRNA, as well as a modest preference for the A-site RNA, as observed with the parent compound

paromomycin (**Figure 5.1**). The absence of the other three rings in DHR23 as compared to paromomycin, reduced its affinity for the A-site RNA by about 10-fold. Even with the 10-fold reduction in affinity, DHR23 was still able to retain a slight level of selectivity for the A-site RNA. These results add some credence to the hypothesis that further reduction of the neamine core to generate A-site selective ligands is possible.
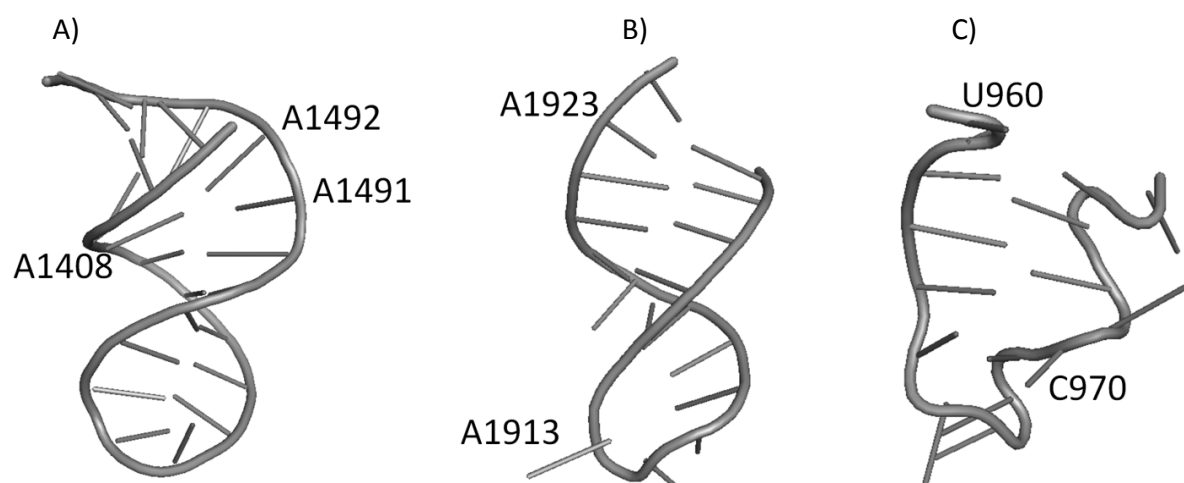
Figure 5.2: A) NMR structure of the bacterial A-site model,[87] B) crystal structure of H69,[77] and C) crystal structure of h31[77] are shown. The figures were generated with PyMOL[49] using the following PDB files: 1A3M, 2WDG, and 2WDI.
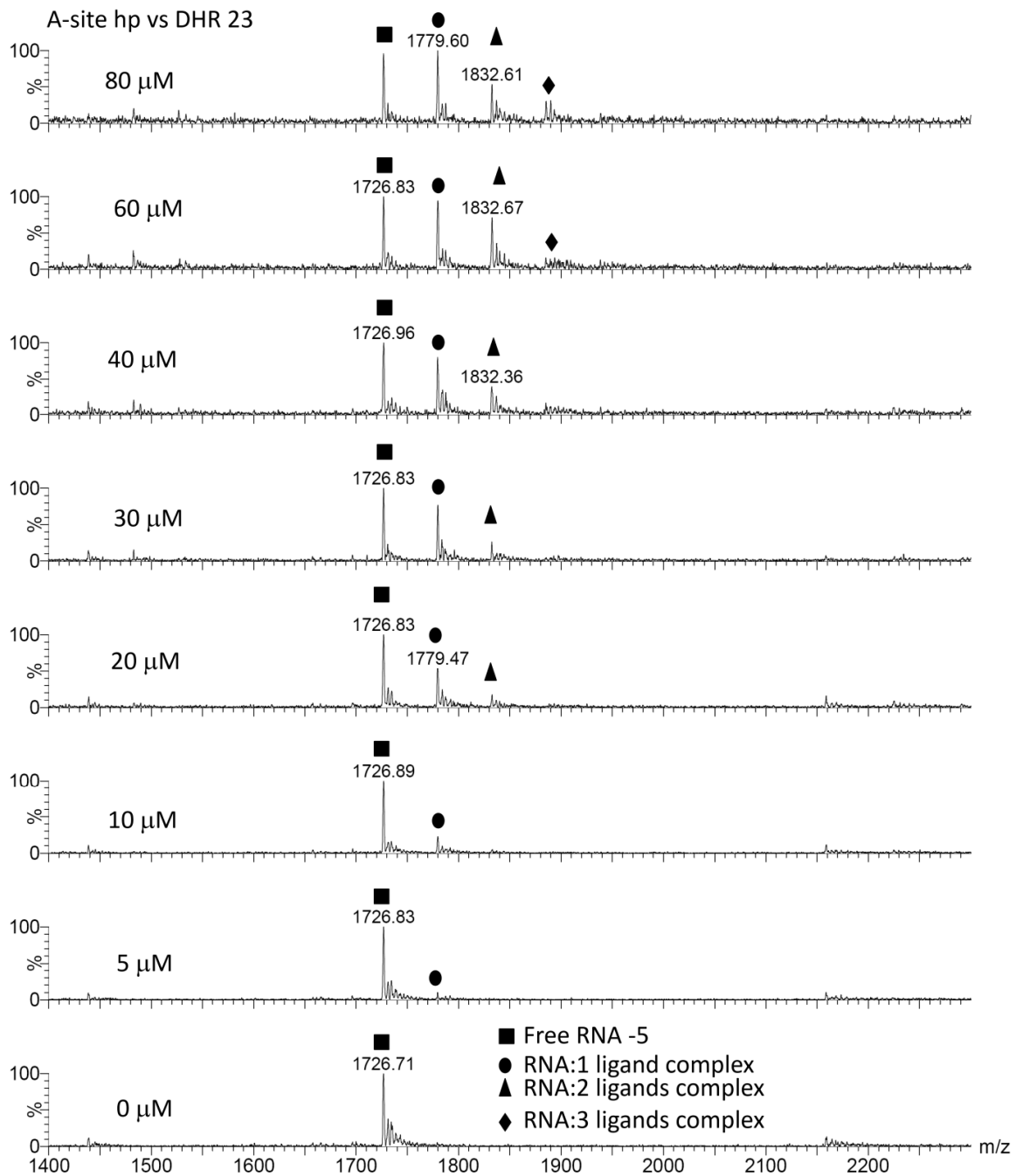
Figure 5.3: ESI-MS spectra of A-site hairpin vs. DHR23 are shown. Buffer conditions were 150 mM ammonium acetate pH 7.
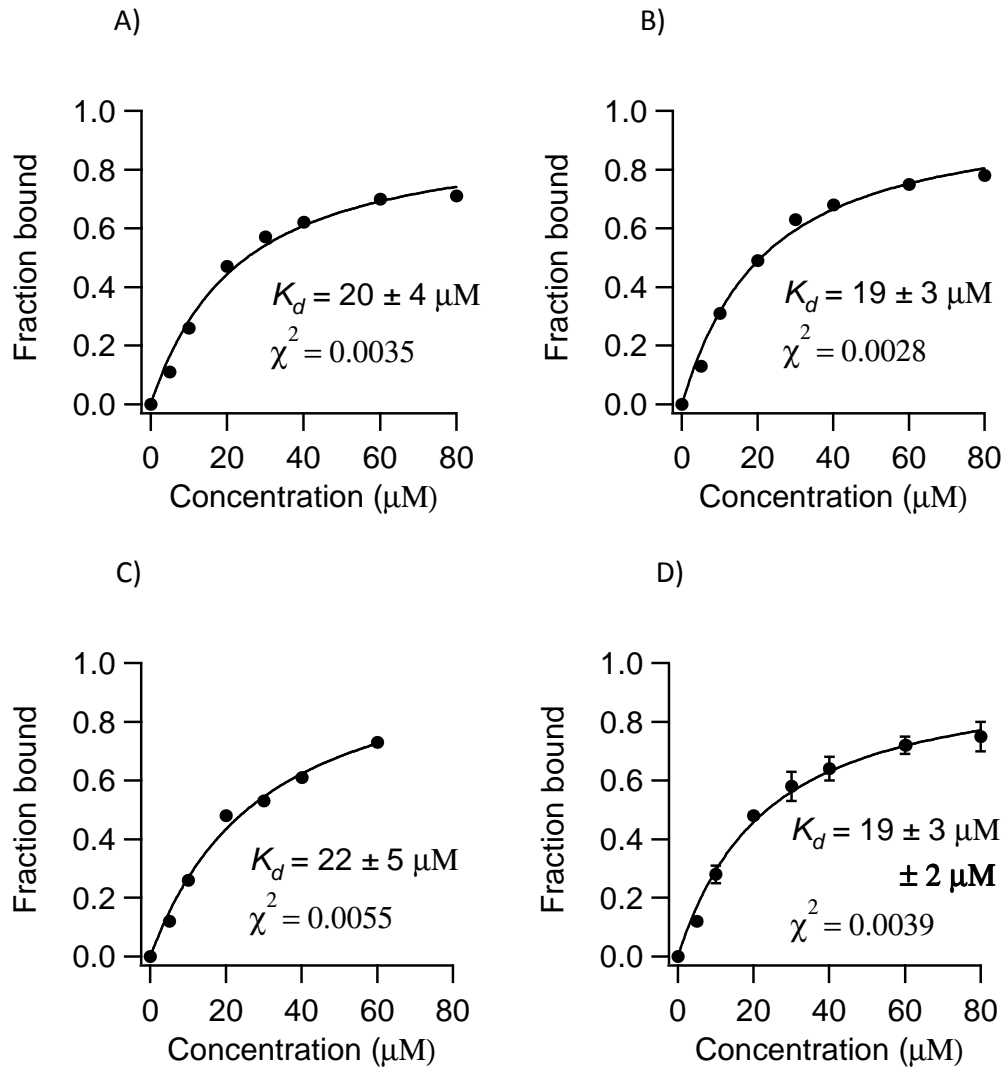
Figure 5.4: Binding curves (A-C) obtained from three different ESI-MS experiments between DHR23 and the A-site hairpin RNA, and (D) the average of the three experiments ± error of fit and **standard deviation** (in bold letters) are shown.

The errors in curves A-C ($\pm$ 4 μM, $\pm$ 3 μM, and $\pm$ 5 μM) represent the error of the fit. In other word, how well the binding model fits the data points. Since curves A-C are single experiments a weighting value of one is given to all the data points, or all data points are assigned the same level of importance. As a result the estimated error may not be accurate. In curve D, the data points represent the average from the three experiments (A-C). The error bars are generated using the standard deviation of each data point in curves A-C. The estimated error ($\pm$ 3 μM), represents how well the binding model fits the data points taking into consideration the weighted value of each data point, based on the standard deviation of the data point. In other words different importance is assigned to each data point based on their standard deviation. This generates a more reliable error estimate. The error in bold letters (**$\pm$ 2 μM**) represents the standard deviation of the three different experiments.

Figure 5.5: ESI-MS spectra of A-site duplex vs. DHR23 are shown. Buffer conditions were 150 mM ammonium acetate pH 7.

Figure 5.6: Binding curves (A-C) obtained from three different ESI-MS experiments between DHR23 and the A-site duplex RNA and (D) the average of the three experiments ± error of fit and **standard deviation** (in bold letters) are shown.
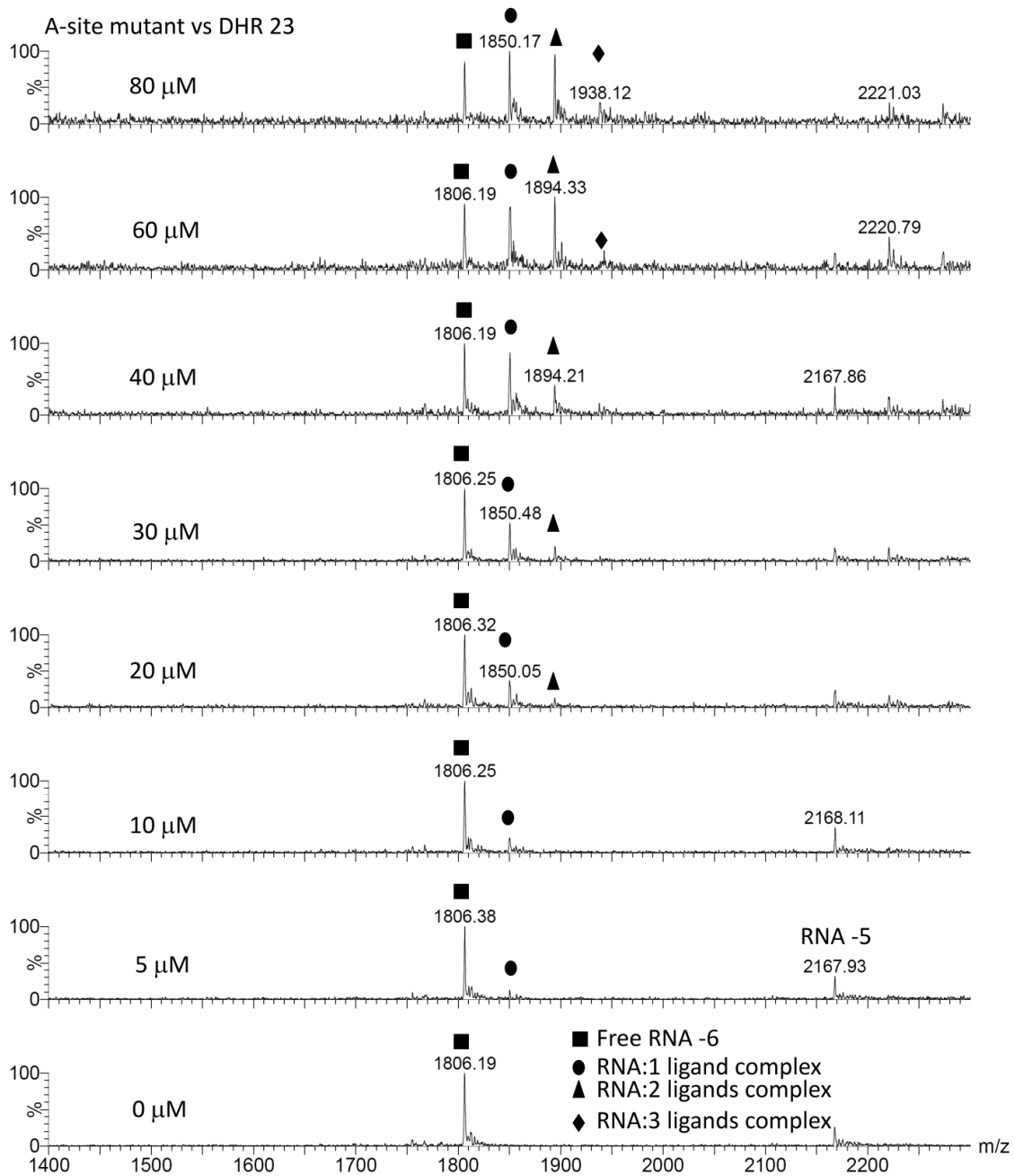
Figure 5.7: ESI-MS spectra of A-site mutant vs. DHR23 are shown. Buffer conditions were 150 mM ammonium acetate pH 7.

Figure 5.8: Binding curves (A-C) obtained from three different ESI-MS experiments between DHR23 and the A-site mutant RNA and (D) the average of the three experiments ± error of fit and **standard deviation** (in bold letters) are shown.
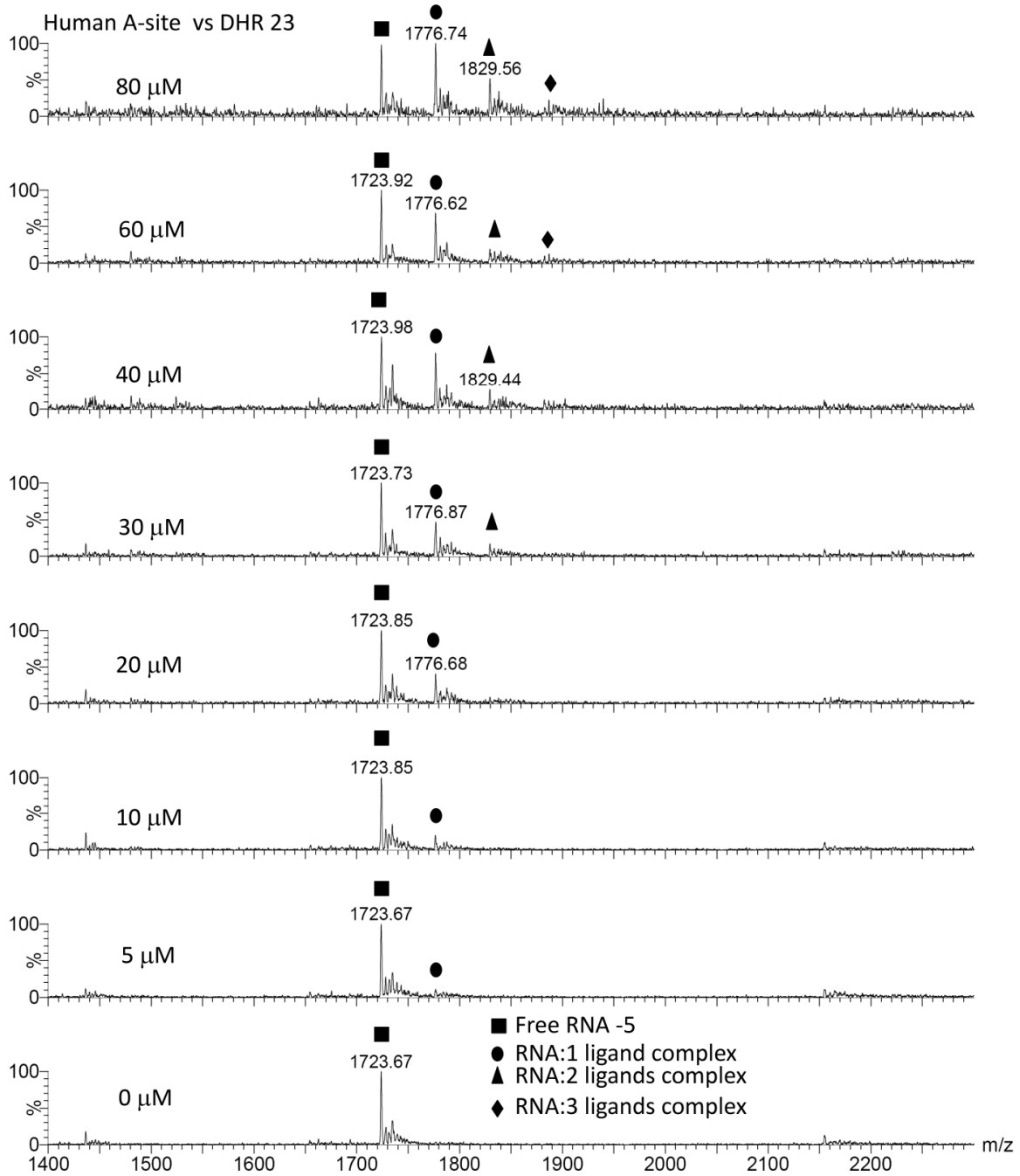
Figure 5.9: ESI-MS spectra of human A-site vs. DHR23 are shown. Buffer conditions were 150 mM ammonium acetate pH 7.
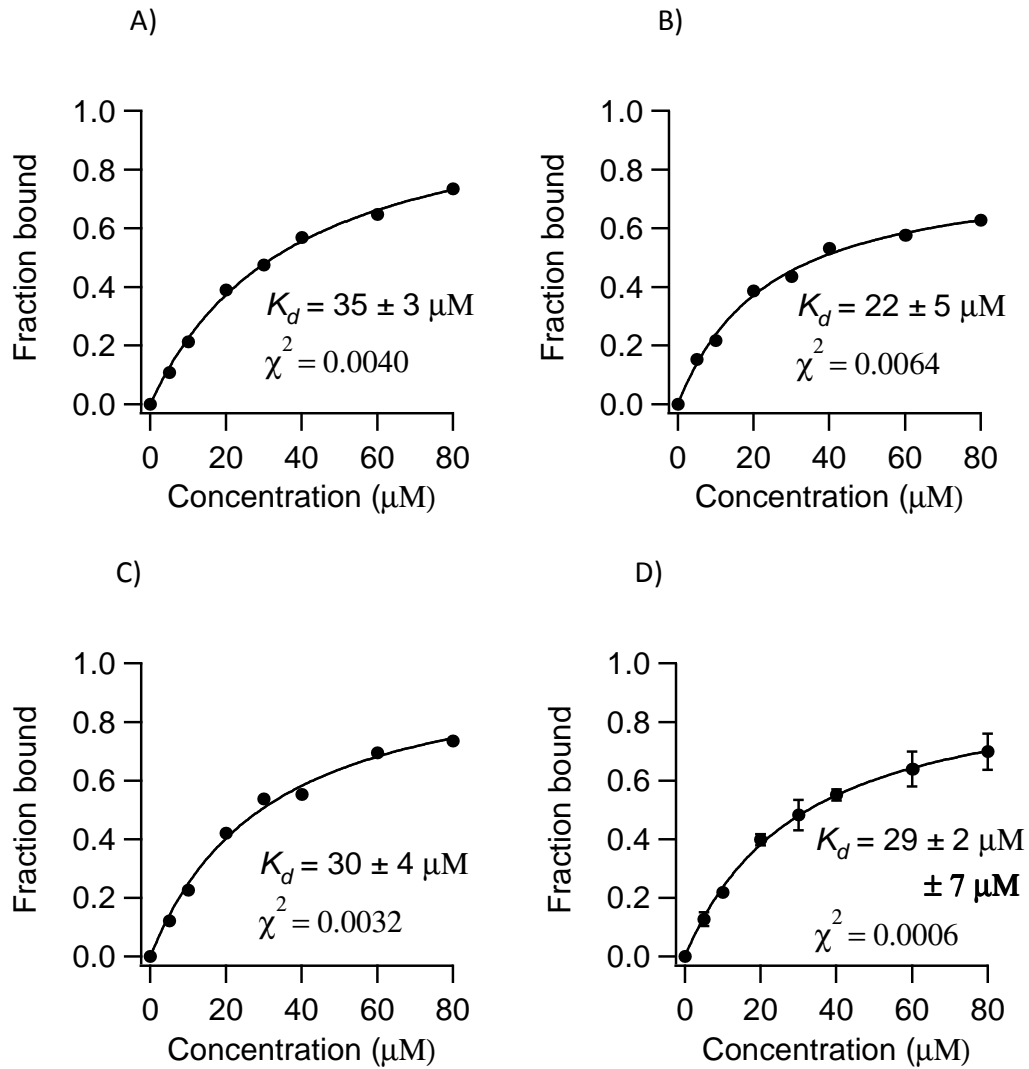
Figure 5.10: Binding curves (A-C) obtained from three different ESI-MS experiments between DHR23 and the human A-site RNA and (D) the average of the three experiments ± error of fit and **standard deviation** (in bold letters) are shown.
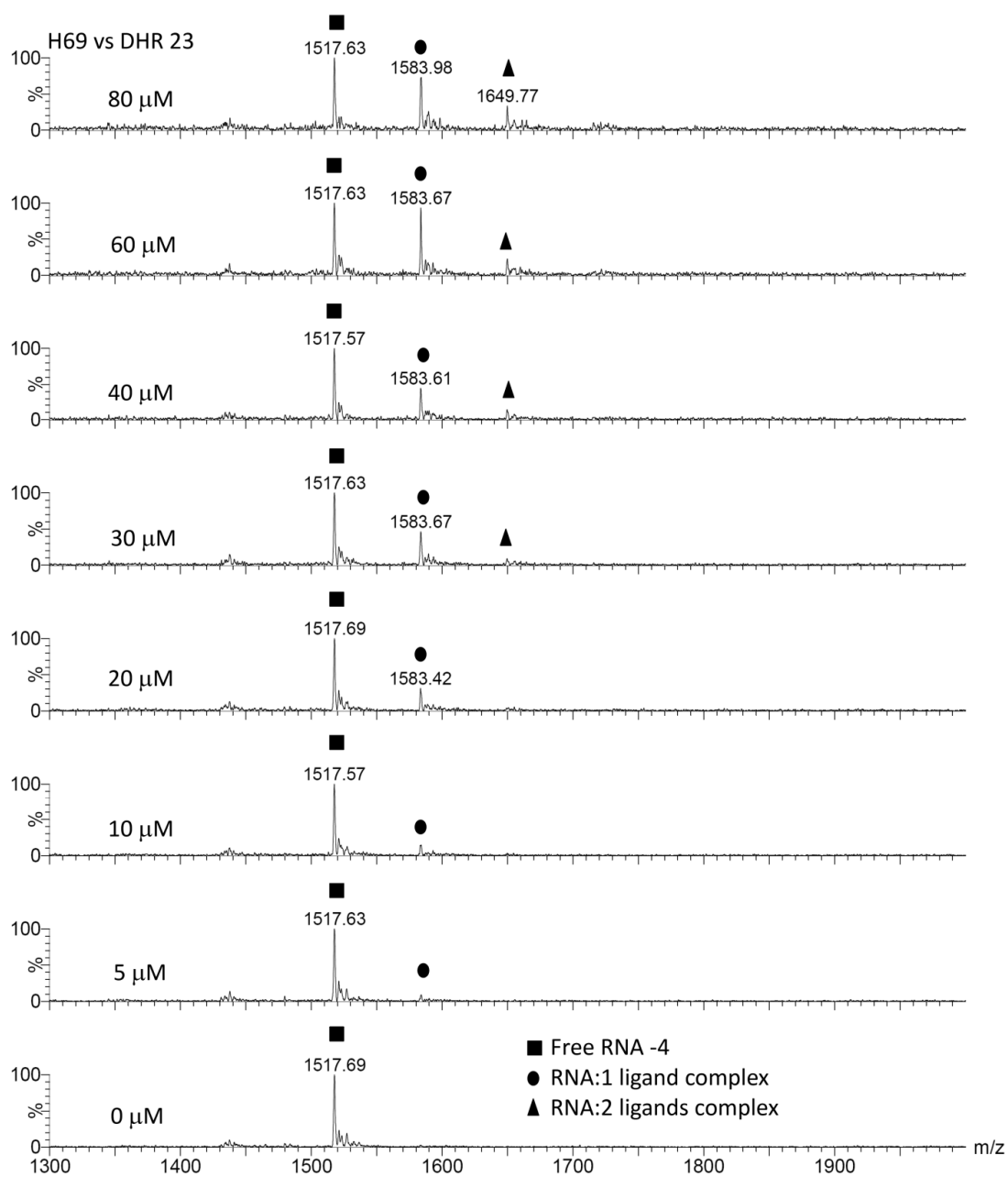
Figure 5.11: ESI-MS spectra of H69 vs. DHR23 are shown. Buffer conditions were 150 mM ammonium acetate pH 7.
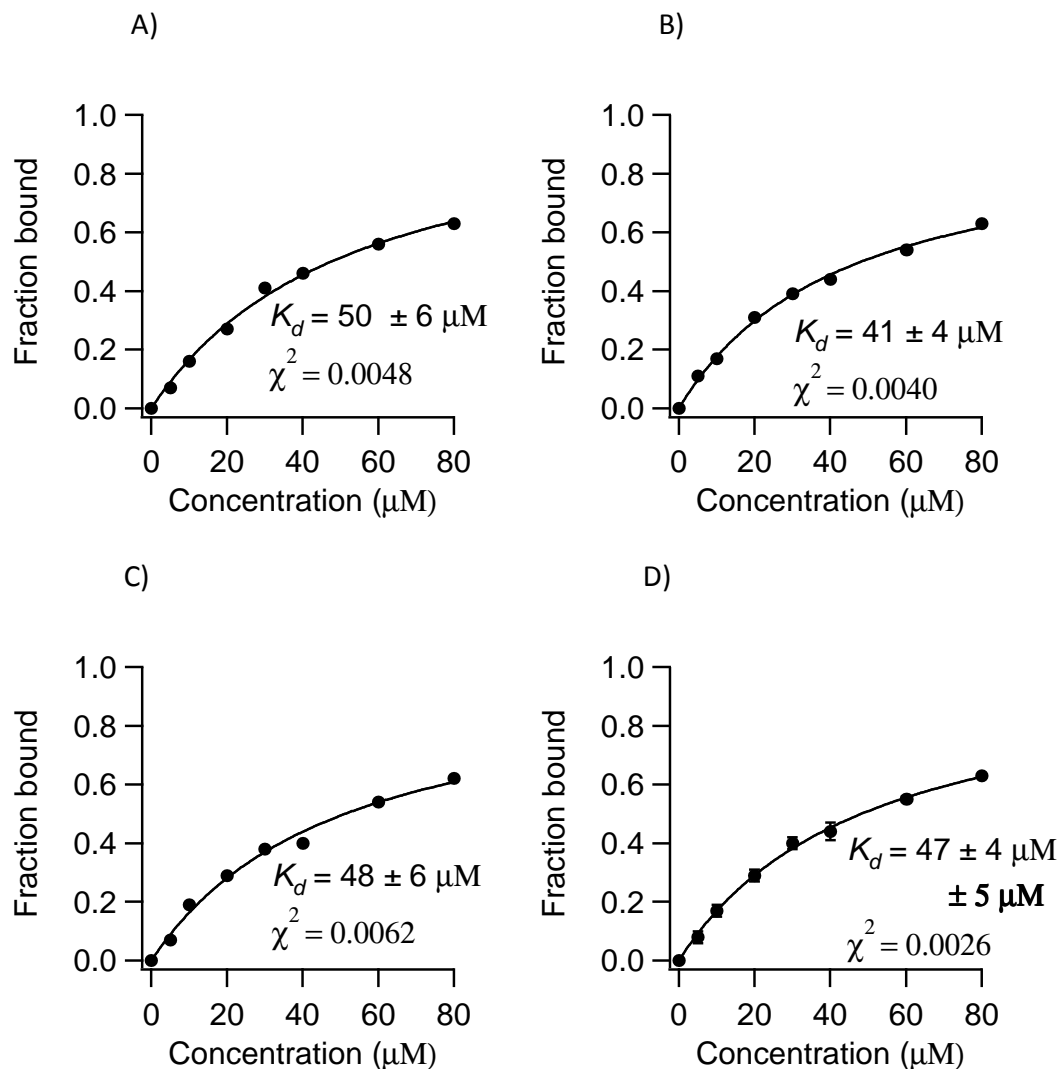
Figure 5.12: Binding curves (A-C) obtained from three different ESI-MS experiments between DHR23 and H69 RNA and (D) the average of the three experiments ± error of fit and **standard deviation** (in bold letters) are shown.
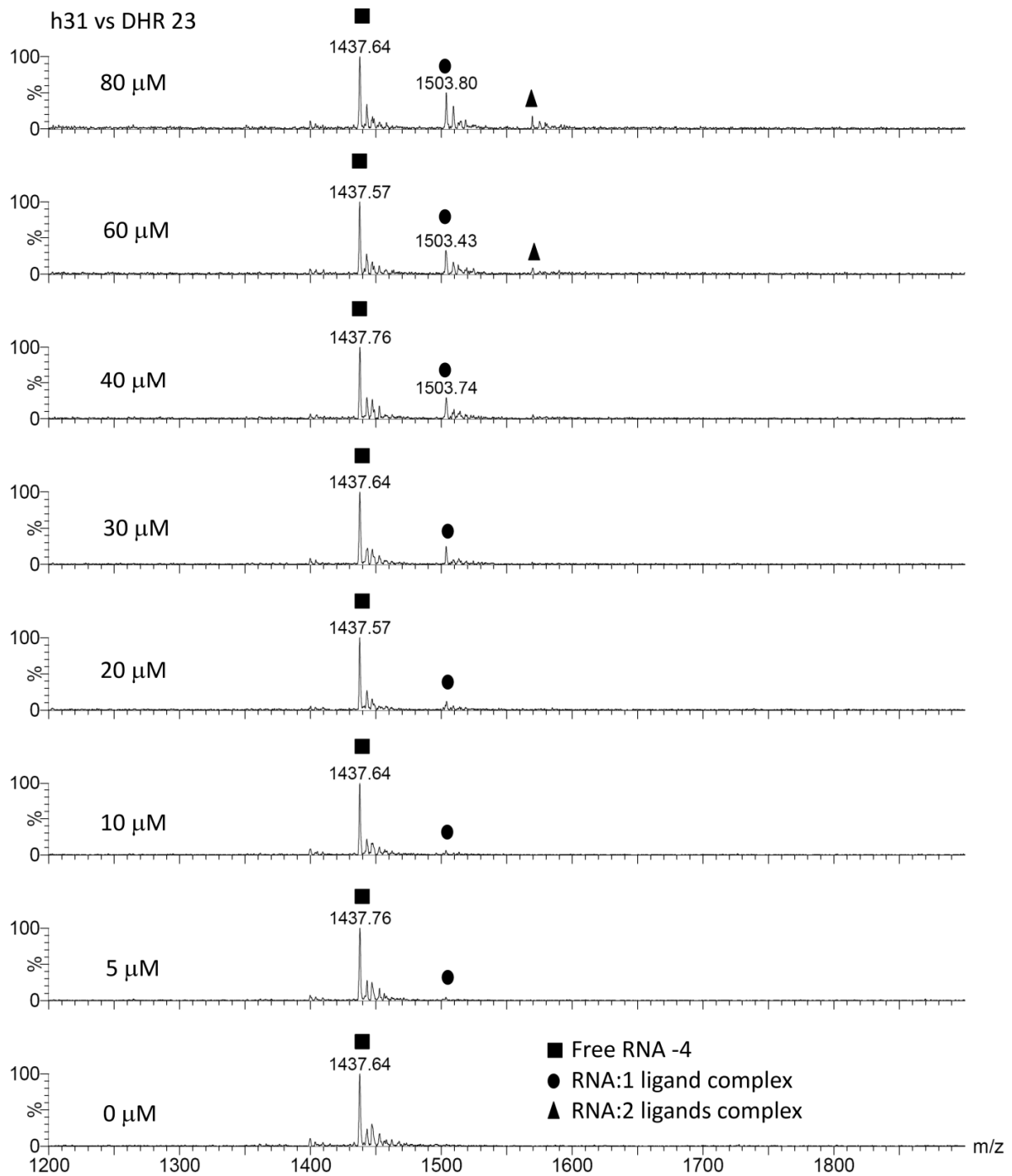
Figure 5.13: ESI-MS spectra of h31 vs. DHR23 are shown. Buffer conditions were 150 mM ammonium acetate pH 7.
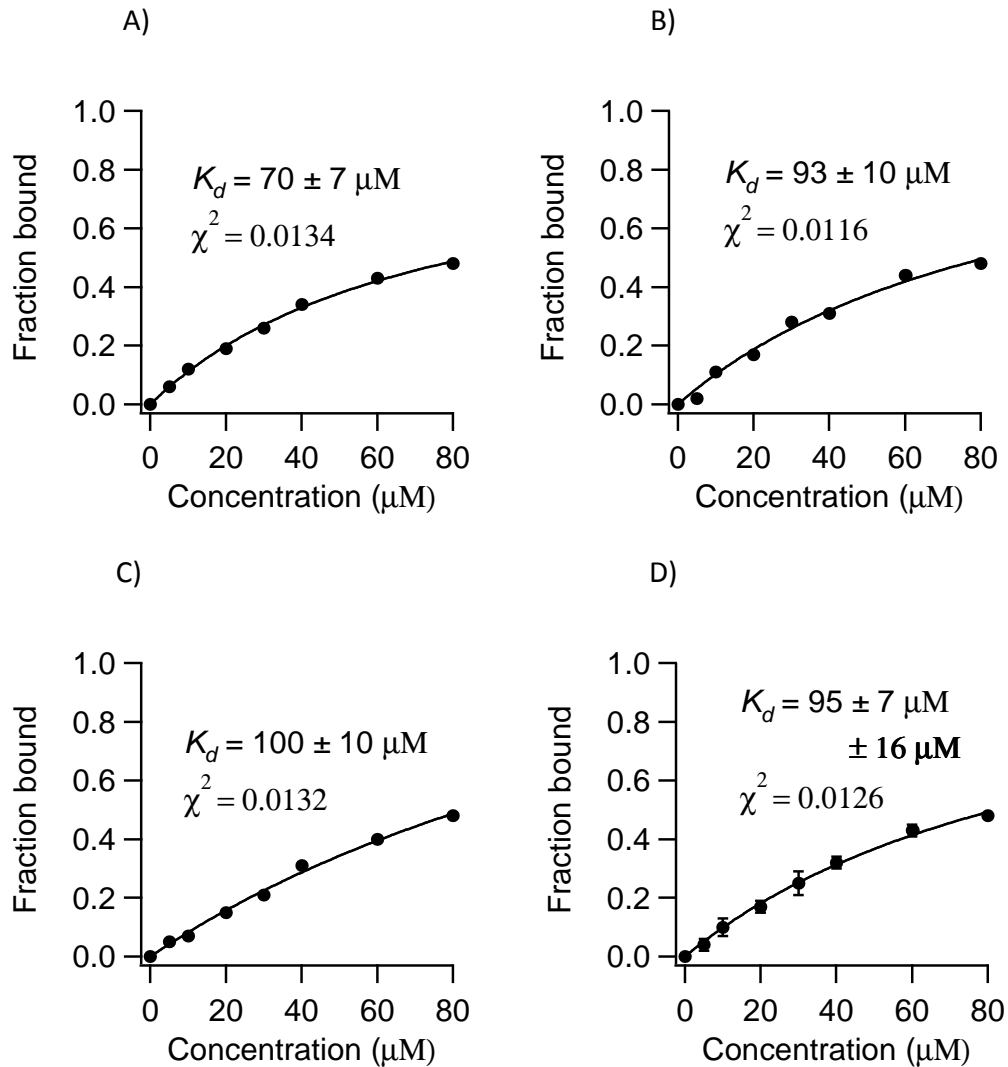
Figure 5.14: Binding curves (A-C) obtained from three different ESI-MS experiments between DHR23 and h31 RNA and (D) the average of the three experiments ± error of fit and **standard deviation** (in bold letters) are shown.
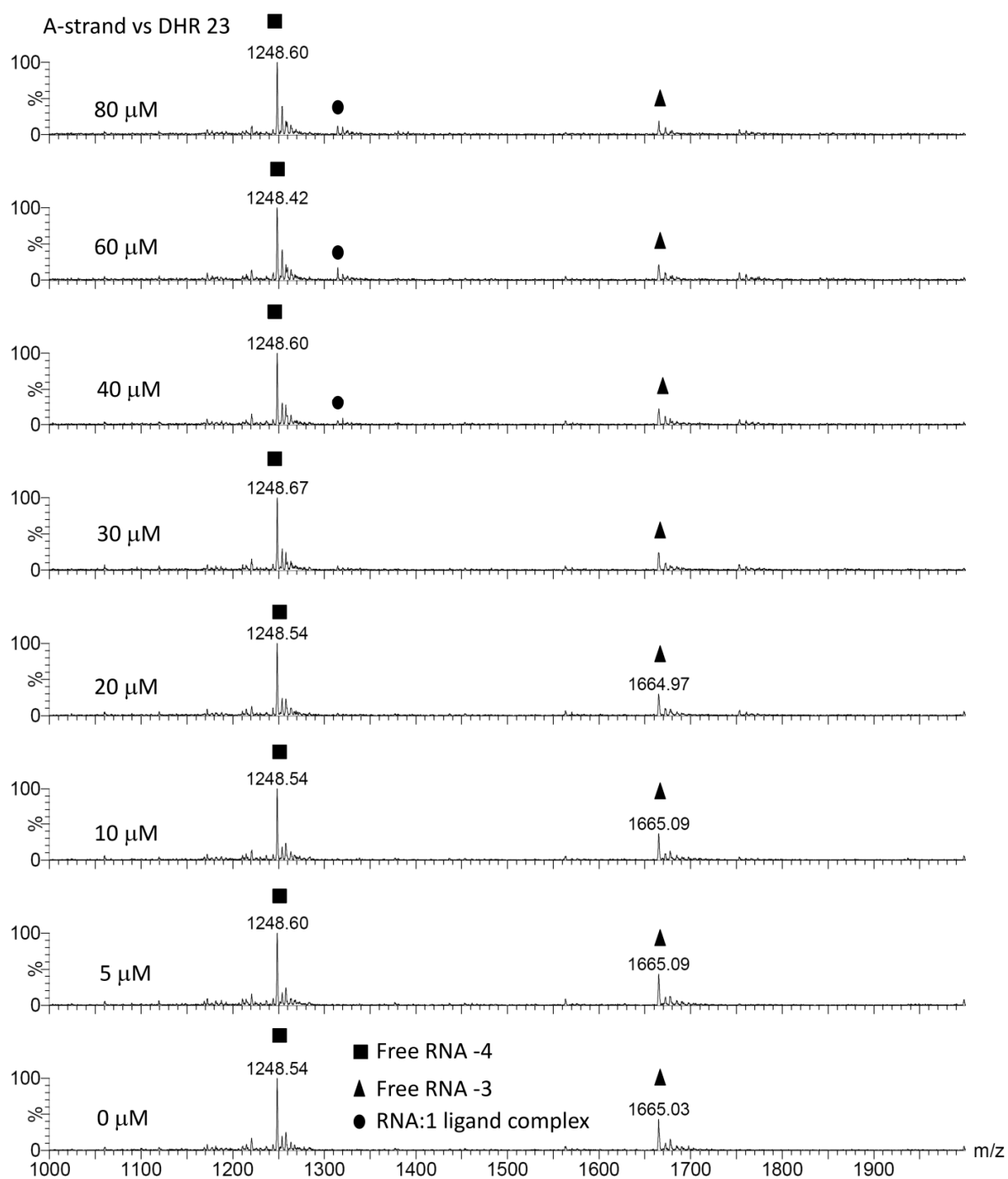
Figure 5.15: ESI-MS spectra of A-strand vs. DHR23 are shown. Buffer conditions were 150 mM ammonium acetate pH 7.
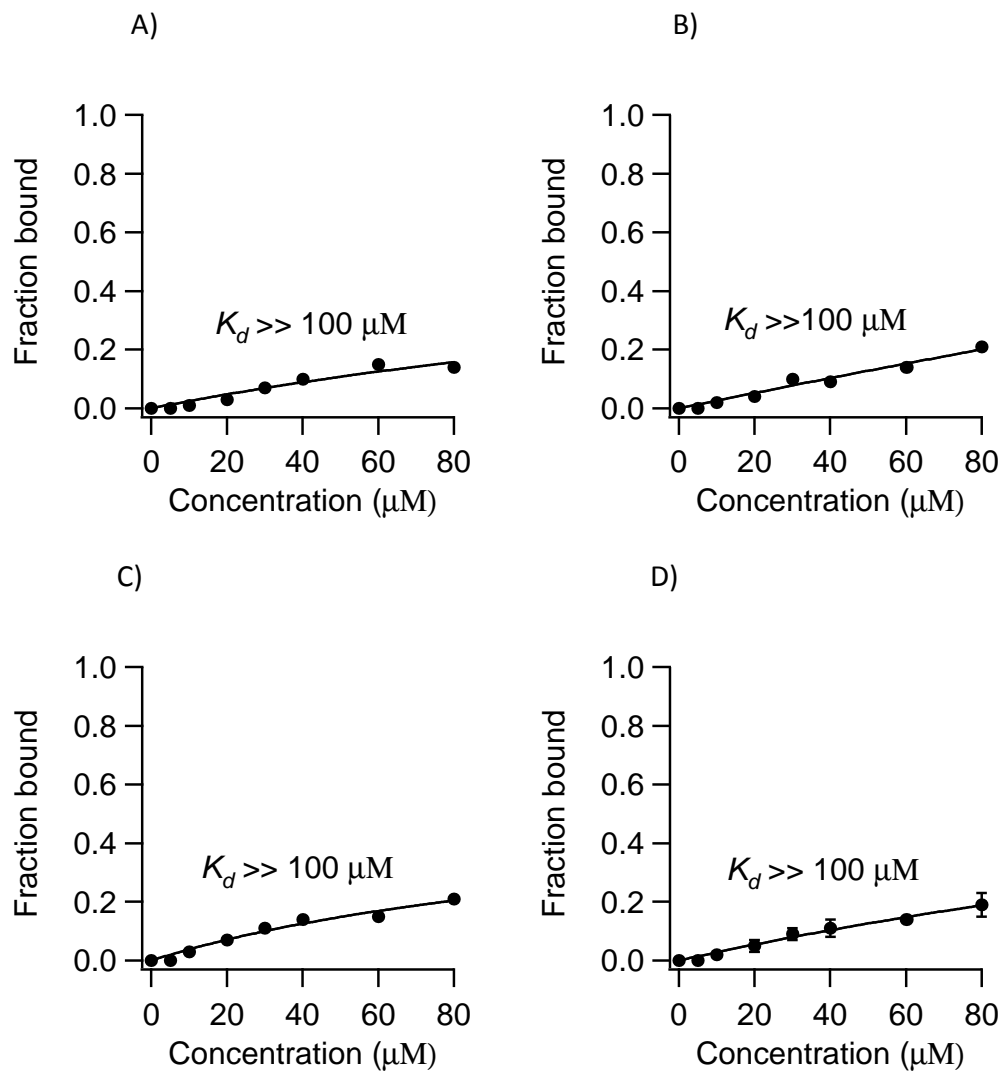
Figure 5.16: Binding curves (A-C) obtained from three different ESI-MS experiments between DHR23 and A-strand RNA and (D) the average of the three experiments are shown.
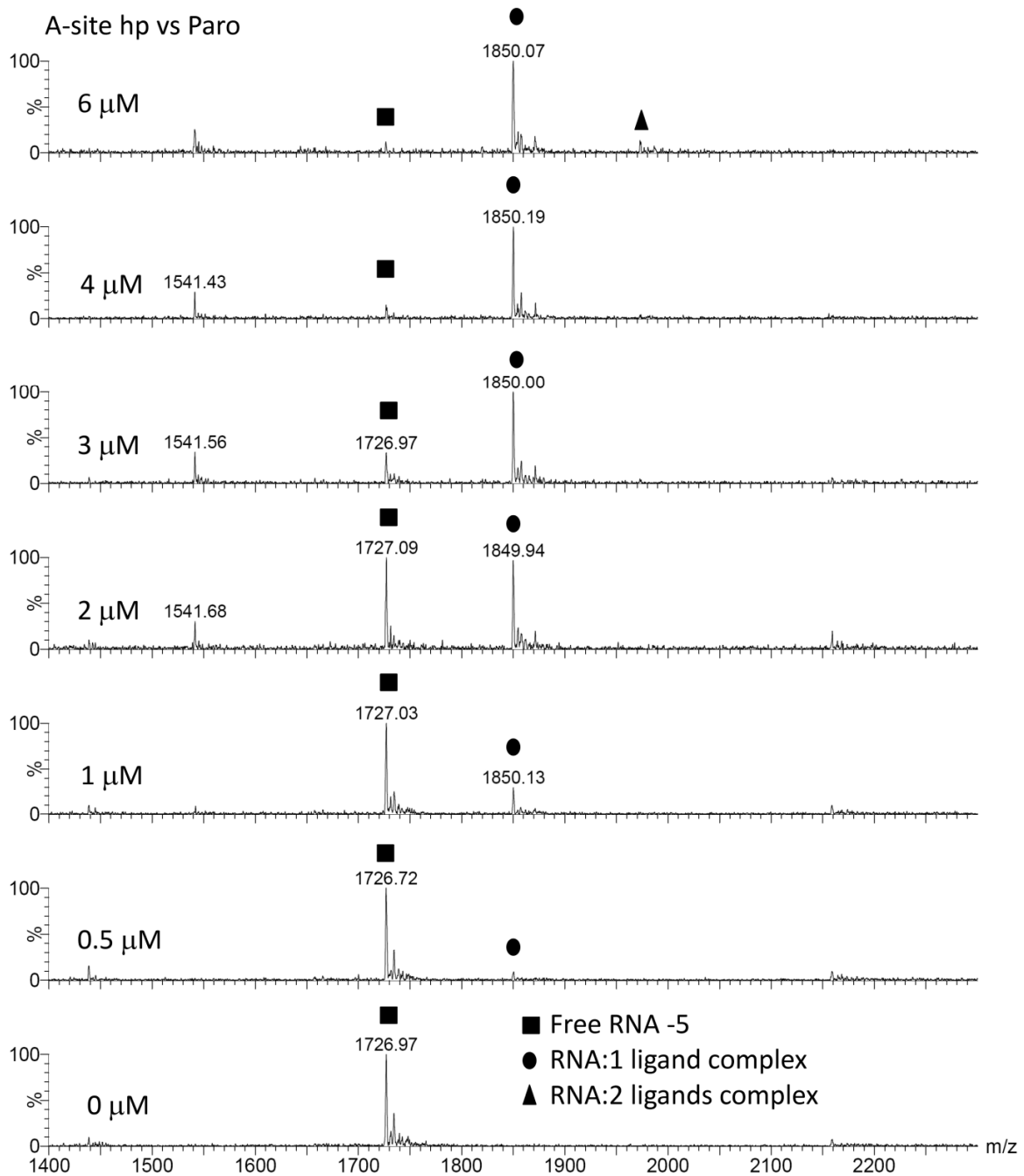
Figure 5.17: ESI-MS spectra of A-site hairpin vs. paromomycin are shown. Buffer conditions were 150 mM ammonium acetate pH 7.
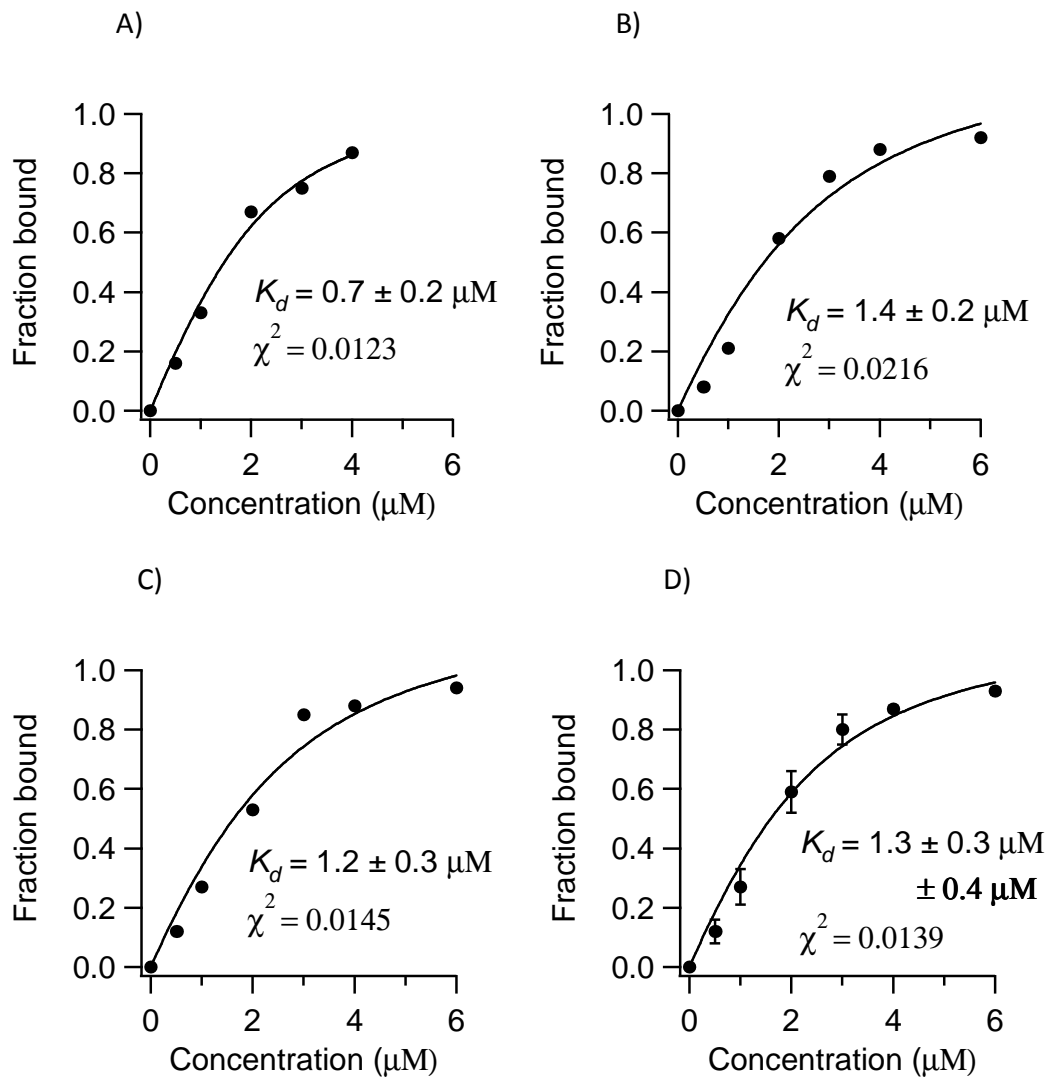
Figure 5.18: Binding curves (A-C) obtained from three different ESI-MS experiments between paromomycin and A-site hairpin RNA and (D) the average of the three experiments ± error of fit and **standard deviation** (in bold letters) are shown.
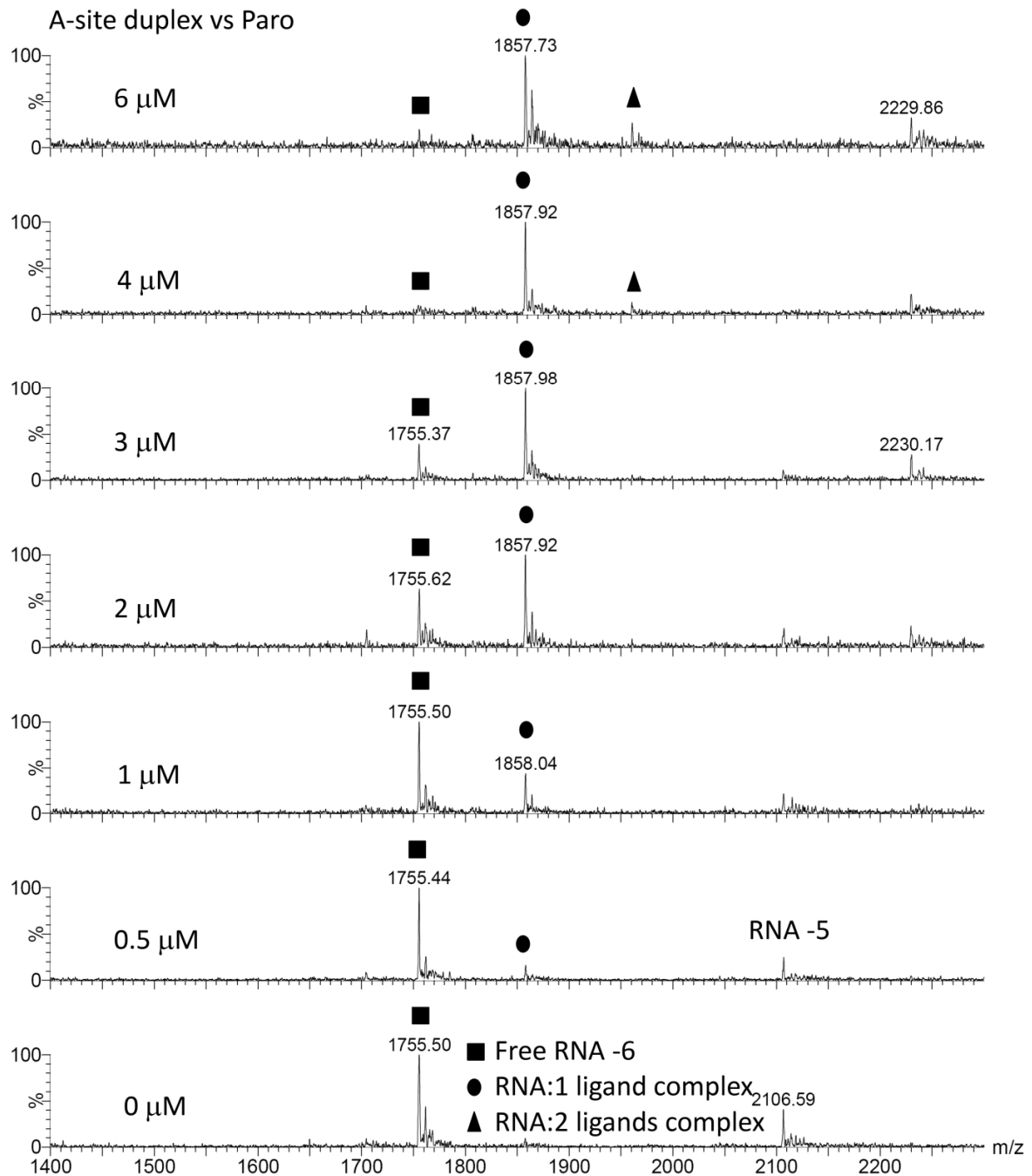
Figure 5.19: ESI-MS spectra of A-site duplex RNA vs. paromomycin are shown. Buffer conditions were 150 mM ammonium acetate pH 7.
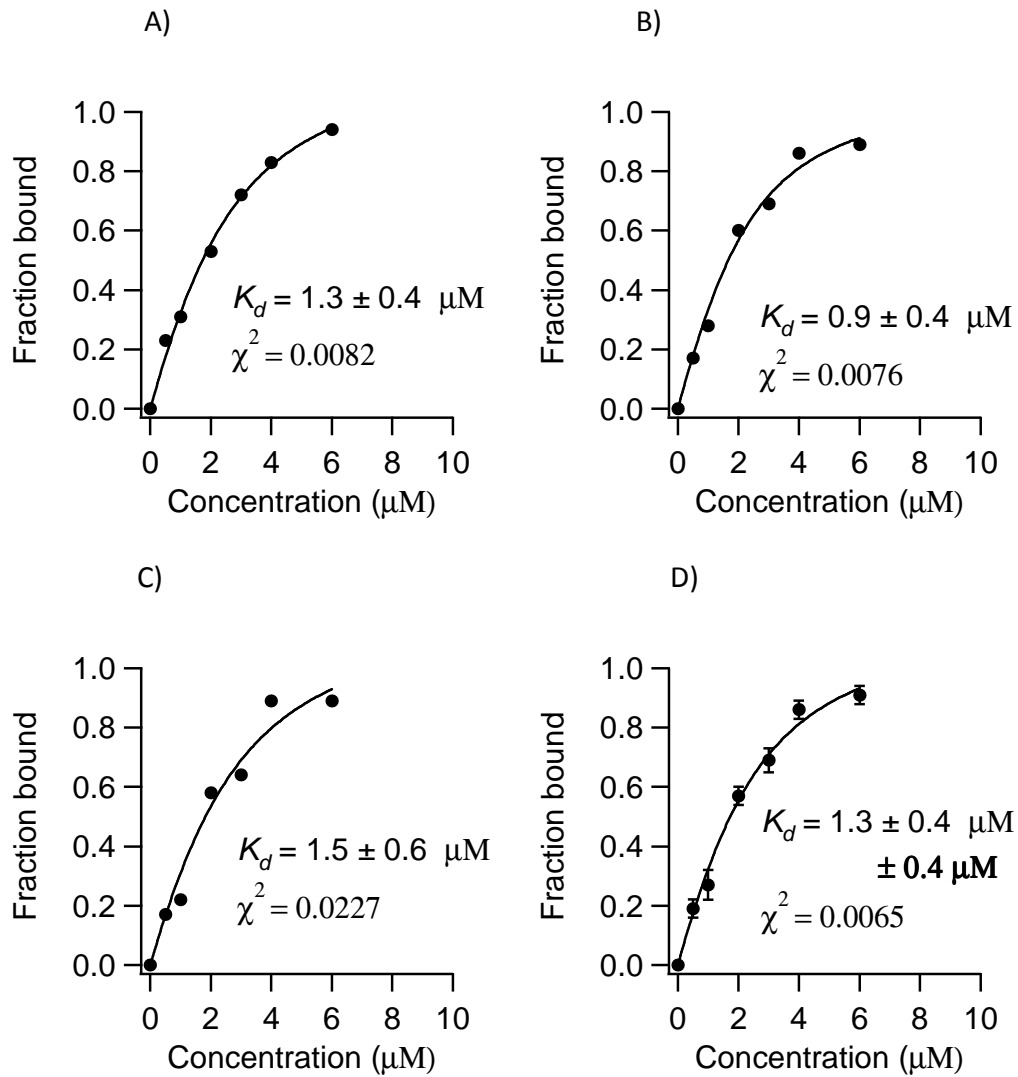
Figure 5.20: Binding curves (A-C) obtained from three different ESI-MS experiments between paromomycin and A-site duplex RNA and (D) the average of the three experiments ± error of fit and **standard deviation** (in bold letters) are shown.
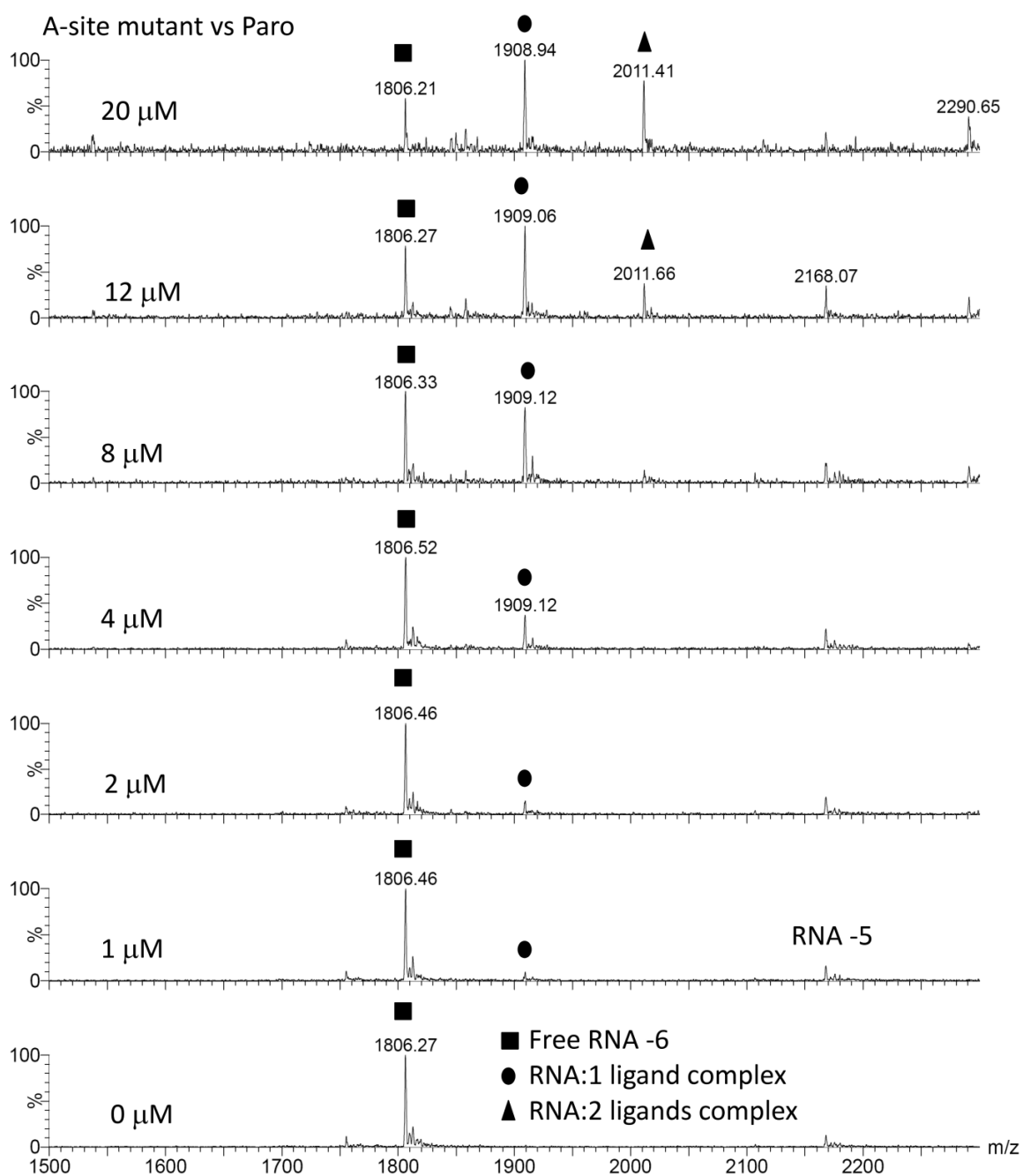
Figure 5.21: ESI-MS spectra of A-site mutant RNA vs. paromomycin are shown. Buffer conditions were 150 mM ammonium acetate pH 7.
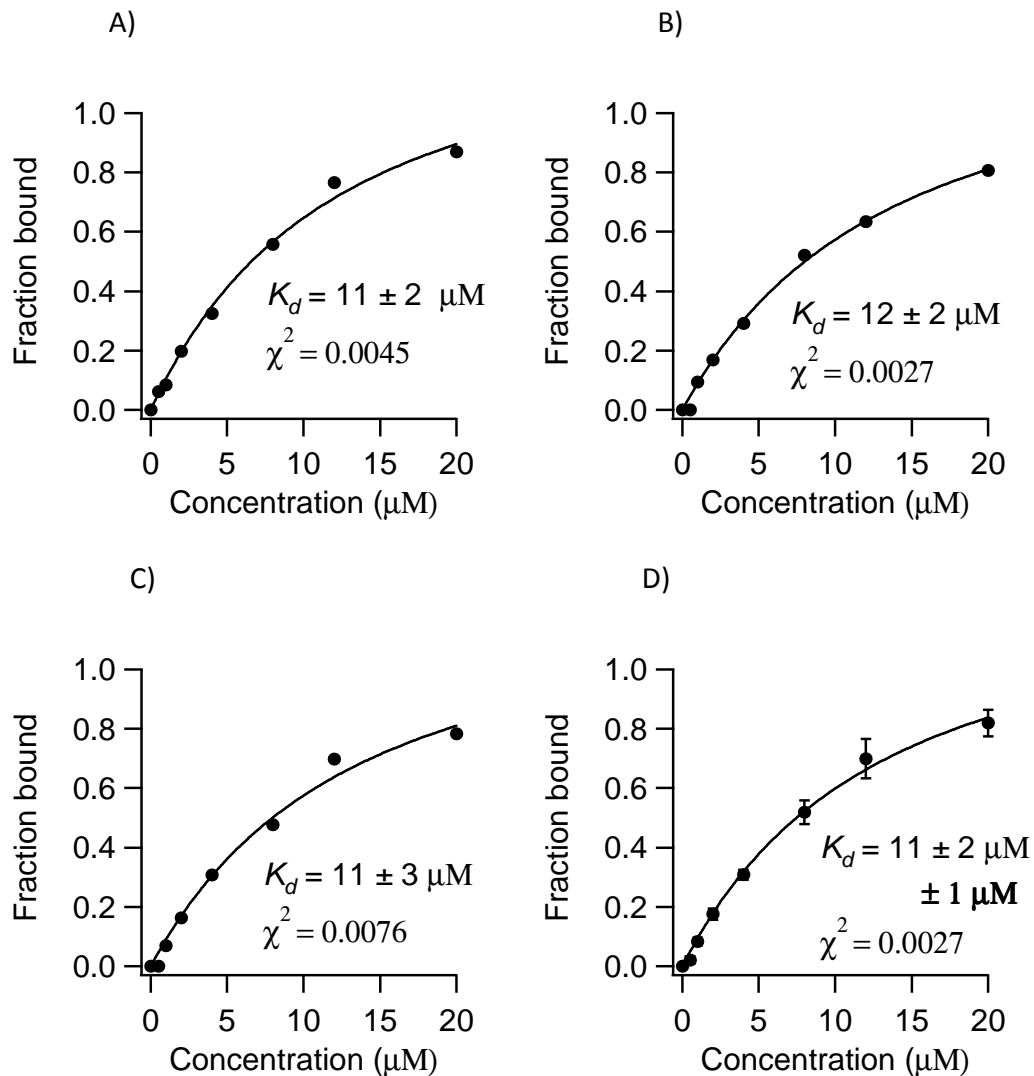
Figure 5.22: Binding curves (A-C) obtained from three different ESI-MS experiments between paromomycin and A-site mutant RNA and (D) the average of the three experiments ± error of fit and **standard deviation** (in bold letters) are shown.
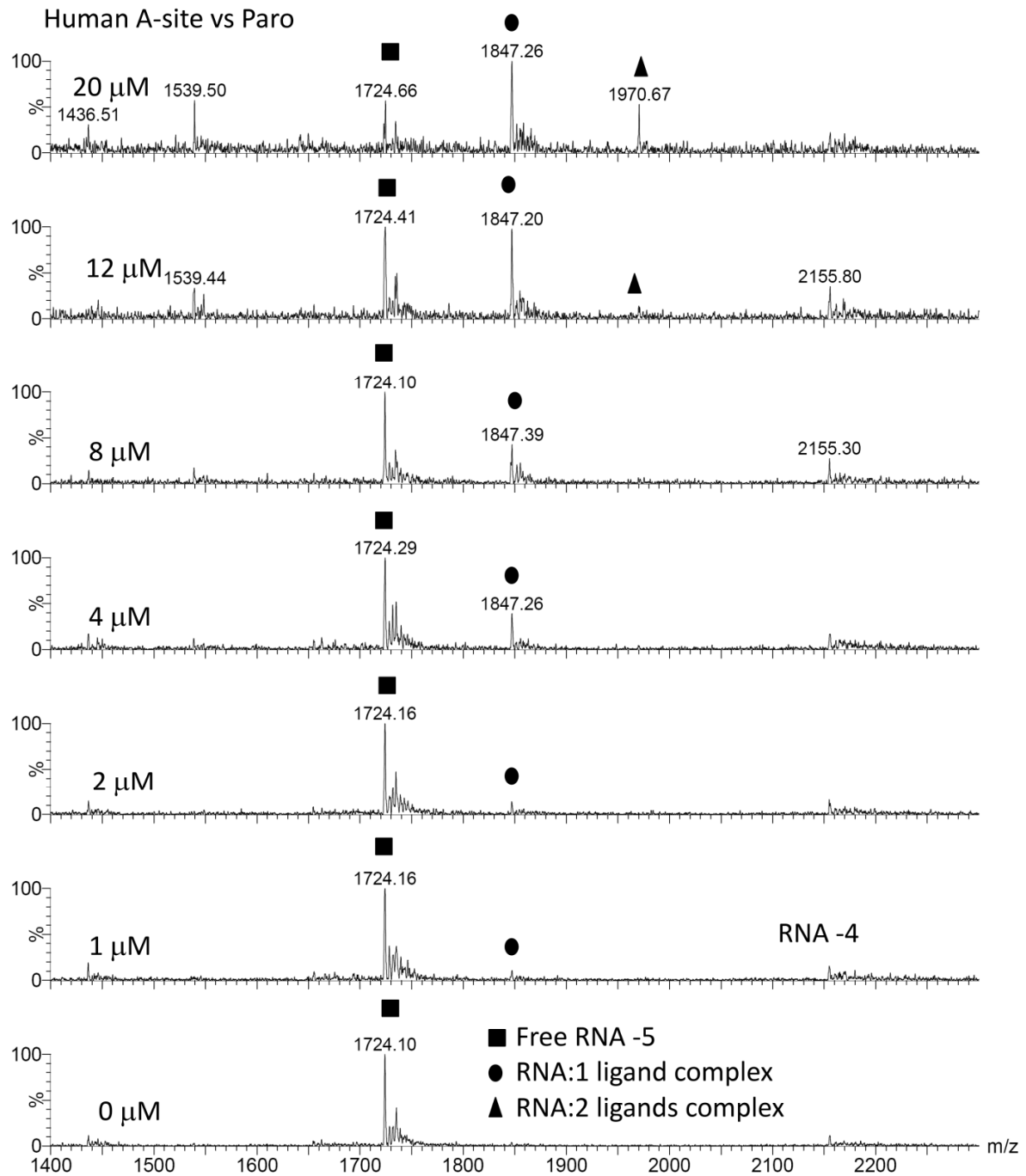
Figure 5.23: ESI-MS spectra of human A-site RNA vs. paromomycin are shown. Buffer conditions were 150 mM ammonium acetate pH 7.
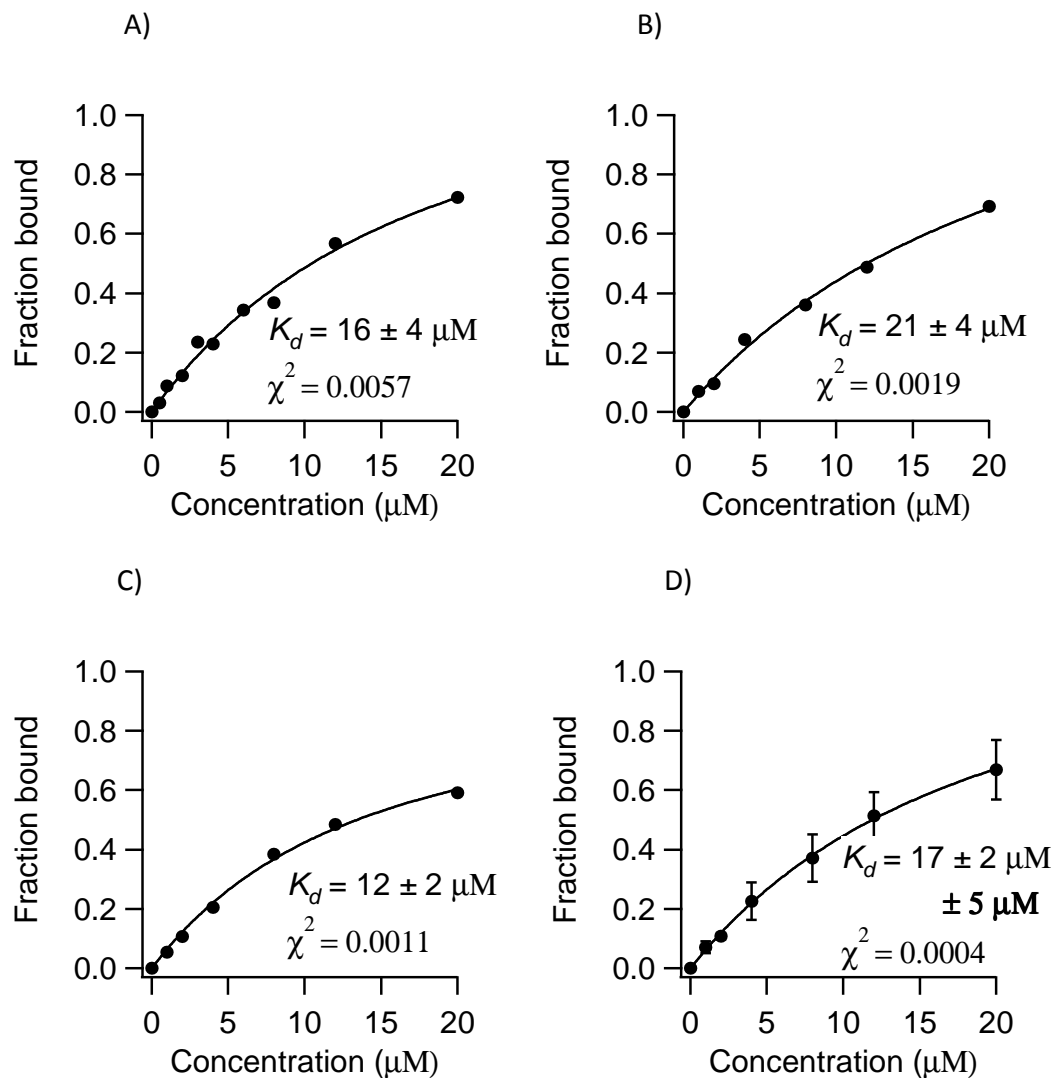
Figure 5.24: Binding curves (A-C) obtained from three different ESI-MS experiments between paromomycin and human A-site RNA and (D) the average of the three experiments ± error of fit and **standard deviation** (in bold letters) are shown.
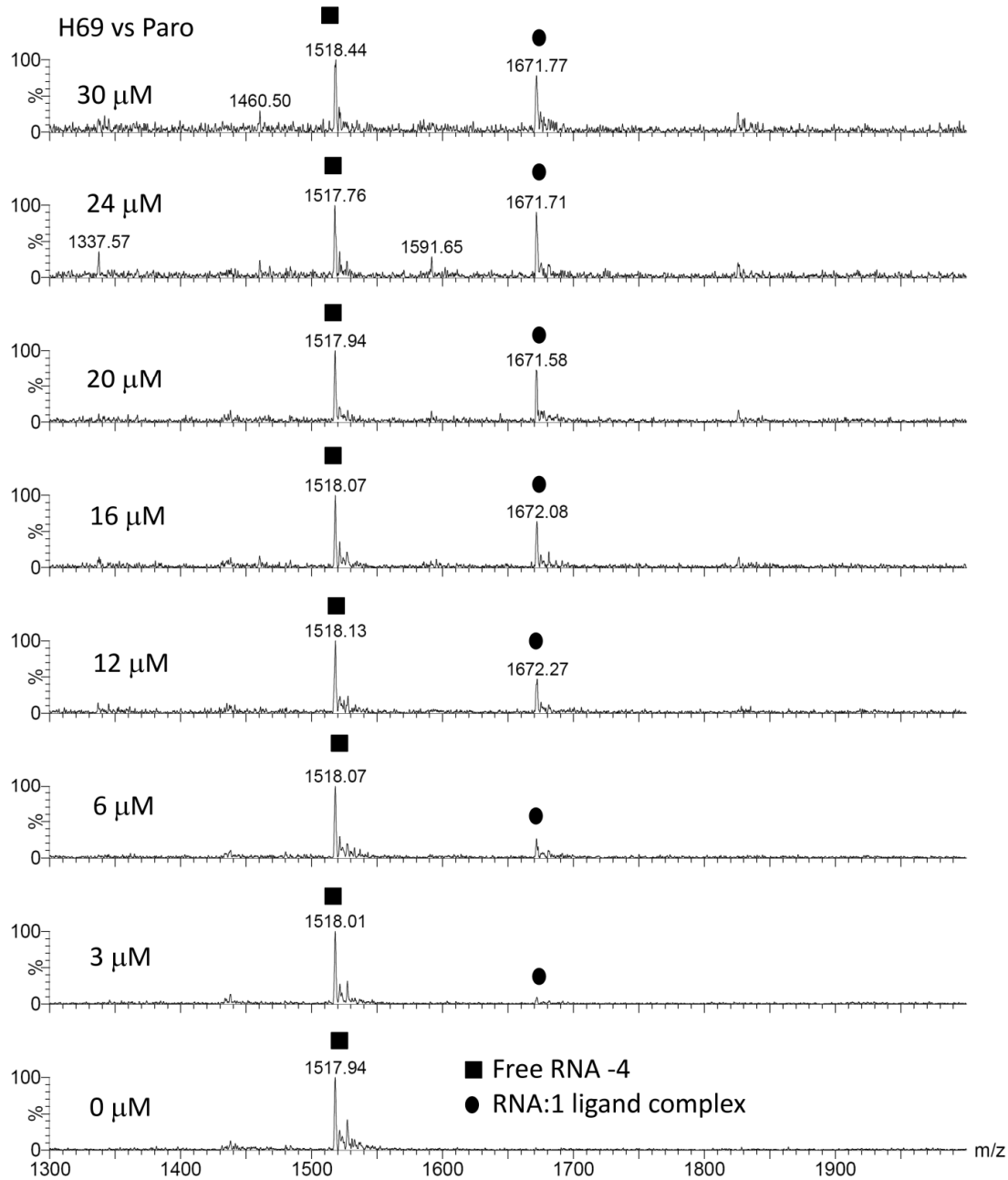
Figure 5.25: ESI-MS spectra of H69 RNA vs. paromomycin are shown. Buffer conditions were 150 mM ammonium acetate pH 7.
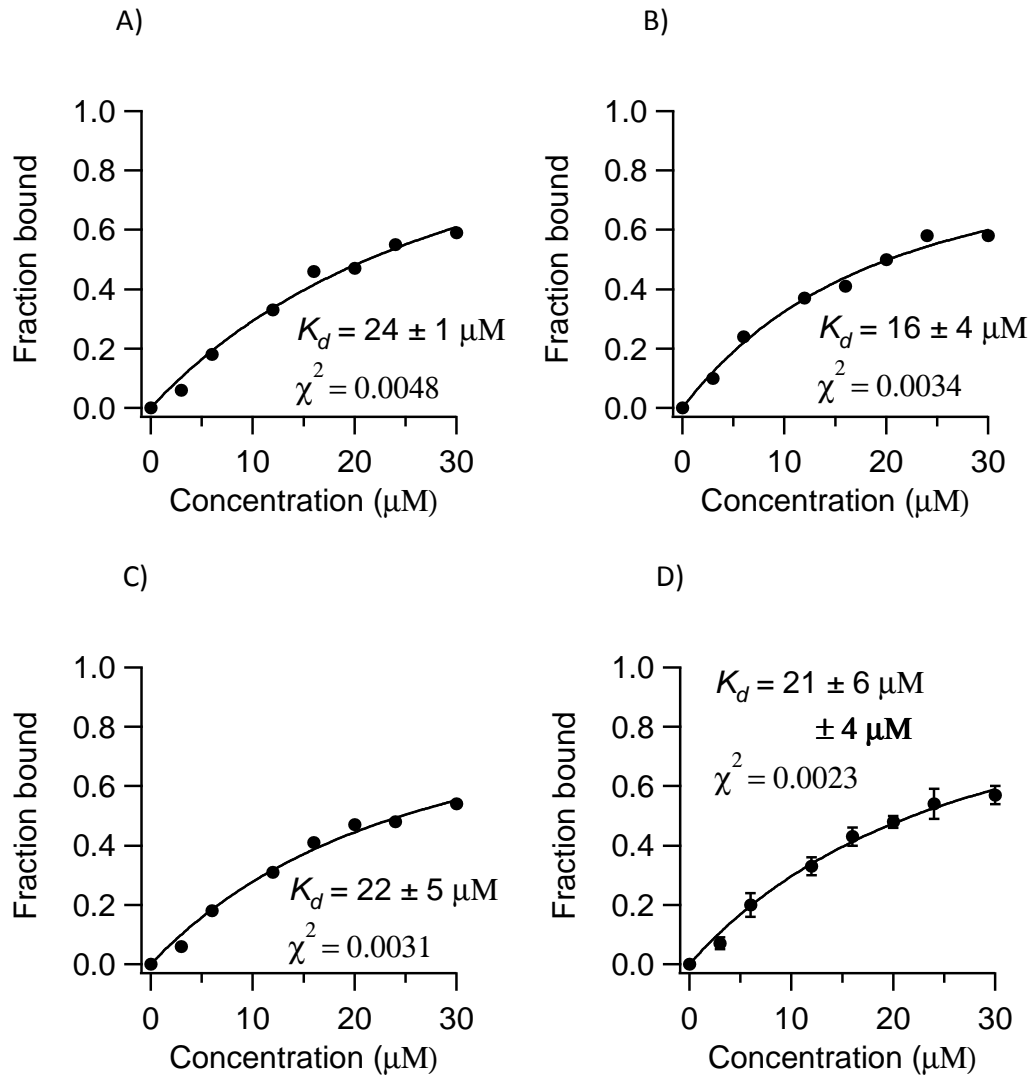
Figure 5.26: Binding curves (A-C) obtained from three different ESI-MS experiments between paromomycin H69 RNA and (D) the average of the three experiments ± error of fit and **standard deviation** (in bold letters) are shown.
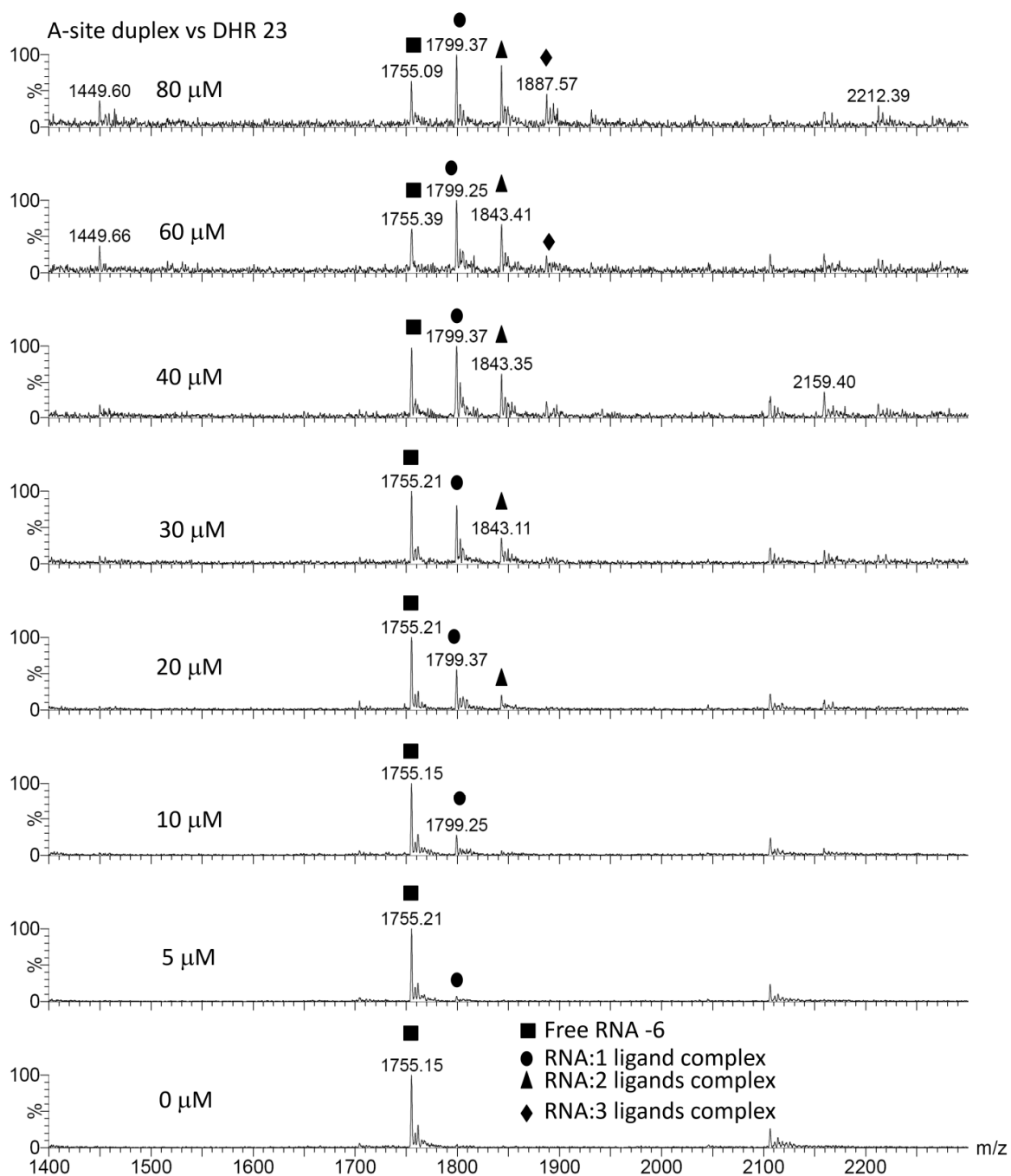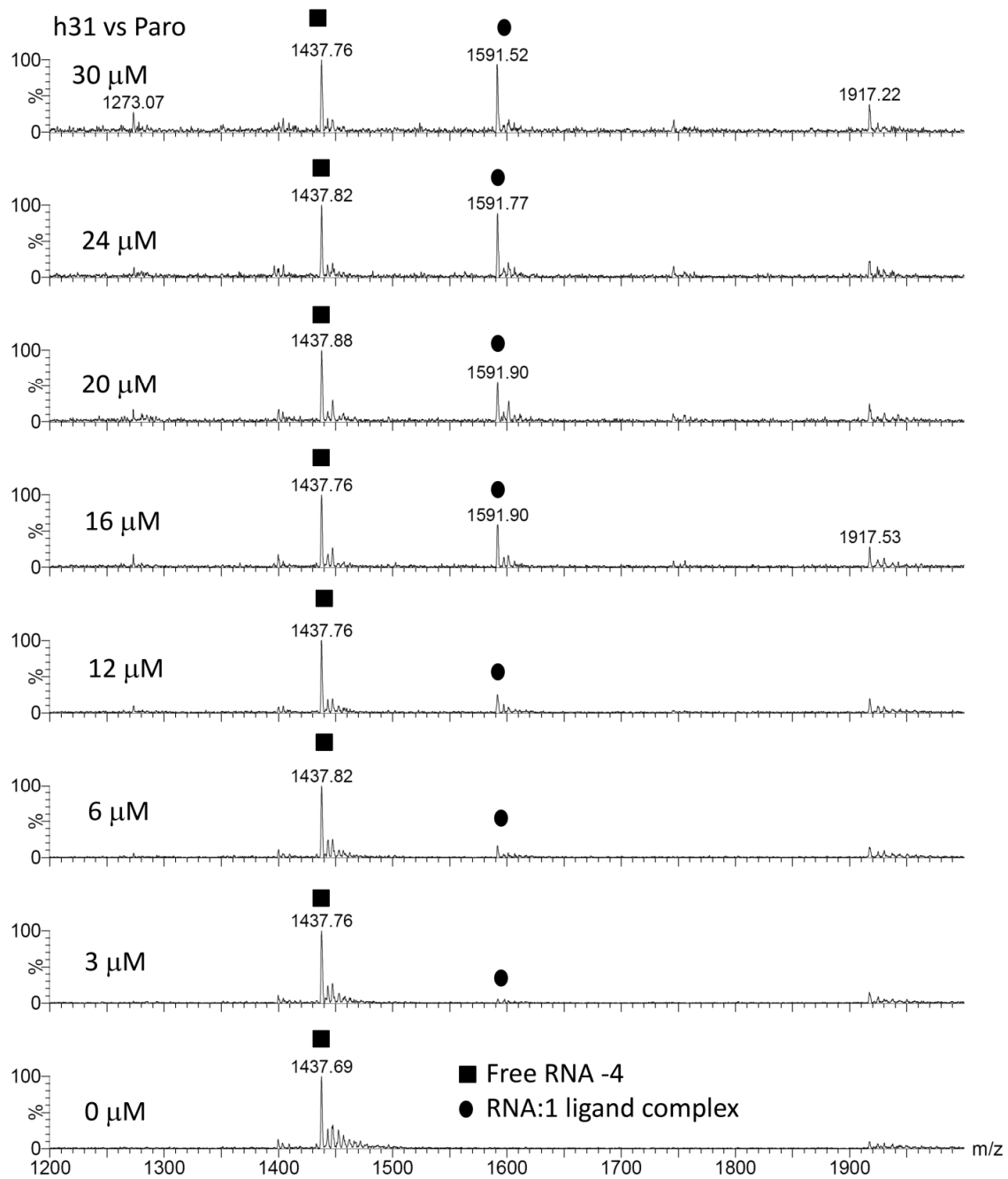
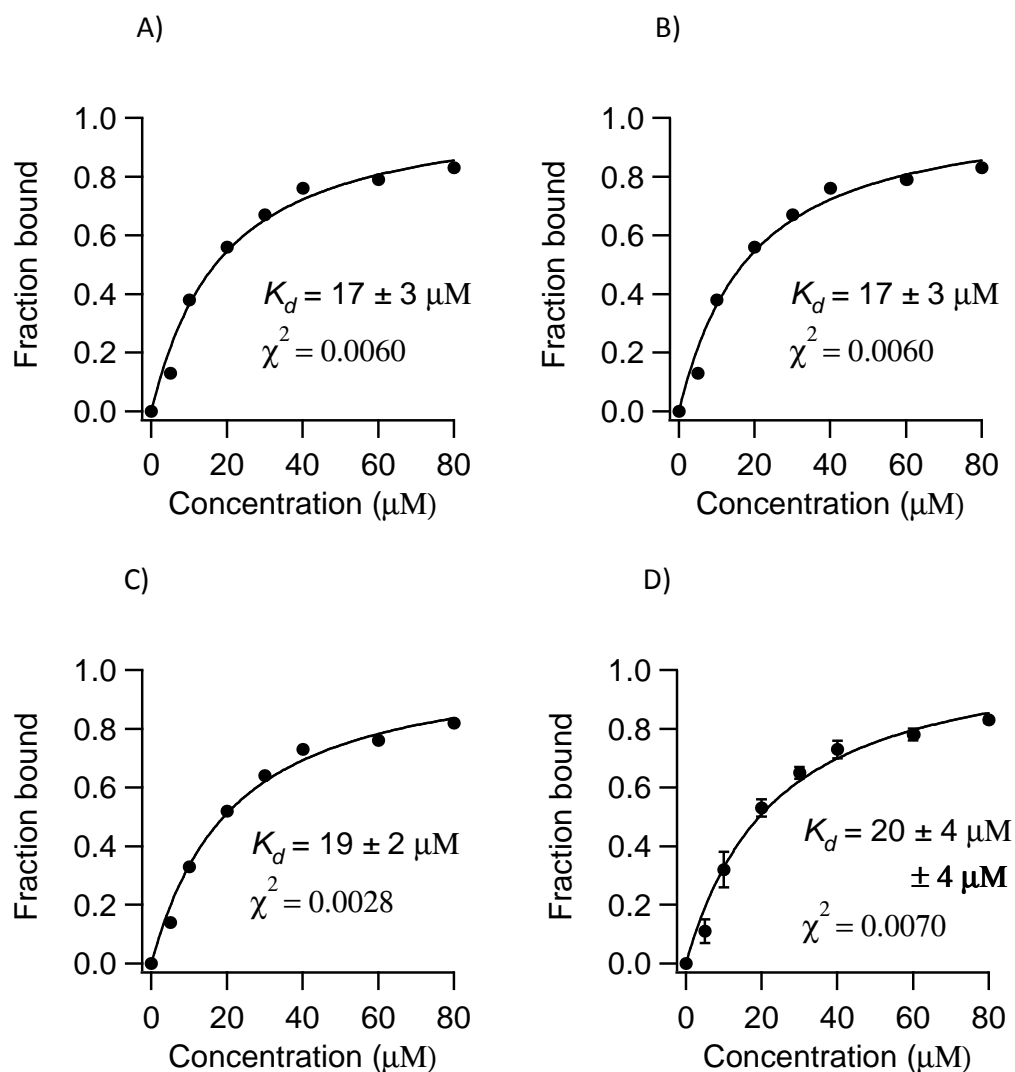**Figure 5.27**: ESI-MS spectra of h31 RNA vs. paromomycin are shown. Buffer conditions were 150 mM ammonium acetate pH 7.
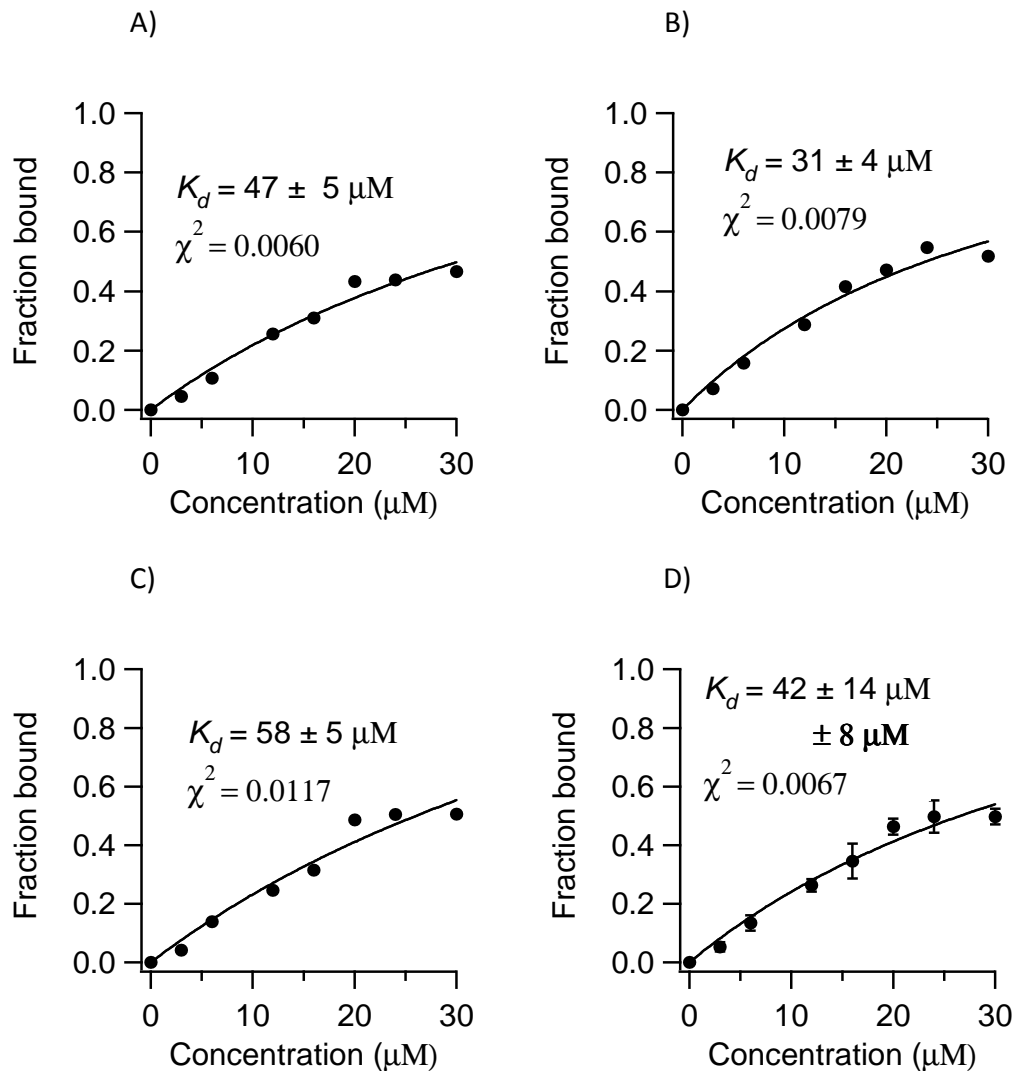
Figure 5.28: Binding curves (A-C) obtained from three different ESI-MS experiments between paromomycin h31 RNA and (D) the average of the three experiments ± error of fit and **standard deviation** (in bold letters) are shown.
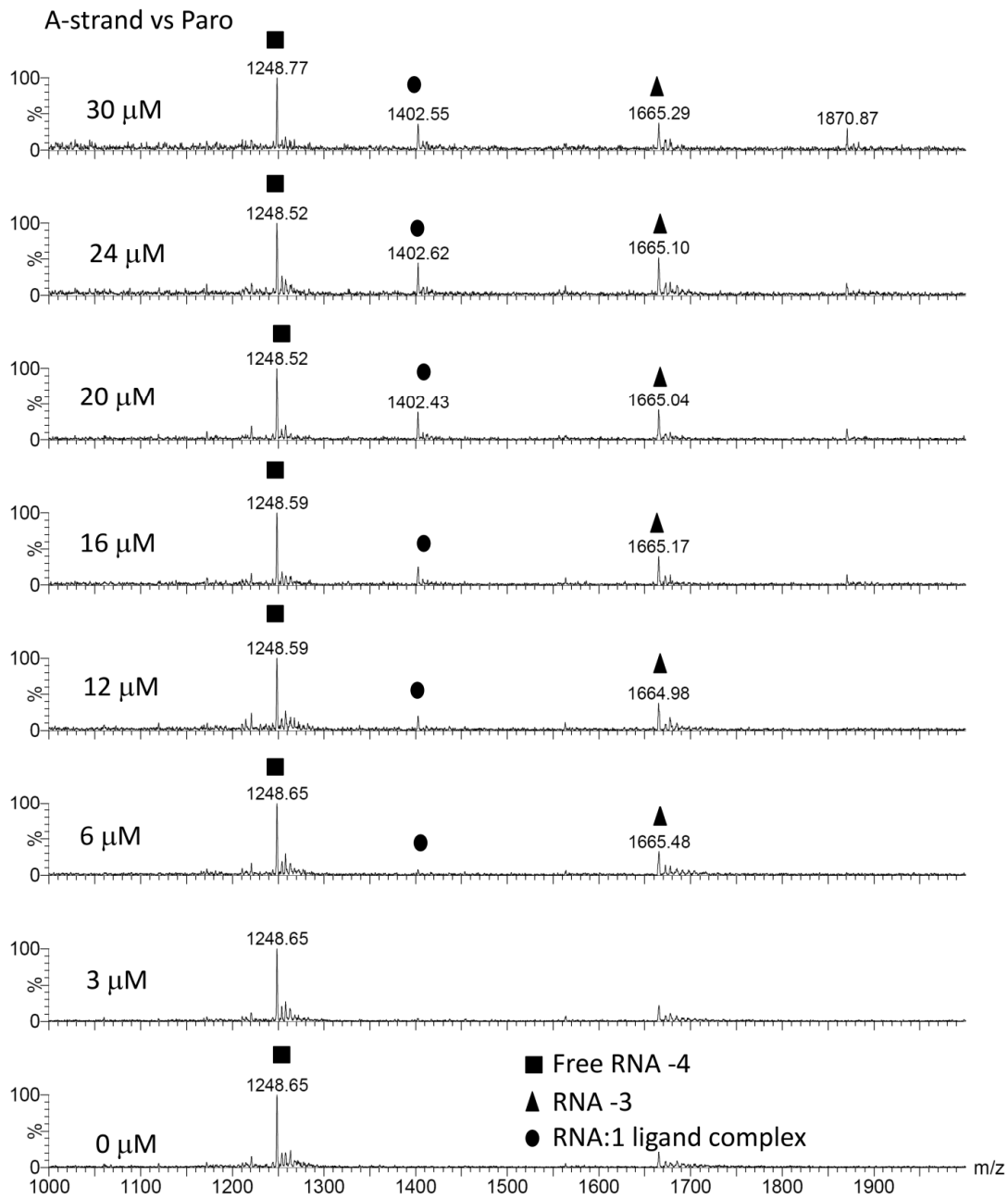
Figure 5.29: ESI-MS spectra of A-strand RNA vs. paromomycin are shown. Buffer conditions were 150 mM ammonium acetate pH 7.
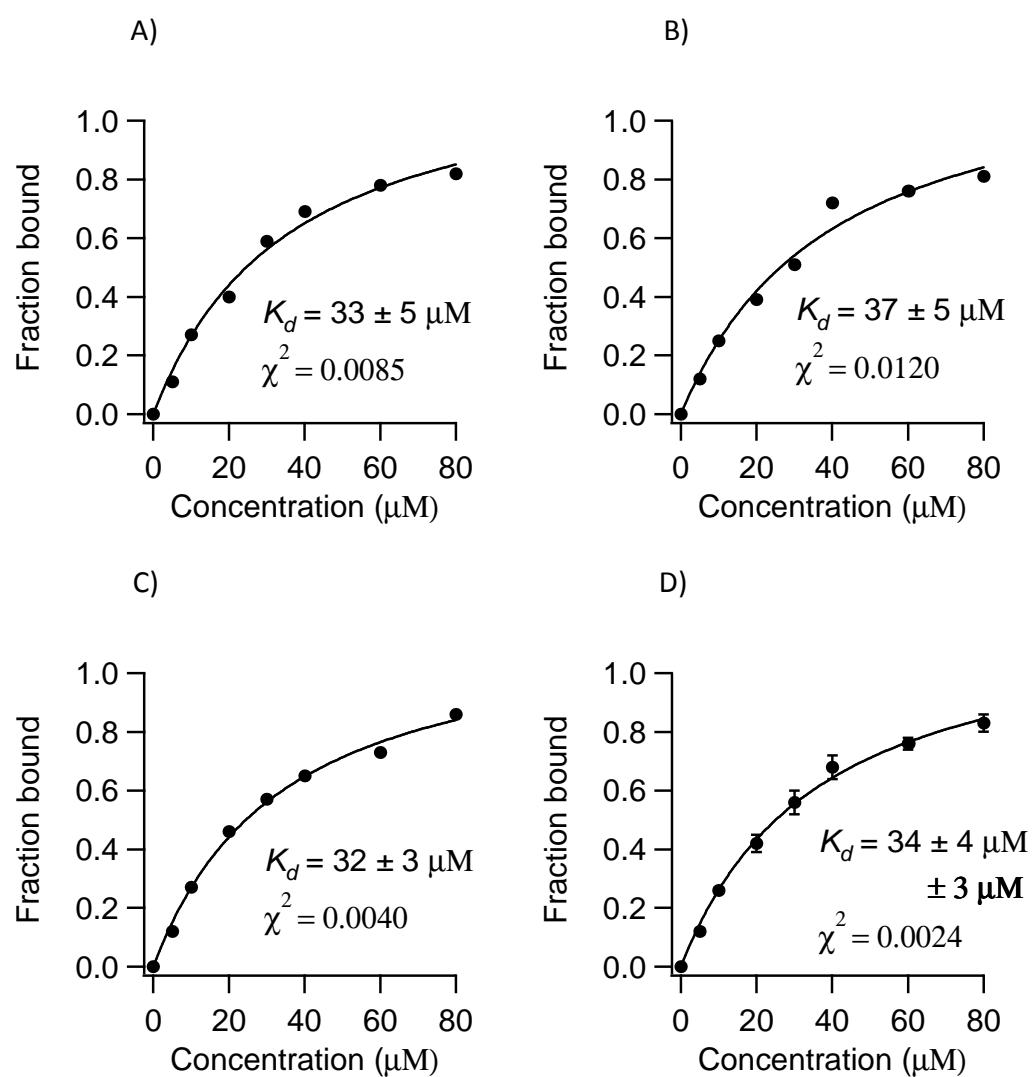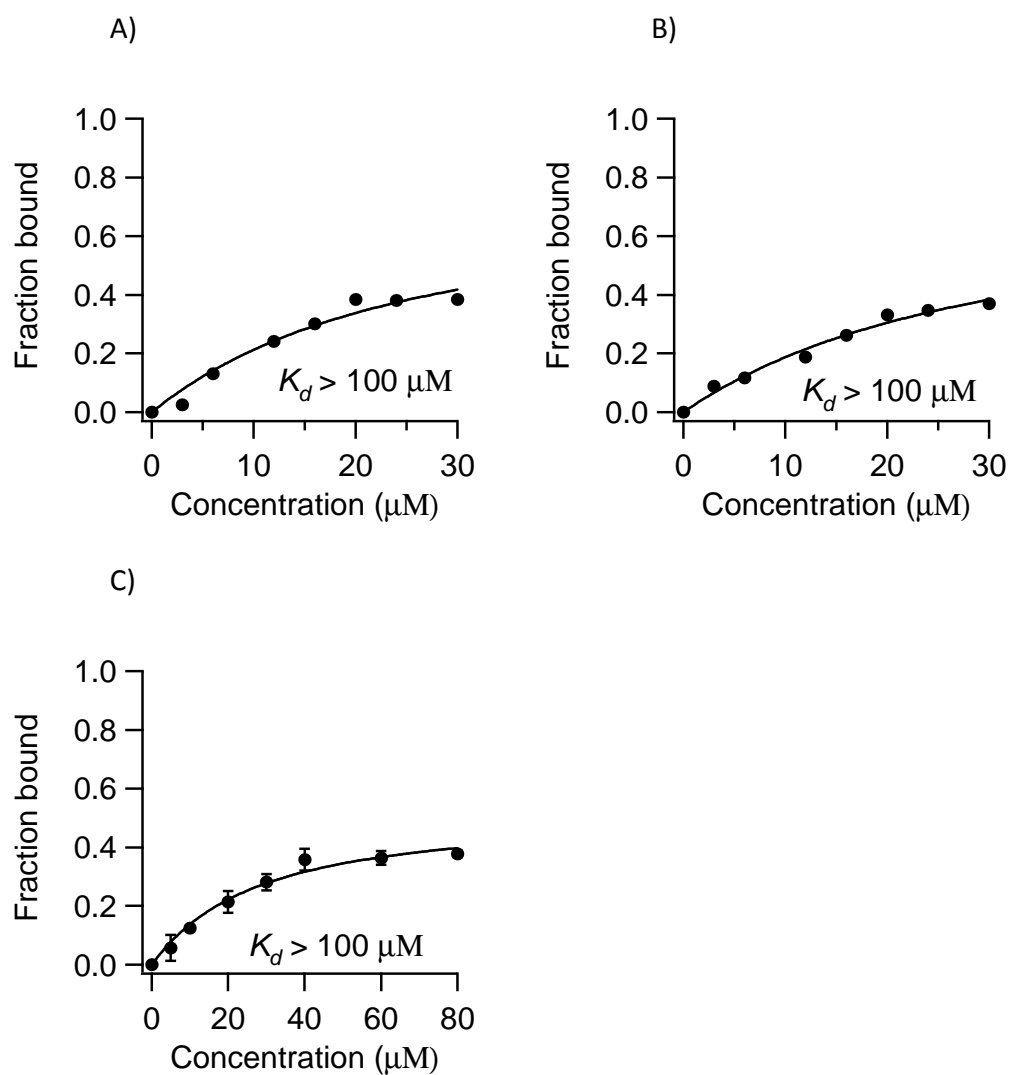
Figure 5.30: Binding curves (A-B) obtained from three different ESI-MS experiments between paromomycin A-strand RNA and (C) the average of the three experiments are shown.

CHAPTER 6

ROLE OF MODIFIED NUCLEOTIDES IN DRUG BINDING: TARGETING THE RIBOSOMAL A SITE*

6.1 Abstract

The decoding region of the ribosome is a well-established drug target for a wide variety of antibiotics. Present in the decoding region of the bacterial ribosome are modified nucleotides that are conserved across phylogeny. Modified nucleotides have been well characterized for the roles they play in antibiotic sensitivity and resistance; however, the roles that modified nucleotides play in antibiotic binding are not well understood. In this study, antibiotic binding studies were performed with modified and unmodified decoding region constructs using electrospray ionization mass spectrometry. Our results show that modified nucleotides may enhance or reduce the affinity of certain antibiotics for the decoding region.

6.2 Introduction

There is a wide variety of post-transcriptionally modified nucleotides present in the ribosome. Over 100 of these modifications have been identified in bacterial and eukaryotic cells.[46]

* The synthesis of modified RNAs reported in this chapter was carried out by Santosh Mahto.

The modified nucleotides are thought to modulate the specific folding of the RNA in a variety of ways, including improving base stacking,[294-296] and increasing or decreasing the potential for hydrogen bonding.[297-299] There are three modifications present in the decoding region of the *E. coli* ribosome; namely, m^3U, m^5C and m^4Cm (**Figure 6.1**B).[31, 34] Nucleotide base methylation may increase base stacking due to its hydrophobicity, block hydrogen bonding when present at Watson-Crick edges (such as in m^3U), or cause structural changes induced by steric hindrance.[296, 298, 300] Furthermore, nucleosides with sugar methylations in the 2'-OH position (such as in m^4Cm) favor the 3'-*endo* sugar conformation and can block interactions at the sugar edge.[301-302]

The roles that modified nucleotides play in antibiotic resistance and susceptibility have been well documented. For example, methylation at the 2'-OH position of nucleotide A1067 located in the large ribosomal subunit of *Streptomyces azureus* confers resistance to the antibiotics thiostrepton and micrococcin.[303] Other base methylations such as mono and dimethylation of A2058 in the 23 S rRNA confer resistance to three different classes of antibiotics; monomethylation of A2058 causes a high level of resistance to lincosamides, but a low level resistance to macrolides and streptogramin B. On the other hand, dimethylation of this nucleotide confers a high resistance to all the three classes of the aforementioned antibiotics.[304-305] Inhibition or lack of housekeeping methylations may also lead to antibiotic resistance as seen in the case of kasugamycin, in which loss of methylations at A1518 and A1519 confer resistance to kasugamycin.[306] The above examples underscore the importance of investigating the impact of rRNA modifications on ligand binding and drug targeting.

Figure 6.1: The *E. coli* rRNA constructs are shown: (A) unmodified and (B) modified decoding region. The blue spheres indicate contacts made by paromomycin and green open spheres indicate contacts made by hygromycin B.

The study of RNA-ligand interactions are beneficial and an important area of research.[36,][158] Some of methods used to investigate the various aspects of RNA-ligand interactions include gel-based methods such as footprinting,[307] and biophysical methods such as ITC,[308] SPR,[309] NMR,[310] and ESI-MS.[182] These methods can be used to obtain parameters such as binding affinities, stoichiometries, kinetics, and binding sites of ligands on RNA (an overview of these techniques was given in Chapter 1). In recent times, ESI-MS has been the method of choice because of its speed and convenience.[182, 311-312] Labeling of the analyte is not necessary, and only a few picomoles of the sample is required for ESI-MS experiments. Also, ESI-MS provides distinct mass signatures that can be unambiguously resolved; therefore, several competition experiments can be performed. Binding experiments have been performed using of various ligands and unmodified decoding region (previously).[313] However, the effects of all naturally occurring modified nucleotides on ligand binding have not been considered. In this study, ESI-MS experiments were carried out using well-studied aminoglycosides, paromomycin, neomycin, kanamycin A and hygromycin B, as well as newly discovered ligands, peptide HPVHHYQ-NH2[314] and an aminoglycoside analogue DHR23 (Figure 6.2). The binding affinities of these ligands to the modified (wild-type) and unmodified decoding region variants (**Figure 6.1**) were compared. This project was done in collaboration with Santosh Mahto.

6.3 Experimental

6.3.1 RNA Preparation

Synthesis of the modified decoding region oligonucleotides has previously been reported.[302, 315] The RNAs were purified and desalted as previously described in Chapter 3. The concentration of RNAs were determined at 90 °C using Beer's law with the following single-stranded extinction coefficients: $\varepsilon_{260\,nm}$ 190,400 cm^{-1}M^{-1} and 242,500 cm^{-1}M^{-1} for the 5' half (21 mer oligonucleotide) and the 3' half (24 mer oligonucleotide), respectively. The oligonucleotides were dissolved in 1 M ammonium acetate buffer and duplex formations were achieved by heating the RNA samples at 94 °C for 3 min and slow cooling to room temperature in a heat block.

6.3.2 Ligands

Paromomycin, neomycin, kanamycin A, and hygromycin B were purchased from Sigma Aldrich (St. Louis MO) and used without further purification. The aminoglycoside analogue, DHR23, was obtained from Shahriar Mobashery (University of Notre Dame). Stock solutions of paromomycin, neomycin, kanamycin A, hygromycin B, and DHR23 were prepared with double-distilled water. Synthesis of the peptide HPVHHYQ-NH$_2$ was done by A.C. Duc.[314] The peptide concentration was calculated by measuring absorbance at 280 nm and using equation

$C = A_{280} / (\#_{tyr} \bullet \varepsilon_{tyr} + \#_{trp} \bullet \varepsilon_{trp}) \bullet \lambda$ in which the extinction coefficient of tyrosine (ε_{tyr}) is 1490 cm^{-1}M^{-1}, the extinction coefficient of tryptophan (ε_{trp}) is 5560 cm^{-1}M^{-1}, λ is the pathlength, and $\#_{tyr}$ and $\#_{trp}$ are the number of tyrosine and tryptophan residues, respectively.

6.3.3 Electrospray Ionization Mass Spectrometry (ESI-MS)

Electrospray ionization mass spectrometry (ESI-MS) experiments were performed on a Quattro LC tandem quadrupole mass spectrometer equipped with electrospray ionization in the negative ion mode (Micromass, Manchester, UK). The tuning parameters, sample preparation, data processing and fraction bound determination were discussed previously in Chapters 2 and 3.

6.4   Results and Discussion

The interaction of paromomycin, neomycin, and kanamycin with the A-site RNA has been studied extensively by different methods under various buffer conditions.[95, 316-318] The K_d values reported for aminoglycoside-RNA interactions range from 5 nM to 100 µM.[6, 163, 319-320] The results from our binding studies are consistent with literature values.[6, 163, 319-320] The data show that the ligands (paromomycin, neomycin, kanamycin and HPVHHYQ) that bind to the lower region on the A site (see **Figure 6.1**) have a negligible or only small preference (0.6 to 0.9-fold difference) for the unmodified decoding region over the modified decoding region (Table 6.1).
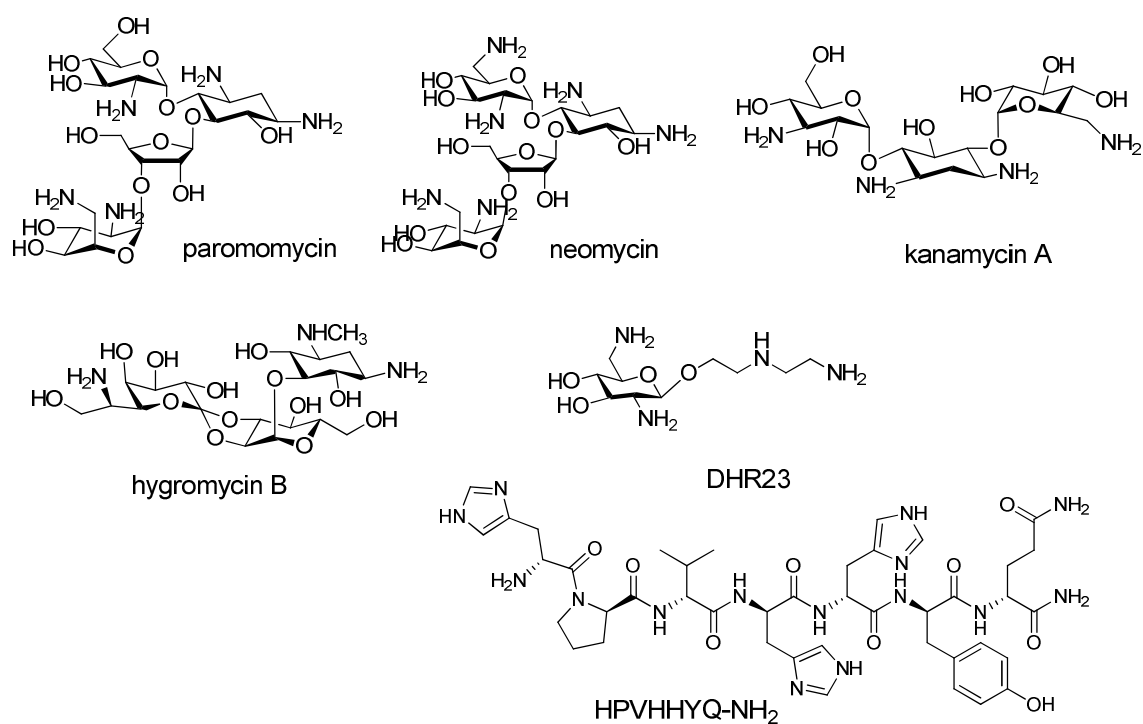
Figure 6.2: Chemical structures of the decoding region-targeting ligands are shown.

Table 6.1: Summary of the binding study results

| Ligands | Dissociation constant, K_d (µM) | | |
	Unmodified decoding region[a]	Modified decoding region[a]	Unmod/mod
Paromomycin	0.7 ± 0.3	0.8 ± 0.3	0.9
Neomycin	2.0 ± 0.4	2.0 ± 0.3	1
Kanamycin A	8 ± 1	12 ± 1	0.7
Hygromycin B	25 ± 4	15 ± 7	1.7
HPVHHYQ-NH$_2$	31 ± 7	50 ± 7	0.6
DHR23	9 ± 2	18 ± 6	0.5

[a] Values reported are an average of three experiments ± one standard deviation

Crystal structures and NMR solution structures reveal that paromomycin binds at G1405, A1408, C1490, G1491, A1493, and U1495 (**Figure 6.1** and **Figure 6.3**).[95, 207, 293, 316, 321] These residues are far from the modified nucleotides with the exception of m^5C at 1407. Therefore, m^5C appears to have no contribution to the binding, perhaps due to lack of a direct contact between the ligands (paromomycin, neomycin, kanamycin A, and HPVHHYQ) and this residue. The other two modified nucleotides (m^4Cm and m^3U) are not close to the binding site.

A)   B)
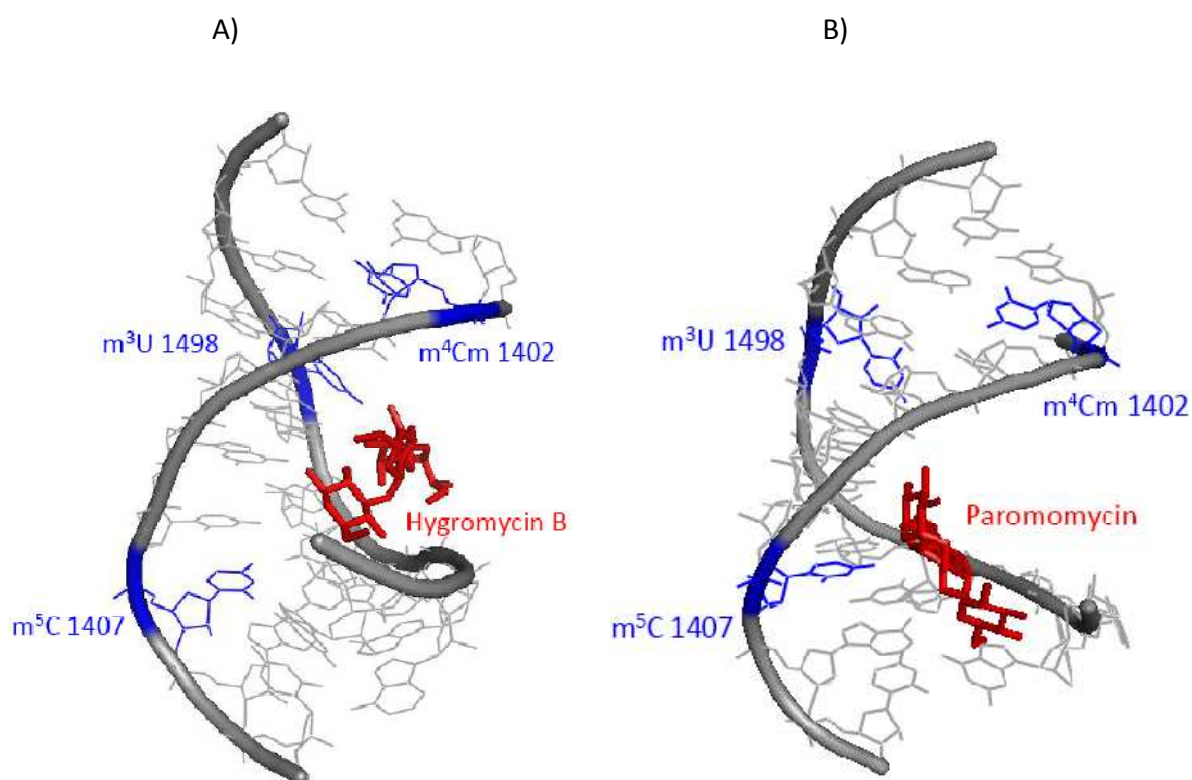
Figure 6.3: The structures of: A) hygromycin B and B) paromomycin bound to the decoding region. The modified nucleotides present in the decoding region are highlighted in blue. The figures were generated with PyMol software[322] using coordinates from PDB files 2Z4K and 1HNZ.[94, 293]

Interestingly, hygromycin B slightly prefers binding to the modified decoding region, with a K_d of 15 μM over the unmodified decoding region, with a K_d of 25 μM (Table 6.1). A Crystal structure of hygromycin B bound to the 30 S subunit reveals that this aminoglycoside binds to the decoding region nucleotides C1403, G1405, A1408, C1496, G1491, A1493, U1495, and the modified nucleotide m[3]U1498 (**Figure 6.1** and **Figure 6.3**A).[94] In this case, the modified nucleotide m[3]U1498 makes contact with hygromycin B. Thus, the modified residue appears to play a role in enhancing the binding affinity by approximately 1.5 fold. The methylation at the N3 position of uridine may favor stronger hydrogen bonding interactions between the O4 position of uridne and hygromycin B (through inductive effect) (**Figure 6.4**). Alternatively the presence of the methyl group may affect the local conformation[299] of the RNA resulting in more favorable interactions with hygromycin B. This result is consistent with earlier findings in which U1498C mutation leads to hygromycin resistance in *Mycobacterium smegmatis*.[323] Mutation of this methylated uridine to a cytidine leads abolishment of hydrogen bonding interactions between O4 of uridine and hygromycin B, which eventually leads to resistance.
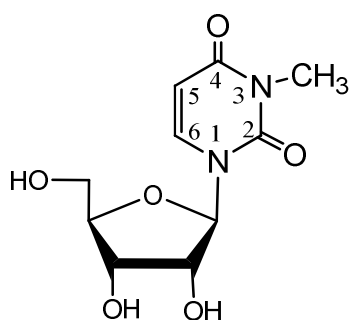
Figure 6.4: The structure of 3-methyluridine is shown.

The peptide HPVHHYQ-NH$_2$, selected through phage display, targets the ribosomal A site.[314] The reported K_ds of the peptide range from 2 to 29 µM with a smaller unmodified RNA construct by different methods such as ITC, footprinting, and ESI and in various buffers.[314] Here, we studied the binding affinity of the peptide HPVHHYQ-NH$_2$ with unmodified and modified decoding region RNAs. It has a slight preference for the unmodified (K_d = 31 µM) over the modified decoding regions (K_d = 50 µM) (Table 6.1). Footprinting data show that the peptide HPVHHYQ-NH$_2$ binds to nucleotides A1492 and A1493 of the A-site loop on the smaller A-site RNA construct.[314] Its binding site is on the opposite side of the loop-modified nucleotide m^{5}C1407, similar to the aminoglycosides. The modification may slightly change the loop structure. Therefore, the slight difference between the binding affinities of the modified and unmodified decoding regions may result from slight structural changes facilitated by the modified nucleotide m^{5}C, which has been shown to destabilize the decoding region.[315] Furthermore, the peptide was selected for binding to unmodified A-site RNA; thus it is not surprising that it has a higher affinity for the unmodified decoding region. Paromomycin and kanamycin A belong to 4,5-linked and 4,6-linked aminoglycoside families, respectively.[114] Even though ring I and II of these two aminoglycoside families (neamine core) adopt similar conformations when bound to the A site, differences exist in the interactions of the other rings with the A site.[6, 208] Since the difference in selectivity of HPVHHYQ for the modified and unmodified decoding region (unmod/mod = 0.6, **Table 6.1**) is very similar to that of kanamycin, it suggests that HPVHHYQ may have a similar binding mode as kanamycin. The data also suggest

that only slight differences in binding modes exist between HPVHHYQ, paromomycin, neomycin, and kanamycin A.

The aminoglycoside analogue DHR23 was found to bind to the A-site RNA with moderate affinity. Results from Chapter 5 show that DHR23 preferentially binds to bacterial A-site RNA, having a K_d of 19 µM compared to bacterial A-site mutants, human A site, helix 69, and helix 31, which had K_{ds} of 34, 29, 47, and 95 µM, respectively. In this study, DHR23 shows a two-fold reduced binding affinity toward the modified decoding region having K_ds of 9 and 18 µM for the unmodified decoding region and modified decoding region, respectively (Table 6.1). Its binding site is different from the parent aminoglycoside and might be closer to the modified region, such that binding interactions may be affected by the presence of methylated residues. Alternatively, slight differences in the RNA conformation due to the modified nucleotide may impact the binding of DHR23. Similar to the data from Chapter 3, the difference in selectivity of DHR23 for the modified and unmodified decoding region suggests that DHR23 has a different binding mode compared to the parent aminoglycoside. Since DHR23 binds to the unmodified RNA slightly better than the corresponding modified decoding region (wild type), resistance to DHR23 would be less likely to occur by inhibition of housekeeping methyltransferase enzymes, as seen in the case of kasugamycin resistance. This result also suggests that it may be prudent to include modified nucleotide constructs (wild type) in the screening process when developing new anti-infectives.

6.5: Conclusions

The results from the binding experiments indicate that modified nucleotides may affect the binding affinity of ligands. For example, hygromycin B had a slightly higher binding affinity for the modified decoding region compared to the unmodified decoding region. On the other hand, DHR23 had a slight preference for the unmodified decoding region. These results go to show that modified nucleotides may play an important role in modulating the binding affinity of ligands if they are present at or near the binding pocket of a ligand. Hence, it is important to utilize modified or wild-type RNA constructs in ligand screening and binding assays. The fact that a single methylation affects the binding of a ligand is not unprecedented. Resistance to capreomycin (a cyclic peptide antibiotic) used as an anti-tuberculosis drug can occur due to lack of C 2'-*O*-methlation at 1409 of 16 S rRNA and 1920 of 23 S rRNA.[324] Conversely, resistance to kanamycin and apramycin occur due to *N1*-methylation of A1408 of 16 S rRNA.[325] Many antibiotic-producing bacteria protect themselves by modifying their target rRNA. Therefore, by utilizing the typical patterns of rRNA post-transcriptional modification in different bacteria, more specific anti-infectives can be developed to counteract the resistance problem.

ESI-MS Spectra and Binding Curves

The ESI-MS spectra and binding curves for this study are shown on the next page.
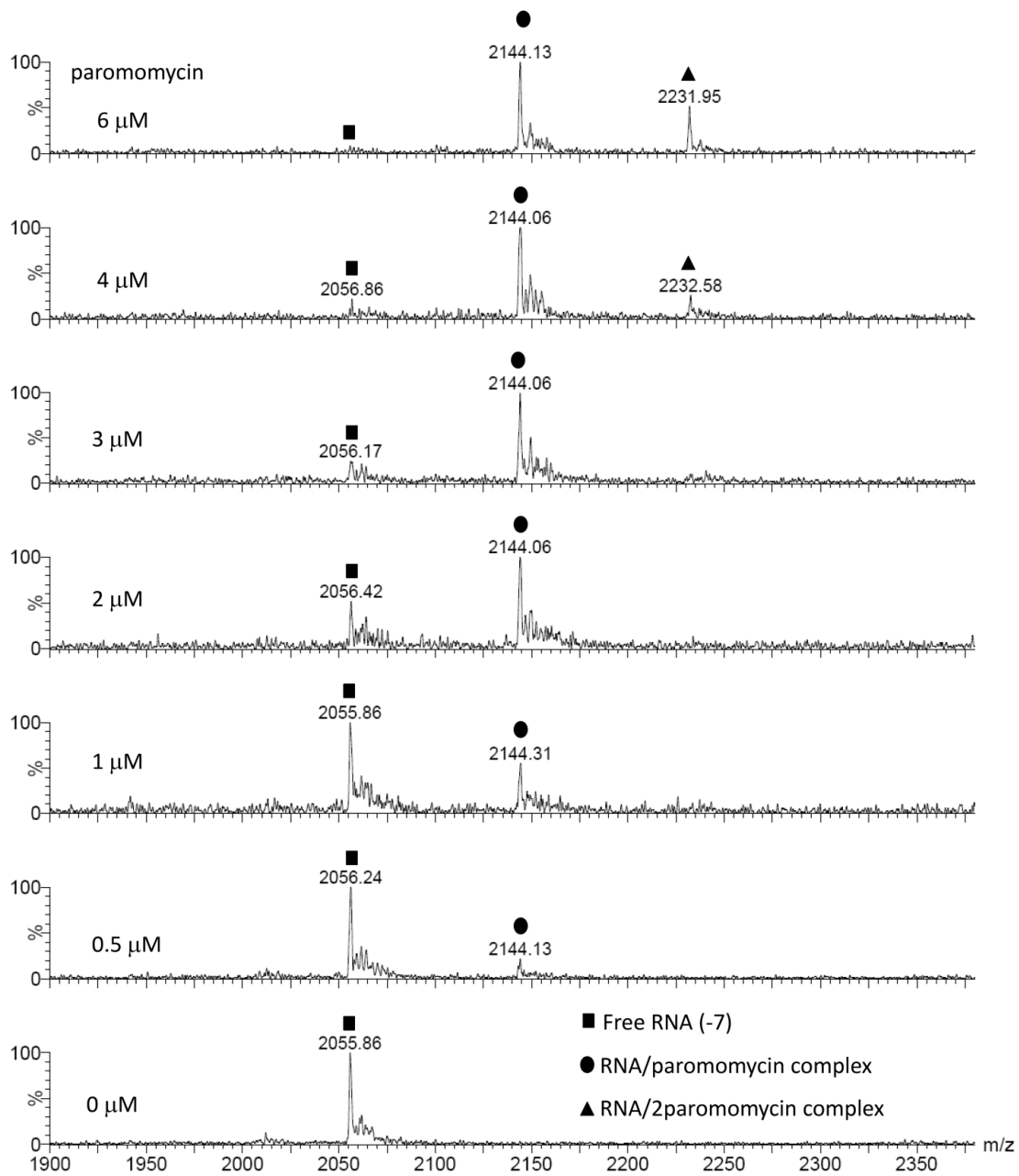
Figure 6.5: ESI-MS data for unmodified decoding region interactions with paromomycin are shown. The experiments were carried out in 150 mM ammonium acetate pH 7.0.
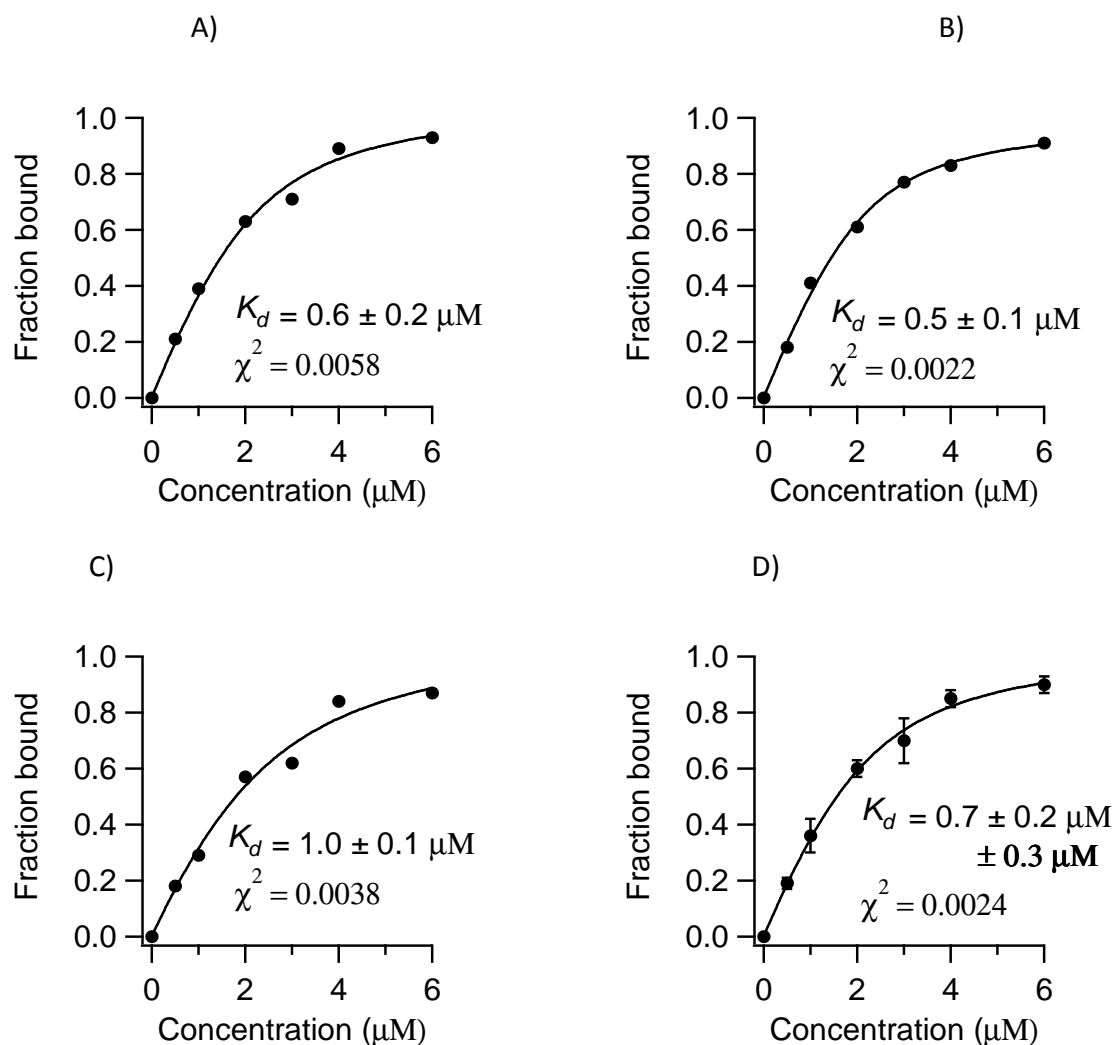
Figure 6.6: Binding curves (A-C) obtained from three different ESI-MS experiments between paromomycin and unmodified decoding region and (D) the average of the three experiments ± error of fit and **standard deviation** (in bold letters) are shown.
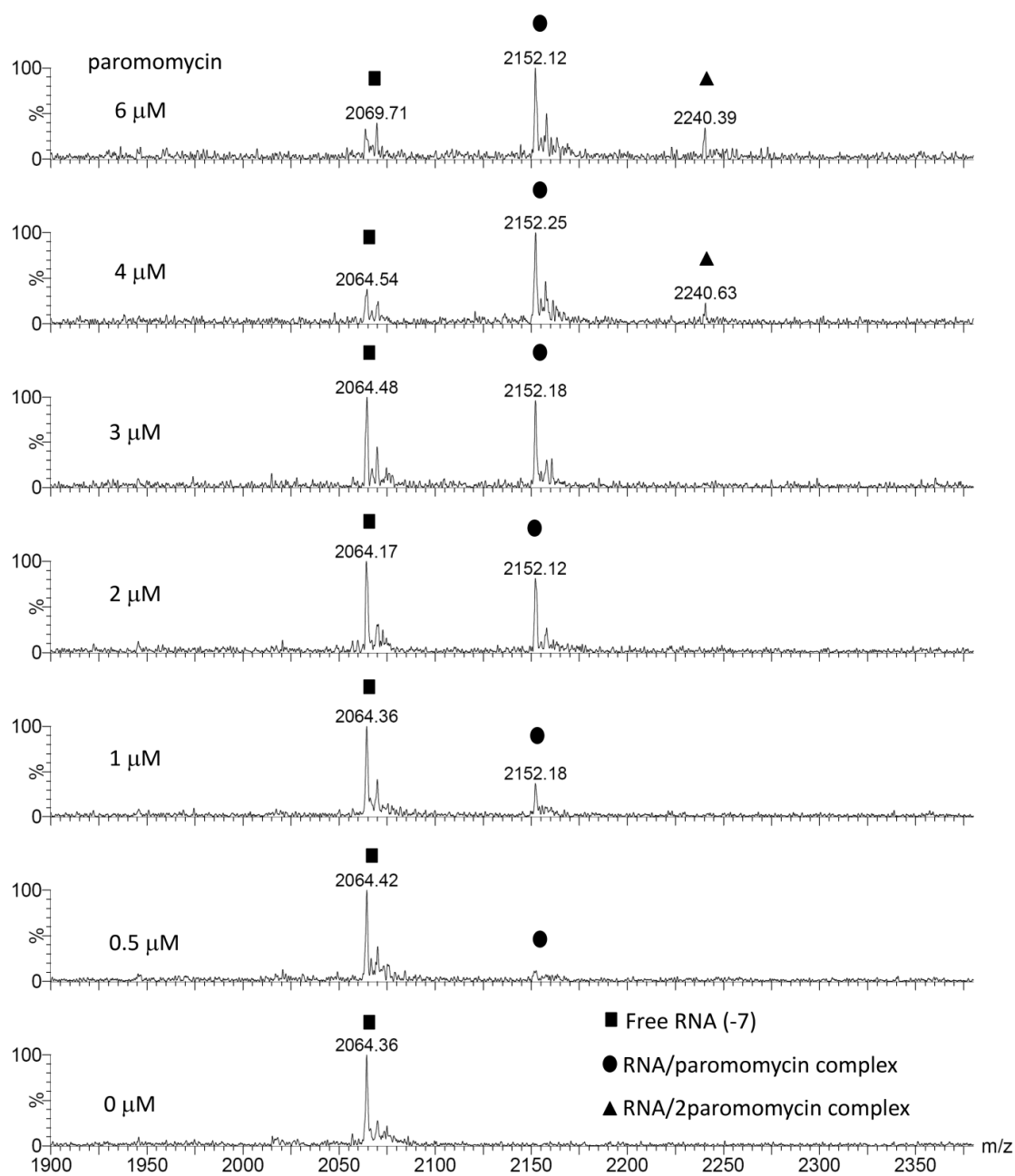
Figure 6.7: ESI-MS data for modified decoding region interactions with paromomycin are shown. The experiments were carried out in 150 mM ammonium acetate pH 7.0.
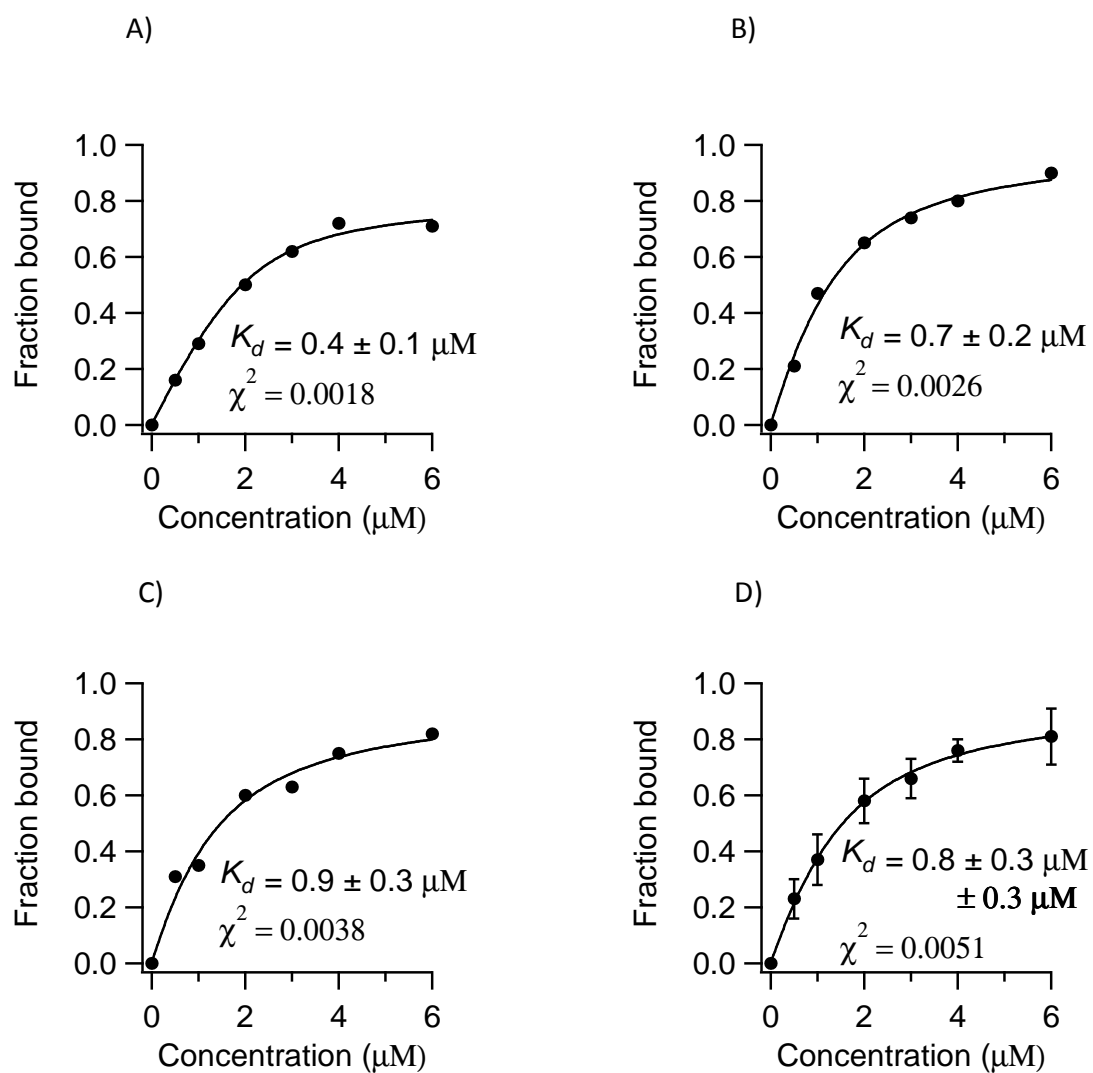
Figure 6.8: Binding curves (A-C) obtained from three different ESI-MS experiments between paromomycin and modified decoding region and (D) the average of the three experiments ± error of fit and **standard deviation** (in bold letters) are shown.
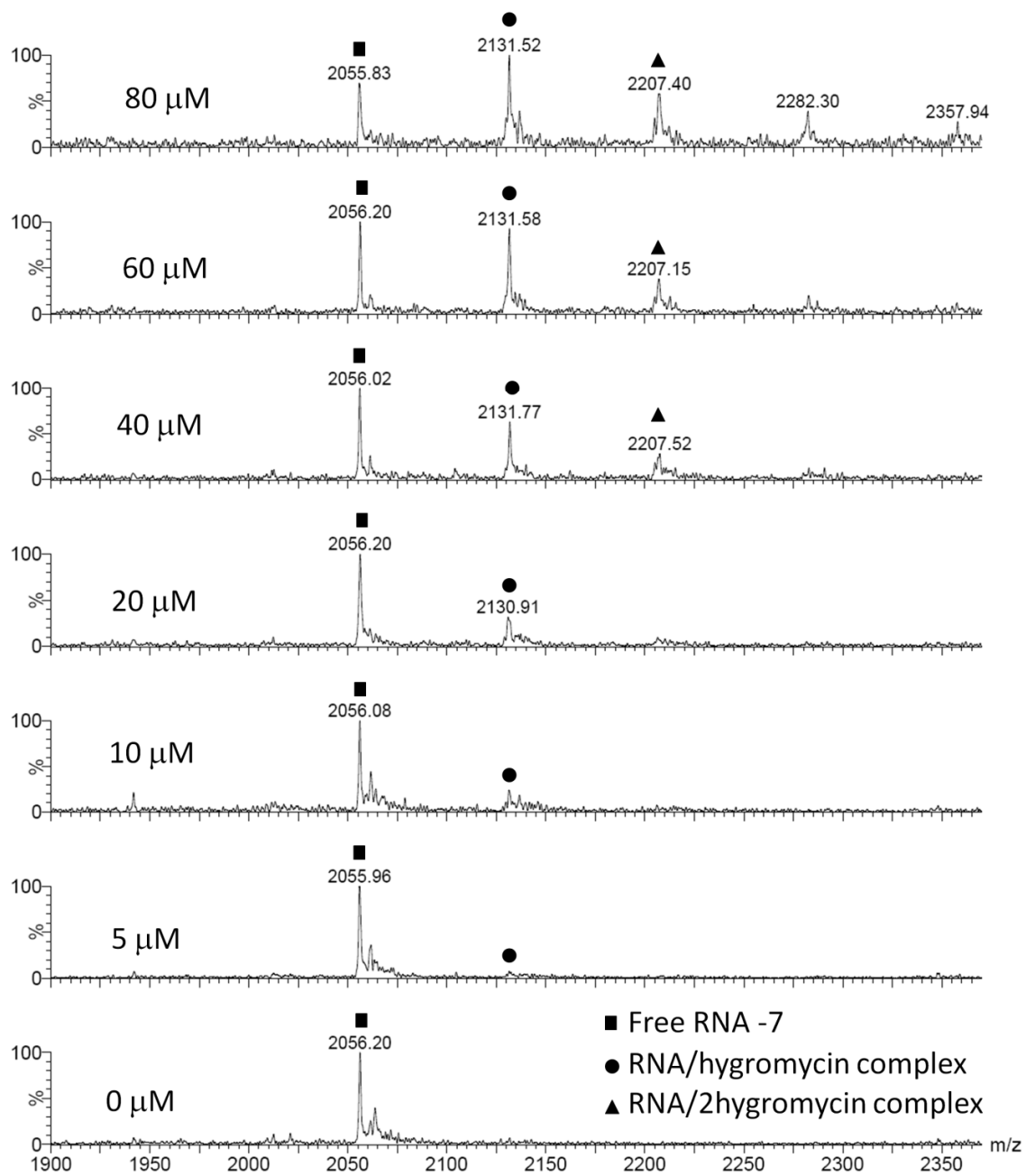
Figure 6.9: ESI-MS data for unmodified decoding region interactions with hygromycin are shown. The experiments were carried out in 150 mM ammonium acetate pH 7.0.
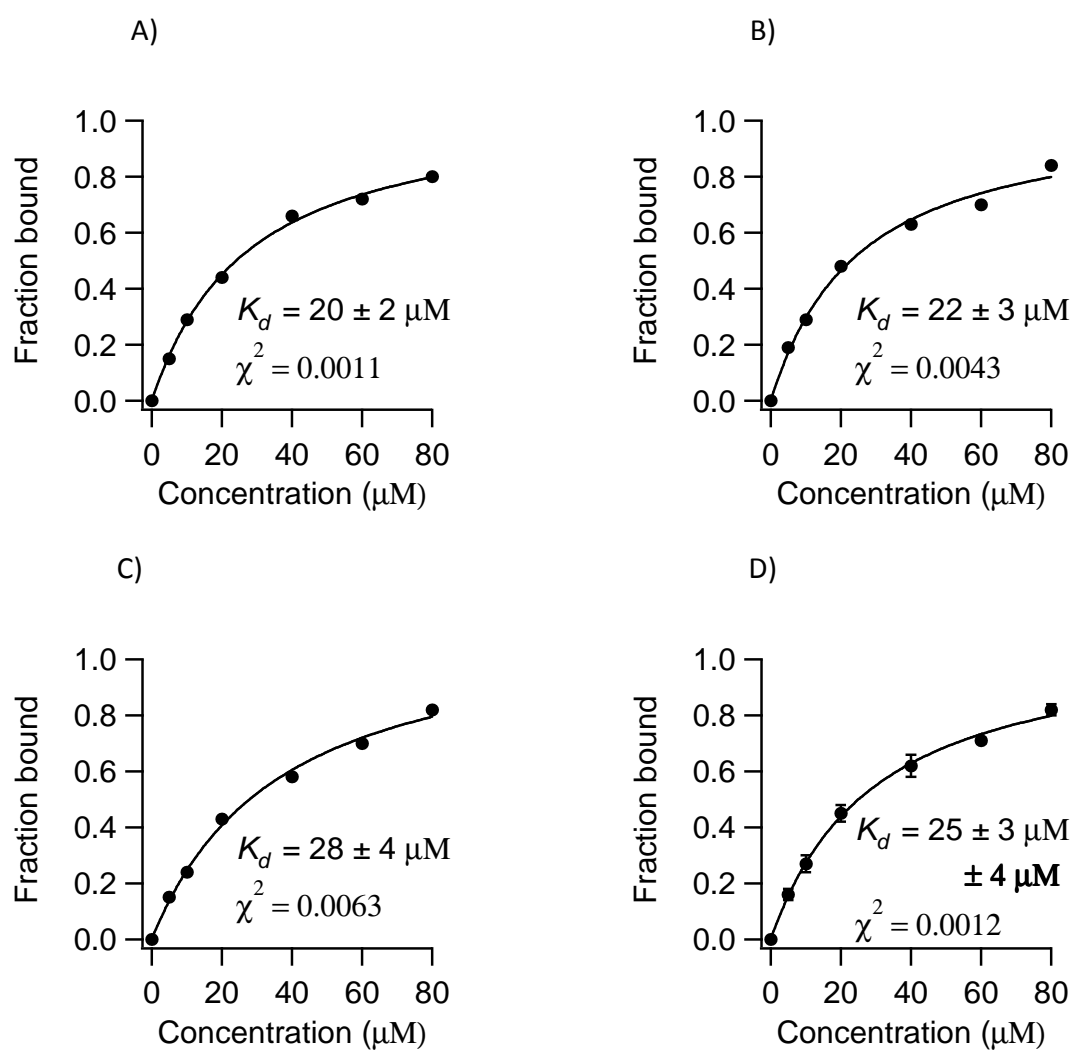
Figure 6.10: Binding curves (A-C) obtained from three different ESI-MS experiments between hygromycin and unmodified decoding region and (D) the average of the three experiments ± error of fit and **standard deviation** (in bold letters) are shown.
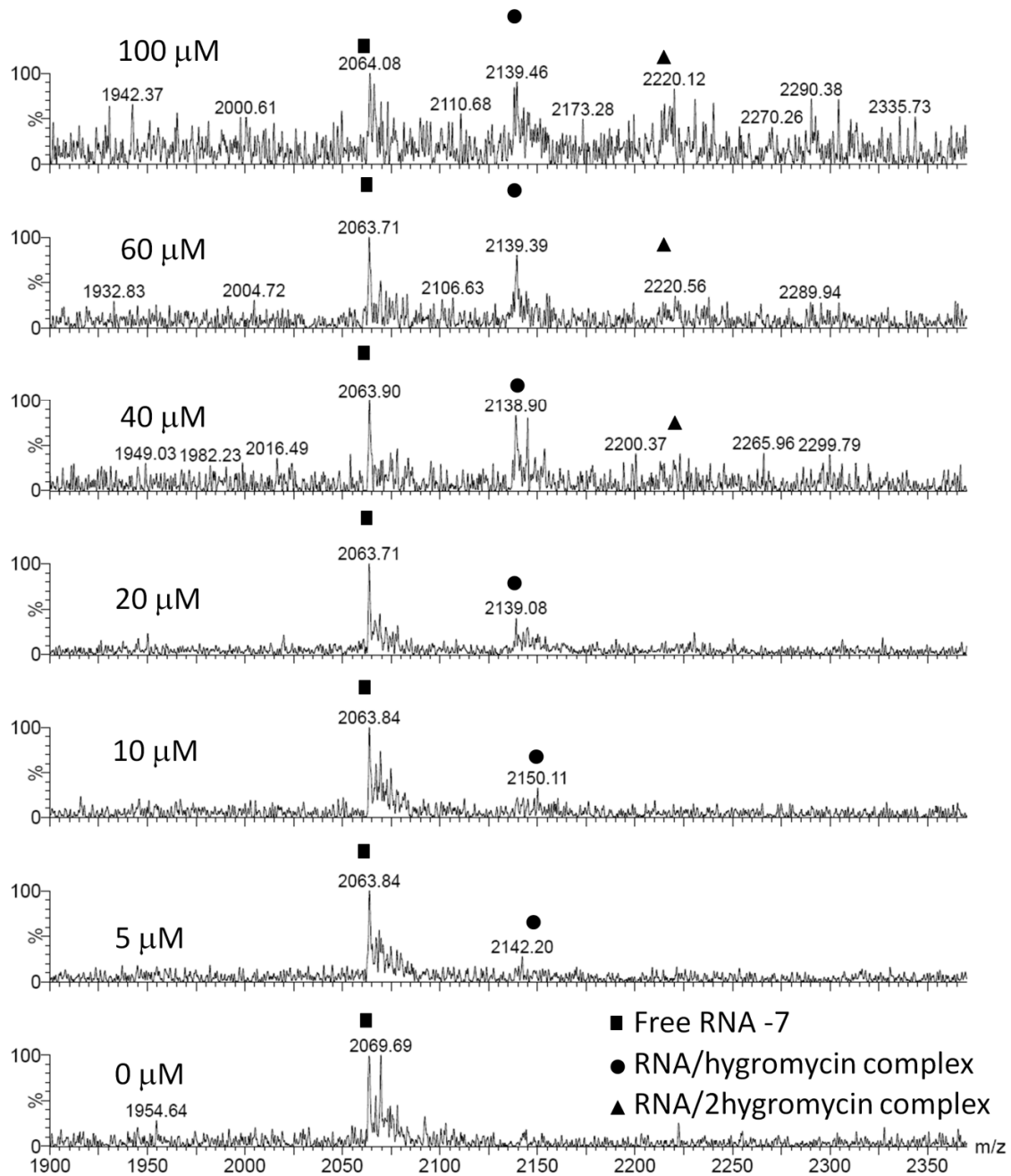
Figure 6.11: ESI-MS data for modified decoding region interactions with hygromycin are shown. The experiments were carried out in 150 mM ammonium acetate pH 7.0.
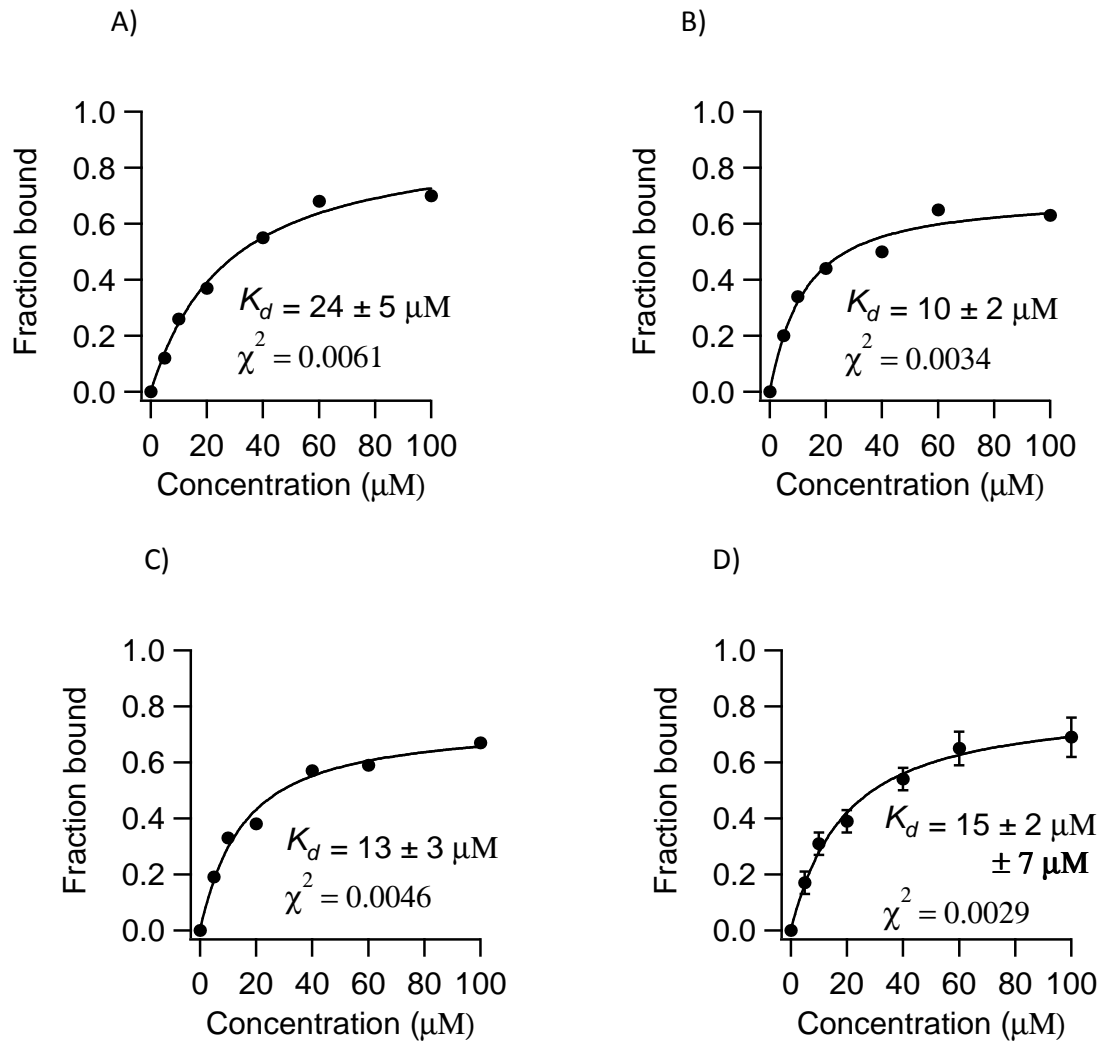
Figure 6.12: Binding curves (A-C) obtained from three different ESI-MS experiments between hygromycin and modified decoding region and (D) the average of the three experiments ± error of fit and **standard deviation** (in bold letters) are shown.
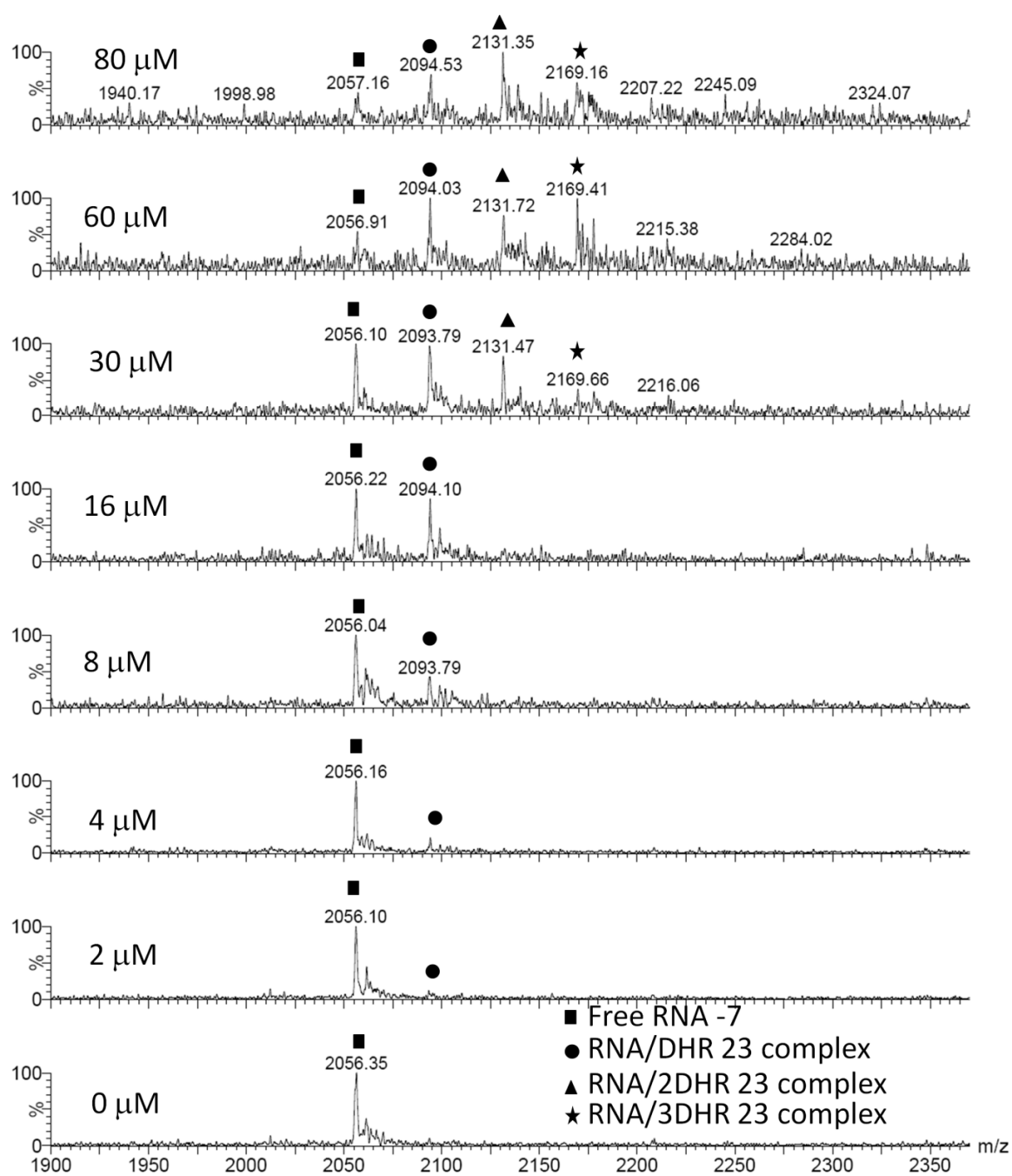
Figure 6.13: ESI-MS data for unmodified decoding region interactions with DHR23 are shown. The experiments were carried out in 150 mM ammonium acetate pH 7.0.
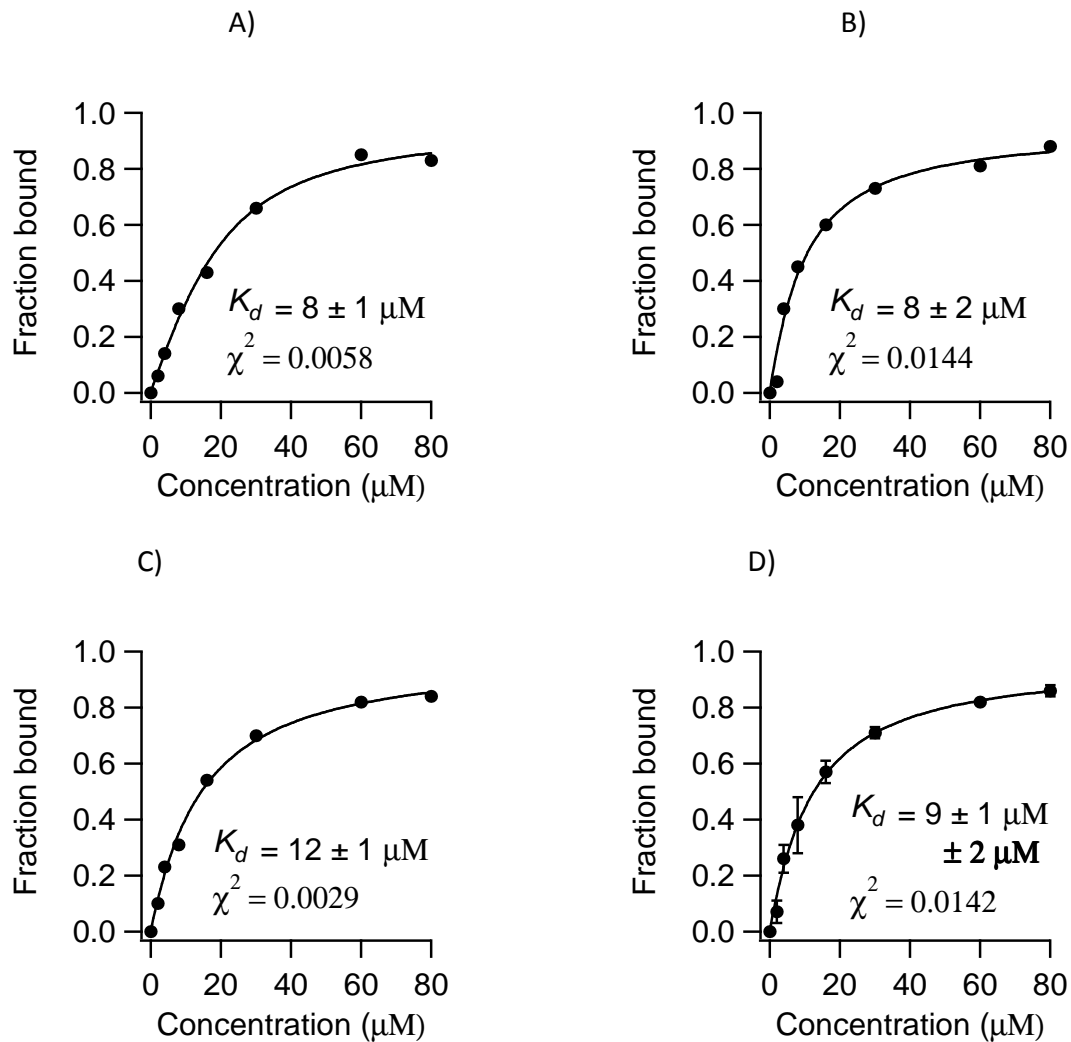
Figure 6.14: Binding curves (A-C) obtained from three different ESI-MS experiments between DHR23 and unmodified decoding region and (D) the average of the three experiments ± error of fit and **standard deviation** (in bold letters) are shown.
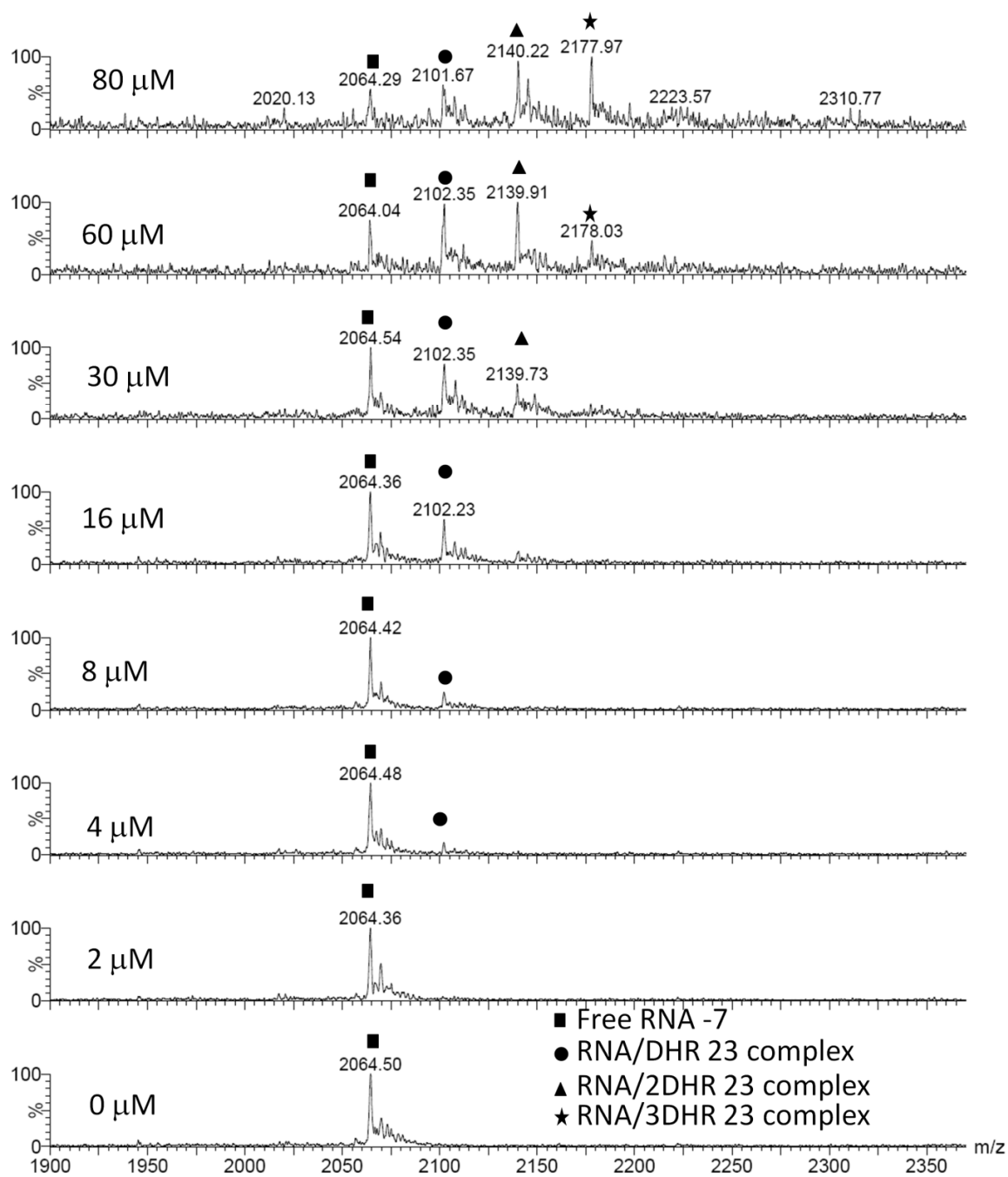
Figure 6.15: ESI-MS data for modified decoding region interactions with DHR23 are shown. The experiments were carried out in 150 mM ammonium acetate pH 7.0.
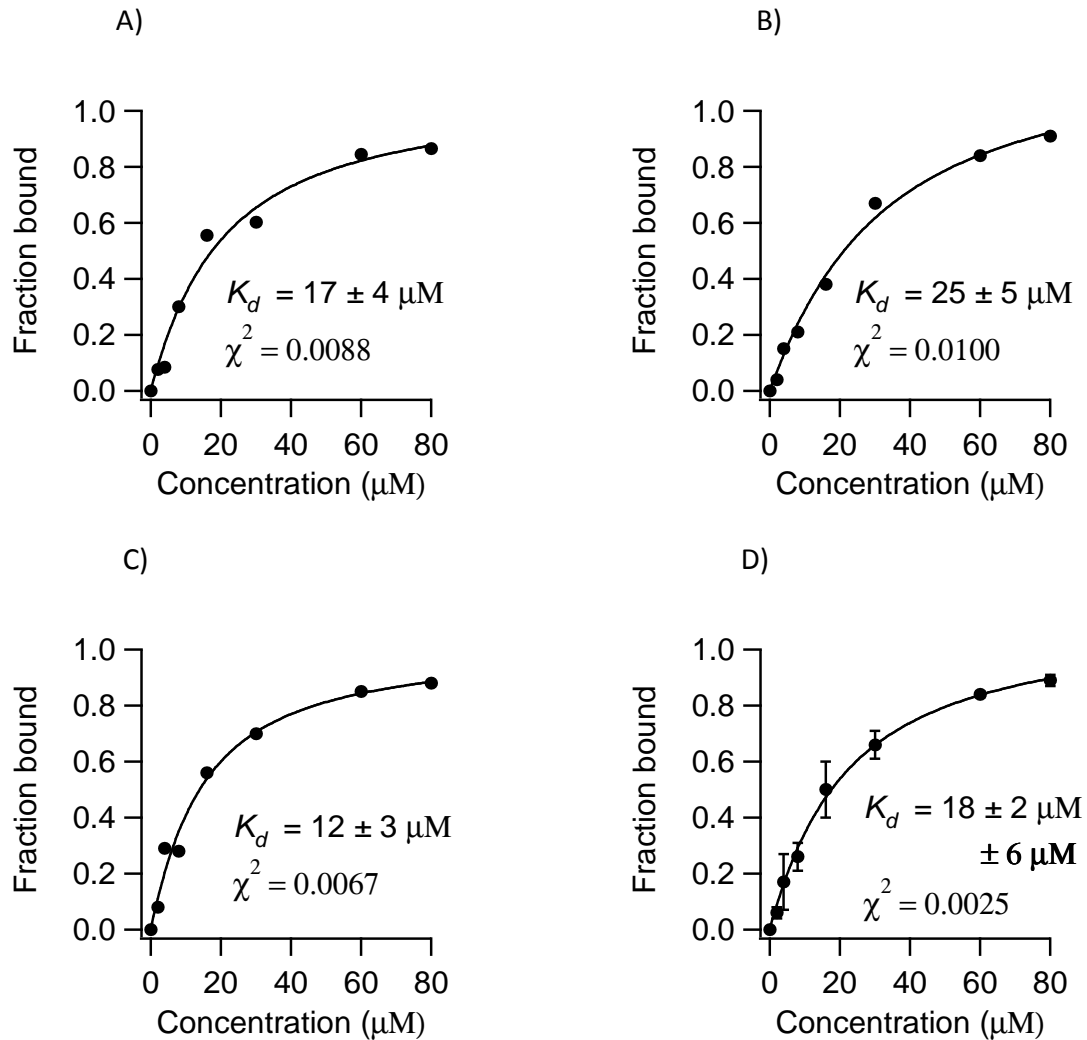
Figure 6.16: Binding curves (A-C) obtained from three different ESI-MS experiments between DHR23 and modified decoding region and (D) the average of the three experiments ± error of fit and **standard deviation** (in bold letters) are shown.
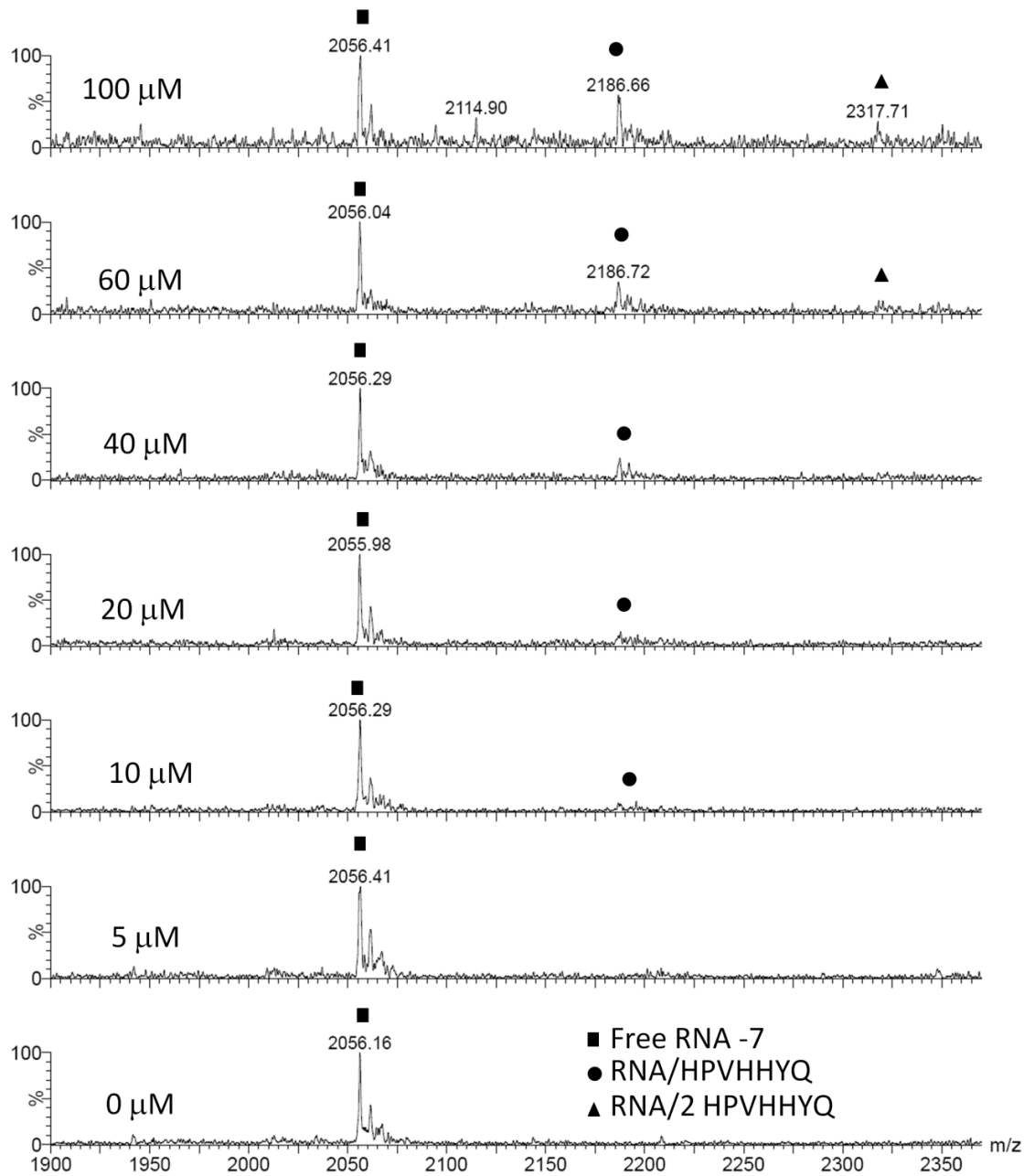
Figure 6.17: ESI-MS data for unmodified decoding region interactions with HPVHHYQ are shown. The experiments were carried out in 150 mM ammonium acetate pH 7.0.

A)

B)

C)

D)
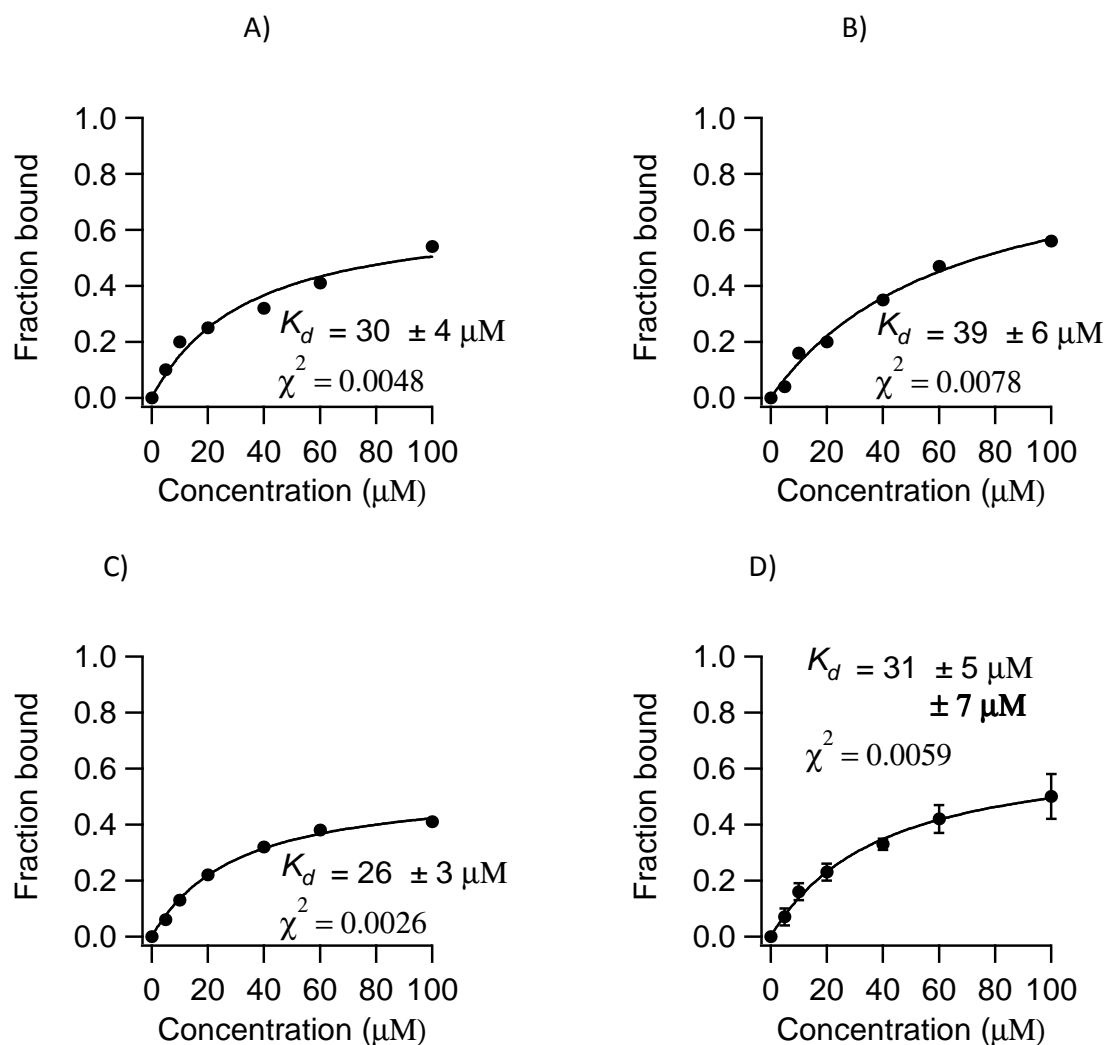
Figure 6.18: Binding curves (A-C) obtained from three different ESI-MS experiments between HPVHHYQ and unmodified decoding region and (D) the average of the three experiments ± error of fit and **standard deviation** (in bold letters) are shown.
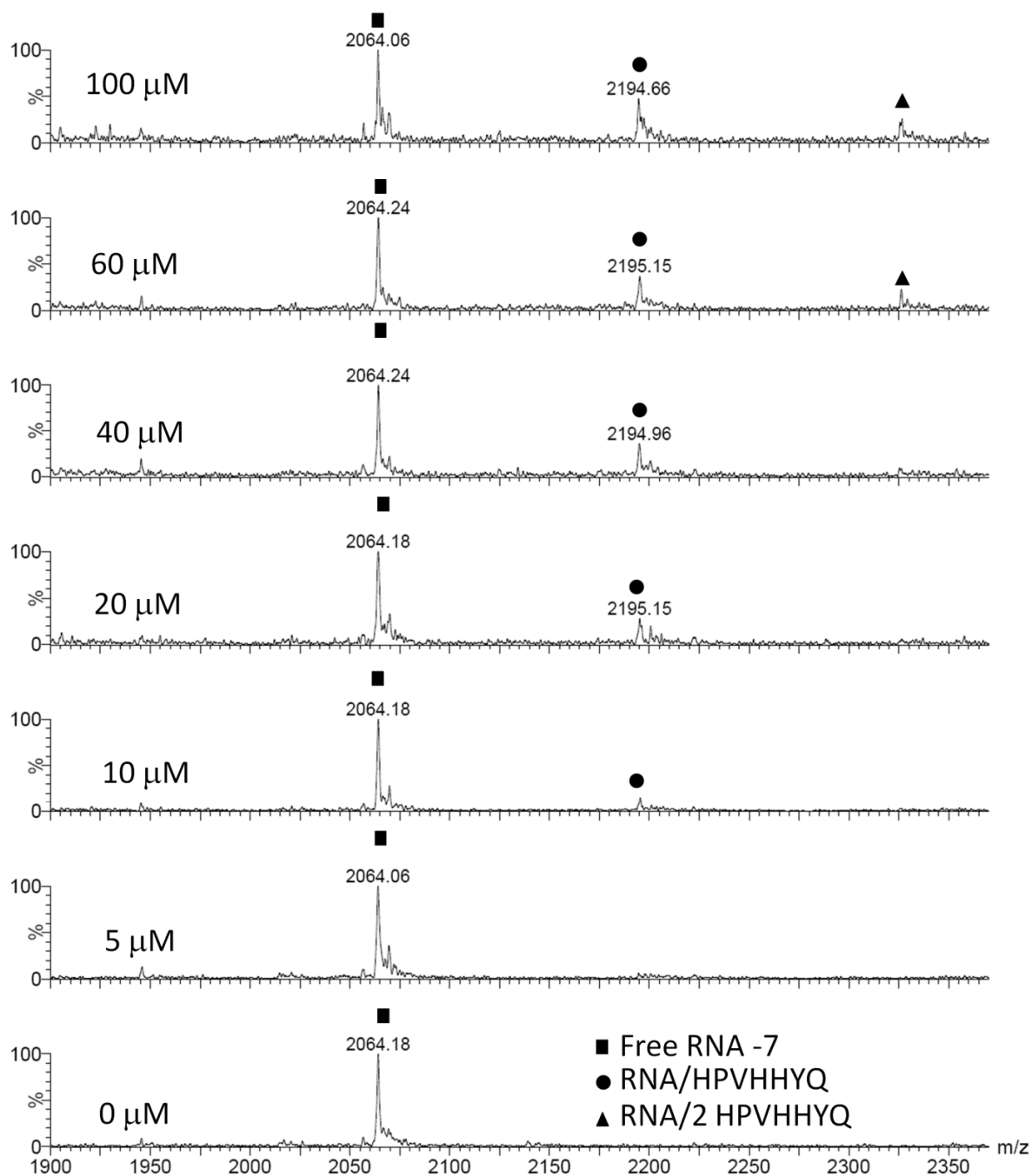
Figure 6.19: ESI-MS data for modified decoding region interactions with HPVHHYQ are shown. The experiments were carried out in 150 mM ammonium acetate pH 7.0.
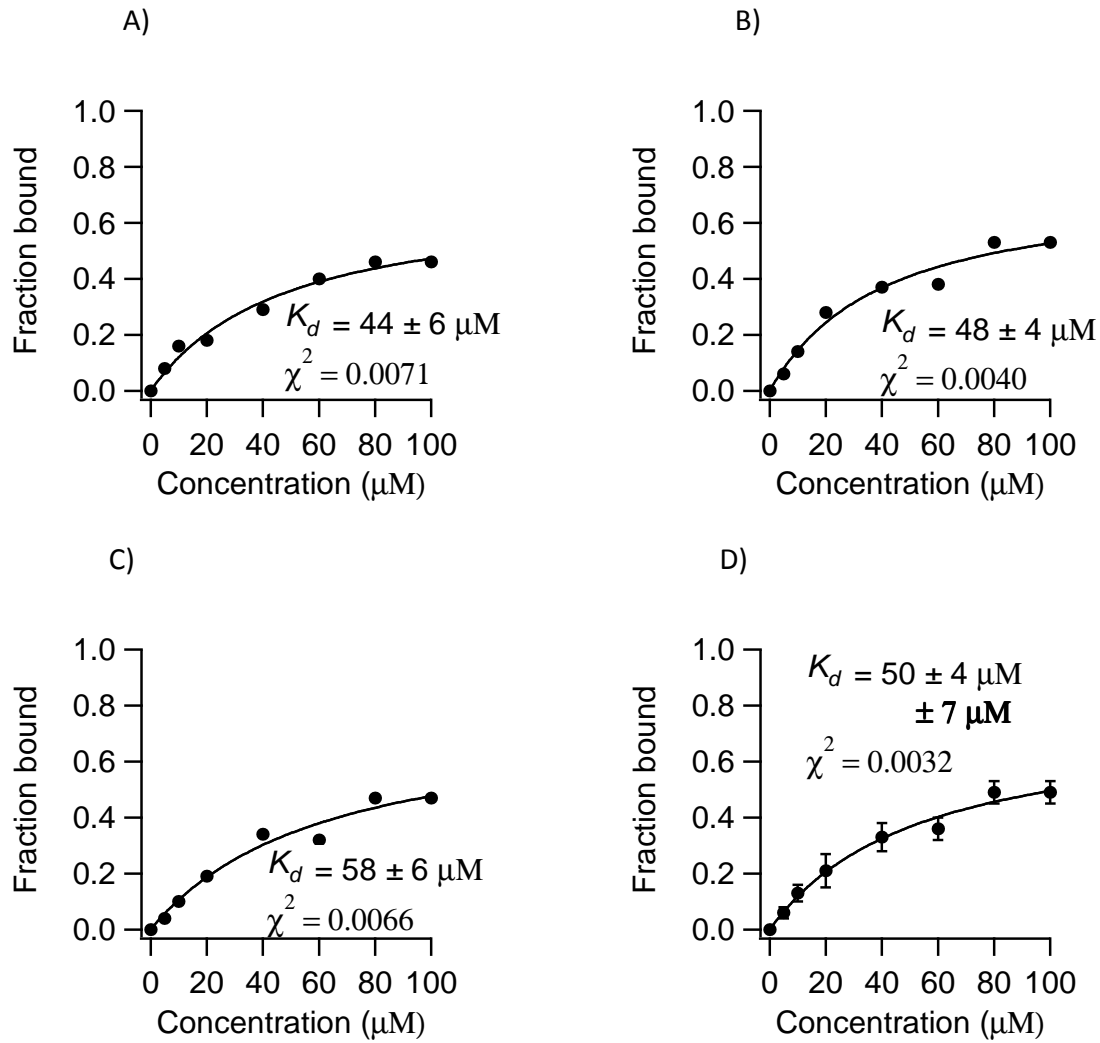
Figure 6.20: Binding curves (A-C) obtained from three different ESI-MS experiments between HPVHHYQ and modified decoding region and (D) the average of the three experiments ± error of fit and **standard deviation** (in bold letters) are shown.
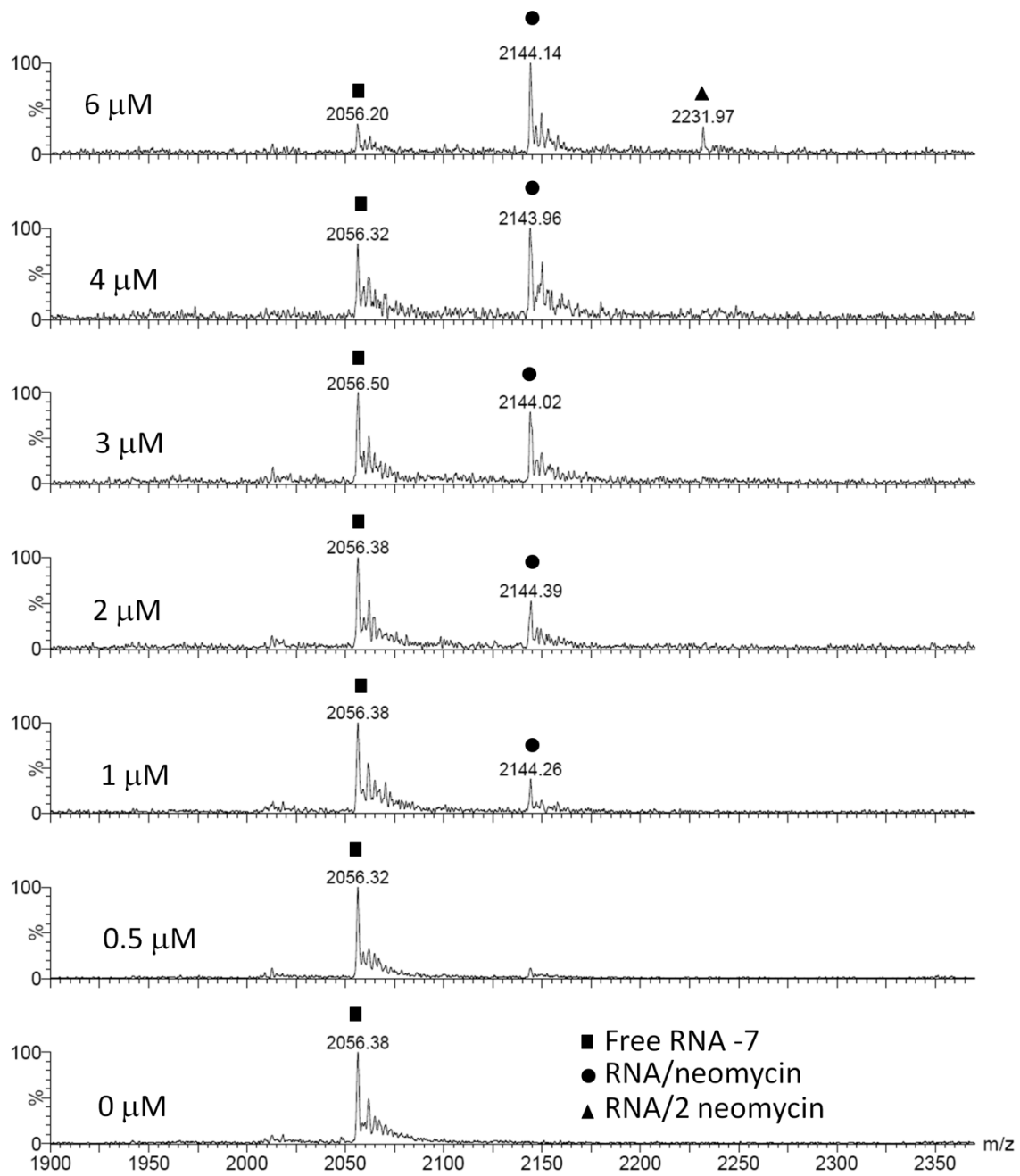
Figure 6.21: ESI-MS data for unmodified decoding region interactions with neomycin are shown. The experiments were carried out in 150 mM ammonium acetate pH 7.0.
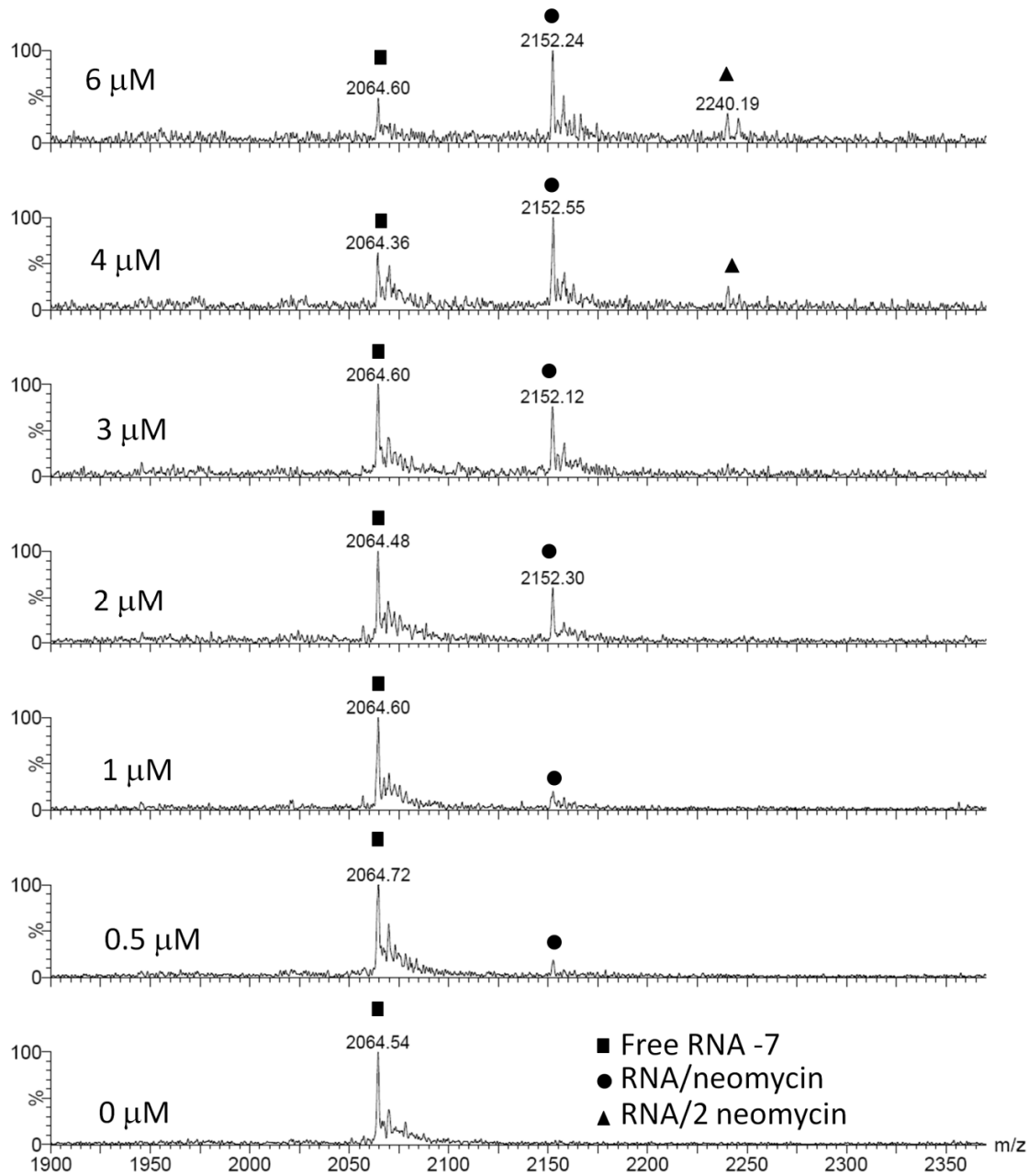
Figure 6.22: ESI-MS data for modified decoding region interactions with neomycin are shown. The experiments were carried out in 150 mM ammonium acetate pH 7.0.
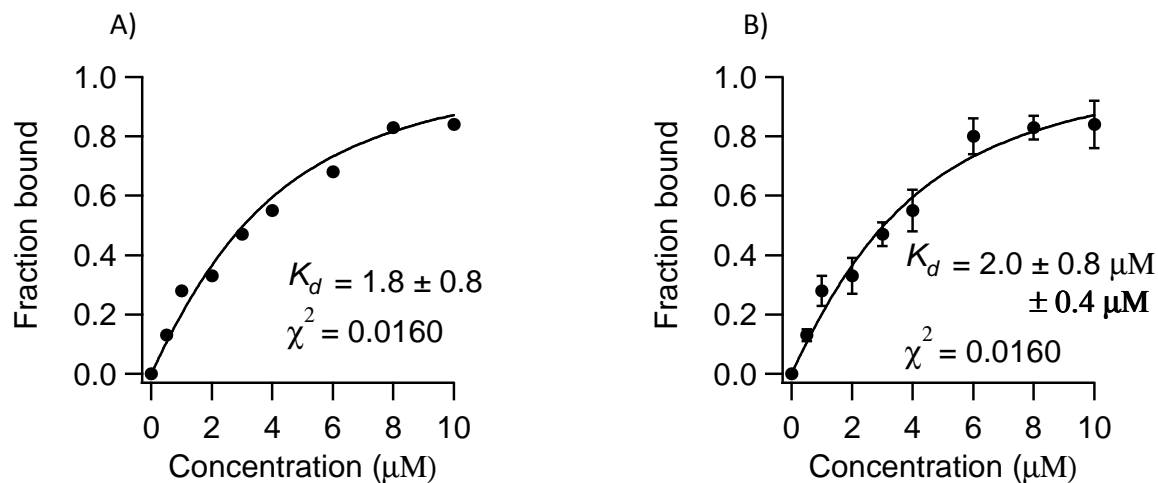
Figure 6.23: Binding curve (A) obtained from two different ESI-MS experiments between neomycin and unmodified decoding region and (B) the average of the two experiments ± error of fit and **standard deviation** (in bold letters) are shown are shown.
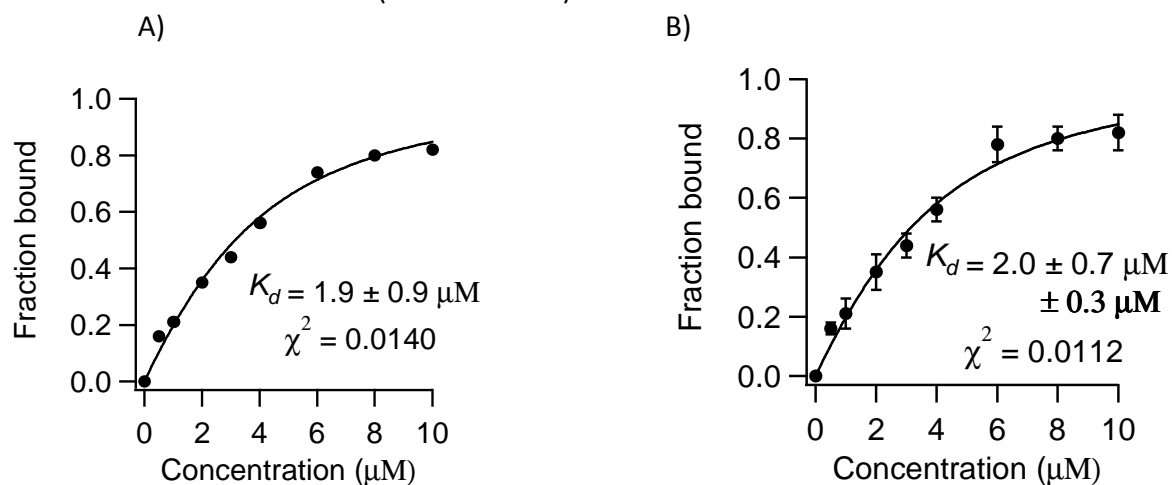
Figure 6.24: Binding curve (A) obtained from two different ESI-MS experiments between neomycin and modified decoding region and (B) the average of the two experiments ± error of fit and **standard deviation** (in bold letters) are shown are shown.
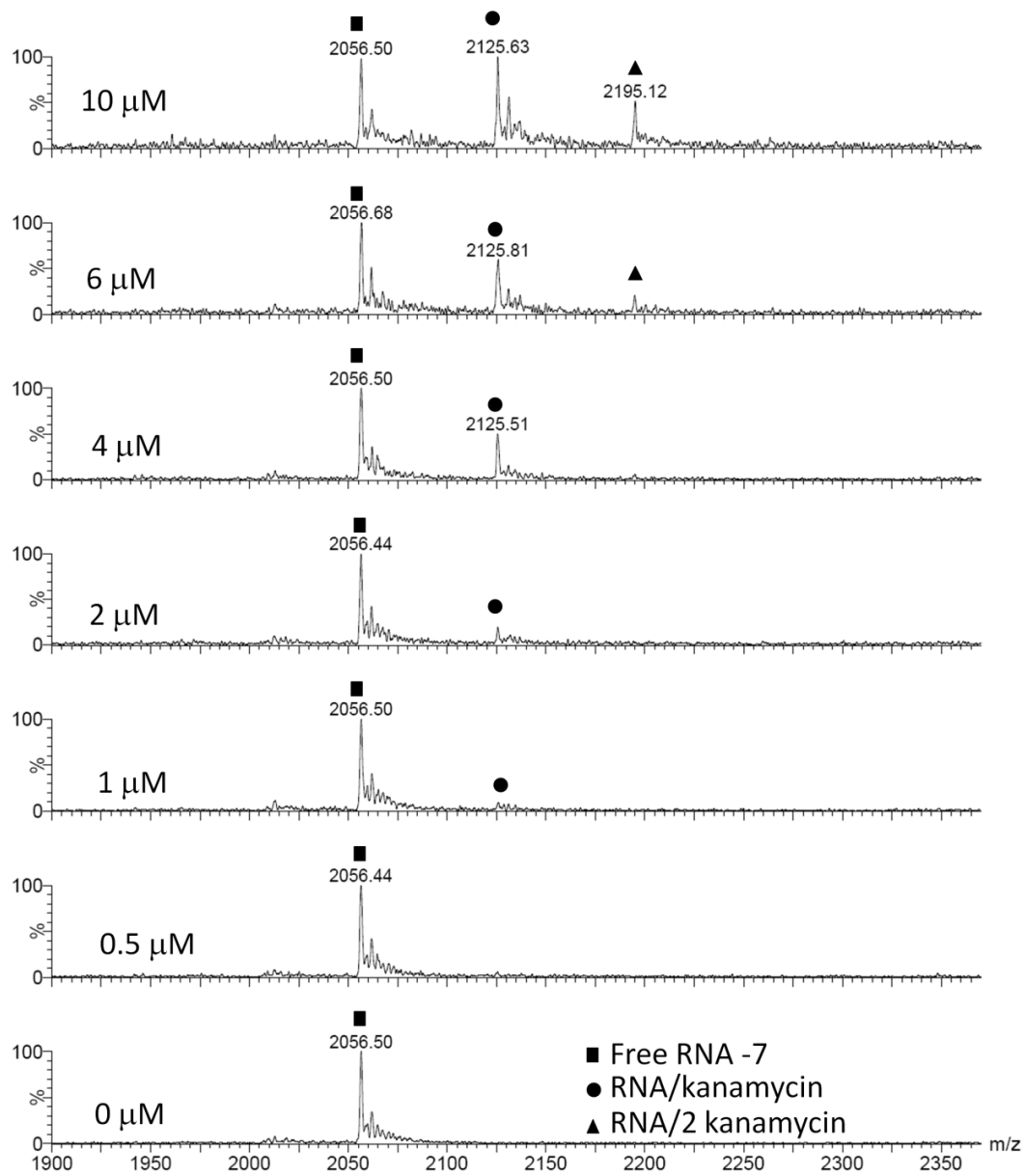
Figure 6.25: ESI-MS data for unmodified decoding region interactions with kanamycin are shown. The experiments were carried out in 150 mM ammonium acetate pH 7.0.
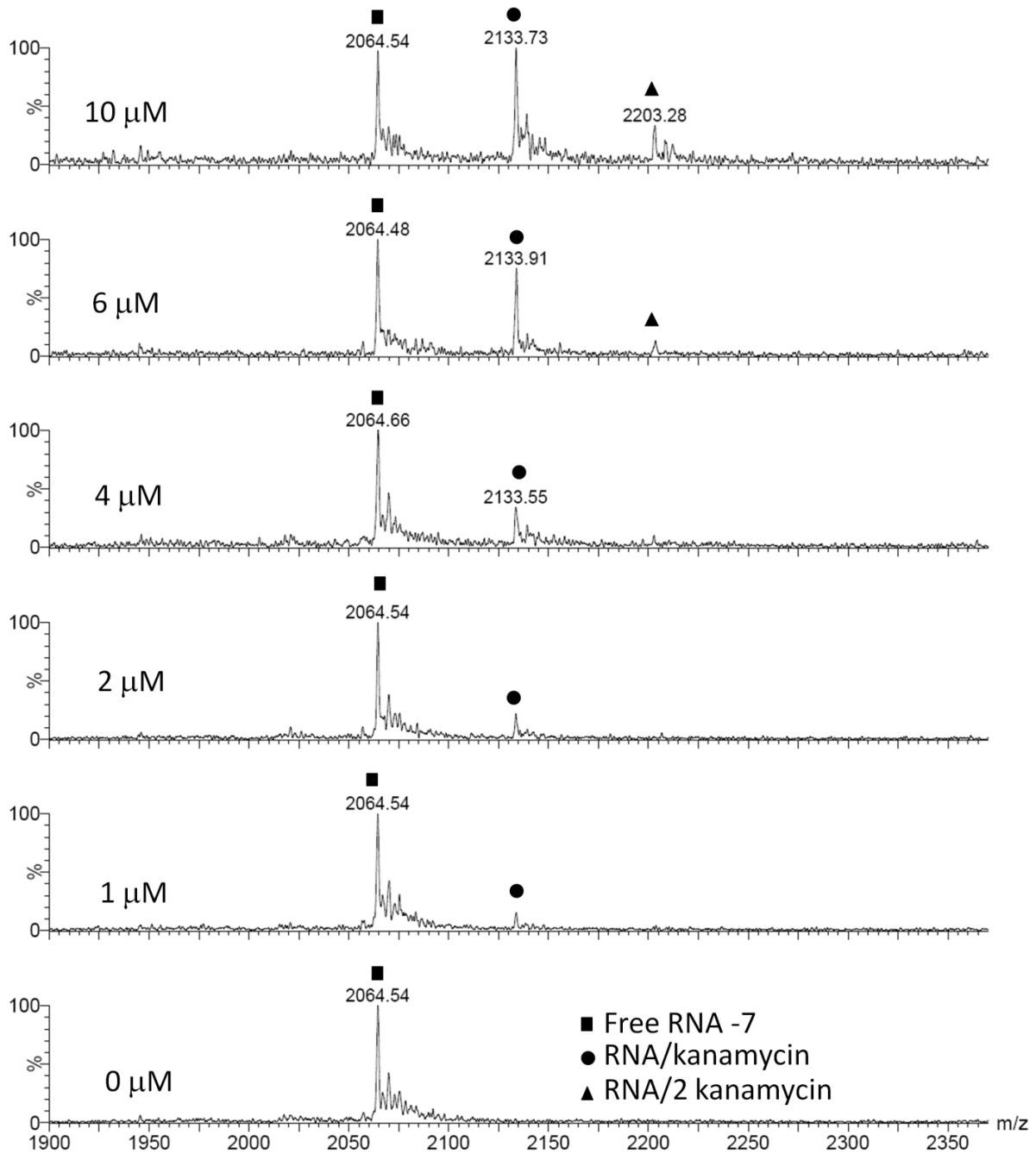
Figure 6.26: ESI-MS data for modified decoding region interactions with kanamycin are shown. The experiments were carried out in 150 mM ammonium acetate pH 7.0.
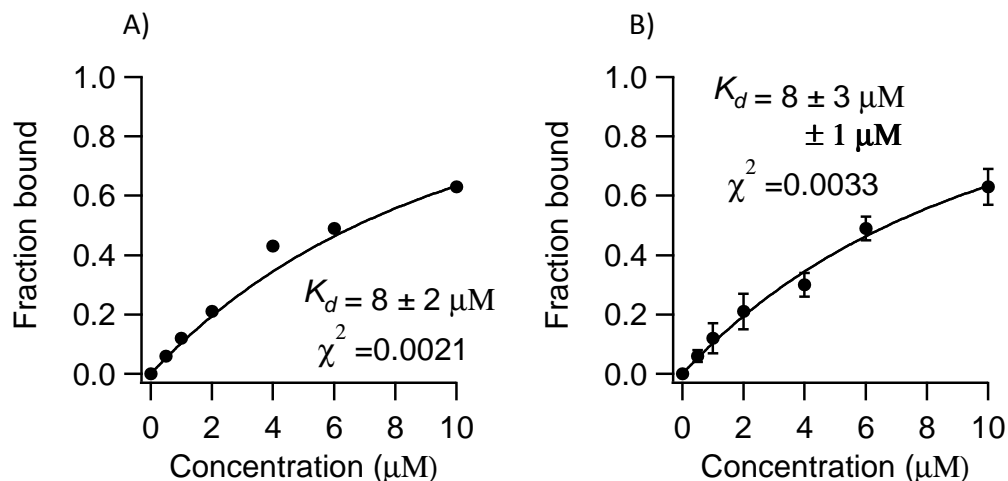
Figure 6.27: Binding curve (A) obtained from two different ESI-MS experiments between kanamycin and unmodified decoding region and (B) the average of the two experiments ± error of fit and **standard deviation** (in bold letters) are shown are shown.
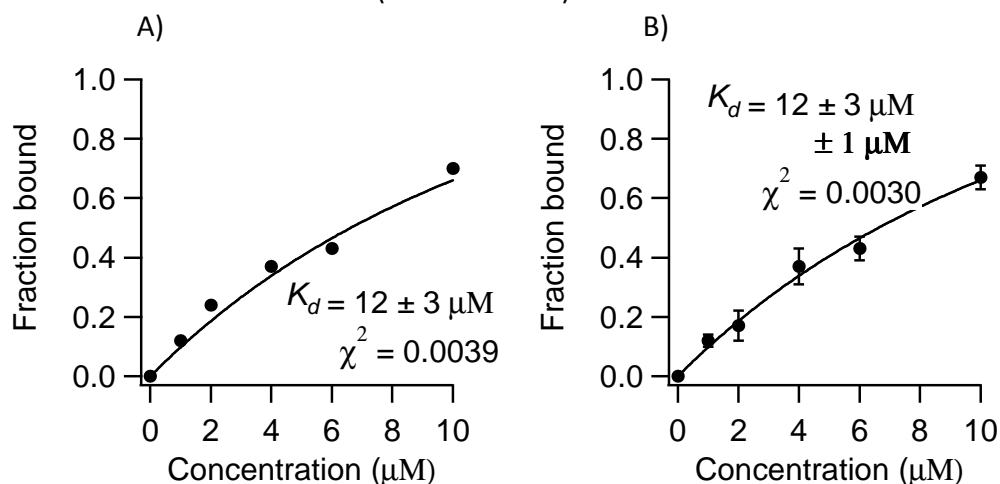
Figure 6.28: Binding curve (A) obtained from thw0 different ESI-MS experiments between kanamycin and modified decoding region and (B) the average of the three experiments ± error of fit and **standard deviation** (in bold letters) are shown are shown.

CHAPTER 7

CONCLUSIONS

The prevalence of antibiotic resistance poses a huge challenge for the healthcare industry as well as research scientists.[2] Development of new antibiotics has made major strides, especially in the field of aminoglycoside research. Some brilliant efforts from many laboratories have helped propel the improvement of the efficacy of current aminoglycosides.[214, 216, 272] However, the race is far from over; more research is needed to combat the resistance problem.[114, 205] Resistance to aminoglycosides can occur in a variety of ways; however, the most common type is enzymatic modification of their hydroxyl and amino groups, which affects the ability of the compounds to bind to the target RNA.[114, 205]

This thesis work focused on improving the efficacy of current aminoglycosides by developing and testing new derivatives. Previous structure studies suggested that the minimal motif for specific binding of aminoglycosides to the A site of the ribosome is neamine.[6] Therefore, using a reductionist approach, a series of aminoglycoside analogues based on the neamine core was tested. The aim was to maintain the minimal structure required for specific binding to the A site, but avoid modification by resistance enzymes. Our methodical approach yielded new insights to aminoglycoside-RNA interactions. The binding affinity of ring I could be enhanced by more than 100-fold through modifications at the five functional group positions. Through incremental changes made to the parent compound in collaboration with Dr. Mobashery and Pei-Wen Chao, we were able to determine that charge formation or hydrogen

bonding at the N1 position of ring I is critical for binding to the A site.[201] Also, addition of a γ-amino-α-hydroxybutyryl group at the N1 position enhanced the binding affinity of ring I by approximately 40-fold. In contrast, addition of a second γ-amino-α-hydroxybutyryl group at N6 decreased the binding affinity by three-fold.[201] These results among others indicate that bulky groups are not well tolerated at the N6 position.

The analogue with the best affinity to the A site (DHR23), was determined through footprinting assays to bind to the internal bulge region of the A-site RNA. This was a very encouraging result because, in spite of the absence of the other three rings in paromomycin, DHR23 was still able to bind to the internal bulge region of the A-site RNA. However, the binding of DHR23 to this region did not elicit the conformational changes similar to that observed upon paromomycin binding.[95, 207, 237] This result suggests that the other rings in paromomycin may position it in a unique way in order to have specific contacts with the RNA, which are absent in DHR23. The lesson learned from this result is that specific binding to the A site is not a guarantee for antibacterial activity; however, including functionalities that can mimic the contacts made by the other rings in paromomycin would be fruitful in generating functionally useful A-site binders.

In the quest to develop new antibiotics, one of the major impediments is the availability of relatively simple high-throughput methods to screen RNA-binding ligands. In our efforts to bridge this gap, a fluorescent indicator (TO-PRO) method was developed.[166] ESI-MS was employed to investigate the mechanism of the assay, and the results obtained provide molecular evidence that correlates the reduction in fluorescence observed in the FID assay with

the displacement of the TO-PRO dye molecule from RNA. The assay was successfully applied to screen a variety of RNA ligands and our results suggest that this assay is an appropriate method for obtaining relative binding affinities of a variety of ligands to RNA, including amino sugars, peptides, and planar aromatic compounds. The FID assay will be amenable to high-throughput screening because it is a sensitive, fluorescence-based method that can be done on 96- or 384- well plate formats. Furthermore, the system is compatible with cationic buffer components, including Mg^{2+}, Na^+, and K^+, which are not suitable for ESI-MS screening.

One reason why aminoglycosides are effective antibiotics is because they preferentially target bacterial ribosomes over eukaryotic ribosomes.[163] This is due to subtle nucleotide differences in the A site of the bacteria as compared to eukaryotes. Binding studies were performed to test specificity of DHR23 compared to paromomycin, and also to identify new potential RNA targets. In the absence of the other rings in paromomycin, DHR23 had a 10-fold decrease in affinity to the bacterial A site. Even with this reduction in affinity, it still retained a slight preference for the bacterial A-site RNA over the human A-site RNA. This selectivity may be an inherent property of amino sugars which makes them structurally compatible with the bacterial A-site internal bulge. This was evident in both the FID and specificity studies in which RNAs such as H69 and TAR RNA that fold into tertiary structure conformations similar to that of the A-site internal bulge[293, 326] provided scaffolds for favorable binding of paromomycin and DHR23. This was contrasted with poor binding of paromomycin and DHR23 to h31, a helix that adopts a conformation very different from the A-site internal bulge region.[106]

In the last part of this thesis work, the effect of modified nucleotides on ligand binding was explored using ESI-MS. There are numerous modified nucleotides present in the ribosome.[46] The modified nucleotides are thought to modulate the specific folding of the RNA in a variety of ways including improving base stacking,[294-296] and increasing or decreasing the potential for hydrogen bonding.[297-299] These properties may affect RNA-ligand interactions. Ligand-binding experiments were performed with modified and unmodified decoding region constructs. Our results indicate that modified nucleotides may affect binding affinity if they are present at or near the ligand-binding pocket. For example, the affinity of hygromycin B for the modified decoding region was enhanced by approximately 1.5-fold due to the presence of the modified nucleotide m^{3}U1498. This increase in affinity could be due to enhanced hydrogen-bond interactions between the modified nucleotide and hygromycin or due subtle conformational changes resulting from the presence of the modified nucleotides, which lead to favorable interactions with the RNA. Conversely, the presence of the modified nucleotide m^{5}C1407 appeared to decrease the affinity of peptide HPVHHYQ for the modified decoding region construct. This result was not surprising because HPVHHYQ was selected through phage display against an unmodified A-site RNA.[314] Thus, these results suggest that as synthesis of modified nucleosides becomes more accessible and less expensive, it would be worthwhile to use modified nucleotides or wild-type nucleotides in ligand screening and selection assays.

In summary, the results from this work have shown that generation of compounds based on these simplified structures in combination with FID screening may lead to selective reagents for RNA internal bulges, loops, mismatches, or other unique secondary structure

elements. Also, including functional groups that mimic the contacts made by rings II-IV of paromomycin and screening with wild-type (modified) RNA constructs may lead to identification of ligands high selectivity and efficacy.

Future plans to improve the efficacy of DHR23 include coupling it with HPVHHYQ, a peptide found to stabilize the flipped out conformation of A1492 and A1493 (**Figure 7.1**).[314] We hypothesize that conjugating the two compounds will have a synergistic effect; imparting on the hybrid compound the specificity of DHR23 and the efficacy of HPVHHYQ. Also, molecular modeling of DHR23 bound to the A site will be helpful to determine the kinds of functionalities that can be added to DHR23 in order to mimic the specific interactions observed between the parent compound paromomycin and the A site. Information from the molecular modeling studies will be valuable in generating functionally useful A-site binders. Another avenue worth exploring is coupling DHR23 to planar molecules such as CR1119 (Chapter 4) (**Figure 7.2**). This may result in generation of molecules that specifically target structured RNA including internal loops and hairpins loops.[327]
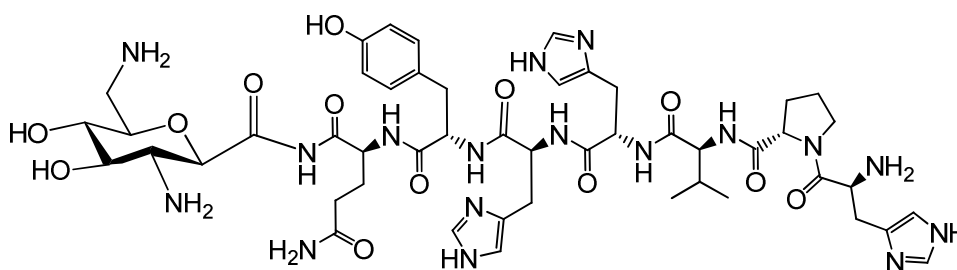
Figure 7.1: Chemical structure of DHR23 conjugated to HPVHHYQ is shown
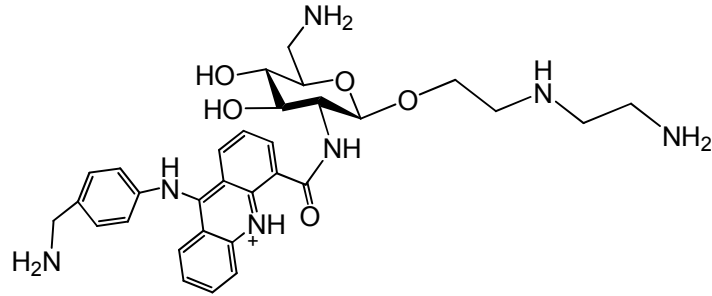
Figure 7.2: Chemical structure of DHR23 conjugated to a truncated CR1119 is shown.

REFERENCES

1.   Goldsworthy, P. D.; McFarlane, A. C. Howard Florey, Alexander Fleming and the fairy tale of penicillin. *Med. J. Aust.* 2002, 176, 176-178.

2.   Maragakis, L. L.; Perencevich, E. N.; Cosgrove, S. E. Clinical and economic burden of antimicrobial resistance. *Expert. Rev. Anti. Infect. Ther.* 2008, 6, 751-763.

3.   Khardori, N. Antibiotics-past, present, and future. *Med. Clin. North. Am.* 2006, 90, 1049-1076.

4.   Tomasz, A. From penicillin-binding proteins to the lysis and death of bacteria: a 1979 view. *Rev. Infect. Dis.* 1979, 1, 434-467.

5.   Drlica, K. Mechanism of fluoroquinolone action. *Curr. Opin. Microbiol.* 1999, 2, 504-508.

6.   Fourmy, D.; Recht, M. I.; Puglisi, J. D. Binding of neomycin-class aminoglycoside antibiotics to the A-site of 16 S rRNA. *J. Mol. Biol.* 1998, 277, 347-362.

7.   Hansen, J. L.; Moore, P. B.; Steitz, T. A. Structures of five antibiotics bound at the peptidyl transferase center of the large ribosomal subunit. *J. Mol. Biol.* 2003, 330, 1061-1075.

8.   Tenson, T.; Lovmar, M.; Ehrenberg, M. The mechanism of action of macrolides, lincosamides and streptogramin B reveals the nascent peptide exit path in the ribosome. *J. Mol. Biol.* 2003, 330, 1005-1014.

9.   Aszodi, J.; Bryskier, A. *Resistance to β-latams, a self-regenerating problem*. Kluwer Academic Publishers: Dordrecht, 2001.

10. Reynolds, P. E. *The genetic and biochemistry of resistance to glycopeptide antibiotics*. Kluwer Academic Publishers: 2001; p 99-115.

11. Hancock, R. E. Alterations in outer membrane permeability. *Annu. Rev. Microbiol.* 1984, 38, 237-264.

12. Kotra, L. P.; Haddad, J.; Mobashery, S. Aminoglycosides: perspectives on mechanisms of action and resistance and strategies to counter resistance. *Antimicrob. Agents Chemother.* 2000, 44, 3249-3256.

13. Liou, G. F.; Yoshizawa, S.; Courvalin, P.; Galimand, M. Aminoglycoside resistance by ArmA-mediated ribosomal 16S methylation in human bacterial pathogens. *J. Mol. Biol.* 2006, 359, 358-364.

14. Masuda, N.; Sakagawa, E.; Ohya, S.; Gotoh, N.; Tsujimoto, H.; Nishino, T. Substrate specificities of MexAB-OprM, MexCD-OprJ, and MexXY-oprM efflux pumps in Pseudomonas aeruginosa. *Antimicrob. Agents Chemother.* 2000, 44, 3322-3327.

15. Tait-Kamradt, A.; Davies, T.; Appelbaum, P. C.; Depardieu, F.; Courvalin, P.; Petitpas, J.; Wondrack, L.; Walker, A.; Jacobs, M. R.; Sutcliffe, J. Two new mechanisms of macrolide resistance in clinical strains of Streptococcus pneumoniae from Eastern Europe and North America. *Antimicrob. Agents Chemother.* 2000, 44, 3395-3401.

16. Matsuoka, M.; Sasaki, T. Inactivation of macrolides by producers and pathogens. *Curr. Drug Targets Infect. Disord.* 2004, 4, 217-240.

17. Gerrits, M. M.; de Zoete, M. R.; Arents, N. L.; Kuipers, E. J.; Kusters, J. G. 16S rRNA mutation-mediated tetracycline resistance in Helicobacter pylori. *Antimicrob. Agents Chemother.* 2002, 46, 2996-3000.

18. Schwarz, S.; Kehrenberg, C.; Doublet, B.; Cloeckaert, A. Molecular basis of bacterial resistance to chloramphenicol and florfenicol. *FEMS Microbiol. Rev.* 2004, 28, 519-542.

19. Bozdogan, B.; Appelbaum, P. C. Oxazolidinones: activity, mode of action, and mechanism of resistance. *Int. J. Antimicrob. Agents* 2004, 23, 113-119.

20. Alekshun, M. N.; Levy, S. B. Molecular mechanisms of antibacterial multidrug resistance. *Cell* 2007, 128, 1037-1050.

21. del Castillo, I.; Vizan, J. L.; Rodriguez-Sainz, M. C.; Moreno, F. An unusual mechanism for resistance to the antibiotic coumermycin A1. *Proc. Natl. Acad. Sci. U. S. A.* 1991, 88, 8860-8864.

22. Ruiz, J. Mechanisms of resistance to quinolones: target alterations, decreased accumulation and DNA gyrase protection. *J. Antimicrob. Chemother.* 2003, 51, 1109-1117.

23. Skold, O. Resistance to trimethoprim and sulfonamides. *Vet. Res.* 2001, 32, 261-273.

24. Davies, J. E. Origins, acquisition and dissemination of antibiotic resistance determinants. *Ciba Found Symp.* 1997, 207, 15-27; discussion 27-35.

25. Davies, J.; Davies, D. Origins and evolution of antibiotic resistance. *Microbiol. Mol. Biol. Rev.* 2010, 74, 417-433.

26.   Martinez, J. L. Antibiotics and antibiotic resistance genes in natural environments. *Science* 2008, 321, 365-367.

27.   Wittmann, H. G. Structure, function and evolution of ribosomes. *Eur. J. Biochem.* 1976, 61, 1-13.

28.   Brosius, J.; Dull, T. J.; Noller, H. F. Complete nucleotide sequence of a 23S ribosomal RNA gene from Escherichia coli. *Proc. Natl. Acad. Sci. U. S. A.* 1980, 77, 201-204.

29.   Carbon, P.; Ehresmann, C.; Ehresmann, B.; Ebel, J. P. The complete nucleotide sequence of the ribosomal 16-S RNA from Excherichia coli. Experimental details and cistron heterogeneities. *Eur J Biochem* 1979, 100, 399-410.

30.   Brownlee, G. G.; Sanger, F.; Barrell, B. G. Nucleotide sequence of 5S-ribosomal RNA from Escherichia coli. *Nature* 1967, 215, 735-6.

31.   Brosius, J.; Palmer, M. L.; Kennedy, P. J.; Noller, H. F. Complete nucleotide sequence of a 16S ribosomal RNA gene from Escherichia coli. *Proc. Natl. Acad. Sci. U. S. A.* 1978, 75, 4801-4805.

32.   Herold, M.; Nierhaus, K. H. Incorporation of six additional proteins to complete the assembly map of the 50 S subunit from Escherichia coli ribosomes. *J. Biol. Chem.* 1987, 262, 8826-8833.

33.   Traub, W.; Elson, D. RNA composition and base pairing. *Science* 1966, 153, 178-180.

34.   Noller, H. F.; Woese, C. R. Secondary structure of 16S ribosomal RNA. *Science* 1981, 212, 403-411.

35. Noller, H. F.; Kop, J.; Wheaton, V.; Brosius, J.; Gutell, R. R.; Kopylov, A. M.; Dohme, F.; Herr, W.; Stahl, D. A.; Gupta, R.; Waese, C. R. Secondary structure model for 23S ribosomal RNA. *Nucleic Acids Res.* 1981, 9, 6167-6189.

36. Chow, C. S.; Bogdan, F. M. A Structural basis for RNA-ligand interactions. *Chem. Rev.* 1997, 97, 1489-1514.

37. Onoa, B.; Tinoco, I., Jr. RNA folding and unfolding. *Curr. Opin. Struct. Biol.* 2004, 14, 374-379.

38. Brodersen, D. E.; Clemons, W. M., Jr.; Carter, A. P.; Wimberly, B. T.; Ramakrishnan, V. Crystal structure of the 30 S ribosomal subunit from Thermus thermophilus: structure of the proteins and their interactions with 16 S RNA. *J. Mol. Biol.* 2002, 316, 725-768.

39. Arnold, R. J.; Reilly, J. P. Observation of Escherichia coli ribosomal proteins and their posttranslational modifications by mass spectrometry. *Anal. Biochem.* 1999, 269, 105-112.

40. David, C. L.; Keener, J.; Aswad, D. W. Isoaspartate in ribosomal protein S11 of Escherichia coli. *J. Bacteriol.* 1999, 181, 2872-2877.

41. Cumberlidge, A. G.; Isono, K. Ribosomal protein modification in Escherichia coli. I. A mutant lacking the N-terminal acetylation of protein S5 exhibits thermosensitivity. *J. Mol. Biol.* 1979, 131, 169-189.

42. Kang, W. K.; Icho, T.; Isono, S.; Kitakawa, M.; Isono, K. Characterization of the gene rimK responsible for the addition of glutamic acid residues to the C-terminus of ribosomal protein S6 in Escherichia coli K12. *Mol. Gen. Genet.* 1989, 217, 281-288.

43. Pace, N. R. Structure and synthesis of the ribosomal ribonucleic acid of prokaryotes. *Bacteriol. Rev.* 1973, 37, 562-603.

44. Lindahl, L.; Zengel, J. M. Ribosomal genes in Escherichia coli. *Annu. Rev. Genet.* 1986, 20, 297-326.

45. http://rna.ucsc.edu/rnacenter/ribosome_images.html.

46. Rozenski, J.; Crain, P. F.; McCloskey, J. A. The RNA Modification Database: 1999 update. *Nucleic Acids Res.* 1999, 27, 196-197.

47. Decatur, W. A.; Fournier, M. J. rRNA modifications and ribosome function. *Trends Biochem. Sci.* 2002, 27, 344-351.

48. de Narvaez, C. C.; Schaup, H. W. In vivo transcriptionally coupled assembly of Escherichia coli ribosomal subunits. *J. Mol. Biol.* 1979, 134, 1-22.

49. *The PyMOL Molecular Graphics System, Version 1.2r3pre, Schrödinger, LLC.*

50. Voorhees, R. M.; Weixlbaumer, A.; Loakes, D.; Kelley, A. C.; Ramakrishnan, V. Insights into substrate stabilization from snapshots of the peptidyl transferase center of the intact 70S ribosome. *Nat. Struct. Mol. Biol.* 2009, 16, 528-533.

51. Williamson, J. R. After the ribosome structures: how are the subunits assembled? *RNA* 2003, 9, 165-167.

52. Lindahl, L. Intermediates and time kinetics of the in vivo assembly of Escherichia coli ribosomes. *J. Mol. Biol.* 1975, 92, 15-37.

53. Woodson, S. A. Recent insights on RNA folding mechanisms from catalytic RNA. *Cell Mol. Life. Sci.* 2000, 57, 796-808.

54. Lorsch, J. R. RNA chaperones exist and DEAD box proteins get a life. *Cell* 2002, 109, 797-800.

55. Watson, J. D. The Synthesis of Proteins Upon Ribosomes. *Bull. Soc. Chim. Biol. (Paris)* 1964, 46, 1399-1425.

56. Selmer, M.; Dunham, C. M.; Murphy, F. V. t.; Weixlbaumer, A.; Petry, S.; Kelley, A. C.; Weir, J. R.; Ramakrishnan, V. Structure of the 70S ribosome complexed with mRNA and tRNA. *Science* 2006, 313, 1935-1942.

57. Hartz, D.; Binkley, J.; Hollingsworth, T.; Gold, L. Domains of initiator tRNA and initiation codon crucial for initiator tRNA selection by Escherichia coli IF3. *Genes Dev.* 1990, 4, 1790-1800.

58. Carter, A. P.; Clemons, W. M., Jr.; Brodersen, D. E.; Morgan-Warren, R. J.; Hartsch, T.; Wimberly, B. T.; Ramakrishnan, V. Crystal structure of an initiation factor bound to the 30S ribosomal subunit. *Science* 2001, 291, 498-501.

59. Yusupova, G. Z.; Yusupov, M. M.; Cate, J. H.; Noller, H. F. The path of messenger RNA through the ribosome. *Cell* 2001, 106, 233-241.

60. Nakamoto, T.; Kalokofsky, D. A possible mechanism for initiation of protein synthesis. *Proc. Natl. Acad. Sci. U. S. A.* 1966, 55, 606-13.

61. Nakamoto, T. A unified view of the initiation of protein synthesis. *Biochem. Biophys. Res. Commun.* 2006, 341, 675-678.

62. Melancon, P.; Leclerc, D.; Destroismaisons, N.; Brakier-Gingras, L. The anti-Shine-Dalgarno region in Escherichia coli 16S ribosomal RNA is not essential for the correct selection of translational starts. *Biochemistry* 1990, 29, 3402-3407.

63. Calogero, R. A.; Pon, C. L.; Canonaco, M. A.; Gualerzi, C. O. Selection of the mRNA translation initiation region by Escherichia coli ribosomes. *Proc. Natl. Acad. Sci. U. S. A.* 1988, 85, 6427-6431.

64. Wu, C. J.; Janssen, G. R. Expression of a streptomycete leaderless mRNA encoding chloramphenicol acetyltransferase in Escherichia coli. *J. Bacteriol.* 1997, 179, 6824-6830.

65. Boni, I. V.; Artamonova, V. S.; Tzareva, N. V.; Dreyfus, M. Non-canonical mechanism for translational control in bacteria: synthesis of ribosomal protein S1. *EMBO J.* 2001, 20, 4222-4232.

66. Tomsic, J.; Vitali, L. A.; Daviter, T.; Savelsbergh, A.; Spurio, R.; Striebeck, P.; Wintermeyer, W.; Rodnina, M. V.; Gualerzi, C. O. Late events of translation initiation in bacteria: a kinetic analysis. *EMBO J.* 2000, 19, 2127-2136.

67. Guillon, J. M.; Heiss, S.; Soutourina, J.; Mechulam, Y.; Laalami, S.; Grunberg-Manago, M.; Blanquet, S. Interplay of methionine tRNAs with translation elongation factor Tu and translation initiation factor 2 in Escherichia coli. *J. Biol. Chem.* 1996, 271, 22321-22325.

68. Bouadloun, F.; Donner, D.; Kurland, C. G. Codon-specific missense errors in vivo. *EMBO J.* 1983, 2, 1351-1356.

69. Lucas-Lenard, J.; Haenni, A. L. Requirement of granosine 5'-triphosphate for ribosomal binding of aminoacyl-SRNA. *Proc. Natl. Acad .Sci. U. S. A.* 1968, 59, 554-560.

70. Shorey, R. L.; Ravel, J. M.; Garner, C. W.; Shive, W. Formation and properties of the aminoacyl transfer ribonucleic acid-guanosine triphosphate-protein complex. *J. Biol. Chem.* 1969, 244, 4555-4564.

71. Rodnina, M. V.; Fricke, R.; Kuhn, L.; Wintermeyer, W. Codon-dependent conformational change of elongation factor Tu preceding GTP hydrolysis on the ribosome. *EMBO J.* 1995, 14, 2613-2619.

72. Valle, M.; Zavialov, A.; Li, W.; Stagg, S. M.; Sengupta, J.; Nielsen, R. C.; Nissen, P.; Harvey, S. C.; Ehrenberg, M.; Frank, J. Incorporation of aminoacyl-tRNA into the ribosome as seen by cryo-electron microscopy. *Nat. Struct. Biol.* 2003, 10, 899-906.

73. Beringer, M.; Rodnina, M. V. The ribosomal peptidyl transferase. *Mol. Cell.* 2007, 26, 311-321.

74. Moazed, D.; Noller, H. F. Interaction of tRNA with 23S rRNA in the ribosomal A, P, and E sites. *Cell* 1989, 57, 585-597.

75. Ogle, J. M.; Brodersen, D. E.; Clemons, W. M., Jr.; Tarry, M. J.; Carter, A. P.; Ramakrishnan, V. Recognition of cognate transfer RNA by the 30S ribosomal subunit. *Science* 2001, 292, 897-902.

76. Ogle, J. M.; Murphy, F. V.; Tarry, M. J.; Ramakrishnan, V. Selection of tRNA by the ribosome requires a transition from an open to a closed form. *Cell* 2002, 111, 721-732.

77. Villa, E.; Sengupta, J.; Trabuco, L. G.; LeBarron, J.; Baxter, W. T.; Shaikh, T. R.; Grassucci, R. A.; Nissen, P.; Ehrenberg, M.; Schulten, K.; Frank, J. Ribosome-induced changes in

elongation factor Tu conformation control GTP hydrolysis. *Proc. Natl. Acad. Sci. U. S. A.* 2009, 106, 1063-1068.

78. Frank, J.; Agrawal, R. K. A ratchet-like inter-subunit reorganization of the ribosome during translocation. *Nature* 2000, 406, 318-322.

79. Frank, J.; Gao, H.; Sengupta, J.; Gao, N.; Taylor, D. J. The process of mRNA-tRNA translocation. *Proc. Natl. Acad. Sci. U. S. A.* 2007, 104, 19671-19678.

80. Taylor, D. J.; Nilsson, J.; Merrill, A. R.; Andersen, G. R.; Nissen, P.; Frank, J. Structures of modified eEF2 80S ribosome complexes reveal the role of GTP hydrolysis in translocation. *EMBO J.* 2007, 26, 2421-2431.

81. Kisselev, L. L.; Buckingham, R. H. Translational termination comes of age. *Trends. Biochem. Sci.* 2000, 25, 561-566.

82. Zavialov, A. V.; Buckingham, R. H.; Ehrenberg, M. A posttermination ribosomal complex is the guanine nucleotide exchange factor for peptide release factor RF3. *Cell* 2001, 107, 115-1124.

83. Kaji, A.; Kiel, M. C.; Hirokawa, G.; Muto, A. R.; Inokuchi, Y.; Kaji, H. The fourth step of protein synthesis: disassembly of the posttermination complex is catalyzed by elongation factor G and ribosome recycling factor, a near-perfect mimic of tRNA. *Cold Spring Harb. Symp. Quant. Biol.* 2001, 66, 515-529.

84. Lodmell, J. S.; Dahlberg, A. E. A conformational switch in Escherichia coli 16S ribosomal RNA during decoding of messenger RNA. *Science* 1997, 277, 1262-1267.

85. Chao, P. W.; Chow, C. S. Monitoring aminoglycoside-induced conformational changes in 16S rRNA through acrylamide quenching. *Bioorg. Med. Chem.* 2007, 15, 3825-3831.

86. Shandrick, S.; Zhao, Q.; Han, Q.; Ayida, B. K.; Takahashi, M.; Winters, G. C.; Simonsen, K. B.; Vourloumis, D.; Hermann, T. Monitoring molecular recognition of the ribosomal decoding site. *Angew. Chem. Int. Ed. Engl.* 2004, 43, 3177-3182.

87. Fourmy, D.; Yoshizawa, S.; Puglisi, J. D. Paromomycin binding induces a local conformational change in the A-site of 16 S rRNA. *J. Mol. Biol.* 1998, 277, 333-345.

88. Pape, T.; Wintermeyer, W.; Rodnina, M. V. Conformational switch in the decoding region of 16S rRNA during aminoacyl-tRNA selection on the ribosome. *Nat. Struct. Biol.* 2000, 7, 104-107.

89. Recht, M. I.; Fourmy, D.; Blanchard, S. C.; Dahlquist, K. D.; Puglisi, J. D. RNA sequence determinants for aminoglycoside binding to an A-site rRNA model oligonucleotide. *J. Mol. Biol.* 1996, 262, 421-436.

90. Purohit, P.; Stern, S. Interactions of a small RNA with antibiotic and RNA ligands of the 30S subunit. *Nature* 1994, 370, 659-662.

91. Miyaguchi, H.; Narita, H.; Sakamoto, K.; Yokoyama, S. An antibiotic-binding motif of an RNA fragment derived from the A-site-related region of Escherichia coli 16S rRNA. *Nucleic Acids Res.* 1996, 24, 3700-3706.

92. Wong, C. H.; Hendrix, M.; Priestley, E. S.; Greenberg, W. A. Specificity of aminoglycoside antibiotics for the A-site of the decoding region of ribosomal RNA. *Chem. Biol.* 1998, 5, 397-406.

93. Mora, D.; Ricci, G.; Guglielmetti, S.; Daffonchio, D.; Fortina, M. G. 16S-23S rRNA intergenic spacer region sequence variation in Streptococcus thermophilus and related dairy streptococci and development of a multiplex ITS-SSCP analysis for their identification. *Microbiology* 2003, 149, 807-813.

94. Brodersen, D. E.; Clemons, W. M., Jr.; Carter, A. P.; Morgan-Warren, R. J.; Wimberly, B. T.; Ramakrishnan, V. The structural basis for the action of the antibiotics tetracycline, pactamycin, and hygromycin B on the 30S ribosomal subunit. *Cell* 2000, 103, 1143-1154.

95. Carter, A. P.; Clemons, W. M.; Brodersen, D. E.; Morgan-Warren, R. J.; Wimberly, B. T.; Ramakrishnan, V. Functional insights from the structure of the 30S ribosomal subunit and its interactions with antibiotics. *Nature* 2000, 407, 340-348.

96. Stanley, R. E.; Blaha, G.; Grodzicki, R. L.; Strickler, M. D.; Steitz, T. A. The structures of the anti-tuberculosis antibiotics viomycin and capreomycin bound to the 70S ribosome. *Nat. Struct. Mol. Biol.* 2010, 17, 289-293.

97. Pioletti, M.; Schlunzen, F.; Harms, J.; Zarivach, R.; Gluhmann, M.; Avila, H.; Bashan, A.; Bartels, H.; Auerbach, T.; Jacobi, C.; Hartsch, T.; Yonath, A.; Franceschi, F. Crystal structures of complexes of the small ribosomal subunit with tetracycline, edeine and IF3. *EMBO J.* 2001, 20, 1829-1839.

98. Harms, J. M.; Wilson, D. N.; Schluenzen, F.; Connell, S. R.; Stachelhaus, T.; Zaborowska, Z.; Spahn, C. M.; Fucini, P. Translational regulation via L11: molecular switches on the ribosome turned on and off by thiostrepton and micrococcin. *Mol. Cell* 2008, 30, 26-38.

99. Bashan, A.; Agmon, I.; Zarivach, R.; Schluenzen, F.; Harms, J.; Berisio, R.; Bartels, H.; Franceschi, F.; Auerbach, T.; Hansen, H. A.; Kossoy, E.; Kessler, M.; Yonath, A. Structural basis of the ribosomal machinery for peptide bond formation, translocation, and nascent chain progression. *Mol. Cell* 2003, 11, 91-102.

100. Schlunzen, F.; Zarivach, R.; Harms, J.; Bashan, A.; Tocilj, A.; Albrecht, R.; Yonath, A.; Franceschi, F. Structural basis for the interaction of antibiotics with the peptidyl transferase centre in eubacteria. *Nature* 2001, 413, 814-821.

101. Schlunzen, F.; Harms, J. M.; Franceschi, F.; Hansen, H. A.; Bartels, H.; Zarivach, R.; Yonath, A. Structural basis for the antibiotic activity of ketolides and azalides. *Structure* 2003, 11, 329-338.

102. Rodnina, M. V.; Savelsbergh, A.; Matassova, N. B.; Katunin, V. I.; Semenkov, Y. P.; Wintermeyer, W. Thiostrepton inhibits the turnover but not the GTPase of elongation factor G on the ribosome. *Proc. Natl. Acad. Sci. U. S. A.* 1999, 96, 9586-9590.

103. Gabashvili, I. S.; Agrawal, R. K.; Spahn, C. M. T.; Grassucci, R. A.; Svergun, D. I.; Frank, J.; Penczek, P. Solution structure of the *E. coli* 70S ribosome at 11.5 Å resolution. *Cell* 2000, 100, 537-549.

104. Yusupov, M. M.; Yusupova, G. Z.; Baucom, A.; Lieberman, K.; Earnest, T. N.; Cate, J. H. D.; Noller, H. F. Crystal structure of the ribosome at 5.5 Å resolution. *Science* 2001, 292, 883-896.

105. Doring, T.; Mitchell, P.; Osswald, M.; Bochkariov, D.; Brimacombe, R. The decoding region of 16S RNA - A cross-linking study of the ribosomal A-site, P-site and E-site using

transfer-RNA derivatized at position-32 in the anticodon loop. *EMBO J.* 1994, 13, 2677-2685.

106.   Korostelev, A.; Trakhanov, S.; Laurberg, M.; Noller, H. F. Crystal structure of a 70S ribosome-tRNA complex reveals functional interactions and rearrangements. *Cell* 2006, 126, 1065-1077.

107.   Selmer, M.; Dunham, C. M.; Murphy, F. V.; Weixlbaumer, A.; Petry, S.; Kelley, A. C.; Weir, J. R.; Ramakrishnan, V. Structure of the 70S ribosome complexed with mRNA and tRNA. *Science* 2006, 313, 1935-1942.

108.   Triman, K. L. Mutational analysis of 23S ribosomal RNA structure and function in Escherichia coli. *Adv. Genet.* 1999, 41, 157-195.

109.   Yassin, A.; Fredrick, K.; Mankin, A. S. Deleterious mutations in small subunit ribosomal RNA identify functional sites and potential targets for antibiotics. *Proc. Natl. Acad. Sci. U. S. A.* 2005, 102, 16620-16625.

110.   Yassin, A.; Mankin, A. S. Potential new antibiotic sites in the ribosome revealed by deleterious mutations in RNA of the large ribosomal subunit. *J. Biol. Chem.* 2007, 282, 24329-24342.

111.   Korzybski, T.; Kowszyk-Gindifer, Z.; Kuryowicz, W. O. *Antibiotics : origin, nature, and properties*. American Society for Microbiology: Washington DC, 1978.

112.   Walter, F.; Vicens, Q.; Westhof, E. Aminoglycoside-RNA interactions. *Curr. Opin. Chem. Biol.* 1999, 3, 694-704.

113. Jenner, L. B.; Demeshkina, N.; Yusupova, G.; Yusupov, M. Structural aspects of messenger RNA reading frame maintenance by the ribosome. *Nat. Struct. Mol. Biol.* 2010, 17, 555-560.

114. Wright, G. D.; Berghuis, A. M.; Mobashery, S. Aminoglycoside antibiotics. Structures, functions, and resistance. *Adv. Exp. Med. Biol.* 1998, 456, 27-69.

115. Cho, J.; Rando, R. R. Specificity in the binding of aminoglycosides to HIV-RRE RNA. *Biochemistry* 1999, 38, 8548-8554.

116. Lapidot, A.; Berchanski, A.; Borkow, G. Insight into the mechanisms of aminoglycoside derivatives interaction with HIV-1 entry steps and viral gene transcription. *FEBS J.* 2008, 275, 5236-5257.

117. Wang, Y.; Hamasaki, K.; Rando, R. R. Specificity of aminoglycoside binding to RNA constructs derived from the 16S rRNA decoding region and the HIV-RRE activator region. *Biochemistry* 1997, 36, 768-779.

118. Berkhout, B.; Silverman, R. H.; Jeang, K. T. Tat trans-activates the human immunodeficiency virus through a nascent RNA target. *Cell* 1989, 59, 273-282.

119. Dingwall, C.; Ernberg, I.; Gait, M. J.; Green, S. M.; Heaphy, S.; Karn, J.; Lowe, A. D.; Singh, M.; Skinner, M. A. Hiv-1 Tat protein stimulates transcription by binding to A U-rich bulge in the stem of the TAR RNA structure. *EMBO J.* 1990, 9, 4145-4153.

120. Frankel, A. D. Activation of HIV transcription by Tat. *Curr. Opin. Genet. Dev.* 1992, 2, 293-298.

121. Kellermayer, R. Translational readthrough induction of pathogenic nonsense mutations. *Eur. J. Med. Genet.* 2006, 49, 445-50.

122. Howard, M.; Frizzell, R. A.; Bedwell, D. M. Aminoglycoside antibiotics restore CFTR function by overcoming premature stop mutations. *Nat. Med.* 1996, 2, 467-469.

123. Bedwell, D. M.; Kaenjak, A.; Benos, D. J.; Bebok, Z.; Bubien, J. K.; Hong, J.; Tousson, A.; Clancy, J. P.; Sorscher, E. J. Suppression of a CFTR premature stop mutation in a bronchial epithelial cell line. *Nat. Med.* 1997, 3, 1280-1284.

124. Howard, M. T.; Anderson, C. B.; Fass, U.; Khatri, S.; Gesteland, R. F.; Atkins, J. F.; Flanigan, K. M. Readthrough of dystrophin stop codon mutations induced by aminoglycosides. *Ann. Neurol.* 2004, 55, 422-426.

125. Morin, J. P.; Viotte, G.; Vandewalle, A.; Van Hoof, F.; Tulkens, P.; Fillastre, J. P. Gentamicin-induced nephrotoxicity: a cell biology approach. *Kidney Int.* 1980, 18, 583-590.

126. Selimoglu, E. Aminoglycoside-induced ototoxicity. *Curr. Pharm. Des.* 2007, 13, 119-126.

127. Mingeot-Leclercq, M. P.; Tulkens, P. M. Aminoglycosides: nephrotoxicity. *Antimicrob. Agents. Chemother.* 1999, 43, 1003-1012.

128. Roland, P. S. New developments in our understanding of ototoxicity. *Ear. Nose. Throat J.* 2004, 83, 15-6; discussion 16-7.

129. Carlier, M. B.; Laurent, G.; Claes, P. J.; Vanderhaeghe, H. J.; Tulkens, P. M. Inhibition of lysosomal phospholipases by aminoglycoside antibiotics: in vitro comparative studies. *Antimicrob. Agents Chemother.* 1983, 23, 440-449.

130. Yu, Y.; Szczepek, A. J.; Haupt, H.; Mazurek, B. Geldanamycin induces production of heat shock protein 70 and partially attenuates ototoxicity caused by gentamicin in the organ of Corti explants. *J. Biomed. Sci.* 2009, 16, 79.

131. Hanessian, S.; Masse, R.; Capmeau, M. L. Aminoglycoside antibiotics: synthesis of 5''-amino-5''-deoxyneomycin and 5''-amino-5''-deoxyparomomycin. *J. Antibiot. (Tokyo)* 1977, 30, 893-896.

132. Houghton, J. L.; Green, K. D.; Chen, W.; Garneau-Tsodikova, S. The future of aminoglycosides: the end or renaissance? *Chembiochem.* 2010, 11, 880-902.

133. Tsitovich, P. B.; Pushechnikov, A.; French, J. M.; Disney, M. D. A chemoenzymatic route to diversify aminoglycosides enables a microarray-based method to probe acetyltransferase activity. *Chembiochem.* 2010, 11, 1656-1660.

134. Rege, K.; Hu, S.; Moore, J. A.; Dordick, J. S.; Cramer, S. M. Chemoenzymatic synthesis and high-throughput screening of an aminoglycoside-polyamine library: identification of high-affinity displacers and DNA-binding ligands. *J. Am. Chem. Soc.* 2004, 126, 12306-12315.

135. Doi, Y.; Yokoyama, K.; Yamane, K.; Wachino, J.; Shibata, N.; Yagi, T.; Shibayama, K.; Kato, H.; Arakawa, Y. Plasmid-mediated 16S rRNA methylase in Serratia marcescens conferring high-level resistance to aminoglycosides. *Antimicrob. Agents Chemother.* 2004, 48, 491-496.

136. Murakami, S.; Nakashima, R.; Yamashita, E.; Yamaguchi, A. Crystal structure of bacterial multidrug efflux transporter AcrB. *Nature* 2002, 419, 587-593.

137. Yu, E. W.; Aires, J. R.; Nikaido, H. AcrB multidrug efflux pump of Escherichia coli: composite substrate-binding cavity of exceptional flexibility generates its extremely wide substrate specificity. *J. Bacteriol.* 2003, 185, 5657-5664.

138. Chow, J. W. Aminoglycoside resistance in enterococci. *Clin. Infect. Dis.* 2000, 31, 586-589.

139. Holmes, D. J.; Cundliffe, E. Analysis of a ribosomal RNA methylase gene from Streptomyces tenebrarius which confers resistance to gentamicin. *Mol. Gen. Genet.* 1991, 229, 229-237.

140. Galimand, M.; Courvalin, P.; Lambert, T. Plasmid-mediated high-level resistance to aminoglycosides in Enterobacteriaceae due to 16S rRNA methylation. *Antimicrob Agents. Chemother.* 2003, 47, 2565-2571.

141. Cubrilo, S.; Babic, F.; Douthwaite, S.; Maravic Vlahovicek, G. The aminoglycoside resistance methyltransferase Sgm impedes RsmF methylation at an adjacent rRNA nucleotide in the ribosomal A site. *RNA* 2009, 15, 1492-1497.

142. Taber, H. W.; Mueller, J. P.; Miller, P. F.; Arrow, A. S. Bacterial uptake of aminoglycoside antibiotics. *Microbiol. Rev.* 1987, 51, 439-457.

143. Mingeot-Leclercq, M. P.; Glupczynski, Y.; Tulkens, P. M. Aminoglycosides: activity and resistance. *Antimicrob. Agents. Chemother.* 1999, 43, 727-737.

144. Perichon, B.; Courvalin, P.; Galimand, M. Transferable resistance to aminoglycosides by methylation of G1405 in 16S rRNA and to hydrophilic fluoroquinolones by QepA-mediated efflux in Escherichia coli. *Antimicrob. Agents Chemother.* 2007, 51, 2464-2469.

145. Savic, M.; Lovric, J.; Tomic, T. I.; Vasiljevic, B.; Conn, G. L. Determination of the target nucleosides for members of two families of 16S rRNA methyltransferases that confer resistance to partially overlapping groups of aminoglycoside antibiotics. *Nucleic Acids Res.* 2009, 37, 5420-5431.

146. Wachino, J.; Shibayama, K.; Kurokawa, H.; Kimura, K.; Yamane, K.; Suzuki, S.; Shibata, N.; Ike, Y.; Arakawa, Y. Novel plasmid-mediated 16S rRNA m1A1408 methyltransferase, NpmA, found in a clinically isolated Escherichia coli strain resistant to structurally diverse aminoglycosides. *Antimicrob. Agents Chemother.* 2007, 51, 4401-4409.

147. Holmes, D. J.; Drocourt, D.; Tiraby, G.; Cundliffe, E. Cloning of an aminoglycoside-resistance-encoding gene, kamC, from Saccharopolyspora hirsuta: comparison with kamB from Streptomyces tenebrarius. *Gene* 1991, 102, 19-26.

148. Beauclerk, A. A.; Cundliffe, E. Sites of action of two ribosomal RNA methylases responsible for resistance to aminoglycosides. *J. Mol. Biol.* 1987, 193, 661-671.

149. Centron, D.; Roy, P. H. Presence of a group II intron in a multiresistant Serratia marcescens strain that harbors three integrons and a novel gene fusion. *Antimicrob. Agents Chemother.* 2002, 46, 1402-1409.

150. Mendes, R. E.; Toleman, M. A.; Ribeiro, J.; Sader, H. S.; Jones, R. N.; Walsh, T. R. Integron carrying a novel metallo-beta-lactamase gene, blaIMP-16, and a fused form of aminoglycoside-resistant gene aac(6')-30/aac(6')-Ib': report from the SENTRY Antimicrobial Surveillance Program. *Antimicrob. Agents Chemother.* 2004, 48, 4693-4702.

151. Dubois, V.; Poirel, L.; Marie, C.; Arpin, C.; Nordmann, P.; Quentin, C. Molecular characterization of a novel class 1 integron containing bla(GES-1) and a fused product of aac3-Ib/aac6'-Ib' gene cassettes in Pseudomonas aeruginosa. *Antimicrob. Agents Chemother.* 2002, 46, 638-645.

152. Kim, C.; Hesek, D.; Zajicek, J.; Vakulenko, S. B.; Mobashery, S. Characterization of the bifunctional aminoglycoside-modifying enzyme ANT(3''-Ii/AAC(6')-IId from Serratia marcescens. *Biochemistry* 2006, 45, 8368-8377.

153. Latham, M. P.; Brown, D. J.; McCallum, S. A.; Pardi, A. NMR methods for studying the structure and dynamics of RNA. *Chembiochem.* 2005, 6, 1492-1505.

154. Johnson, E. C.; Feher, V. A.; Peng, J. W.; Moore, J. M.; Williamson, J. R. Application of NMR SHAPES screening to an RNA target. *J. Am. Chem. Soc.* 2003, 125, 15724-15725.

155. Kime, M. J.; Moore, P. B. Nuclear Overhauser experiments at 500 MHz on the downfield proton spectra of 5S ribonucleic acid and its complex with ribosomal protein L25. *Biochemistry* 1983, 22, 2622-2629.

156. Schasfoort, R. B. M.; Tudos, A. J. *Handbook of surface plasmon resonance*. RSC Pub.: Cambridge, UK, 2008; p xxi, 403 p.

157. Schuck, P. Reliable determination of binding affinity and kinetics using surface plasmon resonance biosensors. *Curr. Opin. Biotechnol.* 1997, 8, 498-502.

158. Thomas, J. R.; Hergenrother, P. J. Targeting RNA with small molecules. *Chem. Rev.* 2008, 108, 1171-1224.

159. Cooper, A.; Johnson, C. M. Isothermal titration microcalorimetry. *Methods Mol. Biol.* 1994, 22, 137-150.

160. Hamasaki, K.; Rando, R. R. A high-throughput fluorescence screen to monitor the specific binding of antagonists to RNA targets. *Anal. Biochem.* 1998, 261, 183-190.

161. Llano-Sotelo, B.; Chow, C. S. RNA-aminoglycoside antibiotic interactions: fluorescence detection of binding and conformational change. *Bioorg. Med. Chem. Lett.* 1999, 9, 213-216.

162. Shandrick, S.; Zhao, Q.; Han, Q.; Ayida, B. K.; Takahashi, M.; Winters, G. C.; Simonsen, K. B.; Vourloumis, D.; Hermann, T. Monitoring molecular recognition of the ribosomal decoding site. *Angew.Chem. Int. Ed. Engl.* 2004, 43, 3177-3182.

163. Kaul, M.; Barbieri, C. M.; Pilch, D. S. Fluorescence-based approach for detecting and characterizing antibiotic-induced conformational changes in ribosomal RNA: comparing aminoglycoside binding to prokaryotic and eukaryotic ribosomal RNA sequences. *J. Am. Chem. Soc.* 2004, 126, 3447-3453.

164. Bradrick, T. D.; Marino, J. P. Ligand-induced changes in 2-aminopurine fluorescence as a probe for small molecule binding to HIV-1 TAR RNA. *RNA* 2004, 10, 1459-1468.

165. Dallmann, A.; Dehmel, L.; Peters, T.; Mugge, C.; Griesinger, C.; Tuma, J.; Ernsting, N. P. 2-Aminopurine incorporation perturbs the dynamics and structure of DNA. *Angew. Chem. Int. Ed. Engl.* 2010, 49, 5989-5992.

166. Asare-Okai, P. N.; Chow, C. S. A modified fluorescent intercalator displacement assay for RNA ligand discovery. *Anal. Biochem.* 2011, 408, 269-276.

167. Zhang, J.; Umemoto, S.; Nakatani, K. Fluorescent indicator displacement assay for ligand-RNA interactions. *J. Am. Chem. Soc.* 2010, 132, 3660-1.

168. McPike, M. P.; Goodisman, J.; Dabrowiak, J. C. Drug-RNA footprinting. *Methods Enzymol.* 2001, 340, 431-449.

169. Li, M.; Duc, A. C.; Klosi, E.; Pattabiraman, S.; Spaller, M. R.; Chow, C. S. Selection of peptides that target the aminoacyl-tRNA site of bacterial 16S ribosomal RNA. *Biochemistry* 2009, 48, 8299-82311.

170. Glish, G. L.; Vachet, R. W. The basics of mass spectrometry in the twenty-first century. *Nat. Rev. Drug. Discov.* 2003, 2, 140-150.

171. Kulkarni, P.; Chellam, S.; Flanagan, J. B.; Jayanty, R. K. Microwave digestion-ICP-MS for elemental analysis in ambient airborne fine particulate matter: rare earth elements and validation using a filter borne fine particle certified reference material. *Anal. Chim. Acta.* 2007, 599, 170-176.

172. Dreisewerd, K. The Desorption Process in MALDI. *Chem. Rev.* 2003, 103, 395-426.

173. Jia, W. J.; Kosmidis, C.; Ledingham, K. W. D.; Scott, C. T. J.; Singhal, R. P. Laser mass spectrometry of biological molecular ions produced by matrix assisted laser desorption ionization (MALDI). *Applied Surface Science* 1996, 106, 108-113.

174. Tanaka, K.; Waki, H.; Ido, Y.; Akita, S.; Yoshida, Y.; Yoshida, T.; Matsuo, T. Protein and polymer analyses up to m/z 100 000 by laser ionization time-of-flight mass spectrometry. *Rapid Commun. Mass Spectrom.* 1988, 2, 151-153.

175. Hart-Smith, G.; Barner-Kowollik, C. Contemporary Mass Spectrometry and the Analysis of Synthetic Polymers: Trends, Techniques and Untapped Potential. *Macromol. Chem. Physic.* 2010, 211, 1507-1529.

176. Dawson, P. H. *Quadrupole mass spectrometry and its applications*. Elsevier Scientific Pub. Co. ; distributor for the U.S. and Canada, Elsevier/North-Holland: Amsterdam New York, 1976; p 349 p.

177. D'Agostino, P. A.; Hancock, J. R.; Provost, L. R.; Semchuk, P. D.; Hodges, R. S. High resolution electrospray mass spectrometry with a magnetic sector instrument: Accurate mass measurement and peptide sequencing. *Rapid Commun. Mass Sp.* 1995, 9, 597-603.

178. D'Agostino, P. A.; Hancock, J. R.; Provost, L. R.; Semchuk, P. D.; Hodges, R. S. High resolution electrospray mass spectrometry with a magnetic sector instrument: Accurate mass measurement and peptide sequencing. *Rapid Commun. Mass Spectrom.* 1995, 9, 597-603.

179. McLuckey, S. A.; Wells, J. M. Mass Analysis at the Advent of the 21st Century. *Chem. Rev.* 2001, 101, 571-606.

180. Ganem, B.; Li, Y. T.; Henion, J. D. Detection of noncovalent receptor ligand complexes by mass-spectrometry. *J. Am. Chem. Soc.* 1991, 113, 6294-6296.

181. Hofstadler, S. A.; Sannes-Lowery, K. A. Applications of ESI-MS in drug discovery: interrogation of noncovalent complexes. *Nat. Rev. Drug Discovery* 2006, 5, 585-595.

182. Rosu, F.; De Pauw, E.; Gabelica, V. Electrospray mass spectrometry to study drug-nucleic acids interactions. *Biochimie* 2008, 90, 1074-1087.

183. Rosu, F.; Gabelica, V.; Houssier, C.; De Pauw, E. Determination of affinity, stoichiometry and sequence selectivity of minor groove binder complexes with double-stranded oligodeoxynucleotides by electrospray ionization mass spectrometry. *Nucleic Acids Res.* 2002, 30, e82.

184. Sannes-Lowery, K. A.; Griffey, R. H.; Hofstadler, S. A. Measuring dissociation constants of RNA and aminoglycoside antibiotics by electrospray ionization mass spectrometry. *Anal. Biochem.* 2000, 280, 264-271.

185. Lakowicz, J. R. *Principles of fluorescence spectroscopy*. 3rd ed.; Springer: New York, 2006; p xxvi, 954 p.

186. Hof, M.; Hutterer, R.; Fidler, V. *Fluorescence spectroscopy in biology : advanced methods and their applications to membranes, proteins, DNA, and cells*. Springer: Berlin ; New York, 2005; p xix, 305 p.

187. Huranova, M.; Jablonski, J. A.; Benda, A.; Hof, M.; Stanek, D.; Caputi, M. In vivo detection of RNA-binding protein interactions with cognate RNA sequences by fluorescence resonance energy transfer. *RNA* 2009, 15, 2063-2071.

188. Collins, T. R.; Hsieh, T. S. Monitoring the topoisomerase II DNA gate conformational change with fluorescence resonance energy transfer. *Methods Mol. Biol.* 2009, 582, 59-70.

189. Uphoff, S.; Holden, S. J.; Le Reste, L.; Periz, J.; van de Linde, S.; Heilemann, M.; Kapanidis, A. N. Monitoring multiple distances within a single molecule using switchable FRET. *Nat. Methods.* 2010.

190.   Foldes-Papp, Z.; Demel, U.; Tilz, G. P. Detection of single molecules: solution-phase single-molecule fluorescence correlation spectroscopy as an ultrasensitive, rapid and reliable system for immunological investigation. *J. Immunol. Methods.* 2002, 260, 117-124.

191.   Zander, C.; Enderlein, J.; Keller, R. A. *Single molecule detection in solution : methods and applications*. 1st ed.; Wiley-VCH: Berlin, 2002; p xvi, 371 p.

192.   Brunel, C.; Romby, P. Probing RNA structure and RNA-ligand complexes with chemical probes. *Methods Enzymol.* 2000, 318, 3-21.

193.   Peattie, D. A. Direct chemical method for sequencing RNA. *Proc. Natl. Acad. Sci. U. S. A.* 1979, 76, 1760-1764.

194.   Levene, P. A.; Bass, L. W. The action of hydrazine hydrate on uridine. *J. Biol. Chem.* 1926, 71, 167-172.

195.   Brown, D. M. The reaction of hydrazine with pyrimidine bases. In *Methods Enzymol.*, Lawrence Grossman, K. M., Ed. Academic Press: 1967; Vol. Volume 12, Part 1, pp 31-34.

196.   Ofengand, J.; Del Campo, M.; Kaya, Y. Mapping pseudouridines in RNA molecules. *Methods* 2001, 25, 365-373.

197.   Recht, M. I.; Douthwaite, S.; Puglisi, J. D. Basis for prokaryotic specificity of action of aminoglycoside antibiotics. *EMBO J.* 1999, 18, 3133-3138.

198.   Ehresmann, C.; Baudin, F.; Mougel, M.; Romby, P.; Ebel, J. P.; Ehresmann, B. Probing the structure of RNAs in solution. *Nucleic Acids Res.* 1987, 15, 9109-9128.

199. Ehrenberg, L.; Fedorcsak, I.; Solymosy, F. Diethyl pyrocarbonate in nucleic acid research. *Prog. Nucleic. Acid. Res. Mol. Biol.* 1976, 16, 189-262.

200. Barton, D.; Nakanishi, K. o.; Meth-Cohn, O. *Comprehensive natural products chemistry*. 1st ed.; Elsevier: Amsterdam ; New York, 1999; p v. 1-8

201. Chao, P. W. Studies of aminoglycoside analogue and rRNA interactions through biophysical approaches. EDT collection for Wayne State University, Detroit, 2008.

202. Jana, S.; Deb, J. K. Molecular understanding of aminoglycoside action and resistance. *Appl. Microbiol. Biotechnol.* 2006, 70, 140-150.

203. Moazed, D.; Noller, H. F. Interaction of antibiotics with functional sites in 16S ribosomal RNA. *Nature* 1987, 327, 389-94.

204. Woodcock, J.; Moazed, D.; Cannon, M.; Davies, J.; Noller, H. F. Interaction of antibiotics with A- and P-site-specific bases in 16S ribosomal RNA. *EMBO J.* 1991, 10, 3099-3103.

205. Llano-Sotelo, B.; Azucena, E. F., Jr.; Kotra, L. P.; Mobashery, S.; Chow, C. S. Aminoglycosides modified by resistance enzymes display diminished binding to the bacterial ribosomal aminoacyl-tRNA site. *Chem. Biol.* 2002, 9, 455-463.

206. Fourmy, D.; Recht, M. I.; Blanchard, S. C.; Puglisi, J. D. Structure of the A site of Escherichia coli 16S ribosomal RNA complexed with an aminoglycoside antibiotic. *Science* 1996, 274, 1367-1371.

207. Vicens, Q.; Westhof, E. Crystal structure of paromomycin docked into the eubacterial ribosomal decoding A site. *Structure* 2001, 9, 647-658.

208.   Vicens, Q.; Westhof, E. Crystal structure of a complex between the aminoglycoside tobramycin and an oligonucleotide containing the ribosomal decoding a site. *Chem. Biol.* 2002, 9, 747-755.

209.   Vicens, Q.; Westhof, E. Crystal structure of geneticin bound to a bacterial 16S ribosomal RNA A site oligonucleotide. *J. Mol. Biol.* 2003, 326, 1175-1188.

210.   Alper, P. B.; Hendrix, M.; Sears, P.; Wong, C. H. Probing the specificity of aminoglycoside ribosomal RNA interactions with designed synthetic analogs. *J. Am. Chem. Soc.* 1998, 120, 1965-1978.

211.   Greenberg, W. A.; Priestley, E. S.; Sears, P. S.; Alper, P. B.; Rosenbohm, C.; Hendrix, M.; Hung, S. C.; Wong, C. H. Design and synthesis of new aminoglycoside antibiotics containing neamine as an optimal core structure: Correlation of antibiotic activity with in vitro inhibition of translation. *J. Am. Chem. Soc.* 1999, 121, 6527-6541.

212.   Haddad, J.; Kotra, L. P.; Llano-Sotelo, B.; Kim, C.; Azucena, E. F.; Liu, M. Z.; Vakulenko, S. B.; Chow, C. S.; Mobashery, S. Design of novel antibiotics that bind to the ribosomal acyltransfer site. *J. Am. Chem. Soc.* 2002, 124, 3229-3237.

213.   Russell, R. J.; Murray, J. B.; Lentzen, G.; Haddad, J.; Mobashery, S. The complex of a designer antibiotic with a model aminoacyl site of the 30S ribosomal subunit revealed by X-ray crystallography. *J. Am. Chem. Soc.* 2003, 125, 3410-3411.

214.   Vourloumis, D.; Winters, G. C.; Simonsen, K. B.; Takahashi, M.; Ayida, B. K.; Shandrick, S.; Zhao, Q.; Han, Q.; Hermann, T. Aminoglycoside-hybrid ligands targeting the ribosomal decoding site. *Chembiochem.* 2005, 6, 58-65.

215. Ding, Y.; Hofstadler, S. A.; Swayze, E. E.; Griffey, R. H. An efficient synthesis of mimetics of neamine for RNA recognition. *Org. Lett.* 2001, 3, 1621-1623.

216. Vourloumis, D.; Takahashi, M.; Winters, G. C.; Simonsen, K. B.; Ayida, B. K.; Barluenga, S.; Qamar, S.; Shandrick, S.; Zhao, Q.; Hermann, T. Novel 2,5-dideoxystreptamine derivatives targeting the ribosomal decoding site RNA. *Bioorg. Med. Chem. Lett.* 2002, 12, 3367-3372.

217. Price, K. E.; Chisholm, D. R.; Misiek, M.; Leitner, F.; Tsai, Y. H. Microbiological evaluation of BB-K 8, a new semisynthetic aminoglycoside. *J. Antibiot.* 1972, 25, 709-731.

218. Kawaguchi, H.; Naito, T.; Nakagawa, S.; Fujisawa, K. I. BB-K 8, a new semisynthetic aminoglycoside antibiotic. *J. Antibiot.* 1972, 25, 695-708.

219. Watanabe, A.; Nagai, J.; Adachi, Y.; Katsube, T.; Kitahara, Y.; Murakami, T.; Takano, M. Targeted prevention of renal accumulation and toxicity of gentamicin by aminoglycoside binding receptor antagonists. *J. Control. Release* 2004, 95, 423-433.

220. Kawaguchi, H. Discovery, chemistry, and activity of amikacin. *J. Infect. Dis.* 1976, 134 S242-S248.

221. Francois, B.; Russell, R. J.; Murray, J. B.; Aboul-ela, F.; Masquida, B.; Vicens, Q.; Westhof, E. Crystal structures of complexes between aminoglycosides and decoding A site oligonucleotides: role of the number of rings and positive charges in the specific binding leading to miscoding. *Nucleic Acids Res.* 2005, 33, 5677-5690.

222. Matthey, T.; Hansen, J. P.; Drewsen, M. Coulomb bicrystals of species with identical charge-to-mass ratios. *Phys. Rev. Lett.* 2003, 91, 165001.

223. Scaringe, S. A.; Wincott, F. E.; Caruthers, M. H. Novel RNA synthesis method using 5'-O-silyl-2'-O-orthoester protecting groups. *J. Am. Chem. Soc.* 1998, 120, 1820-1821.

224. Fasman, G. D. *Handbook of biochemistry and molecular biology*. 3d ed.; CRC Press: Cleveland, 1975; p 5 v. in 9.

225. Krzyzosiak, W.; Denman, R.; Nurse, K.; Hellmann, W.; Boublik, M.; Gehrke, C. W.; Agris, P. F.; Ofengand, J. In vitro synthesis of 16S ribosomal RNA containing single base changes and assembly into a functional 30S ribosome. *Biochemistry* 1987, 26, 2353-2364.

226. Cunningham, P. R.; Ofengand, J. Use of inorganic pyrophosphatase to improve the yield of in vitro transcription reactions catalyzed by T7 RNA polymerase. *Biotechniques* 1990, 9, 713-714.

227. Bruce, A. G.; Uhlenbeck, O. C. Reactions at the termini of tRNA with T4 RNA ligase. *Nucleic Acids Res.* 1978, 5, 3665-3677.

228. Moazed, D.; Noller, H. F. Transfer RNA shields specific nucleotides in 16S ribosomal RNA from attack by chemical probes. *Cell* 1986, 47, 985-994.

229. Moazed, D.; Stern, S.; Noller, H. F. Rapid chemical probing of conformation in 16 S ribosomal RNA and 30 S ribosomal subunits using primer extension. *J. Mol. Biol.* 1986, 187, 399-416.

230. Findlay, D.; Herries, D. G.; Mathias, A. P.; Rabin, B. R.; Ross, C. A. The active site and mechanism of action of bovine pancreatic ribonuclease. *Nature* 1961, 190, 781-784.

231. Raines, R. T. Ribonuclease A. *Chem. Rev.* 1998, 98, 1045-1066.

232. delCardayre, S. B.; Raines, R. T. Structural determinants of enzymatic processivity. *Biochemistry* 1994, 33, 6031-7.

233. Sorrentino, S.; Libonati, M. Human pancreatic-type and nonpancreatic-type ribonucleases: a direct side-by-side comparison of their catalytic properties. *Arch. Biochem. Biophys.* 1994, 312, 340-348.

234. Moazed, D.; Noller, H. F. Chloramphenicol, erythromycin, carbomycin and vernamycin B protect overlapping sites in the peptidyl transferase region of 23S ribosomal RNA. *Biochimie* 1987, 69, 879-84.

235. Felsenfeld, G.; Sandeen, G.; Vonhippel, P. H. The Destabilizing Effect of Ribonuclease on the Helical DNA Structure. *Proc. Natl. Acad. Sci. U. S. A.* 1963, 50, 644-651.

236. Fisher, B. M.; Schultz, L. W.; Raines, R. T. Coulombic effects of remote subsites on the active site of ribonuclease A. *Biochemistry* 1998, 37, 17386-17401.

237. Fourmy, D.; Recht, M. I.; Blanchard, S. C.; Puglisi, J. D. Structure of the A site of Escherichia coli 16S ribosomal RNA complexed with an aminoglycoside antibiotic. *Science* 1996, 274, 1367-71.

238. Meroueh, S. O.; Mobashery, S. Conformational transition in the aminoacyl t-RNA site of the bacterial ribosome both in the presence and absence of an aminoglycoside antibiotic. *Chem. Biol. Drug Des.* 2007, 69, 291-297.

239. Laurberg, M.; Asahara, H.; Korostelev, A.; Zhu, J.; Trakhanov, S.; Noller, H. F. Structural basis for translation termination on the 70S ribosome. *Nature* 2008, 454, 852-857.

240. Boger, D. L.; Fink, B. E.; Brunette, S. R.; Tse, W. C.; Hedrick, M. P. A simple, high-resolution method for establishing DNA binding affinity and sequence selectivity. *J. Am. Chem. Soc.* 2001, 123, 5878-5891.

241. Boger, D. L.; Tse, W. C. Thiazole orange as the fluorescent intercalator in a high resolution FID assay for determining DNA binding affinity and sequence selectivity of small molecules. *Bioorg. Med. Chem.* 2001, 9, 2511-2518.

242. Monchaud, D.; Allain, C.; Bertrand, H.; Smargiasso, N.; Rosu, F.; Gabelica, V.; De Cian, A.; Mergny, J. L.; Teulade-Fichou, M. R. Ligands playing musical chairs with G-quadruplex DNA: A rapid and simple displacement assay for identifying selective G-quadruplex binders. *Biochimie* 2008, 90, 1207-1223.

243. Tse, W. C.; Boger, D. L. A fluorescent intercalator displacement assay for establishing DNA binding selectivity and affinity. *Acc. Chem. Res.* 2004, 37, 61-69.

244. Lewis, M. A.; Long, E. C. Fluorescent intercalator displacement analyses of DNA binding by the peptide-derived natural products netropsin, actinomycin, and bleomycin. *Bioorg. Med. Chem.* 2006, 14, 3481-90.

245. Krishnamurthy, M.; Schirle, N. T.; Beal, P. A. Screening helix-threading peptides for RNA binding using a thiazole orange displacement assay. *Bioorg. Med. Chem.* 2008, 16, 8914-8921.

246. Meyer, S. T.; Hergenrother, P. J. Small molecule ligands for bulged RNA secondary structures. *Org. Lett.* 2009, 11, 4052-4055.

247. Zhang, J.; Umemoto, S.; Nakatani, K. Fluorescent indicator displacement assay for ligand-RNA interactions. *J. Am. Chem. Soc.* 2010, 132, 3660-3661.

248. Kempen, E. C.; Brodbelt, J. S. A method for the determination of binding constants by electrospray ionization mass spectrometry. *Anal. Chem.* 2000, 72, 5411-5416.

249. Daniel, J. M.; McCombie, G.; Wendt, S.; Zenobi, R. Mass spectrometric determination of association constants of adenylate kinase with two noncovalent inhibitors. *J. Am. Soc. Mass Spectrom.* 2003, 14, 442-448.

250. Stults, J. T.; Marsters, J. C. Improved electrospray ionization of synthetic oligodeoxynucleotides. *Rapid Commun. Mass Spectrom.* 1991, 5, 359-363.

251. Limbach, P. A.; Crain, P. F.; McCloskey, J. A. Molecular mass measurments of intact ribonucleic acids via electrospray ionization quadrupole mass spectrometry. *J. Am. Soc. Mass Spectrom.* 1995, 6, 27-39.

252. Cheng, X.; Chen, R.; Bruce, J. E.; Schwartz, B. L.; Anderson, G. A.; Hofstadler, S. A.; Gale, D. C.; Smith, R. D.; Gao, J.; Sigal, G. B.; Mammen, M.; Whitesides, G. M. Using Electrospray Ionization FTICR Mass Spectrometry To Study Competitive Binding of Inhibitors to Carbonic Anhydrase. *J. Am. Chem. Soc.* 1995, 117, 8859–8860.

253. Smith, R. D.; Bruce, J. E.; Wu, Q. Y.; Lei, Q. P. New mass spectrometric methods for the study of noncovalent associations of biopolymers. *Chem. Soc. Rev.* 1997, 26, 191-202.

254. Loo, J. A. Studying noncovalent protein complexes by electrospray ionization mass spectrometry. *Mass Spectrom. Rev.* 1997, 16, 1-23.

255. Huang, C. Y. Determination of binding stoichiometry by the continuous variation method: the Job plot. *Methods Enzymol.* 1982, 87, 509-525.

256. Satz, A. L.; Bruice, T. C. Synthesis of fluorescent microgonotropens (FMGTs) and their interactions with dsDNA. *Bioorg. Med. Chem.* 2000, 8, 1871-1880.

257. Purohit, P.; Stern, S. Interactions of a small RNA with antibiotic and RNA ligands of the 30S subunit. *Nature* 1994, 370, 659-62.

258. Hermann, T.; Westhof, E. Aminoglycoside binding to the hammerhead ribozyme: a general model for the interaction of cationic antibiotics with RNA. *J Mol Biol* 1998, 276, 903-12.

259. Hermann, T.; Westhof, E. Saccharide-RNA recognition. *Biopolymers* 1998, 48, 155-65.

260. Gottlieb, D.; Bhattacharyya, P. K. Some properties of an antibiotic obtained from a species of streptomyces. *J.Bacteriol.* 1948, 55, 409-417.

261. Long, K. S.; Porse, B. T. A conserved chloramphenicol binding site at the entrance to the ribosomal peptide exit tunnel. *Nucleic Acids Res.* 2003, 31, 7208-7215.

262. Moazed, D.; Noller, H. F. Chloramphenicol, erythromycin, carbomycin and vernamycin-B protect overlapping sites in the peptidyl transferase region of 23S-ribosomal RNA. *Biochimie* 1987, 69, 879-884.

263. Long, K. S.; Crothers, D. M. Interaction of human-immunodeficiency-virus type-1 Tat-derived peptides with TAR RNA. *Biochemistry* 1995, 34, 8885-8895.

264. Mei, H. Y.; Galan, A. A.; Halim, N. S.; Mack, D. P.; Moreland, D. W.; Sanders, K. B.; Truong, H. N.; Czarnik, A. W. Inhibition of an HIV-1 Tat-derived peptide binding to TAR RNA by aminoglycoside antibiotics. *Bioorg. Med. Chem. Lett.* 1995, 5, 2755-2760.

265. Weeks, K. M.; Ampe, C.; Schultz, S. C.; Steitz, T. A.; Crothers, D. M. Fragments of the HIV-1 Tat protein specifically bind TAR RNA. *Science* 1990, 249, 1281-5.

266. Chaloin, O.; Peter, J. C.; Briand, J. P.; Masquida, B.; Desgranges, C.; Muller, S.; Hoebeke, J. The N-terminus of HIV-1 Tat protein is essential for Tat-TAR RNA interaction. *Cell. Mol. Life Sci.* 2005, 62, 355-361.

267. Sannes-Lowery, K. A.; Hu, P. F.; Mack, D. P.; Mei, H. Y.; Loo, J. A. HIV 1 Tat peptide binding do to TAR RNA by electrospray ionization mass spectrometry. *Anal. Chem.* 1997, 69, 5130-5135.

268. Hendrix, M.; Priestley, E. S.; Joyce, G. F.; Wong, C. H. Direct observation of aminoglycoside-RNA interactions by surface plasmon resonance. *J. Am. Chem. Soc.* 1997, 119, 3641-3648.

269. Ryu, D. H.; Rando, R. R. Aminoglycoside binding to human and bacterial A-site rRNA decoding region constructs. *Bioorg. Med. Chem.* 2001, 9, 2601-2608.

270. Ryu, D. H.; Rando, R. R. Decoding region bubble size and aminoglycoside antibiotic binding. *Bioorg. Med. Chem. Lett.* 2002, 12, 2241-2244.

271. Chui, H. M.; Desaulniers, J. P.; Scaringe, S. A.; Chow, C. S. Synthesis of helix 69 of *Escherichia coli* 23S rRNA containing its natural modified nucleosides, m3Ψ and Ψ. *J. Org. Chem.* 2002, 67, 8847-8854.

272. Haddad, J.; Kotra, L. P.; Llano-Sotelo, B.; Kim, C.; Azucena, E. F., Jr.; Liu, M.; Vakulenko, S. B.; Chow, C. S.; Mobashery, S. Design of novel antibiotics that bind to the ribosomal acyltransfer site. *J. Am. Chem. Soc.* 2002, 124, 3229-3237.

273. Hwang, S.; Tamilarasu, N.; Ryan, K.; Huq, I.; Richter, S.; Still, W. C.; Rana, T. M. Inhibition of gene expression in human cells through small molecule-RNA interactions. *Proc. Natl. Acad. Sci. U. S. A.* 1999, 96, 12997-13002.

274. Davies, J.; Gorini, L.; Davis, B. D. Misreading of RNA codewords induced by aminoglycoside antibiotics. *Mol. Pharmacol.* 1965, 1, 93-106.

275. Puglisi, J. D., Blanchard, S. C., Dahlquist, K. D., Eason, R. G., Fourmy, D., Lynch, S. R., Recht, M. I., and Yoshizawa, S. *Aminoglycoside Antibiotics and Decoding. In The Ribosome: Structure, Function, Antibiotics, and Cellular Interactions*. ASM Press: Washington, DC, 2000.

276. Prayle, A.; Watson, A.; Fortnum, H.; Smyth, A. Side effects of aminoglycosides on the kidney, ear and balance in cystic fibrosis. *Thorax* 2010, 65, 654-8.

277. Wang, S.; Huber, P. W.; Cui, M.; Czarnik, A. W.; Mei, H. Y. Binding of neomycin to the TAR element of HIV-1 RNA induces dissociation of Tat protein by an allosteric mechanism. *Biochemistry* 1998, 37, 5549-5557.

278. Liang, F. S.; Greenberg, W. A.; Hammond, J. A.; Hoffmann, J.; Head, S. R.; Wong, C. H. Evaluation of RNA-binding specificity of aminoglycosides with DNA microarrays. *Proc. Natl. Acad. Sci. U. S. A.* 2006, 103, 12311-12316.

279. Clouet-d'Orval, B.; Stage, T. K.; Uhlenbeck, O. C. Neomycin inhibition of the hammerhead ribozyme involves ionic interactions. *Biochemistry* 1995, 34, 11186-11190.

280. Tor, Y.; Hermann, T.; Westhof, E. Deciphering RNA recognition: aminoglycoside binding to the hammerhead ribozyme. *Chem. Biol.* 1998, 5, R277-283.

281. Wang, H.; Tor, Y. Electrostatic Interactions in RNA Aminoglycosides Binding. *J. Am. Chem. Soc.* 1997, 119, 8734-8735.

282. Arya, D. P.; Xue, L.; Willis, B. Aminoglycoside (neomycin) preference is for A-form nucleic acids, not just RNA: results from a competition dialysis study. *J. Am. Chem. Soc.* 2003, 125, 10148-10149.

283. Blount, K. F.; Zhao, F.; Hermann, T.; Tor, Y. Conformational constraint as a means for understanding RNA-aminoglycoside specificity. *J. Am. Chem. Soc.* 2005, 127, 9818-9829.

284. Faber, C.; Sticht, H.; Schweimer, K.; Rosch, P. Structural rearrangements of HIV-1 Tat-responsive RNA upon binding of neomycin B. *J. Biol. Chem.* 2000, 275, 20660-20666.

285. Jiang, L.; Majumdar, A.; Hu, W.; Jaishree, T. J.; Xu, W.; Patel, D. J. Saccharide-RNA recognition in a complex formed between neomycin B and an RNA aptamer. *Structure* 1999, 7, 817-827.

286. Varani, G. Exceptionally stable nucleic acid hairpins. *Annu. Rev. Biophys. Biomol. Struct.* 1995, 24, 379-404.

287. Woese, C. R.; Winker, S.; Gutell, R. R. Architecture of ribosomal RNA: constraints on the sequence of "tetra-loops". *Proc. Natl. Acad. Sci. U. S. A.* 1990, 87, 8467-8471.

288. Liu, X.; Thomas, J. R.; Hergenrother, P. J. Deoxystreptamine dimers bind to RNA hairpin loops. *J. Am. Chem. Soc.* 2004, 126, 9196-9197.

289. Gutell, R. R. Collection of small subunit (16S- and 16S-like) ribosomal RNA structures: 1994. *Nucleic Acids Res.* 1994, 22, 3502-3507.

290. Recht, M. I.; Douthwaite, S.; Dahlquist, K. D.; Puglisi, J. D. Effect of mutations in the A site of 16 S rRNA on aminoglycoside antibiotic-ribosome interaction. *J. Mol. Biol.* 1999, 286, 33-43.

291. Lynch, S. R.; Puglisi, J. D. Structure of a eukaryotic decoding region A-site RNA. *J. Mol. Biol.* 2001, 306, 1023-1035.

292. Scheunemann, A. E.; Graham, W. D.; Vendeix, F. A. P.; Agris, P. F. Binding of aminoglycoside antibiotics to helix 69 of 23S rRNA. *Nucleic Acids Res.* 2010, 38, 3094-3105.

293. Borovinskaya, M. A.; Pai, R. D.; Zhang, W.; Schuwirth, B. S.; Holton, J. M.; Hirokawa, G.; Kaji, H.; Kaji, A.; Cate, J. H. Structural basis for aminoglycoside inhibition of bacterial ribosome recycling. *Nat. Struct. Mol. Biol.* 2007, 14, 727-732.

294. Yarian, C. S.; Basti, M. M.; Cain, R. J.; Ansari, G.; Guenther, R. H.; Sochacka, E.; Czerwinska, G.; Malkiewicz, A.; Agris, P. F. Structural and functional roles of the N1- and N3-protons of psi at tRNA's position 39. *Nucleic Acids Res.* 1999, 27, 3543-3549.

295. Durant, P. C.; Davis, D. R. Stabilization of the anticodon stem-loop of tRNALys,3 by an A+-C base-pair and by pseudouridine. *J. Mol. Biol.* 1999, 285, 115-131.

296. Agris, P. F. The importance of being modified: roles of modified nucleosides and Mg2+ in RNA structure and function. *Prog. Nucleic Acid Res. Mol. Biol.* 1996, 53, 79-129.

297. Charette, M.; Gray, M. W. Pseudouridine in RNA: what, where, how, and why. *IUBMB Life* 2000, 49, 341-51.

298. Helm, M.; Giege, R.; Florentz, C. A Watson-Crick base-pair-disrupting methyl group (m1A9) is sufficient for cloverleaf folding of human mitochondrial tRNALys. *Biochemistry* 1999, 38, 13338-13346.

299. Micura, R.; Pils, W.; Hobartner, C.; Grubmayr, K.; Ebert, M. O.; Jaun, B. Methylation of the nucleobases in RNA oligonucleotides mediates duplex-hairpin conversion. *Nucleic Acids Res.* 2001, 29, 3997-4005.

300. Kierzek, E.; Kierzek, R. The thermodynamic stability of RNA duplexes and hairpins containing N6-alkyladenosines and 2-methylthio-N6-alkyladenosines. *Nucleic Acids Res.* 2003, 31, 4472-4480.

301. Auffinger, P.; Westhof, E. Rules governing the orientation of the 2'-hydroxyl group in RNA. *J. Mol. Biol.* 1997, 274, 54-63.

302. Mahto, S. K.; Chow, C. S. Synthesis and solution conformation studies of the modified nucleoside N(4),2'-O-dimethylcytidine (m(4)Cm) and its analogues. *Bioorg. Med. Chem.* 2008, 16, 8795-8800.

303. Thompson, J.; Schmidt, F.; Cundliffe, E. Site of action of a ribosomal RNA methylase conferring resistance to thiostrepton. *J. Biol. Chem.* 1982, 257, 7915-7917.

304. Weisblum, B. Erythromycin resistance by ribosome modification. *Antimicrob. Agents Chemother.* 1995, 39, 577-585.

305. Pernodet, J. L.; Fish, S.; Blondelet-Rouault, M. H.; Cundliffe, E. The macrolide-lincosamide-streptogramin B resistance phenotypes characterized by using a specifically deleted, antibiotic-sensitive strain of Streptomyces lividans. *Antimicrob. Agents Chemother.* 1996, 40, 581-585.

306. Helser, T. L.; Davies, J. E.; Dahlberg, J. E. Mechanism of kasugamycin resistance in *Escherichia coli*. *Nat. New Biol.* 1972, 235, 6-9.

307. Rippe, R. A.; Brenner, D. A.; Tugores, A. Techniques to measure nucleic acid-protein binding and specificity: nuclear extract preparations, DNase I footprinting, and mobility shift assays. *Methods Mol. Biol.* 2001, 160, 459-479.

308. Feig Andrew, L. Applications of isothermal titration calorimetry in RNA biochemistry and biophysics. *Biopolymers* 2007, 87, 293-301.

309. Nguyen, B.; Tanious Farial, A.; Wilson, W. D. Biosensor-surface plasmon resonance: quantitative analysis of small molecule-nucleic acid interactions. *Methods* 2007, 42, 150-161.

310. Fuertig, B.; Richter, C.; Woehnert, J.; Schwalbe, H. NMR spectroscopy of RNA. *ChemBioChem* 2003, 4, 936-962.

311. Daniel, J. M.; Friess, S. D.; Rajagopalan, S.; Wendt, S.; Zenobi, R. Quantitative determination of noncovalent binding interactions using soft ionization mass spectrometry. *Int. J. Mass Spectrom.* 2002, 216, 1-27.

312. Akashi, S. Investigation of molecular interaction within biological macromolecular complexes by mass spectrometry. *Medicinal research reviews* 2006, 26, 339-68.

313. Stern, S.; Purohit, P. An oligonucleotide analog approach to the decoding region of 16S rRNA. *Biochem. Cell Biol.* 1995, 73, 899-905.

314. Li, M.; Duc, A. C.; Klosi, E.; Pattabiraman, S.; Spaller, M. R.; Chow, C. S. Selection of peptides that target the aminoacyl-tRNA site of bacterial 16S ribosomal RNA. *Biochemistry* 2009, 48, 8299-8311.

315. Mahto, S. Exploring the roles of modified nucleotides in the bacterial decoding region and antisense applications. Wayne State University, Detroit, 2009.

316. Lynch, S. R.; Puglisi, J. D. Structural origins of aminoglycoside specificity for prokaryotic ribosomes. *J. Mol. Biol.* 2001, 306, 1037-1058.

317. Magnet, S.; Blanchard, J. S. Molecular insights into aminoglycoside action and resistance. *Chem. Rev.* 2005, 105, 477-498.

318. Chao, P.-W.; Chow, C. S. Monitoring aminoglycoside-induced conformational changes in 16S rRNA through acrylamide quenching. *Bioorg. Med. Chem.* 2007, 15, 3825-3831.

319. Yang, G.; Trylska, J.; Tor, Y.; McCammon, J. A. Binding of aminoglycosidic antibiotics to the oligonucleotide A-site model and 30S ribosomal subunit: Poisson-Boltzmann model, thermal denaturation, and fluorescence studies. *J. Med. Chem.* 2006, 49, 5478-5490.

320. Kondo, J.; Hainrichson, M.; Nudelman, I.; Shallom-Shezifi, D.; Barbieri, C. M.; Pilch, D. S.; Westhof, E.; Baasov, T. Differential selectivity of natural and synthetic aminoglycosides

towards the eukaryotic and prokaryotic decoding A sites. *ChemBioChem* 2007, 8, 1700-1709.

321. Lynch, S. R.; Gonzalez, R. L.; Puglisi, J. D. Comparison of X-Ray Crystal structure of the 30S subunit-antibiotic complex with NMR structure of decoding site oligonucleotide-paromomycin complex. *Structure* 2003, 11, 43-53.

322. Chao, P. M.; Huang, H. L.; Liao, C. H.; Huang, S. T.; Huang, C. J. A high oxidised frying oil content diet is less adipogenic, but induces glucose intolerance in rodents. *Br J Nutr* 2007, 98, 63-71.

323. Pfister, P.; Risch, M.; Brodersen, D. E.; Bottger, E. C. Role of 16S rRNA Helix 44 in Ribosomal Resistance to Hygromycin B. *Antimicrob. Agents Chemother.* 2003, 47, 1496-1502.

324. Johansen, S. K.; Maus, C. E.; Plikaytis, B. B.; Douthwaite, S. Capreomycin binds across the ribosomal subunit interface using tlyA-encoded 2'-O-methylations in 16S and 23S rRNAs. *Mol. Cell* 2006, 23, 173-182.

325. Beauclerk, A. A. D.; Cundliffe, E. Sites of action of two ribosomal RNA methylases responsible for resistance to aminoglycosides. *J. Mol. Biol.* 1987, 193, 661-671.

326. Van Melckebeke, H.; Devany, M.; Di Primo, C.; Beaurain, F.; Toulme, J. J.; Bryce, D. L.; Boisbouvier, J. Liquid-crystal NMR structure of HIV TAR RNA bound to its SELEX RNA aptamer reveals the origins of the high stability of the complex. *Proc. Natl. Acad. Sci. U. S. A.* 2008, 105, 9210-5.

327. Carlson, C. B.; Vuyisich, M.; Gooch, B. D.; Beal, P. A. Preferred RNA binding sites for a threading intercalator revealed by in vitro evolution. *Chem. Biol.* 2003, 10, 663-672.

ABSTRACT

METHOD DEVELOPMENT AND APLLICATIONS TO SCREENING AND CHARACTERIZATION OF rRNA-TARGETING SMALL MOLECULES

by

PAPA NII ASARE-OKAI

May 2011

Advisor: Prof. Christine S. Chow

Major: Chemistry (Biochemistry)

Degree: Doctor of Philosophy

A series of single-ring aminoglycoside analogues was tested for binding to a model RNA representing the A site using electrospray ionization mass spectrometry (ESI-MS). Several of the synthetic analogues with low molecular weights were found to bind to the RNA with affinities comparable to the parental aminoglycoside neamine, with apparent dissociation constants in the low micromolar range. Salt dependence of the affinity constants for the single-ring analogues revealed a predominantly electrostatic binding mode. Footprinting experiments revealed that one of the compounds (DHR23) has a similar binding site as the antibiotic paromomycin. Dimethyl sulphate (DMS) chemical probing results also suggest that the binding of DHR23 to the A site leads to stabilization of the stacked-in conformation of A1492 and A1493.

To aid in the ligand-identification process, a modified fluorescence intercalator displacement (FID) assay for screening RNA-binding ligands was established using 3-methyl-2-

((1-(3-(trimethylammonio)propyl)-4-quinolinylidene)methyl)benzothiazolium (TO-PRO) as the fluorescent indicator. ESI-MS results provide direct evidence that correlates the reduction in fluorescence intensity observed in the FID assay with displacement of the dye molecule from RNA. The assay was successfully applied to screen a variety of RNA-binding ligands with a set of small hairpin RNAs. Ligands that bind with moderate affinity to the chosen RNA constructs were identified.

Furthermore, the specificity of one compound, DHR23, as well as a range of other ligands were tested for binding to a set of RNA models, as well as the modified and unmodified decoding-region RNA constructs. The results show that DHR23 has preferred binding to structured RNA as compared to ssRNA, as well as a modest preference for the A-site RNA. Also, our results indicate that modified nucleotides at or near the ligand-binding pocket may affect binding affinity of small molecules.

In summary, the results from this work have shown that generation of compounds based on these simplified structures in combination with FID screening may lead to selective reagents for RNA internal bulges, loops, mismatches, or other unique secondary-structure elements.

AUTOBIOGRAPHICAL STATEMENT

PAPA NII ASARE-OKAI

ADVISOR: Prof. Christine S. Chow

DISSERTATION TITLE: METHOD DEVELOPMENT AND APPLICATIONS TO SCREENING AND CHARACTERIZATION OF rRNA-TARGETING SMALL MOLECULES

EDUCATION

Ph.D. Chemistry, Wayne State University, Detroit MI, U.S.A. 2011

B. Sc. Biochemistry, Calvin College, Grand Rapids MI, U.S.A. 2004

High School Diploma, Presbyterian Boys' Secondary School, Accra, Ghana, 1998

PUBLICATIONS

Asare-Okai, P.; Chow, C. S. A modified fluorescent intercalator displacement assay for RNA-ligand discovery. *Anal. Biochem.* 2011, 408, 269-276.

Chao, P.; **Asare-Okai, P**.; Hesek, D.; Lee, M.; Mason, J.; Mobashery, S.; and Chow, C.S. Small molecules targeting the ribosomal aminoacyltransfer site (submitted to J. Med. Chem. 2010).

Asare-Okai, P.; Mahto, S. K.; Chow, C. S. Role of modified nucleotides in drug binding: targeting the ribosomal A- site (manuscript in preparation).

Asare-Okai, P.; Williams, B.; Weber, M.; Rijal, K.; and Chow, C. S. Exploring the effects of *cis*-Pt and its analogues on the topology of ccDNA (manuscript in preparation).